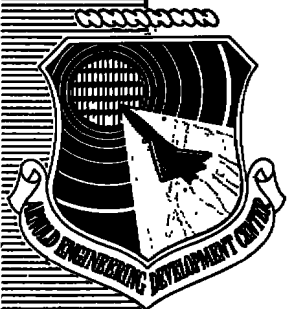AEDC-TR-76-159

Cy.2

NUMERICAL ANALYSIS OF TURBULENT

SEPARATED SUBSONIC DIFFUSER FLOWS

ENGINE TEST FACILITY
ARNOLD ENGINEERING DEVELOPMENT CENTER
AIR FORCE SYSTEMS COMMAND
ARNOLD AIR FORCE STATION, TENNESSEE 37389

February 1977

Final Report for Period October 1973 — June 1976

Approved for public release; distribution unlimited.

Prepared for

DIRECTORATE OF TECHNOLOGY (DY)
ARNOLD ENGINEERING DEVELOPMENT CENTER
ARNOLD AIR FORCE STATION, TENNESSEE 37389

APPROVAL STATEMENT

This technical report has been reviewed and is approved for publication.

FOR THE COMMANDER

ELTON R. THOMPSON
Research & Development
    Division
Directorate of Technology

ROBERT O. DIETZ
Director of Technology

REPORT DOCUMENTATION PAGE		READ INSTRUCTIONS BEFORE COMPLETING FORM
1 REPORT NUMBER AEDC-TR-76-159	2 GOVT ACCESSION NO.	3 RECIPIENT'S CATALOG NUMBER
4 TITLE (and Subtitle) NUMERICAL ANALYSIS OF TURBULENT SEPARATED SUBSONIC DIFFUSER FLOWS		5 TYPE OF REPORT & PERIOD COVERED Final Report - October 1973 - June 1976
		6 PERFORMING ORG. REPORT NUMBER
7 AUTHOR(s) J. C. Chien, ARO, Inc.		8 CONTRACT OR GRANT NUMBER(s)
9 PERFORMING ORGANIZATION NAME AND ADDRESS Arnold Engineering Development Center (DY) Air Force Systems Command Arnold Air Force Station, Tennessee 37389		10 PROGRAM ELEMENT. PROJECT, TASK AREA & WORK UNIT NUMBERS Program Element 65807F
11 CONTROLLING OFFICE NAME AND ADDRESS Arnold Engineering Development Center (DYFS) Arnold Air Force Station Tennessee 37389		12 REPORT DATE February 1977
		13 NUMBER OF PAGES 157
14 MONITORING AGENCY NAME & ADDRESS(If different from Controlling Office)		15. SECURITY CLASS. (of this report) UNCLASSIFIED
		15a DECLASSIFICATION/DOWNGRADING SCHEDULE N/A

16 DISTRIBUTION STATEMENT (of this Report)

Approved for public release; distribution unlimited.

17 DISTRIBUTION STATEMENT (of the abstract entered in Block 20, If different from Report)

18 SUPPLEMENTARY NOTES

Available in DDC

19. KEY WORDS (Continue on reverse side if necessary and identify by block number)

numerical analysis	subsonic flow	flow field
air	diffusers	Navier-Stokes equations
turbulence model	flow separation	

20 ABSTRACT (Continue on reverse side if necessary and identify by block number)

A general finite difference formulation of the incompressible
Navier-Stokes equations in terms of the vorticity and the stream
function is presented for turbulent internal flows. Turbulent
models such as algebraic eddy viscosity models, and the low Reynolds
number two-equation k-ε models were systematically studied. Numeri-
cal solutions are presented for both separated and non-separated
subsonic diffuser flows with either a sublayer coordinate stretching

DD $_{1\ JAN\ 73}^{FORM}$ 1473   EDITION OF 1 NOV 65 IS OBSOLETE

20. ABSTRACT (Continued)

or a law of the wall matching procedure. Excellent agreement with experimental data is obtained for the fully developed channel flow. Agreement with data from an 8-deg conical diffuser is also good. The detailed flow-field structure for separated diffuser flows can be obtained including the prediction of the separation point.

AFSC
Arnold AFS Tenn

PREFACE

The work reported herein was conducted by the Arnold Engineering Development Center (AEDC), Air Force Systems Command (AFSC), under Program Element 65807F. The results of the research presented were obtained by ARO, Inc. (a Sverdrup Corporation Company), operating contractor for the AEDC, AFSC, Arnold Air Force Station, Tennessee, under ARO Project Numbers RF409, R33P-60A, and R33A-02A. The author of this report was J. C. Chien, ARO, Inc. The manuscript (ARO Control No. ARO-ETF-TR-76-122) was submitted for publication on October 15, 1976.

CONTENTS

ILLUSTRATIONS

5

TABLE

APPENDIXES

1.0 INTRODUCTION

Diffusers are an important component in many areas of application, such as propulsion systems, wind tunnels, test facilities, etc. Yet the prediction of diffuser flows remains one of the most difficult fluid dynamics problems, especially when the inlet conditions to the diffuser are highly nonuniform. Since the optimum operating condition for a diffuser, i.e., maximum pressure recovery, has been shown experimentally to occur with some flow separation (Ref. 1), a realistic solution for the flow field can be obtained only by solving the full Navier-Stokes equations. In addition, the diffuser flows of practical interest are turbulent in nature. The performance of a diffuser depends not only on the shape of the inlet velocity profile but also on the turbulence level. The modeling of turbulence with the large pressure gradient existing in the diffuser flows requires a more sophisticated approach than the use of simple eddy viscosity models (Ref. 2).

Currently, the diffuser design information is obtained almost solely from empirical data (Refs. 1 and 3). Many of the available diffuser performance maps and correlations provide only static pressure recovery. Very few detailed turbulence properties of diffuser flows, established experimentally, are available (Refs. 2 and 4) for non-separated cases. Data for separated diffuser flows is even more sparse because conventional instruments, such as the hot wire anemometer, cannot provide meaningful measurement in regions where the flow direction reverses with time. This situation may improve in the future as the recently developed laser velocimeter (LV) becomes more available and reliable (Refs. 5 and 6) so that the flow field data can be obtained for use in the development and verification of analytical prediction methods.

In the past, the flow in a diffuser has been analyzed by assuming that diffuser flow can be approximated by a thin boundary layer adjacent to the wall and an inviscid core in the center of the diffuser. The boundary-layer equation and the inviscid core equation are then solved with or without interaction (Refs. 7, 8, and 9). No rigorous method is available to analyze diffuser flows with a highly nonuniform inlet profile with or without separation (Refs. 10 and 11).

The purpose of the investigation reported herein is to develop numerical prediction methods for the calculation of turbulent, incompressible, separated, subsonic diffuser flows with nonuniform inlet conditions.

The theory development, the turbulence models, the coordinate transformation, and the numerical finite difference solution procedures are presented along with comparison of the results with available experimental data.

2.0 GOVERNING EQUATIONS

2.1 NAVIER-STOKES EQUATIONS AND REYNOLDS STRESSES

The basic equations which describe the motion of laminar or turbulent flow of an incompressible fluid are the Navier-Stokes equations. In turbulent flow, it becomes necessary to use some averaging procedure (or statistical method) to provide useful information about the gross features of the flows which are random in nature. Among the methods available, the time-averaged method has been widely used for constant density non-reacting flows. The resultant equations, as shown by Osborne Reynolds (Ref. 12), can be written in 2-D Cartesian or cylindrical coordinates:

Continuity Equation

$$\frac{\partial}{\partial x}(r^\delta u) + \frac{\partial}{\partial r}(r^\delta v) = 0 \qquad (1)$$

X-Momentum Equation

$$u\frac{\partial u}{\partial x} + v\frac{\partial u}{\partial r} = -\frac{\partial}{\partial x}\left(\frac{p}{\rho}\right) + \left\{2\frac{\partial}{\partial x}\left(\nu\frac{\partial u}{\partial x}\right)\right.$$
$$\left. + \left(\frac{1}{r}\right)^\delta \frac{\partial}{\partial r}\left[\nu r^\delta\left(\frac{\partial v}{\partial x} + \frac{\partial u}{\partial r}\right)\right]\right\} - \left\{\frac{\partial}{\partial x}\left(\overline{u'^2}\right) + \left(\frac{1}{r}\right)^\delta \frac{\partial}{\partial r}\left(r^\delta \overline{u'v'}\right)\right\} \qquad (2)$$

Y-Momentum Equation

$$u\frac{\partial v}{\partial x} + v\frac{\partial v}{\partial r} = -\frac{\partial}{\partial r}\left(\frac{p}{\rho}\right) + \left\{2\frac{\partial}{\partial r}\left(\nu\frac{\partial v}{\partial r}\right)\right.$$
$$\left. + \frac{\partial}{\partial x}\left[\nu\left(\frac{\partial v}{\partial x} + \frac{\partial u}{\partial r}\right)\right] + \frac{2\nu\delta}{r}\left(\frac{\partial v}{\partial r} - \frac{v}{r}\right)\right\} - \left\{\left(\frac{1}{r}\right)^\delta \frac{\partial}{\partial r}\left(r^\delta \overline{v'^2}\right) + \frac{\partial}{\partial x}\left(\overline{u'v'}\right) - \delta\frac{\overline{w'^2}}{r}\right\} \qquad (3)$$

where if $\delta = 0$, r represents y in Cartesian coordinates, and if
$\delta = 1$, r represents the radial coordinate.

In Eqs. (1) through (3), the flow variables (u, v, p, and ρ) are time-averaged quantities. The turbulence quantities, such as $\overline{u'^2}$, $\overline{v'^2}$, $\overline{w'^2}$, and $\overline{u'v'}$ are usually called Reynolds stresses.

2.2 THE EDDY VISCOSITY CONCEPT

The eddy viscosity concept, which relates the Reynolds stresses to the product of the time-averaged velocity gradient and an eddy viscosity, can be attributed to Boussinesq (Ref. 12). With this concept, Reynolds stresses can be defined as

$$\overline{u'^2} = -2\nu_t \frac{\partial u}{\partial x} + \frac{2}{3}k$$

$$\overline{v'^2} = -2\nu_t \frac{\partial v}{\partial r} + \frac{2}{3}k$$

$$\overline{w'^2} = -2\nu_t \frac{v}{r} + \frac{2}{3}k \qquad (4)$$

$$\overline{u'v'} = -\nu_t \left(\frac{\partial u}{\partial r} + \frac{\partial v}{\partial x}\right)$$

$$k \equiv (\overline{u'^2} + \overline{v'^2} + \overline{w'^2})/2$$

where ν_t is the eddy viscosity and k is the turbulent kinetic energy (TKE).

By substituting Eq. (4) into Eqs. (2) and (3), one obtained the momentum equations in the following forms:

$$u\frac{\partial u}{\partial x} + v\frac{\partial u}{\partial r} = -\frac{\partial}{\partial x}\left(\frac{p}{\rho} + \frac{2}{3}k\right) + 2\frac{\partial}{\partial x}\left[(\nu + \nu_t)\frac{\partial u}{\partial x}\right]$$
$$+ \left(\frac{1}{r}\right)^{\delta} \frac{\partial}{\partial r}\left[r^{\delta}(\nu + \nu_t)\left(\frac{\partial v}{\partial x} + \frac{\partial u}{\partial r}\right)\right] \qquad (5)$$

$$u\frac{\partial v}{\partial x} + v\frac{\partial v}{\partial r} = -\frac{\partial}{\partial r}\left(\frac{p}{\rho} + \frac{2}{3}k\right) + \frac{\partial}{\partial x}\left[(\nu + \nu_t)\left(\frac{\partial v}{\partial x} + \frac{\partial u}{\partial r}\right)\right]$$
$$+ 2\frac{\partial}{\partial r}\left[(\nu + \nu_t)\frac{\partial v}{\partial r}\right] + \delta\frac{2}{r}(\nu + \nu_t)\left(\frac{\partial v}{\partial r} - \frac{v}{r}\right) \qquad (6)$$

Equations (5) and (6) are similar in form to the original Navier-Stokes equations if one replaces (p/ρ + 2/3 k) by (p/ρ) and (ν + ν_t) by ν. Thus, methods developed for solving the Navier-Stokes equations can be

11

used to solve Eqs. (5) and (6), which allows both laminar and turbulent flows to be solved within one numerical framework.

2.3 VORTICITY-STREAM FUNCTION FORMULATION

Equations (5) and (6) are coupled nonlinear partial differential equations. It can be seen that the pressure term appears only in the gradient form, i.e., $\partial/\partial x(p/\rho)$ and $\partial/\partial r(p/\rho)$. In most cases, the pressure distribution is unknown. Therefore, it is advantageous to remove the explicit pressure gradient terms from Eqs. (5) and (6). This is done by a cross-differentiation (or a curl operation). The resultant equation written in terms of the vorticity becomes

$$
\left\{\frac{\partial^2\Omega}{\partial x^2}+\frac{\partial^2\Omega}{\partial r^2}\right\} - \frac{1}{(\nu+\nu_t)}\left\{(u-2\frac{\partial\nu_t}{\partial x})\frac{\partial\Omega}{\partial x}+(v-2\frac{\partial\nu_t}{\partial r}-\frac{\delta}{r}(\nu+\nu_t))\frac{\partial\Omega}{\partial r}\right\}
$$
$$
+\frac{1}{(\nu+\nu_t)}\left\{\delta\Omega[\frac{\nu}{r}+\frac{1}{r}\frac{\partial\nu_t}{\partial r}-\frac{(\nu+\nu_t)}{r^2}]+(\frac{\partial^2\nu_t}{\partial x^2}-\frac{\partial^2\nu_t}{\partial r^2})(\frac{\partial v}{\partial x}+\frac{\partial u}{\partial r})\right. \tag{7}
$$
$$
\left.+2(\frac{\partial^2\nu_t}{\partial x\partial r})(\frac{\partial v}{\partial r}-\frac{\partial u}{\partial x})\right\} = 0
$$

where Ω is the vorticity defined as

$$
\Omega \equiv \frac{\partial v}{\partial x} - \frac{\partial u}{\partial r} \tag{8}
$$

The continuity equation (Eq. (1)) must be modified to obtain a solution because it is a first-order differential equation as opposed to the vorticity equation (Eq. (7)), which is a second-order equation. A second-order differential equation can be formulated to replace the continuity equation by introducing a stream function,

$$
u = (\frac{1}{r})^\delta \frac{\partial\psi}{\partial r}
$$
$$
v = -(\frac{1}{r})^\delta \frac{\partial\psi}{\partial x} \tag{9}
$$

The stream function defined in Eq. (9) satisfied continuity Eq. (1) automatically. By combining Eqs. (9) and (8), a single second-order differential equation for the stream function (ψ) is obtained

12

$$\left\{ \frac{\partial^2 \psi}{\partial x^2} + \frac{\partial^2 \psi}{\partial r^2} \right\} - \left(\frac{\delta}{r}\right)\frac{\partial \psi}{\partial r} + r^{\delta}\Omega = 0 \tag{10}$$

Equations (7) and (10) replace Eqs. (5), (6), and (1) to form a "Vorticity-Stream Function" formulation.

2.4 THE PRESSURE EQUATION

Since the pressure term was eliminated in the first stage of the formulation, it needs to be recovered after the Ω and ψ solutions are obtained. Two methods are available, namely: (1) the integration of momentum Eqs. (5) and (6), and (2) the solution of a pressure equation. The first method is straightforward. Since the pressure appeared in the momentum equation in the gradient form, i.e., $\partial/\partial x(p/\rho)$ and $\partial/\partial r(p/\rho)$, one can integrate the momentum equation from a reference point where the pressure is known to provide a continuous distribution along any path, i.e.,

X-Integration

$$P_2 - P_1 = \rho \int_1^2 \left\{ -\left(u\frac{\partial u}{\partial x} + v\frac{\partial u}{\partial r}\right) - \frac{\partial}{\partial x}\left(\frac{2}{3}k\right) \right.$$
$$\left. + 2\frac{\partial}{\partial x}\left[(\nu+\nu_t)\frac{\partial u}{\partial x}\right] + \left(\frac{1}{r}\right)^{\delta}\frac{\partial}{\partial r}\left[r^{\delta}(\nu+\nu_t)\left(\frac{\partial v}{\partial x}+\frac{\partial u}{\partial r}\right)\right] \right\} dx \tag{11}$$

r-Integration

$$P_2 - P_1 = \rho \int_1^2 \left\{ -\left(u\frac{\partial v}{\partial x} + v\frac{\partial v}{\partial r}\right) - \frac{\partial}{\partial r}\left(\frac{2}{3}k\right) \right.$$
$$\left. + 2\frac{\partial}{\partial x}\left[(\nu+\nu_t)\left(\frac{\partial v}{\partial x}+\frac{\partial u}{\partial r}\right)\right] + 2\frac{\partial}{\partial r}\left[(\nu+\nu_t)\frac{\partial v}{\partial r}\right] + 2\frac{\delta}{r}(\nu+\nu_t)\left(\frac{\partial v}{\partial r}-\frac{v}{r}\right) \right\} dr \tag{12}$$

The accuracy of the pressure calculated by Eqs. (11) and (12) generally depends on the numerical integration quadrature in addition to the accuracy of the numerically calculated variables, such as u, v, k, etc. The method is commonly used to evaluate the wall pressure distribution where Eqs. (11) and (12) can be simplified because of the non-slip wall boundary condition, i.e., u = v = 0 at the wall. The approach can also provide an initial pressure distribution to be used as an initial guess in the solution of the pressure equation given below.

The second method requires the solution of a pressure equation which can be derived by a further differentiation (or a gradient operation) of momentum Eqs. (5) and (6),

$$\frac{\partial^2 p}{\partial x^2} + \frac{\partial^2 p}{\partial r^2} + \frac{\xi}{r}\frac{\partial p}{\partial r} = \Omega^2 - u\left\{\frac{\partial \Omega}{\partial r} + \frac{\xi}{r}\Omega\right\} + v\left\{\frac{\partial \Omega}{\partial x}\right\}$$
$$- \left\{\frac{\partial^2}{\partial x^2}\left(\frac{u^2+v^2}{2}\right) + \frac{\partial^2}{\partial r^2}\left(\frac{u^2+v^2}{2}\right) + \frac{\xi}{r}\frac{\partial}{\partial r}\left(\frac{u^2+v^2}{2}\right)\right\} \tag{13}$$

Although Eq. (13) can provide uniquely defined pressure distributions as opposed to the path dependent integration procedure, one needs to solve an additional equation along with the related boundary conditions. Even with the pressure distribution uniquely determined, the accuracy still depends on the numerical method used. However, in contrast to the first method, the error does not accumulate along a particular path of integration.

The pressure equation (Eq. (13)) is a Poisson's equation with source terms appearing on the right-hand side of the equation. In the present analysis, Eq. (13) is solved iteratively by a point iteration method. The specification of the boundary condition for the pressure equation requires special attention and is discussed in detail in Section 6.1.

3.0 MATHEMATICAL MODELS OF TURBULENCE

The concept of the eddy viscosity (ν_t) introduced in the previous section simplified the modeling of the Reynolds stresses. Thus, instead of considering the Reynolds stresses directly, one can work with a single eddy viscosity. The modeling of turbulence, in this case, is directly related to the modeling of the eddy viscosity. Because the eddy viscosity is not a physical property of the fluid, one needs a mathematical relation to calculate it. In general, the models of the eddy viscosity can be divided into three groups depending on the degree of sophistication, namely, (1) constant values, (2) algebraic relations to the mean flow property and (3) differential equation representations of the turbulence properties (Refs. 13 and 14).

3.1 CONSTANT VISCOSITY MODEL

The simplest eddy viscosity model is

$$\nu_t = constant \tag{14}$$

in which the eddy viscosity is given a constant value throughout the flow field. This modeling, although crude, can provide approximate solutions when used in the calculation of certain simple flow problems, such as the far field of a free turbulent round jet. The model is also useful in the early stage of the development of a particular numerical method or procedure because the resultant governing equations are the same as those derived from laminar flows with a constant molecular viscosity. The only difference is that the eddy viscosity is usually several orders of magnitude larger than the molecular viscosity. Without the spatial variation of the eddy viscosity, one can concentrate directly on the stability or the convergence of a particular numerical method used in the analysis.

The vorticity equation (Eq. (7)) in the present vorticity-stream function formulation can be simplified to the following form by using the constant eddy viscosity model:

$$\left\{\frac{\partial^2 \Omega}{\partial x^2} + \frac{\partial^2 \Omega}{\partial r^2}\right\} - \frac{1}{(\nu + \nu_t)}\left\{u\frac{\partial \Omega}{\partial x} + (v - \frac{\delta}{r})\frac{\partial \Omega}{\partial r}\right\} + \frac{1}{(\nu + \nu_t)}\left\{\delta \Omega[\frac{v}{r} - \frac{(\nu + \nu_t)}{r^2}]\right\} = 0 \tag{15}$$

Equations (14), (15), and (10) were used in the calculation of a planar diffuser flow field with a fully developed parabolic entrance velocity profile. The detailed numerical results for separated and non-separated flows, along with an evaluation of convergence characteristics of the numerical method used, are discussed in Section 6.1.

3.2 ALGEBRAIC VISCOSITY MODEL

In the algebraic viscosity model for boundary-layer flows, the eddy viscosity is related to the mean velocity field parameters through an algebraic relationship. There are two types of algebraic models commonly used, namely, a local model and a global model. The former, such as Prandtl's mixing length theory, relates the eddy viscosity to the local velocity gradient. On the other hand, a global model such as

the one proposed by Clauser (Ref. 15) relates the eddy viscosity to the integral quantities such as the displacement thickness of a boundary layer. The Prandtl's mixing length model is

$$\nu_t = \ell^2 \left| \frac{\partial u}{\partial y} \right| \tag{16}$$

where ℓ is the mixing length. In the wall region, the mixing length is given by Van Driest (Ref. 16) as

$$\ell = 0.41 \, y \left[1 - \exp\left(-\frac{y}{26\nu}\sqrt{\frac{\tau_w}{\rho}}\right) \right] \tag{17}$$

where τ_w is the shear stress at the wall.

The Van Driest model has been widely used and modified to include other effects such as the pressure gradient $(\partial p/\partial x)$, wall suction, etc. (Ref. 17). The model has been used to obtain fairly good results for certain boundary-layer flows (Refs. 18 through 21). It is used in the present analysis to calculate the velocity distribution for a fully developed channel flow. The fully developed velocity profile is then used as the inlet condition for a diffuser flow calculation. For fully developed channel flows, the total shear stress can be written as

$$\frac{\tau}{\rho} = (\nu + \nu_t)\frac{\partial u}{\partial y} \tag{18}$$

With the assumption that shear stress is constant near the wall, i.e., $\tau \approx \tau_w$, Eqs. (16), (17), and (18) are used to derive the velocity gradient:

$$\frac{\partial u^+}{\partial y^+} = \Omega^+ = \frac{2}{1 + \sqrt{1 + 4(0.41)^2 \, y^{+2} \left[1 - \exp(-y^+/26)\right]^2}} \tag{19}$$

where

$$\frac{\partial u^+}{\partial y^+} = \Omega^+ = \frac{u \cdot \nu}{y \cdot v^{*2}}$$

and

$$y^+ = \frac{y \cdot v^+}{\nu} \tag{20}$$

From the vorticity distribution, given by Eq. (19), the velocity and the stream function distributions can be easily obtained by numerical integration.

For more complicated turbulent flows, such as those with strong adverse pressure gradients and with separation, Prandtl's mixing length model is not adequate to obtain satisfactory results. Although extensions and modifications of the model are possible, they usually require experience in the turbulence modeling of a particular flow problem. Often, a trial-and-error approach or a numerical optimization procedure is employed to obtain the desired eddy viscosity distribution.

3.3 DIFFERENTIAL EQUATION VISCOSITY MODEL

In the differential equation models, the eddy viscosity (ν_t) is related to the characteristics of the turbulent motion, such as the turbulent kinetic energy, which are obtained by solution of additional differential equations. Two models in this category are commonly used, namely, (1) the Prandtl's one-equation turbulent kinetic energy model and (2) the Prandtl-Kolmogorov two-equation model (Ref. 13).

For the Prandtl's turbulent kinetic energy model, the eddy viscosity is related to the product of a length scale and the square root of the turbulent kinetic energy, i.e.,

$$\nu_t = \ell \cdot \sqrt{k} \qquad (21)$$

where ℓ is a length scale. The turbulent kinetic energy (k) is obtained from a differential equation and the length scale (ℓ) is specified algebraically. For simple turbulent flows, several length scale formula have been proposed (Ref. 13). Unfortunately, the specification of the length scale still requires experience and, more often, a trial-and-error approach. Therefore, the method is not general and cannot be used for complex turbulent flows with ease. Nevertheless, Prandtl's turbulent kinetic energy model contains more information about the turbulent motion than does his mixing length theory.

The TKE equation, which can be derived from the Navier-Stokes equation (Ref. 12), is written as

$$u_i \frac{\partial k}{\partial x_i} = -\frac{\partial}{\partial x_i} \left[-\nu \frac{\partial k}{\partial x_i} + \overline{u_i \left(\frac{u_j' u_j'}{2} + \frac{p'}{\rho} \right)} \right]$$

$$- \overline{u_i' u_j'} \frac{\partial u_i}{\partial x_j} - \nu \overline{\left(\frac{\partial u_i'}{\partial x_j} \frac{\partial u_i'}{\partial x_j} \right)}$$

(22)

where the summation convention has been used.

Equation (22) contains convection, diffusion, and source terms. Because the turbulent kinetic energy is dependent on the history of the turbulence motion, the eddy viscosity model (Eq. (21)) also depends on the history of the turbulence motion. Examples of turbulent flows with a strong history dependent nature are flows with separations, flows with strong adverse pressure gradient, etc.

For the Prandtl-Kolmogorov two-equation model, the length scale (ℓ) is obtained from a transport equation. For high Reynolds number regions of the flow where the molecular viscosity effect is small, the length scale associated with the turbulent kinetic energy dissipation ($\epsilon = (k)^{3/2}/\ell_\epsilon$) is used in Eq. (21) to obtain

$$\nu_t = C_\mu \cdot \frac{k^2}{\epsilon}$$

(23)

where C_μ is assumed to be a constant (0.09) at high Reynolds number. Although additional equations for ϵ and k are needed, the specification of the length scale is completely eliminated which makes the model attractive for the calculation of complex turbulent flows.

3.3.1 High Reynolds Number Two-Equation k-ϵ Model

For high Reynolds number, the governing equations for the turbulent kinetic energy and its dissipation are modeled as (Ref. 22)

k-Equation

$$\left\{ \frac{\partial^2 k}{\partial x^2} + \frac{\partial^2 k}{\partial r^2} \right\} - \frac{1}{\nu_t} \left\{ \left[u - \frac{\partial \nu_t}{\partial x} \right] \frac{\partial k}{\partial x} + \left[v - \frac{\partial \nu_t}{\partial r} - \delta \frac{\nu_t}{r} \right] \frac{\partial k}{\partial r} \right\}$$

$$+ \left\{ 2 \left[\left(\frac{\partial u}{\partial x} \right)^2 + \left(\frac{\partial v}{\partial r} \right)^2 + \delta \left(\frac{v}{r} \right)^2 \right] + \left(\frac{\partial u}{\partial r} + \frac{\partial v}{\partial x} \right)^2 \right\} - \frac{\epsilon}{\nu_t} = 0$$

(24)

ϵ -Equation

$$\left\{\frac{\partial^2 \epsilon}{\partial x^2} + \frac{\partial^2 \epsilon}{\partial r^2}\right\} - \frac{\sigma_\epsilon}{\nu_t}\left\{\left[u - \frac{\partial}{\partial x}(\frac{\nu_t}{\sigma_\epsilon})\right]\frac{\partial \epsilon}{\partial x} + \left[v - \frac{\partial}{\partial r}(\frac{\nu_t}{\sigma_\epsilon}) - \frac{\delta}{r}\frac{\nu_t}{\sigma_\epsilon}\right]\frac{\partial \epsilon}{\partial r}\right\}$$

$$+ C_1 \sigma_\epsilon \frac{\epsilon}{k}\left\{2\left[(\frac{\partial u}{\partial x})^2 + (\frac{\partial v}{\partial r})^2 + \delta(\frac{v}{r})^2\right] + (\frac{\partial u}{\partial r} + \frac{\partial v}{\partial x})^2\right\} - C_2 \frac{\epsilon^2}{k}\frac{\sigma_\epsilon}{\nu_t} = 0 \qquad (25)$$

where

$$C_1 = 1.44 \quad , \quad C_2 = 1.92 \quad \text{and} \quad \sigma_\epsilon = 1.1$$

The value of constants used follows that of Launder (Ref. 22), and ϵ is the so-called isotropic part of the total TKE dissipation.

In deriving Eqs. (24) and (25), it was assumed that the effect of the molecular viscosity is negligible. The assumption is valid in the fully turbulent regions at high Reynolds number where the turbulent eddy viscosity (ν_t) is usually several order of magnitude larger than the molecular viscosity (ν). Inside the viscous wall sublayer, however, the assumption is no longer valid because the molecular viscosity does play a dominant role there. For this reason, a special sublayer formulation is necessary which can be accomplished, for example, by matching the solution from the fully turbulent region to an analytical law of the wall solution. Two types of analytical expressions are commonly used, namely, a logarithmic law of the wall and a power law velocity profile. The former is given as

$$u = v^*\left[2.5 \ln(y v^*/\nu) + 5.5\right] \qquad (26)$$

where y is the distance from the wall and v* is the friction velocity defined as $\sqrt{\tau_w/\rho}$.

In the present study, the high Reynolds number k-ϵ model with the law of the wall matching is used in the calculation of a conical diffuser flow field with a fully developed turbulent pipe flow at the entrance. The results are presented in Section 6.3.

3.3.2 Low Reynolds Number Two-Equation k-ϵ Model

For turbulent separated diffuser flow calculations, the prediction of the point of separation and the reverse flow field in the separated region is of major importance. The high Reynolds number k-ϵ model

19

with the law of the wall matching procedure is not applicable in the separated flow calculation because Eq. (26) becomes singular at the point of separation, i.e., $v^* = \sqrt{\tau_w/\rho} = 0$. In addition the validity of the law of the wall profile (Eq. (26)) in a flow with a strong adverse pressure gradient is also questionable (Refs. 23 and 24). Therefore, it is necessary to include the sublayer in the formulation so that the point of separation can be predicted. In the present analysis, this is accomplished by the use of (1) a low Reynolds number two-equation k-ε model that includes the effect of the molecular viscosity, and (2) a coordinate transformation which stretches the sublayer region to provide many computational grid points in that region.

For low Reynolds number, C_μ in Eq. (23) is redefined in the present study as

$$C_\mu = \frac{A}{3(a + A/b)} \tag{27}$$

where $A = \sqrt{2k}\,y/\nu$, y is measured from the wall, and a and b are constants. The k-equation becomes

$$\left\{\frac{\partial^2 k}{\partial x^2} + \frac{\partial^2 k}{\partial r^2}\right\} - \frac{1}{(\nu + \nu_t)}\left\{\left[u - \frac{\partial \nu_t}{\partial x}\right]\frac{\partial k}{\partial x} + \left[v - \frac{\partial \nu_t}{\partial r} - \delta\frac{(\nu + \nu_t)}{r}\right]\frac{\partial k}{\partial r}\right\}$$
$$+ \frac{\nu_t}{(\nu + \nu_t)}\left\{2\left[\left(\frac{\partial u}{\partial x}\right)^2 + \left(\frac{\partial v}{\partial r}\right)^2 + \left(\frac{v}{r}\right)^2\delta\right] + \left(\frac{\partial u}{\partial r} + \frac{\partial v}{\partial x}\right)^2\right\} \tag{28}$$
$$- \frac{1}{(\nu + \nu_t)}\left\{\varepsilon + 2\nu\frac{k}{y^2}\right\} = 0$$

The last term of Eq. (28) is the total TKE dissipation which consists of the isotropic and the non-isotropic parts of the dissipation. The ε-equation becomes

$$\left\{\frac{\partial^2 \varepsilon}{\partial x^2} + \frac{\partial^2 \varepsilon}{\partial r^2}\right\} - \frac{1}{(\nu + \nu_t/\sigma_\varepsilon)}\left\{\left[u - \frac{\partial}{\partial x}\left(\frac{\nu_t}{\sigma_\varepsilon}\right)\right]\frac{\partial k}{\partial x} + \left[v - \frac{\partial}{\partial r}\left(\frac{\nu_t}{\sigma_\varepsilon}\right) - \frac{\delta}{r}\frac{\nu_t}{\sigma_\varepsilon}\right]\frac{\partial k}{\partial r}\right\}$$
$$+ C_1\frac{\nu_t}{(\nu + \nu_t/\sigma_\varepsilon)}\frac{\varepsilon}{k}\left\{2\left[\left(\frac{\partial u}{\partial x}\right)^2 + \left(\frac{\partial v}{\partial r}\right)^2 + \left(\frac{v}{r}\right)^2\delta\right] + \left(\frac{\partial u}{\partial r} + \frac{\partial v}{\partial x}\right)^2\right\} \tag{29}$$
$$- C_2\frac{1}{(\nu + \nu_t/\sigma_\varepsilon)}\frac{\varepsilon^2}{k} = 0$$

where

$$C_1 = 1.44 \quad , \quad C_2 = 1.92 \left[1 - 0.3 \exp(-R^2) \right] \quad , \quad \sigma_\varepsilon = 1.1 \qquad (30)$$

and

$$R = k^2 / (\nu \varepsilon) \qquad (31)$$

Note that Eqs. (27), (28), and (29) reduce to Eqs. (23), (24), and (25), respectively, when ν is neglected. The low Reynolds number terms in Eqs. (27), (28), and (29) are derived in the following paragraphs.

3.3.2.1 Derivation of the Total Turbulent Kinetic Energy Dissipation at the Wall

The exact expression for the total turbulent kinetic energy dissipation is (Ref. 12):

$$\varepsilon_T = \nu \left\{ 2\left[\overline{\left(\frac{\partial u'}{\partial x}\right)^2} + \overline{\left(\frac{\partial v'}{\partial y}\right)^2} + \overline{\left(\frac{\partial w'}{\partial z}\right)^2} \right] + \overline{\left(\frac{\partial u'}{\partial y} + \frac{\partial v'}{\partial x}\right)^2} + \overline{\left(\frac{\partial v'}{\partial z} + \frac{\partial w'}{\partial y}\right)^2} + \overline{\left(\frac{\partial u'}{\partial z} + \frac{\partial w'}{\partial x}\right)^2} \right\} \qquad (32)$$

At the wall, velocity gradients such as $\partial u'/\partial x$, $\partial u'/\partial z$, $\partial v'/\partial x$, $\partial v'/\partial z$, $\partial w'/\partial x$, and $\partial w'/\partial z$ vanish. In addition, from the continuity equation, $\partial v'/\partial y$ also vanishes. Therefore, the total turbulent kinetic energy dissipation at the wall can be simplified to

$$\varepsilon_{T,w} = \nu \left\{ \overline{\left(\frac{\partial u'}{\partial y}\right)^2} + \overline{\left(\frac{\partial w'}{\partial y}\right)^2} \right\} \qquad (33)$$

Equation (33) can be evaluated at the wall in the following manner:

$$\begin{aligned}
\varepsilon_{T,w} &= \nu \left\{ \overline{\left(\frac{\partial u'}{\partial y}\right)^2} + \overline{\left(\frac{\partial w'}{\partial y}\right)^2} \right\} \\
&\approx \nu \left\{ \overline{\left(\frac{\Delta u'}{\Delta y}\right)^2} + \overline{\left(\frac{\Delta w'}{\Delta y}\right)^2} \right\} \\
&= \nu \left\{ \overline{\left(\frac{u'}{y}\right)^2} + \overline{\left(\frac{w'}{y}\right)^2} \right\}_{y=\Delta y} \\
&= \nu \left\{ (\overline{u'^2} + \overline{w'^2}) / y^2 \right\}_{y=\Delta y}
\end{aligned} \qquad (34)$$

where y is measured from the wall. Equation (34) can also be written in terms of the TKE as

$$\mathcal{E}_{T,W} = \nu \left\{ \frac{2k}{y^2} \right\}_{y=\Delta y} - \nu \left\{ \frac{\overline{v'^2}}{y^2} \right\}_{y=\Delta y} \tag{35}$$

The last term in Eq. (35) is small compared to the first term near the wall and, therefore, may be neglected. The final expression for the total turbulent kinetic energy dissipation at the wall becomes

$$\mathcal{E}_{T,W} = 2\nu \left\{ \frac{k}{y^2} \right\}_{y=\Delta y} \tag{36}$$

This term was ignored in the high Reynolds number formulation of the turbulent kinetic energy equation (Eq. (24)). But, it should be included in the low Reynolds number formulation in regions where the molecular viscosity effect is not negligible. In the high Reynolds number regions, the total TKE dissipation consists of only the isotropic part of the dissipation. The isotropic part decreases rapidly near the wall and vanishes completely at the wall. Since the total TKE dissipation term is needed in the calculation of the low Reynolds number TKE equation not only at the wall but also throughout the viscous sublayer, a formula that represents the non-isotropic part of the turbulent kinetic energy dissipation needs to be developed. In the present study, Eq. (36) is used not only at the wall to represent the TKE dissipation but also throughout the flow field to represent the non-isotropic part of the TKE dissipation. The total TKE dissipation is represented by

$$\mathcal{E}_T = \left\{ \mathcal{E} + 2\nu \frac{k}{y^2} \right\} \tag{37}$$

throughout the flow field. Equation (37) appears as the last term in the low Reynolds number formulation (Eq. (28)).

3.3.2.2 Derivation of the Coefficient (C_μ) for the Low Reynolds Number Model

In order to determine the coefficient (C_μ) from Eq. (23), one needs to have a realistic distribution of ν_t and k^2/ϵ near the wall. Since one of the ultimate goals of the present analysis is the prediction of separated diffuser flows, the eddy viscosity models proposed by Mellon and Herring (Ref. 25), Glusko (Ref. 26), and Alber (Ref. 27) for nearly separated or separated boundary-layer flows are used. These authors represent the eddy viscosity in the sublayer region by

$$\nu_t = \nu \left(\frac{A^2}{a + (A/b)} \right) \tag{38}$$

where A is the characteristic length in the sublayer defined as $\sqrt{2k}\ y/\nu$ and a and b are constants. The total turbulent kinetic energy dissipation is modeled by Mellon and Herring as

$$\mathcal{E}_T = (2k)^{3/2} \Big/ \left[\frac{\nu}{\sqrt{2k}} \frac{A^2}{(1+A/12)} \right] \tag{39}$$

The isotropic part of the TKE dissipation can be obtained from Eqs. (39) and (37) as

$$\mathcal{E} = k^2/(3\nu A) \tag{40}$$

Equation (40) can also be written as

$$\frac{k^2}{\mathcal{E}} = 3\nu A \tag{41}$$

By substituting Eqs. (41) and (38) into Eq. (23), the final expression for the coefficient (C_μ) is

$$C_\mu = \frac{A}{3(a + A/b)} \tag{42}$$

In this study, the value of a is taken to be 1,100, while the value of b is determined by taking the high Reynolds number limit of C_μ, i.e.,

$$C_\mu \Big|_{A \to Large} \approx \frac{b}{3} = 0.09 \tag{43}$$

where the value 0.09 appears to be representative for high Reynolds number flows (Refs. 28 and 29). Thus, the coefficient (b) determined from Eq. (43) is

$$b = 0.27 \tag{44}$$

The function C_μ is plotted in Fig. 1. It should be noted that direct measurement of the dissipation term ϵ is difficult. Thus, the validity of the analytical model expressions can be verified only through the comparison

of the numerically computed and experimentally measurable quantities in turbulent flows.

3.3.3 Discussions on the Present and Launder's Model

There are some basic differences between the present and Launder's model. The approach used by Launder, et al., in determining the coefficient (C_μ) was based on the less general Van Driest form of the mixing length formula (Eq. (17)) which determined the eddy viscosity distribution in a constant shear Couette flow. The eddy viscosity, thus determined, was used on the left-hand side of Eq. (23). The ϵ-equation was then "adjusted and calculated" so that a reasonable turbulent kinetic energy distribution was obtained in the viscous sublayer region. Finally, with k and ϵ determined, Eq. (23) was inverted to provide a preliminary estimate of C_μ. The functional form of C_μ obtained from Eq. (23) was then used to provide the final expression which is given in Table 1.

During the course of the numerical optimization, Launder found that an additional artificial term is needed in the ϵ-equation in order to have a maximum value of the TKE distribution at $y^+ \approx 20$ as indicated by experimental data. The final form of Launder's artificial term is also given in Table 1.

Consider the modeling of the non-isotropic part of TKE dissipation term. From Table 1, it can be seen that both models use the TKE distribution (k). For the purpose of demonstration, a typical TKE distribution in a fully developed channel flow is given in Fig. 2. The turbulent kinetic energy reaches a maximum value near the wall and decreases monotonically toward the wall and the centerline. Since the present dissipation model is directly proportional to the turbulent kinetic energy, it is always positive. The present model provides a non-zero value at the maximum TKE location (y^+_{max}). Because the slope of the TKE distribution vanishes at the peak location, the Launder's model for ($\epsilon_T - \epsilon$) is zero (see Fig. 2). As a result, Launder's model underestimates the energy dissipation in the neighborhood of y^+_{max} which probably affects the solution in such a way that both the TKE and its second derivative cannot reach the experimental value.

With the present model, Eq. (28) becomes

$$\frac{\partial^2 k}{\partial r^2} + \frac{\nu_t}{(\nu + \nu_t)}\left(\frac{\partial u}{\partial r}\right)^2 - \frac{1}{(\nu + \nu_t)}\left\{\epsilon + 2\nu\frac{k}{y^2}\right\} = 0 \qquad (45)$$

24

With the Launder's model, Eq. (28) becomes

$$\frac{\partial^2 k}{\partial r^2} + \frac{\nu_t}{(\nu+\nu_t)}\left(\frac{\partial u}{\partial r}\right)^2 - \frac{1}{(\nu+\nu_t)}\left\{\epsilon\right\} = 0 \qquad (46)$$

The last term of Eq. (46) represents only the isotropic part of the energy dissipation. To overcome this difficulty, Launder created an artificial term (Table 1) in the ϵ-equation so that the magnitude of the isotropic part of TKE dissipation (ϵ) can be increased to a higher level.

4.0 COORDINATE SYSTEMS AND TRANSFORMATIONS

The governing equations introduced in the previous sections must be solved in conjunction with boundary conditions for the particular flow problem of interest. The key to the successful use of a given formulation is strongly a function of the coordinate system used and the numerical method adopted in the calculation. Several types of coordinate systems and transformations may be used depending on the problem to be solved. Since the governing equations and boundary conditions usually are discretized in finite difference form and then solved algebraically on digital computers, important factors, such as the computer storage, the computing time, and the accuracy of the solution, need to be considered in the formulation of a computer program. The size of the computer storage limits the number of discretized variables one can use for a particular flow problem. It also limits the accuracy of the solution because of the finite number of grid points available to describe the flow field. Naturally, the more the grid points the higher the accuracy.

4.1 UNIFORM AND NONUNIFORM SYSTEMS

The simplest way to describe a flow field is to use a uniform coordinate system that has equal spacing in each of its coordinates (see Fig. 3). The advantages are (1) the physical location can be easily identified which eases the interpretation of the solution, and (2) fewer calculations are needed because the grid spacing needs to be calculated only once in a program. In the present study, the uniform system is used in Section 6.1 to calculate the flow field in a diffuser with a parabolic inlet velocity profile. The diffuser geometry used has constant

width inlet and exit sections which fit the coordinate system nicely except at the boundary of the diverging section. The diverging section can be represented by generating the coordinate lines from the diverging section so that grid points lie along the diverging wall (see Fig. 3b). This approach works well when the diverging angle is neither too large nor too small.

When large velocity gradients occur in the flow field, the uniform system is no longer adequate to describe the flow. In that situation, a nonuniform system is necessary. By arranging more grid lines in the region where large velocity gradients occur (Fig. 3c), the accuracy of the solution can be improved. But the approach requires experience on a particular flow problem, and in most cases, the manual arrangement of the coordinates is inevitable. In addition, the accuracy of the result from a nonuniform system is difficult to interpret in terms of grid spacings. Nevertheless, the nonuniform coordinate system is highly flexible in the early stages of program development so that the basic features of the solution can be obtained. This approach was adopted for the calculation of a turbulent separated diffuser flow with an algebraic turbulence model in Section 6.2.

4.2 COORDINATE TRANSFORMATION

4.2.1 Body-Aligned Coordinate Transformation

For diffusers with a small diverging angle, it becomes very difficult to use the nonuniform coordinate system such as the one shown in Fig. 3c. A body-aligned coordinate system is essential for a proper solution in this case, and it also works well for curved walls. The coordinate transformation used in the present analysis is

$$\bar{x} = x \quad , \quad \bar{r} = \frac{r}{S(x)} \tag{47}$$

where $S(x)$ represents the lateral coordinate of the diffuser wall. Equation (47) is a linear stretching function. The corresponding transformation factors are

$$\frac{\partial \bar{x}}{\partial x} = 1 \quad , \quad \frac{\partial \bar{x}}{\partial r} = 0 \quad , \quad \frac{\partial \bar{r}}{\partial r} = \frac{1}{S(x)} \quad , \quad \frac{\partial \bar{r}}{\partial x} = -\bar{r} \frac{S'(x)}{S(x)} \tag{48}$$

where $S'(x)$ represent $dS(x)/dx$. The transformation given by Eq. (47)

transforms a physical domain of a diffuser into a rectangular shape (see Fig. 4). The governing equations developed in the previous sections are transformed into the $\bar{x}$, $\bar{r}$ plane by using the chain rule differentiation,

$$\frac{\partial}{\partial x} = \frac{\partial}{\partial \bar{x}} - \left(\frac{\partial \bar{r}}{\partial x}\right)\frac{\partial}{\partial \bar{r}} \quad , \quad \frac{\partial}{\partial r} = \left(\frac{\partial \bar{r}}{\partial r}\right)\frac{\partial}{\partial \bar{r}} \quad , \quad \frac{\partial^2}{\partial r^2} = \left(\frac{\partial \bar{r}}{\partial r}\right)^2 \frac{\partial^2}{\partial \bar{r}^2}$$

$$\frac{\partial^2}{\partial x^2} = \frac{\partial^2}{\partial \bar{x}^2} - 2\left(\frac{\partial \bar{r}}{\partial x}\right)\frac{\partial^2}{\partial \bar{x} \partial \bar{r}} + \left(\frac{\partial \bar{r}}{\partial x}\right)^2 \frac{\partial^2}{\partial \bar{r}^2} \tag{49}$$

$$\frac{\partial^2}{\partial x \partial r} = \frac{\partial}{\partial \bar{x} \partial \bar{r}}\left(\frac{\partial \bar{r}}{\partial r}\right) - \left(\frac{\partial \bar{r}}{\partial r}\right)\left(\frac{\partial \bar{r}}{\partial x}\right)\frac{\partial^2}{\partial \bar{r}^2}$$

Although the transformed domain shape becomes simple, the number of terms in the governing equations grows. In the present analysis, Eq. (47) is used to transform an 8-deg conical diffuser into a rectangular shape. The computation was then carried out in the transformed domain. The results are presented in Section 6.3.

4.2.2 Coordinate Transformation with a Sublayer Stretching

The existence of a thin sublayer commonly found in the turbulent wall boundary layer makes it very difficult to solve the whole problem in the physical domain with a uniform coordinate system. It becomes necessary to stretch the sublayer region in such a way that the sharp gradient in flow variables can be reasonably resolved. In the present analysis, a composite coordinate transformation is used to provide good resolution throughout the flow field. For a fully developed channel flow velocity profile, the sublayer velocity distribution is a linear function of the distance from the wall, i.e.,

$$u^+ = y^+ \tag{50}$$

where $u^+ = u/v*$ and $y^+ = y\, v*/\nu$. The velocity gradient of the sublayer profile, i.e., $\partial u / \partial y = v*^2/\nu$, provides the basic stretching factor for $\partial \tilde{y} / \partial y$ in the coordinate transformation given by

$$y = \frac{\alpha}{\beta} \tan \beta \tilde{y} \quad , \quad 0 \leqslant y \leqslant y_0 \tag{51}$$

where y is the coordinate measured from the wall with $y = 1$ at the centerline, $\tilde{y}$ is the stretched coordinate, and α, β, and y_0 are parameters

in the transformation. In the core region, the stretching factor $(\partial\tilde{y}/\partial y)$ is gradually changed to unity at the centerline where no stretching is needed because of the low gradients in the velocity profile. The smooth transition is provided by the core transformation function

$$ y = c\tilde{y} + \ln\left[\cosh(\tilde{y} - \tilde{y}_0)\right] + F \, , \quad y_s \le y \le 1.0 \qquad (52) $$

where c and F are parameters in the transformation. By proper matching of the two transformation functions, one can determine the coefficients and thus provide a continuous transformation for the whole flow field. A typical coordinate transformation given by Eqs. (51) and (52) is shown in Fig. 5. The detailed derivation of the parameters used in the transformation is given in Appendix A.

The ability of the coordinate transformation to provide good resolution in the transformed coordinate plane is demonstrated by considering the velocity and the turbulent kinetic energy distributions in a channel flow shown in physical coordinates in Fig. 6a. It can be seen that large gradients of the velocity and turbulent kinetic energy profiles exist near the wall. Poor resolution can be expected in the sublayer region when one attempts to use a uniform coordinate system to describe the profiles. However, when Eqs. (51) and (52) are used to stretch the sublayer and the core region, sharp gradients in velocity profiles diminish as indicated in Fig. 6b. Thus, the detail velocity and turbulent kinetic energy profiles can be adequately described in the transformed coordinates. For this reason, the coordinate transformation plays an important role in obtaining an accurate numerical solution.

4.2.3 A Complete Coordinate Transformation for a Diffuser Flow

Both the body-aligned coordinate transformation and the sublayer stretching are necessary to provide a good spatial resolution throughout a diffuser flow field. The complete coordinate transformation is achieved first by mapping the diffuser shape into a rectangular domain then followed by a sublayer stretching (see Fig. 7). The complete transformation is given as

$$ x = \tilde{x} \qquad (53) $$

In the sublayer region,

$$ r = S(x)\left\{1 - \frac{\alpha}{\beta}\tan\beta\left(\tilde{r}_{max} - \tilde{r}\right)\right\} , \quad \tilde{r}_0 \le \tilde{r} \le \tilde{r}_{max} \qquad (54) $$

In the core region,

$$r = S(x)\left\{1 - \left[C(\tilde{r}_{max} - \tilde{r}) + \ln\left[\cosh(\tilde{r}_o - \tilde{r})\right] + F\right]\right\}, \qquad (55)$$

$$0 \le \tilde{r} \le \tilde{r}_o$$

where r is measured from the centerline, S(x) represents the diffuser wall shape, $\tilde{r}_o$ is the transformed matching location, and $\tilde{r}_{max}$ is the transformed wall shape. The complete transformation factors are:

In the sublayer region from Eq. (54),

$$\frac{\partial \tilde{r}}{\partial r} = \frac{1}{\alpha S(x)} \cos^2\left[\beta(\tilde{r}_{max} - \tilde{r})\right]$$

$$\frac{\partial \tilde{r}}{\partial x} = -\left(\frac{\partial \tilde{r}}{\partial r}\right) S'(x) \frac{r}{S(x)}$$

$$\frac{\partial^2 \tilde{r}}{\partial r^2} = \frac{2\beta}{\alpha S(x)} \left(\frac{\partial \tilde{r}}{\partial r}\right) \cos\left[\beta(\tilde{r}_{max} - \tilde{r})\right] \sin\left[\beta(\tilde{r}_{max} - \tilde{r})\right]$$

$$\frac{\partial^2 \tilde{r}}{\partial x^2} = -\frac{S'(x)}{S(x)}\left(\frac{\partial \tilde{r}}{\partial x}\right) + 2\beta \tan\left[\beta(\tilde{r}_{max} - \tilde{r})\right]\left(\frac{\partial \tilde{r}}{\partial x}\right)^2 \qquad (56)$$

$$- \left(\frac{\partial \tilde{r}}{\partial r}\right)\left\{S''(x)\frac{r}{S(x)} - \left(\frac{S'(x)}{S(x)}\right)^2 r\right\}$$

$$\frac{\partial^2 \tilde{r}}{\partial x \partial r} = \frac{2\beta}{\alpha S(x)} \cos\left[\beta(\tilde{r}_{max} - \tilde{r})\right]\left(\frac{\partial \tilde{r}}{\partial x}\right) \sin\left[\beta(\tilde{r}_{max} - \tilde{r})\right]$$

$$- \frac{S'(x)}{S(x)}\left(\frac{\partial \tilde{r}}{\partial r}\right)$$

In the core region, from Eq. (55),

$$\frac{\partial \tilde{r}}{\partial r} = \frac{1}{S(x)\left[C + \tanh(\tilde{r}_o - \tilde{r})\right]}$$

$$\frac{\partial \tilde{r}}{\partial x} = -S'(x)\frac{r}{S(x)}\left(\frac{\partial \tilde{r}}{\partial r}\right)$$

$$\frac{\partial^2 \tilde{r}}{\partial r^2} = \left(\frac{\partial \tilde{r}}{\partial r}\right)^2 \frac{\operatorname{sech}^2(\tilde{r}_o - \tilde{r})}{\left[C + \tanh(\tilde{r}_o - \tilde{r})\right]} \qquad (57)$$

$$\frac{\partial^2 \tilde{r}}{\partial x \partial r} = \left(\frac{\partial \tilde{r}}{\partial r}\right)\left(\frac{\partial \tilde{r}}{\partial x}\right) \frac{\operatorname{sech}^2(\tilde{r}_o - \tilde{r})}{\left[C + \tanh(\tilde{r}_o - \tilde{r})\right]} - \frac{S'(x)}{S(x)}\left(\frac{\partial \tilde{r}}{\partial r}\right)$$

$$\frac{\partial^2 \tilde{r}}{\partial x^2} = -S'(x)\frac{r}{S(x)}\left(\frac{\partial^2 \tilde{r}}{\partial x \partial r}\right) - \left(\frac{\partial \tilde{r}}{\partial r}\right)\left[S''(x)\frac{r}{S(x)} + \left(\frac{S'(x)}{S(x)}\right)^2 r\right]$$

29

The transformation factors given by Eqs. (56) and (57) will be used in the next section to derive the governing equations in the transformed coordinates. In the present analysis, the coordinate transformation given by Eqs. (53), (54), and (55) was used in the calculation of separated and non-separated diffuser flows. The results are presented in Section 6.4.

5.0 FINITE DIFFERENCE FORMULATION AND NUMERICAL SOLUTION PROCEDURE

The governing equations and the turbulence models presented in the previous sections are a system of coupled non-linear partial differential equations. The system cannot be solved analytically and, therefore, must be solved by numerical methods. The system of equations becomes even more complicated when it is written in the transformed coordinates such as those described in Section 4.2.3. In the present analysis, a standard form of the transformed equations is first derived to represent the common features of the governing equations. A general finite difference formulation is then developed so that stable and convergent solutions can be obtained for a wide range of Reynolds number. The stability limitation associated with the central difference scheme and the accuracy problem inherent to the up-wind difference scheme are avoided by the use of the locally evaluated decay functions in the finite-difference formulation.

5.1 COMPLETE GOVERNING EQUATIONS IN THE TRANSFORMED COORDINATES AND THE STANDARD FORM EQUATION

For the separated or non-separated diffuser flow calculations, the coordinate transformation given by Eqs. (53), (54), and (55) is necessary to provide adequate resolution in both the core and the viscous sublayer region. The vorticity-stream function formulation and the two-equation low Reynolds number turbulence model written in the transformed coordinates are:

Vorticity Equation (Ω):

$$\frac{\partial^2 \Omega}{\partial \tilde{x}^2} + \frac{\partial^2 \Omega}{\partial \tilde{r}^2}\left[\left(\frac{\partial \tilde{r}}{\partial x}\right)^2 + \left(\frac{\partial \tilde{r}}{\partial r}\right)^2\right] - \frac{1}{(\nu + \nu_t)}\left\{u - 2\left[\frac{\partial \nu_t}{\partial \tilde{x}} + \left(\frac{\partial \tilde{r}}{\partial x}\right)\frac{\partial \nu_t}{\partial \tilde{r}}\right]\right\}\frac{\partial \Omega}{\partial \tilde{x}}$$

$$- \frac{1}{(\nu + \nu_t)}\left\{\left[v - 2\left(\frac{\partial \nu_t}{\partial \tilde{r}}\left(\frac{\partial \tilde{r}}{\partial r}\right)\right) - \frac{\delta}{r}(\nu + \nu_t)\right]\left(\frac{\partial \tilde{r}}{\partial r}\right) + \left[u - 2\left(\frac{\partial \nu_t}{\partial \tilde{x}} + \left(\frac{\partial \tilde{r}}{\partial x}\right)\frac{\partial \nu_t}{\partial \tilde{r}}\right)\right]\left(\frac{\partial \tilde{r}}{\partial x}\right)\right.$$

$$\left. - (\nu + \nu_t)\left[\left(\frac{\partial^2 \tilde{r}}{\partial x^2}\right) + \left(\frac{\partial^2 \tilde{r}}{\partial r^2}\right)\right]\right\}\frac{\partial \Omega}{\partial \tilde{r}} + 2\left(\frac{\partial \tilde{r}}{\partial x}\right)\frac{\partial^2 \Omega}{\partial \tilde{x}\partial \tilde{r}} + \delta\left\{\frac{v}{r} + \frac{1}{r}\frac{\partial \nu_t}{\partial \tilde{r}}\left(\frac{\partial \tilde{r}}{\partial r}\right) - \frac{(\nu + \nu_t)}{r^2}\right\}\frac{\Omega}{(\nu + \nu_t)}$$

$$+ \frac{1}{(\nu + \nu_t)}\left\{\frac{\partial^2 \nu_t}{\partial \tilde{x}^2}\left[\frac{\partial u}{\partial \tilde{r}}\left(\frac{\partial \tilde{r}}{\partial r}\right) + \frac{\partial v}{\partial \tilde{x}} + \left(\frac{\partial \tilde{r}}{\partial x}\right)\frac{\partial v}{\partial \tilde{r}}\right] + \frac{\partial^2 \nu_t}{\partial \tilde{r}^2}\left\{\left[\left(\frac{\partial \tilde{r}}{\partial x}\right)^2 - \left(\frac{\partial \tilde{r}}{\partial r}\right)^2\right]\left[\frac{\partial u}{\partial \tilde{r}}\left(\frac{\partial \tilde{r}}{\partial r}\right) + \frac{\partial v}{\partial \tilde{x}}\right.\right.\right. \quad (58)$$

$$+ \left(\frac{\partial \tilde{r}}{\partial x}\right)\frac{\partial v}{\partial \tilde{r}}\right] + 2\left(\frac{\partial \tilde{r}}{\partial r}\right)\left(\frac{\partial \tilde{r}}{\partial x}\right)\left[\frac{\partial v}{\partial \tilde{r}}\left(\frac{\partial \tilde{r}}{\partial r}\right) - \left(\frac{\partial u}{\partial \tilde{x}} + \left(\frac{\partial \tilde{r}}{\partial x}\right)\frac{\partial u}{\partial \tilde{r}}\right)\right]\right\} + \frac{\partial \nu_t}{\partial \tilde{r}}\left\{\left(\frac{\partial^2 \tilde{r}}{\partial x^2} - \frac{\partial^2 \tilde{r}}{\partial r^2}\right)\left[\frac{\partial u}{\partial \tilde{r}}\left(\frac{\partial \tilde{r}}{\partial r}\right)\right.\right.$$

$$+ \frac{\partial v}{\partial \tilde{x}} + \left(\frac{\partial \tilde{r}}{\partial x}\right)\frac{\partial v}{\partial \tilde{r}}\right] + 2\left(\frac{\partial^2 \tilde{r}}{\partial x \partial r}\right)\left[\frac{\partial v}{\partial \tilde{r}}\left(\frac{\partial \tilde{r}}{\partial r}\right) - \left(\frac{\partial u}{\partial \tilde{x}} + \left(\frac{\partial \tilde{r}}{\partial x}\right)\frac{\partial u}{\partial \tilde{r}}\right)\right]\right\} + \frac{\partial^2 \nu_t}{\partial \tilde{x}\partial \tilde{r}}\left\{2\left(\frac{\partial \tilde{r}}{\partial x}\right)\cdot\right.$$

$$\left.\left[\frac{\partial u}{\partial \tilde{r}}\left(\frac{\partial \tilde{r}}{\partial r}\right) + \frac{\partial v}{\partial \tilde{x}} + \left(\frac{\partial \tilde{r}}{\partial x}\right)\frac{\partial v}{\partial \tilde{r}}\right] + 2\left(\frac{\partial \tilde{r}}{\partial r}\right)\left[\frac{\partial v}{\partial \tilde{r}}\left(\frac{\partial \tilde{r}}{\partial r}\right) - \left(\frac{\partial u}{\partial \tilde{x}} + \left(\frac{\partial \tilde{r}}{\partial x}\right)\frac{\partial u}{\partial \tilde{r}}\right)\right]\right\}\right\} = 0$$

Stream Function (ψ):

$$\frac{\partial^2 \psi}{\partial \tilde{x}^2} + \frac{\partial^2 \psi}{\partial \tilde{r}^2}\left[\left(\frac{\partial \tilde{r}}{\partial x}\right)^2 + \left(\frac{\partial \tilde{r}}{\partial r}\right)^2\right] - \frac{\partial \psi}{\partial \tilde{r}}\left[-\frac{\partial^2 \tilde{r}}{\partial x^2} - \frac{\partial^2 \tilde{r}}{\partial r^2}\right] - \frac{\partial \psi}{\partial \tilde{r}}\frac{\delta}{r}\left(\frac{\partial \tilde{r}}{\partial r}\right) + 2\left(\frac{\partial \tilde{r}}{\partial x}\right)\frac{\partial^2 \psi}{\partial \tilde{x}\partial \tilde{r}} + r^\delta \Omega = 0$$

$$(59)$$

Velocity Recovery (u, v):

$$u = \frac{1}{r^\delta}\left(\frac{\partial \tilde{r}}{\partial r}\right)\frac{\partial \psi}{\partial \tilde{r}} \qquad (60)$$

$$v = -\frac{1}{r^\delta}\left[\frac{\partial \psi}{\partial \tilde{x}} + \frac{\partial \psi}{\partial \tilde{r}}\left(\frac{\partial \tilde{r}}{\partial x}\right)\right] \qquad (61)$$

Turbulent Kinetic Energy Equation (k):

$$\frac{\partial^2 k}{\partial \tilde{x}^2} + \frac{\partial^2 k}{\partial \tilde{r}^2}\left[\left(\frac{\partial \tilde{r}}{\partial x}\right)^2 + \left(\frac{\partial \tilde{r}}{\partial r}\right)^2\right] - \frac{1}{(\nu + \nu_t)}\left\{u - \left[\frac{\partial \nu_t}{\partial \tilde{x}} + \left(\frac{\partial \tilde{r}}{\partial x}\right)\frac{\partial \nu_t}{\partial \tilde{r}}\right]\right\}\frac{\partial k}{\partial \tilde{x}}$$

$$- \frac{1}{(\nu + \nu_t)}\left\{\left[v - \frac{\partial \nu_t}{\partial \tilde{r}}\left(\frac{\partial \tilde{r}}{\partial r}\right) - \frac{\delta}{r}(\nu + \nu_t)\right]\left(\frac{\partial \tilde{r}}{\partial r}\right) + \left[u - \left(\frac{\partial \nu_t}{\partial \tilde{x}} + \left(\frac{\partial \tilde{r}}{\partial x}\right)\frac{\partial \nu_t}{\partial \tilde{r}}\right)\right]\left(\frac{\partial \tilde{r}}{\partial x}\right)\right.$$

$$\left. - (\nu + \nu_t)\left[\left(\frac{\partial^2 \tilde{r}}{\partial x^2}\right) + \left(\frac{\partial^2 \tilde{r}}{\partial r^2}\right)\right]\right\}\frac{\partial k}{\partial \tilde{r}} + 2\left(\frac{\partial \tilde{r}}{\partial x}\right)\frac{\partial^2 k}{\partial \tilde{x}\partial \tilde{r}} + \frac{\nu_t}{(\nu + \nu_t)}\left\{2\left\{\left[\frac{\partial u}{\partial \tilde{x}}\right.\right.\right. \qquad (62)$$

$$+ \left(\frac{\partial \tilde{r}}{\partial x}\right)\frac{\partial u}{\partial \tilde{r}}\right]^2 + \left[\frac{\partial v}{\partial \tilde{r}}\left(\frac{\partial \tilde{r}}{\partial r}\right)\right]^2 + \delta\left(\frac{v}{r}\right)^2\right\} + \left[\frac{\partial u}{\partial \tilde{r}}\left(\frac{\partial \tilde{r}}{\partial r}\right) + \frac{\partial v}{\partial \tilde{x}} + \left(\frac{\partial \tilde{r}}{\partial x}\right)\frac{\partial v}{\partial \tilde{r}}\right]^2\right\}$$

$$- \frac{1}{(\nu + \nu_t)}\left\{\frac{C_\mu k}{\nu_t} + \frac{2\nu}{y^2}\right\} \cdot k = 0$$

where y is measured from the wall.

Turbulent Kinetic Energy Dissipation (ϵ):

$$\frac{\partial^2 \epsilon}{\partial \tilde{x}^2} + \frac{\partial^2 \epsilon}{\partial \tilde{r}^2}\left[(\frac{\partial \tilde{r}}{\partial x})^2 + (\frac{\partial \tilde{r}}{\partial r})^2\right] - \frac{1}{(\nu + \nu_t/\sigma_\epsilon)}\left\{ u - \left[\frac{\partial}{\partial \tilde{x}}(\frac{\nu_t}{\sigma_\epsilon}) + (\frac{\partial \tilde{r}}{\partial x})\frac{\partial}{\partial \tilde{r}}(\frac{\nu_t}{\sigma_\epsilon})\right]\right\}\frac{\partial \epsilon}{\partial \tilde{x}}$$

$$- \frac{1}{(\nu + \nu_t/\sigma_\epsilon)}\left\{\left[v - (\frac{\partial \tilde{r}}{\partial r})\frac{\partial}{\partial \tilde{r}}(\frac{\nu_t}{\sigma_\epsilon}) - \frac{5}{r}(\nu + \nu_t/\sigma_\epsilon)\right](\frac{\partial \tilde{r}}{\partial r}) + \left[u - (\frac{\partial}{\partial \tilde{x}}(\frac{\nu_t}{\sigma_\epsilon})\right.\right.$$

$$\left.\left. + (\frac{\partial \tilde{r}}{\partial x})\frac{\partial}{\partial \tilde{r}}(\frac{\nu_t}{\sigma_\epsilon})\right](\frac{\partial \tilde{r}}{\partial x}) - (\nu + \nu_t/\sigma_\epsilon)\left[(\frac{\partial^2 \tilde{r}}{\partial x^2}) + (\frac{\partial^2 \tilde{r}}{\partial r^2})\right]\right\}\frac{\partial \epsilon}{\partial \tilde{r}} + 2(\frac{\partial \tilde{r}}{\partial x})\frac{\partial^2 \epsilon}{\partial \tilde{x} \partial \tilde{r}} \quad (63)$$

$$+ C_1 \frac{C_\mu k}{(\nu + \nu_t/\sigma_\epsilon)}\left\{2\left[(\frac{\partial u}{\partial \tilde{x}} + (\frac{\partial \tilde{r}}{\partial x})\frac{\partial u}{\partial \tilde{r}})^2 + [\frac{\partial v}{\partial \tilde{r}}(\frac{\partial \tilde{r}}{\partial r})]^2 + \delta(\frac{v}{r})^2\right]\right.$$

$$\left. + \left[\frac{\partial u}{\partial \tilde{r}}(\frac{\partial \tilde{r}}{\partial r}) + \frac{\partial v}{\partial \tilde{x}} + (\frac{\partial \tilde{r}}{\partial x})\frac{\partial v}{\partial \tilde{r}}\right]^2\right\} - C_2 \frac{\epsilon^2}{k}\frac{1}{(\nu + \nu_t/\sigma_\epsilon)} = 0$$

The Prandtl-Kolmogorov eddy viscosity formula is

$$\nu_t = C_\mu \frac{k^2}{\epsilon} \quad (64)$$

The coefficients (C_1, C_2, σ_ϵ, and C_μ) are given as

$$C_1 = 1.44 \quad, \quad C_2 = 1.92\left[1 - 0.3\exp(-R^2)\right] \quad, \quad \sigma_\epsilon = 1.1$$

$$C_\mu = A/[3(1100 + A/0.27)] \quad (65)$$

where

$$A = \sqrt{2k}\,\ell/\nu \quad, \quad R = k^2/(\nu\epsilon)$$

The equations are lengthy and complicated, especially, when the transformation factors are calculated from Eqs. (56) and (57). To simplify the analysis, Eqs. (58), (59), (62), and (63) can be cast in a standard form which retains the basic features such as the diffusion, the convection, the production and the dissipation of a flow variable. The standard form derived is

$$\left\{a_1\frac{\partial^2 \phi}{\partial \tilde{x}^2} + a_2\frac{\partial^2 \phi}{\partial \tilde{r}^2}\right\} - \left\{b_1\frac{\partial \phi}{\partial \tilde{x}} + b_2\frac{\partial \phi}{\partial \tilde{r}}\right\} + d = 0 \quad (66)$$

where ϕ represents the flow variables, i.e., Ω, ψ, k, and ϵ. The corresponding coefficients (a_1, a_2, b_1, b_2, and d) are given below for each of the variables, Ω, ψ, k, and ϵ.

Ω-equation:

$$a_1 = 1$$

$$a_2 = \left[\left(\frac{\partial \tilde{r}}{\partial x}\right)^2 + \left(\frac{\partial \tilde{r}}{\partial r}\right)^2\right]$$

$$b_1 = \frac{1}{(\nu + \nu_t)}\left\{u - 2\left[\frac{\partial \nu_t}{\partial \tilde{x}} + \left(\frac{\partial \tilde{r}}{\partial x}\right)\frac{\partial \nu_t}{\partial \tilde{r}}\right]\right\}$$

$$b_2 = \frac{1}{(\nu + \nu_t)}\left\{\left[v - 2\left(\frac{\partial \tilde{r}}{\partial r}\right)\frac{\partial \nu_t}{\partial \tilde{r}} - \frac{\delta}{r}(\nu + \nu_t)\right]\left(\frac{\partial \tilde{r}}{\partial r}\right)\right.$$

$$\left. + \left[u - 2\left(\frac{\partial \nu_t}{\partial \tilde{x}} + \left(\frac{\partial \tilde{r}}{\partial x}\right)\frac{\partial \nu_t}{\partial \tilde{r}}\right)\right]\left(\frac{\partial \tilde{r}}{\partial x}\right) - (\nu + \nu_t)\left[\left(\frac{\partial^2 \tilde{r}}{\partial x^2}\right) + \left(\frac{\partial^2 \tilde{r}}{\partial r^2}\right)\right]\right\}$$

$$d = 2\left(\frac{\partial \tilde{r}}{\partial x}\right)\frac{\partial^2 \Omega}{\partial \tilde{x}\partial \tilde{r}} + \delta\left\{\frac{v}{r} + \frac{1}{r}\left(\frac{\partial \tilde{r}}{\partial r}\right)\frac{\partial \nu_t}{\partial \tilde{r}} - \frac{(\nu + \nu_t)}{r^2}\right\}\frac{\Omega}{(\nu + \nu_t)}$$

$$+ \frac{1}{(\nu + \nu_t)}\left\{\frac{\partial^2 \nu_t}{\partial \tilde{x}^2}\left[\frac{\partial u}{\partial \tilde{r}}\left(\frac{\partial \tilde{r}}{\partial r}\right) + \frac{\partial v}{\partial \tilde{x}} + \left(\frac{\partial \tilde{r}}{\partial x}\right)\frac{\partial v}{\partial \tilde{r}}\right]\right.$$

$$+ \frac{\partial^2 \nu_t}{\partial \tilde{r}^2}\left\{\left[\left(\frac{\partial \tilde{r}}{\partial x}\right)^2 - \left(\frac{\partial \tilde{r}}{\partial r}\right)^2\right]\left[\frac{\partial u}{\partial \tilde{r}}\left(\frac{\partial \tilde{r}}{\partial r}\right) + \frac{\partial v}{\partial \tilde{x}} + \left(\frac{\partial \tilde{r}}{\partial x}\right)\frac{\partial v}{\partial \tilde{r}}\right]\right.$$

$$\left. + 2\left(\frac{\partial \tilde{r}}{\partial r}\right)\left(\frac{\partial \tilde{r}}{\partial x}\right)\left[\frac{\partial v}{\partial \tilde{r}}\left(\frac{\partial \tilde{r}}{\partial r}\right) - \left(\frac{\partial u}{\partial \tilde{x}} + \left(\frac{\partial \tilde{r}}{\partial x}\right)\frac{\partial u}{\partial \tilde{r}}\right)\right]\right\}$$

(67)

$$+ \frac{\partial \nu_t}{\partial \tilde{r}}\left\{\left(\frac{\partial^2 \tilde{r}}{\partial x^2} - \frac{\partial^2 \tilde{r}}{\partial r^2}\right)\left[\frac{\partial u}{\partial \tilde{r}}\left(\frac{\partial \tilde{r}}{\partial r}\right) + \frac{\partial v}{\partial \tilde{x}} + \left(\frac{\partial \tilde{r}}{\partial x}\right)\frac{\partial v}{\partial \tilde{r}}\right]\right.$$

$$\left. + 2\left(\frac{\partial^2 \tilde{r}}{\partial x\partial r}\right)\left[\frac{\partial v}{\partial \tilde{r}}\left(\frac{\partial \tilde{r}}{\partial r}\right) - \left(\frac{\partial u}{\partial \tilde{x}} + \left(\frac{\partial \tilde{r}}{\partial x}\right)\frac{\partial u}{\partial \tilde{r}}\right)\right]\right\}$$

$$+ \frac{\partial^2 \nu_t}{\partial \tilde{x}\partial \tilde{r}}\left\{2\left(\frac{\partial \tilde{r}}{\partial x}\right)\left[\frac{\partial u}{\partial \tilde{r}}\left(\frac{\partial \tilde{r}}{\partial r}\right) + \frac{\partial v}{\partial \tilde{x}} + \left(\frac{\partial \tilde{r}}{\partial x}\right)\frac{\partial v}{\partial \tilde{r}}\right]\right.$$

$$\left.\left. + 2\left(\frac{\partial \tilde{r}}{\partial r}\right)\left[\frac{\partial v}{\partial \tilde{r}}\left(\frac{\partial \tilde{r}}{\partial r}\right) - \left(\frac{\partial u}{\partial \tilde{x}} + \left(\frac{\partial \tilde{r}}{\partial x}\right)\frac{\partial u}{\partial \tilde{r}}\right)\right]\right\}\right\}$$

ψ - equation:

$$a_1 = 1$$

$$a_2 = \left[\left(\frac{\partial \tilde{r}}{\partial x}\right)^2 + \left(\frac{\partial \tilde{r}}{\partial r}\right)^2\right]$$

$$b_1 = 0$$

$$b_2 = -\frac{\partial^2 \tilde{r}}{\partial x^2} - \frac{\partial^2 \tilde{r}}{\partial r^2} - \frac{\delta}{r}\left(\frac{\partial \tilde{r}}{\partial r}\right)$$

$$d = 2\frac{\partial^2 \psi}{\partial \tilde{x}\partial \tilde{r}}\left(\frac{\partial \tilde{r}}{\partial x}\right) + r^\delta \Omega$$

(68)

k-equation:

$$a_1 = 1$$

$$a_2 = \left[\left(\frac{\partial \tilde{r}}{\partial x}\right)^2 + \left(\frac{\partial \tilde{r}}{\partial r}\right)^2 \right]$$

$$b_1 = \left\{ u - \left[\frac{\partial \nu_t}{\partial \tilde{x}} + \left(\frac{\partial \tilde{r}}{\partial x}\right) \frac{\partial \nu_t}{\partial \tilde{r}} \right] \right\} \frac{1}{(\nu + \nu_t)}$$

$$b_2 = \frac{1}{(\nu + \nu_t)} \left\{ \left[v - \left(\frac{\partial \tilde{r}}{\partial r}\right) \frac{\partial \nu_t}{\partial \tilde{r}} - \frac{\delta}{r}(\nu + \nu_t) \right] \left(\frac{\partial \tilde{r}}{\partial r}\right) \right. $$
$$\left. + \left[u - \left(\frac{\partial \nu_t}{\partial \tilde{x}} + \left(\frac{\partial \tilde{r}}{\partial x}\right) \frac{\partial \nu_t}{\partial \tilde{r}} \right) \right]\left(\frac{\partial \tilde{r}}{\partial x}\right) - (\nu + \nu_t)\left[\left(\frac{\partial^2 \tilde{r}}{\partial x^2}\right) + \left(\frac{\partial^2 \tilde{r}}{\partial r^2}\right) \right] \right\} \tag{69}$$

$$d = 2\left(\frac{\partial \tilde{r}}{\partial x}\right) \frac{\partial^2 k}{\partial \tilde{x} \partial \tilde{r}} + \left\{ 2 \left[\left(\frac{\partial u}{\partial \tilde{x}} + \left(\frac{\partial \tilde{r}}{\partial x}\right)\frac{\partial u}{\partial \tilde{r}}\right)^2 + \left[\frac{\partial v}{\partial \tilde{r}}\left(\frac{\partial \tilde{r}}{\partial r}\right)\right]^2 + \delta\left(\frac{v}{r}\right)^2 \right] \right.$$
$$\left. + \left[\frac{\partial u}{\partial \tilde{r}}\left(\frac{\partial \tilde{r}}{\partial r}\right) + \frac{\partial v}{\partial \tilde{x}} + \left(\frac{\partial \tilde{r}}{\partial x}\right)\frac{\partial v}{\partial \tilde{r}} \right]^2 \right\} \frac{\nu_t}{(\nu + \nu_t)} - \frac{1}{(\nu + \nu_t)}\left\{ \frac{C_\mu k}{\nu_t} + \frac{2\nu}{y^2} \right\} k$$

ϵ-equation:

$$a_1 = 1$$

$$a_2 = \left[\left(\frac{\partial \tilde{r}}{\partial x}\right)^2 + \left(\frac{\partial \tilde{r}}{\partial r}\right)^2 \right]$$

$$b_1 = \frac{1}{(\nu + \nu_t/\sigma_\epsilon)} \left\{ u - \left[\frac{\partial}{\partial \tilde{x}}\left(\frac{\nu_t}{\sigma_\epsilon}\right) + \left(\frac{\partial \tilde{r}}{\partial x}\right)\frac{\partial}{\partial \tilde{r}}\left(\frac{\nu_t}{\sigma_\epsilon}\right) \right] \right\}$$

$$b_2 = \frac{1}{(\nu + \nu_t/\sigma_\epsilon)} \left\{ \left[v - \left(\frac{\partial \tilde{r}}{\partial r}\right)\frac{\partial}{\partial \tilde{r}}\left(\frac{\nu_t}{\sigma_\epsilon}\right) - \frac{\delta}{r}(\nu + \nu_t/\sigma_\epsilon) \right]\left(\frac{\partial \tilde{r}}{\partial r}\right) \right.$$
$$+ \left[u - \left(\frac{\partial}{\partial \tilde{x}}\left(\frac{\nu_t}{\sigma_\epsilon}\right) + \left(\frac{\partial \tilde{r}}{\partial x}\right)\frac{\partial}{\partial \tilde{r}}\left(\frac{\nu_t}{\sigma_\epsilon}\right) \right) \right]\left(\frac{\partial \tilde{r}}{\partial x}\right) \tag{70}$$
$$\left. - (\nu + \nu_t/\sigma_\epsilon)\left[\left(\frac{\partial^2 \tilde{r}}{\partial x^2}\right) + \left(\frac{\partial^2 \tilde{r}}{\partial r^2}\right) \right] \right\}$$

$$d = 2\left(\frac{\partial \tilde{r}}{\partial x}\right)\frac{\partial^2 \epsilon}{\partial \tilde{x} \partial \tilde{r}} + C_1 \frac{C_\mu k}{(\nu + \nu_t/\sigma_\epsilon)} \left\{ 2\left[\left(\frac{\partial u}{\partial \tilde{x}} + \left(\frac{\partial \tilde{r}}{\partial x}\right)\frac{\partial u}{\partial \tilde{r}}\right)^2 \right. \right.$$
$$\left. + \left[\frac{\partial v}{\partial \tilde{r}}\left(\frac{\partial \tilde{r}}{\partial r}\right)\right]^2 + \delta\left(\frac{v}{r}\right)^2 \right] + \left[\frac{\partial u}{\partial \tilde{r}}\left(\frac{\partial \tilde{r}}{\partial r}\right) + \frac{\partial v}{\partial \tilde{x}} + \left(\frac{\partial \tilde{r}}{\partial x}\right)\frac{\partial v}{\partial \tilde{r}} \right]^2 \right\}$$
$$- C_2 \frac{\epsilon^2}{k}\frac{1}{(\nu + \nu_t/\sigma_\epsilon)}$$

5.2 A GENERAL FINITE DIFFERENCE FORMULATION WITH DECAY FUNCTIONS

The partial differential equation (Eq. (66)) can be written as

$$L\{\phi\} + d = 0 \tag{71}$$

where L represents a differential operator. Equation (71) written in a conventional finite difference form is

$$L_f\{\phi\} + d_f = e \tag{72}$$

where L_f is a finite-difference operator and e represents the difference

$$e = \left[L_f\{\phi\} + d_f \right] - \left[L\{\phi\} + d \right] \tag{73}$$

In the present approach (Ref. 30), the finite-difference equation is written as

$$L_f\{\phi, G\} + d_f = \gamma \tag{74}$$

where the additional function (G) is named as the "decay function" which is used to minimize the truncation error (γ). The expression for the decay function (G) is derived in Appendix B.

The present finite difference formulation of the standard Eq. (66) is

$$a_1 \left\{ \frac{\phi_{i+1,j} - 2\phi_{i,j} + \phi_{i-1,j}}{\delta \tilde{x}^2} \frac{1}{G_i} - \left(\frac{b_1}{a_1}\right) \frac{\phi_{i+1,j} - \phi_{i-1,j}}{2\delta \tilde{x}} \right\}$$
$$+ a_2 \left\{ \frac{\phi_{i,j+1} - 2\phi_{i,j} + \phi_{i,j-1}}{\delta \tilde{r}^2} \frac{1}{G_j} - \left(\frac{b_2}{a_2}\right) \frac{\phi_{i,j+1} - \phi_{i,j-1}}{2\delta \tilde{r}} \right\} + d_{i,j} = 0 \tag{75}$$

where the decay functions (G_i and G_j) are determined from

$$G_i = \left(\frac{2}{R_i}\right) \left[1 - 2(e^{R_i} - 1) \right] \left(e^{2R_i} - 1 \right)^{-1} \tag{76}$$

35

$$G_j = \left(\frac{2}{R_j}\right)\left[1 - 2\left(e^{R_j} - 1\right)\right]\left(e^{2R_j} - 1\right)^{-1} \tag{77}$$

and the grid Reynolds numbers (R_i and R_j) are defined as

$$R_i \equiv \frac{b_1}{a_1}\delta\tilde{x} \quad , \quad R_j \equiv \frac{b_2}{a_2}\delta\tilde{r} \tag{78}$$

The decay function is shown in Fig. 8. For the conventional central difference scheme, the decay functions (G_i and G_j) are set equal to unity, i.e.,

$$a_1\left\{\frac{\phi_{i+1,j} - 2\phi_{i,j} + \phi_{i-1,j}}{\delta\tilde{x}^2} - \left(\frac{b_1}{a_1}\right)\frac{\phi_{i+1,j} - \phi_{i-1,j}}{2\delta\tilde{x}}\right\}$$
$$+ a_2\left\{\frac{\phi_{i,j+1} - 2\phi_{i,j} + \phi_{i,j-1}}{\delta\tilde{r}^2} - \left(\frac{b_2}{a_2}\right)\frac{\phi_{i,j+1} - \phi_{i,j-1}}{2\delta\tilde{r}}\right\} + d_{i,j} = 0 \tag{79}$$

The well-known stability limitation for Eq. (79) is (Refs. 31 and 32):

$$R_i \equiv \frac{b_1}{a_1}\delta\tilde{x} \leqslant 2 \quad , \quad R_j \equiv \frac{b_2}{a_2}\delta\tilde{r} \leqslant 2 \tag{80}$$

which for the conventional central difference scheme severely limits the grid sizes ($\delta\tilde{x}$ and $\delta\tilde{r}$) when the coefficients (b_1/a_1 and b_2/a_2) are very large. In order to obtain a stable and convergence solution, the total number of grid must be increased when the small grid meshes are needed, which creates computer core storage problems. The stability problem is avoided by using the decay functions given by Eqs. (76) and (77). Equation (75) is written as

$$\left(\frac{a_1}{G_i}\right)\left\{\frac{\phi_{i+1,j} - 2\phi_{i,j} + \phi_{i-1,j}}{\delta\tilde{x}^2} - \left(\frac{b_1}{a_1}G_i\right)\frac{\phi_{i+1,j} - \phi_{i-1,j}}{2\delta\tilde{x}}\right\}$$
$$+ \left(\frac{a_2}{G_j}\right)\left\{\frac{\phi_{i,j+1} - 2\phi_{i,j} + \phi_{i,j-1}}{\delta\tilde{r}^2} - \left(\frac{b_2}{a_2}G_j\right)\frac{\phi_{i,j+1} - \phi_{i,j-1}}{2\delta\tilde{r}}\right\} + d_{i,j} = 0 \tag{81}$$

Equation (81) is similar to Eq. (79) except that the coefficient (a_1 is replaced by a_1/G_i and b_1/a_1 is replaced by $(b_1/a_1)G_i$, etc.

Therefore, the stability limitation (Eq. (80)) can be written as

$$\left(\frac{b_1}{a_1} G_i\right)\delta\tilde{x} \leqslant 2 \quad , \quad \left(\frac{b_2}{a_2} G_j\right)\delta\tilde{r} \leqslant 2 \tag{82}$$

After re-arrangement, Eq. (82) becomes

$$G_i \leqslant \frac{2}{R_i} \quad , \quad G_j \leqslant \frac{2}{R_j} \tag{83}$$

which is the upper bound for G_i and G_j shown in Fig. 8. It can be seen from Fig. 8 that the decay functions (G_j) given by Eq. (77) is lower than the upper bound of the stability limitation. Therefore, there is no stability limitation on the grid size ($\delta\tilde{x}$ or $\delta\tilde{r}$) with the present general finite difference formulation because Eq. (83) is automatically satisfied with G_i, G_j determined from Eqs. (76) and (77). The unconditional stability is achieved because additional analytical information has been incorporated into the derivation of decay functions (G_i and G_j) (Appendix B). This characteristic of the present formulation makes it possible to solve the complicated equations given by Eqs. (66) through (70) and obtain stable convergence solutions.

The calculation of the decay functions (G_i and G_j) can be simplified by the following approximation.

$$\begin{aligned} G &= 1.0 - 0.625\,(R)^2 \quad , \quad |R| \leqslant 2 \\ &= \frac{2}{|R|} - \frac{1}{(R)^2} \quad\quad , \quad |R| > 2 \end{aligned} \tag{84}$$

for both G_i and G_j, and R_i and R_j. The approximation (Eq. (84)) is also shown in Fig. 8.

It is also interesting to examine the high grid Reynolds number limit of the present formulation. When the grid Reynolds number is large, the decay function can be approximated as

$$G \approx \frac{2}{|R|} \tag{85}$$

By using Eq. (85), the finite difference formulation (Eq. (81)) becomes

$$\left(\frac{|R_i|a_1}{2}\right)\left\{\frac{\phi_{i+1,j}-2\phi_{i,j}+\phi_{i-1,j}}{\delta\tilde{x}^2}-\left(\frac{b_1}{a_1}\frac{2}{|R_i|}\right)\frac{\phi_{i+1,j}-\phi_{i-1,j}}{2\delta\tilde{x}}\right\}$$
$$+\left(\frac{|R_j|a_2}{2}\right)\left\{\frac{\phi_{i,j+1}-2\phi_{i,j}+\phi_{i,j-1}}{\delta\tilde{r}^2}-\left(\frac{b_2}{a_2}\frac{2}{|R_j|}\right)\frac{\phi_{i,j+1}-\phi_{i,j-1}}{2\delta\tilde{r}}\right\}+d_{i,j}=0 \quad (86)$$

For $R_i, R_j > 0$ and by using Eq. (78), Eq. (86) can be written as

$$-\left\{b_1\frac{\phi_{i,j}-\phi_{i-1,j}}{\delta\tilde{x}}+b_2\frac{\phi_{i,j}-\phi_{i,j-1}}{\delta\tilde{r}}\right\}+d_{i,j}=0 \quad (87)$$

Equation (87) is the up-wind difference formulation of the high grid Reynolds number inviscid equation:

$$-\left\{b_1\frac{\partial\phi}{\partial\tilde{x}}+b_2\frac{\partial\phi}{\partial\tilde{r}}\right\}+d=0 \quad (88)$$

which may be derived directly from Eq. (66) by neglecting the viscous terms. Note that Eq. (88) is valid outside the boundary layer region. Thus, the present finite difference formulation approaches the conventional central difference scheme at low grid Reynolds number but gradually changes into the up-wind difference scheme as the local grid Reynolds number (R_i, R_j) increases. This transition is provided by the decay functions (G_i and G_j), which are determined through the use of local analytical solutions (Appendix B).

5.3 NUMERICAL SOLUTION PROCEDURE

When the finite difference equation (Eq. (75)) is applied at each grid point for each flow variable, a large system of algebraic equations is formed. The system of equations and the corresponding boundary conditions are solved in the present analysis by a standard Gauss-Seidel point-iteration scheme (Refs. 33 and 34). This approach has several advantages, namely, (1) a relatively small amount of computer storage is required (one location for each variable), (2) the program is easily written, and (3) under- or over-relaxations can be easily incorporated so that the rate of convergence can be optimized.

The general solution procedure is shown in Fig. 9. The iteration procedure begins with an initial guess of the flow field which can be obtained by assuming that the flow profiles are similar to the inlet profiles. The inlet profiles must be specified, as well as the wall geometry and boundary conditions. The flow-field variables and boundary values are updated point-by-point from iteration to iteration until convergence is reached.

6.0 RESULTS AND DISCUSSION

In this section, the techniques which have been developed are applied to the computation of turbulent internal flows. A series of computations is discussed in the order of increasing complexity. First, solutions for planar diffuser flows, with constant eddy viscosity, are described. The solution of a conical diffuser flow, with algebraic eddy viscosity models and a wall matching procedure, is then presented. Because of limitations in the algebraic eddy viscosity models, solutions obtained with the two-equation turbulence model and the wall matching procedure are then presented. Finally, the two-equation turbulence model, along with the numerical technique for computing the wall region, is applied to planar channel and planar diffuser flows.

6.1 SOLUTION FOR A PLANAR DIFFUSER FLOW WITH A CONSTANT EDDY VISCOSITY

The formulation presented in the previous sections was applied to the calculation of flow in the planar diffuser shown in Fig. 10. The complete finite difference formulation with a constant eddy viscosity is given in Appendix C. The exit to inlet area ratio is two, and the diffuser half-angle is 26.5 deg. The nonuniform inlet velocity is represented by a parabolic profile for a fully developed channel flow. The inlet station is placed one inlet channel width ahead of the diverging section so that the upstream influence of the diverging section on the inlet profiles is negligible. A long exit section (8 inlet channel heights) is used in the calculation to provide enough distance for the flow to reach a parallel flow condition, i.e., $\partial/\partial x = 0$. The exit section, although not always existing in diffuser applications, is convenient for computational purposes because a parallel flow boundary condition can be easily incorporated in the program.

Six cases were calculated which correspond to the Reynolds numbers, based on the inlet centerline velocity (U_c), the channel width (h), and ($\nu + \nu_t$) of 6, 60, 120, 600, and 3,000. The variation of the Reynolds number was easily achieved by changing the value of the eddy viscosity. The solutions are also applicable to laminar flows if ($\nu + \nu_t$) is taken to be ν.

The calculated centerline velocity distribution (normalized by the the average inlet velocity ($\bar{U}$) is shown in Fig. 11. At low Reynolds number, the centerline velocity remains at a constant value of 1.5 in the inlet section except in the region near the diverging section. The velocity begins to decrease in this region before the flow enters the diverging section. The upstream effect is related to the elliptic nature of the flow. The disturbance created by the turning of the flow in the diverging section propagates upstream to cause the flow to slow down. The magnitude of the "upstream effect" decreases as the Reynolds number increases. At a Reynolds number of 3,000, the centerline velocity varies only slightly from the inlet to the exit. The physical mechanism of the changing behavior of the flow in the diverging section as a function of Reynolds number can be understood more easily by examining the velocity profiles and streamline patterns given in Figs. 12. At low Reynolds number, the streamline follows the wall smoothly (Fig. 12a). At Re = 60, the flow separates from the wall at x/h ≈ 1.5. In the separated flow region, the reverse flow velocity is very low (Fig. 12b). The point of separation moves upstream toward the inlet corner of the diffuser as the Reynolds number increases (Fig. 12c). It is interesting to note that, once the separation point moves to the upstream corner, the central flow becomes jet-like.

The centerline and the wall static pressure distributions are shown in Figs. 13 and 14, respectively. Direct comparison of the two sets of data shows very little vertical pressure gradient. The linear pressure drop in the constant area inlet section corresponds to fully developed channel flow (Ref. 35). Since the flow near the wall, in general, turns more than the flow near the centerline, the pressure distribution across the diffuser shows a larger nonuniformity at the inlet corner section than at any other section. At low Reynolds number, the pressure rises sharply in the diverging section, but the rise tends to diminish as the Reynolds number increases. For the jet flow cases, Re = 3,000 for example, the pressure remains constant which is typical of completely "stalled" diffuser flows.

To investigate the quality and accuracy of the present numerical formulation, a conventional upwind difference formulation was also

employed in the solution of the planar diffuser problem. The six test cases were calculated by using the upwind difference scheme to 400 iterations. The final residue ratio is well below 1×10^{-7}. The six cases were re-calculated by using the upwind scheme for the 200 iterations, followed by the present formulations to 400 iterations. A typical centerline velocity distribution is shown in Fig. 15. The upwind difference scheme predicts a faster velocity decay than the present method. Typical behavior of the two solution techniques is indicated in Fig. 16 by the history of the centerline velocity convergence at $x/h = 2.0$. The difference between the two solutions becomes most pronounced at $Re = 120$. As would be expected, the difference gradually diminishes with increasing Reynolds number. At low Reynolds numbers, i.e., $Re \rightarrow 0$, the difference between the two schemes also approaches zero because the contribution from the convection terms vanishes and the flow is completely controlled by the diffusion mechanism.

The convergence should be considered in the evaluation of any iteration process. The velocity residue ratio ($\Delta U/U$) is shown in Fig. 17 in terms of the iteration number. The upwind scheme was used for the first 200 iterations. The residue ratio reached a value below 1×10^{-6} in 150 iterations. The change in numerical method to the present scheme with decay functions at the 200th iteration causes the residue ratio to rise. But it decreases rapidly within the next 100 iterations. The solution obtained at the end of 400 iterations is essentially the converged solution. Once the Ω-ψ solution is obtained, the pressure equation (Eq. (13)) is solved iteratively. The rate of convergence of the centerline pressure at $x/h = 2$ is shown in Fig. 18. One possible explanation for the slow rate of convergence compared to that shown in Fig. 17 is that the boundary condition for the pressure equation is of the gradient type which usually requires many iterations for convergence.

6.2 NUMERICAL SOLUTION OF A CONICAL DIFFUSER

The calculations made with a constant viscosity model have been useful to define the nature of the flow-field solutions and to gain experience with the numerical method. However, real turbulent diffuser flows are poorly described by a constant eddy viscosity; in a real flow, the eddy viscosity vanishes as the wall is approached. In this section, algebraic models are used in the calculation of the separated flow in a 23-deg conical diffuser. Two eddy viscosity

models are used, namely the Prandtl's mixing length model and a "convective" model. The region very close to the diffuser wall is analyzed by the use of the law of the wall; therefore, the boundary condition for the numerical solution of the remainder of the flow field is an effective slip velocity distribution along the wall. The slip velocity is related to the local skin friction coefficient by the law of the wall, so one can assume either a skin friction coefficient distribution or a slip velocity distribution.

The geometry of the diffuser and the computational grid are shown in Fig. 19. A nonuniform grid system is used to provide adequate flow definition near the wall. The numerical formulation for a nonuniform grid system does not pose any serious difficulties, except that simple approximations for the decay functions, such as given by Eq. (84), are not readily available. Therefore, the decay functions must be evaluated at every grid point with exponential functions. The derivation of the decay functions for a nonuniform grid system is given in Appendix B.

The mixing length model used in the present analysis is

$$\nu_t = \ell^2 \left| \frac{\partial u}{\partial y} \right|$$

(89)

where $\ell = 0.4\, y$ in the region near the wall and $\ell = 0.09\, \delta$ for the remainder of the flow. The thickness (δ) is an assumed function of x. The wall slip velocity was specified so that separation was fixed at $x/D = 0.619$. Predicted wall and centerline pressure distributions are shown in Fig. 20. The wall pressure drop in the diffuser inlet section is realistic, but the pressure distribution downstream of separation is unrealistic in that the wall pressure reaches a maximum and then decreases. This unrealistic behavior of the pressure distribution is attributed to the eddy viscosity model. The mixing length model, with a rather conventional specification of the length scale distribution, cannot provide an adequate solution for the flow downstream of separation.

More reasonable flow-field solutions can be obtained by specifying a "convective" model, which approximately includes the tendency of the viscosity to be convected along streamlines (Fig. 21). Wall and centerline pressure distributions computed with the convective eddy viscosity model are shown in Fig. 22; the unrealistic peak in the pressure distributions has been eliminated. The predicted distribution of the axial component of velocity is compared with experiment

(Ref. 36) in Fig. 23. A comparison of the predicted and experimental wall pressure distributions is shown in Fig. 24, along with the assumed distribution of the wall slip velocity. The experimental results are reasonably well predicted.

In the results which have been discussed, the wall slip velocity distribution was held constant. The feasibility of relaxing the slip velocity distribution as the flow-field solution is relaxed was investigated. A smooth converged wall slip velocity distribution can indeed be obtained as long as the separation point is specified. And, in principle, one can iterate on the location of the separation point. But in practice, the logarithmic wall region profile becomes singular at the separation point. Perhaps another wall region profile, such as a power law, could be used in the vicinity of separation. But the validity of any assumed profile in the vicinity of separation is questionable. Clearly, an adequate solution requires that the equations of motion for the wall sublayer be solved along with the solution of the remainder of the flow field. A complete numerical solution requires a low Reynolds number turbulence model and coordinate stretching in the sublayer.

The results presented in this section, although not predictions in the true sense of the word, show that accurate flow-field solutions can be obtained if reasonable eddy viscosity and wall slip velocity distributions are assumed. But adequate predictions of the entire flow field requires a turbulence model which takes into consideration that the turbulence is convected by the mean flow field.

6.3 NUMERICAL SOLUTION WITH A HIGH REYNOLDS NUMBER TWO-EQUATION k-ε MODEL AND A WALL MATCHING PROCEDURE

In this section, the two-equation k-ε model is used for the flow outside the wall sublayer, while the wall slip velocity boundary condition is retained. The purpose of this study was to validate the k-ε model for the high Reynolds number portion of the flow.

6.3.1 Numerical Solution for a Fully Developed Channel Flow with a Wall Matching Procedure

The detailed numerical formulation for the channel flow is given in Appendix D. It is commonly known that a region described by the law of the wall exists in a turbulent boundary layer when the Reynolds number is high. The velocity profile is described by the simple

logarithmic law (Eq. (26)). The existence of the "law of the wall region" provides a birdge between the sublayer and the numerically calculated core region. The basic criterion which allows the use of Eq. (26) in the commonly valid region is that both the velocity (u) and the friction velocity (v*) must be continuous at the matching location (y_o). Since Eq. (26) contains two unknowns (u and v*), one of them, v* in this case, must be determined iteratively so that continuous solution can be obtained. The determination of v* requires the additional assumption that the shear stress is constant from the wall to the matching location. The validity of this assumption and its effect on the accuracy will be discussed below.

There are two methods for determining the friction velocity; the direct and the indirect:

In the direct shear stress determination, the friction velocity v* is calculated from

$$v^* = \sqrt{\tau_w/\varsigma} = \sqrt{\tau/\varsigma}\Big|_{y_o} = \sqrt{\nu_t \cdot \frac{\partial u}{\partial y}}\Big|_{y_o} \tag{90}$$

at the matching location ($\dot{y}_o$). The velocity gradient ($\partial u/\partial y$) and the eddy viscosity are determined numerically from the core region solution. This simple and straightforward method, unfortunately, does not provide accurate determination of the friction velocity because both the eddy viscosity (ν_t) and the velocity gradient must be determined iteratively. As a result, the value of the friction velocity (v*) fluctuates from iteration to iteration. Hence, the velocity determined from Eq. (26) does not give a smooth convergent value. The other factor which affects the accuracy of the numerically determined velocity gradient ($\partial u/\partial y$) is the grid size. Coarse grid sizes can have a significant effect on the numerical value of $\partial u/\partial y$ because large velocity gradients normally exist in the matching region. Thus, it is better to replace the direct method with the indirect method.

In the indirect friction velocity calculation, the method uses two grid points in the matching region to determine the correct matching condition for u and v*. First, Eq. (26) is applied to a point at ($y_o + \delta y$) to determine v* iteratively as

$$v^{*(n+1)} = \Big\{ u/[2.5\ln(y \cdot v^*/\nu)+5.5]\Big\}^n_{y=(y_o+\delta y)} \tag{91}$$

where n is the iteration number. With v* determined, the correct velocity at the matching location is calculated from

$$u_o = v^* \left\{ 2.5 \ln \left(y \cdot v^*/\nu \right) + 5.5 \right\}_{y=y_o} , \quad y_o : \text{specified}. \quad (92)$$

This method does not require the evaluation of the eddy viscosity (ν_t) nor the velocity gradient and thus eliminates the unnecessary fluctuation in determining v* and u_o. The method has been successfully employed to obtain convergent solutions for the channel flow and the 8-deg conical diffuser flow described in Section 6.3.2.

In addition to the boundary conditions for u_o and v*, one needs to have boundary values for the turbulent kinetic energy and its dissipation. To determine the turbulent kinetic energy (k) at the matching location, it is usually assumed that the production of the turbulent kinetic energy is balanced with the dissipation, i.e.,

$$\nu_t \cdot \left(\frac{\partial u}{\partial r} \right)^2 = \varepsilon \quad (93)$$

By using Eq. (93) and the Prandtl-Kolmogorov eddy viscosity formula (Eq. (23)), one obtains

$$k = \sqrt{\nu_t^2 \left(\frac{\partial u}{\partial r} \right)^2 / C_\mu} = v^{*2}/\sqrt{C_\mu} \quad (94)$$

Similarly, by combining Eq. (93), the law of the wall (Eq. (26)), and the definition of the shear stress (τ), one can determine ε_o as

$$\varepsilon_o = \nu_t \left(\frac{\partial u}{\partial r} \right)^2 = \left(\frac{\tau}{\rho} \right) \left(\frac{\partial u}{\partial r} \right) = v^{*2} \left(\frac{2.5 \, v^*}{y_o} \right) = \frac{2.5 \, v^{*3}}{y_o} \quad (95)$$

The numerical solution for a fully developed channel flow was obtained with a standard Gauss-Seidel iteration procedure. At the end of each iteration, the boundary condition at the matching location is updated by using Eqs. (91), (92), (94), and (95). The initial guess is provided by the logarithmic law of the wall. The initial viscosity is calculated from the Prandtl's mixing length theory (Eq. (16)). The distribution of the mixing length is obtained from

$$\frac{\ell}{(0.5 \, h)} = 0.14 - 0.08 \left(1 - \frac{r}{0.5 \, h} \right)^2 - 0.06 \left(1 - \frac{r}{0.5 \, h} \right)^4 \quad (96)$$

which is the Nikuradse's formula for pipe flow. The initial turbulent kinetic energy and its dissipation are calculated from

$$k = \nu_t \cdot \left(\frac{\partial u}{\partial y}\right) / \sqrt{C_\mu} \qquad (97)$$

and

$$\varepsilon = C_\mu \frac{k^2}{\nu_t} \qquad (98)$$

The computation was carried out with 51 grid points.

In the iteration procedure, the eddy viscosity was held constant for the first 700 iterations so that the distributions of the turbulent kinetic energy and its dissipation can be brought to a convergent state. The Prandtl-Kolmogorov eddy viscosity model is used thereafter with an under-relaxation factor (η) of 0.1, i.e.,

$$\nu_t^{(n+1)} = (1-\eta)\nu_t^n + \eta \cdot \left(C_\mu \frac{k^2}{\varepsilon}\right)^{(n+1)} \qquad (99)$$

The convergence of the vorticity at the matching location is shown in Fig. 25 for a Reynolds number of 30,533 based on the centerline velocity (U_c) and the half channel width (h). The solution proceeded through 1,200 iterations. The fairly constant value of the vorticity indicates that the solution has reached a steady value. The calculated velocity profile is shown in Fig. 26. Agreement with Laufer's experimental data (Ref. 37) at Re = 30,800 is excellent. The matching location specified in the calculation was y_0 = 0.06. The calculated velocity profile near the wall follows closely the law of the wall. A small deviation from the law of the wall profile occurs near the centerline so that the symmetry condition can be satisfied. The logarithmic law of the wall does not satisfy the symmetry condition.

The calculated turbulent kinetic energy distribution across the channel is shown in Fig. 27. The maximum TKE occurs at the matching location where the profile closely follows the experimental data by Clark (Ref. 38). The present solution slightly overpredicted the turbulent kinetic energy near the centerline. In general, however, the agreement is good.

The calculated shear stress distribution is given in Fig. 28. The profile is fairly linear as it should be for a fully developed

channel flow. For a linear shear stress distribution, the shear stress at the matching location is always lower than that at the wall. The difference can be minimized by making the location closer to the wall. In general, this can be achieved only by increasing the Reynolds number of the flow since the matching location must be outside the sublayer in order to use the law of the wall.

6.3.2 Numerical Solution of an 8-deg Conical Diffuser Flow with a Fully Developed Inlet Velocity Profile

One of the few experimental investigations of diffuser flow field is reported by Okwoubi and Azad (Ref. 39). Velocity distributions were obtained at various stations in an 8-deg conical diffuser. The inlet condition of the experiment is a well-defined fully developed pipe flow profile, which can be easily represented by the present numerical procedure. In the present numerical calculation, the inlet profile is specified through the use of the Van Driest formula. The inlet condition was allowed to relax to the self-consistent fully developed pipe flow profile in the iteration process. A coordinate transformation is necessary to map the diverging section and the tail section into a constant diameter pipe. The calculation is then performed in the transformed plane. The detailed numerical formulation of the governing equations is given in Appendix E. The diffuser geometry is shown in Fig. 29.

The calculated velocity field in the 8-deg conical diffuser is shown in Fig. 30. The development of the velocity profile from that of a fully developed channel flow into a free shear profile is clearly demonstrated in the figure. The change in the turbulent flow behavior can also be seen in Fig. 31 in terms of the turbulent kinetic energy distributions at the inlet and a far downstream station. At the inlet station, the TKE has a maximum value at the core-sublayer matching location near the wall and monotonically decreases to the centerline. On the other hand, the maximum TKE appears in the middle of the diffuser at a far downstream station which is typical of results associated with a free shear profile. In Fig. 32, the turbulent shear stress distribution is also given at the two stations. The linear shear stress distribution at the inlet gradually changes into a sine function profile of a free shear layer at a far downstream station. The location of the maximum shear stress in the diffuser diverging section is shown in Fig. 33. The predicted position of maximum shear stress agrees fairly well with the experimental data of Ref. 39 indicating that the turbulence transport is well modeled in the present numerical solution. In Fig. 34, the centerline velocity

distribution in the diverging section of the diffuser is also shown to agree well with experimental data. The predicted value, in general, is slightly lower than the experimental value, but the experimental data show some scattering especially in the middle of the diffuser. A comparison of the experimental and predicted velocity profile across the diffuser is shown at four stations in Fig. 35. The agreement between the experiment and theory at the inlet and at the $x/D = 5.95$ is excellent. At the intermediate stations, however, the predicted centerline velocity is about 3 percent lower than the data. This discrepancy was probably caused by the wall matching procedure near the wall. The experimental data show that the velocity profile near the wall in the diverging sections is not represented by the logarithmic law of the wall. In the present approach, since the stream function is used, a slight overprediction of the wall slip velocity in the diverging section can be magnified through the $(1/r)$ factor associated with the axisymmetric flow formulation (Appendix E).

Calculations for the 8-deg conical diffuser flow were performed with 41 lateral grid points across the flow, which is considered more than adequate to provide accurate numerical solution. The program developed also can be applied to variable shape 2-D or axisymmetric channel flow problems.

6.4 NUMERICAL SOLUTION WITH A LOW REYNOLDS NUMBER TWO-EQUATION k-ϵ MODEL

The k-ϵ model, along with the wall matching procedure, has been shown to yield reasonable results for flows in which the law of the wall is applicable. However, as pointed out in Section 6.2, the validity of the law of the wall is questionable in the vicinity of the separation point. In order to avoid the problems associated with the law of the wall, the whole flow field including the sublayer region is solved by the finite difference formulation so that the point of separation and the separated flow field can be predicted. The numerical formulation of the whole flow field requires the use of the low Reynolds number version of the k-ϵ model as well as a sublayer coordinate stretching technique.

6.4.1 Numerical Results for a Fully Developed Channel Flow

The numerical formulation of a fully developed channel flow with a low Reynolds number two-equation k-ϵ model requires the sublayer

coordinate stretching to provide adequate resolution through the flow field. The detailed finite difference formulation of a fully developed channel flow is given in Appendix F.

The velocity profiles with Reynolds numbers ($\bar{U}h/\nu$) ranging from 1,700 to 207,000 are shown in Fig. 36. In the sublayer region, all velocity profiles follow the linear velocity distribution, i.e., $U^+ = y^+$. As the Reynolds number increases, the velocity profile gradually approaches the law of the wall in the core region. The velocity profiles in the physical coordinate are presented in Fig. 37. The profile shape changes from near parabolic at the low Reynolds number to a fuller profile at higher Reynolds number. At Reynolds number 1,657, the profile agrees well with experimental data of Patel and Head (Ref. 40). Results at higher Reynolds number also agree well with Laufer's data (Ref. 37).

The turbulent shear stress distribution is given in Fig. 38. At high Reynolds number, the turbulent shear stress distribution approaches the linear profile of the total shear stress because the contribution from the molecular viscosity is small. The maximum turbulent shear stress also appears near the wall. As the Reynolds number decreases, the location of the maximum turbulent shear moves away from the wall and deviates from the linear distribution of the total shear stress because of the significant contribution from the molecular viscosity. The present calculated shear stress distribution at Re = 5,360 agrees well with Eckelmann's experimental data (Ref. 41) at Re = 5,600.

The TKE distribution is given in Fig. 39. The location of the maximum TKE also moves toward the wall as the Reynolds number increases. The numerical result closely follows the experimental data of Clark (Ref. 38) except near the centerline.

The effect of the total number of grid points on the accuracy of the numerical solution is shown in Fig. 40. With only 41 grid points, the calculated total shear stress deviates substantially from the exact solution. On the other hand, the 101-point case is in excellent agreement with the exact solution.

In Fig. 41, the ratio of the centerline velocity and the mean velocity (averaged across the channel) is shown versus the Reynolds number. The value of the velocity ratio ($U_c/\bar{U}$) is directly related to the flatness of the velocity profile. For a uniform velocity profile, $U_c/\bar{U}$ is equal to one. For Reynolds number below 1,000, $U_c/\bar{U}$ is equal to 1.5, which indicates that the velocity profile is parabolic.

The velocity ratio decreases from a value of 1.5 as the Reynolds number increases. The velocity ratio will presumably reach 1.0 asymptotically as the Reynolds number goes to infinity. The skin friction coefficient is presented in Fig. 42. The agreement between the numerical result and the experimental data (Ref. 42) in both Figs. 41 and 42 is very good.

When the low Reynolds number model is used to calculate the eddy viscosity in the numerical iteration, it is necessary to use an under-relaxation factor on ν_t as in Eq. (99) to provide smooth convergence. The effect of the relaxation factor (η) on the solution convergence is shown in Fig. 43. Large oscillations occur when the relaxation factor (η) is greater than 0.05. It was found that the best value of η is the inverse of the number of lateral grid points which in this case is 0.01. When the relaxation factor is greater than 0.01, the sublayer thickness oscillates as the iterations proceed. The oscillation phenomenon becomes more pronounced at high Reynolds numbers. Therefore, the proper selection of the under-relaxation factor for the eddy viscosity associated with the low Reynolds number two-equation model is very important to ensure the smooth convergence of the numerical iteration process.

6.4.2 Numerical Solution of Separated and Non-Separated Diffuser Flow in a Stretched Coordinate System

A series of preliminary calculation was made for a family of planar diffuser flows to illustrate the nature of the solution. The test case selected is a two-dimensional planar diffuser with a 4:1 aspect ratio (Fig. 44) investigated by Reneau, et al., (Ref. 1). The Reynolds number based on the inlet mean velocity ($\tilde{U}_I$) and the height (h_I) is 1.2×10^5. The inlet profile was a fully developed channel flow profile. It was shown that the maximum pressure recovery occurred with a total diffuser angle of 20 deg. This experimental evidence is used to provide limited verification for the present numerical solutions because more detailed experimental data are not available. The coordinate transformations are given in Eqs. (53) through (57), and the set of governing equations is given in Eqs. (66) through (70). Fifty-one lateral grid points are used across the diffuser which includes both the core region and the sublayer region. The number of grid points is considered adequate to provide a qualitative description of the flow field but not necessarily an accurate result. The numerical procedure is given in Fig. 9. In the iteration process, the first 600 iterations are used to determine the flow field at the first three stations so that a fully developed channel flow

profile can be obtained. With the inlet condition known, the next 600 iterations are used to compute the diffuser flow field. The calculated skin friction coefficient is shown in Fig. 45 for six different angles. Based on the skin friction distributions, flow separation does not occur in the first three cases, namely, 2θ = 3.58, 7.15, and 14.25 deg. The point of separation, which appears in the last three cases, moves upstream as the diffuser angle increases. The rise in the skin friction coefficient around the inlet corner (X/h_I = 2.0) is a result of the elliptic nature of the flow, i.e., disturbances propagate upstream from the diverging section. Such behavior cannot be obtained from a conventional boundary-layer formulation in which there is no feedback mechanism. The skin friction coefficient near the exit corner (X/h_I = 6) in the separated region shows some oscillation (Figs. 45e and f), which indicates that the solution is not fully converged. However, the solution is stable upstream of the separation point.

The development of the velocity profile in the diffuser is shown in Fig. 46. As the diffuser angle increases, the fully developed channel flow profile gradually develops into a wake profile near the wall. For the separated profiles, the sublayer is so thin that it looks as if the velocity profile has a discontinuity near the wall. The velocity profile in the sublayer with an enlarged scale is shown in Fig. 47 for 2θ = 34.7 deg. The reverse flow velocity near the wall at X/h_I = 6 is about 14 percent of the local centerline velocity. The predicted turbulent kinetic energy distribution is shown in Fig. 48. The distinctive feature of the turbulent kinetic energy distribution is that the location of the maximum TKE moves away from the wall in the diverging section. In general, the magnitude of the maximum TKE increases as the diffuser diverging angle increases. For 2θ = 34.7 deg, the maximum TKE at X/h_I = 6 is roughly double the maximum inlet value.

Although there are no detailed flow-field data available to verify the predicted flow-field structure, the centerline velocity distribution is an indication of the pressure recovery. In Fig. 49, the centerline velocity distribution is given in terms of the total diffuser angle. The minimum centerline velocity at X/h_I = 6 occurs at 2θ = 20 deg, which corresponds to the experimentally defined optimum diffuser angle by Reneau, et al. (Ref. 1). A comparison between the present fully developed inlet velocity profile and that of curve 5 in Ref. 1 is given in Fig. 50.

To provide some indication of the accuracy of the present solution, the total shear stress distribution at the inlet station is

51

shown in Fig. 51. Although the linearity of the total shear stress is preserved in the core region, the slope of the profile is somewhat lower than the exact analytical solution. The accuracy check is consistent with that given in Fig. 40. Clearly, the number of grid points used in the computation is only marginal. An increase to an 81- or 101-point system should provide excellent result as was found for fully developed channel flow (Section 6.4.1 and Fig. 40).

7.0 CONCLUDING REMARKS

A numerical method has been developed to provide the detailed flow-field structure of two-dimensional, turbulent, imcompressible stalled and non-stalled subsonic diffuser flows with nonuniform inlet conditions. The general formulation is also applicable to a wide variety of incompressible internal flow problems. An important feature of the numerical method is the use of the "decay function" technique, in which local analytical information is used in the finite difference formulation to ensure stability of the solution. A coordinate transformation including sublayer stretching was developed to provide adequate flow definition throughout the whole flow field. Further study of the coordinate transformation could provide optimization of the grid network.

A hierarchy of solutions were obtained, based on turbulent transport models of increasing complexity, i.e., constant viscosity, algebraic, and two-equation models. In general, treatment of the wall layer with a matching procedure, based on the law of the wall, yields fairly good results for non-separated flows, but is unsatisfactory for separated flows. Therefore, a method was developed to compute the whole flow field numerically, including the viscous sublayer. The approach involves coordinate stretching and a low Reynolds number two-equation turbulent model. Predictions of fully developed channel flows, obtained with the sublayer stretching, are in good agreement with experimental results. Predictions of the performance of planar diffusers are also in reasonable agreement with experimental results. However, additional correlation between the numerical method and experiment is needed, particularly for stalled axisymmetric flows. Unfortunately, the currently available data are very limited, particularly for evaluating the quality of the flow structure.

The present numerical analysis should be extended to include compressible and non-adiabatic flows.

REFERENCES

1. Reneau, L. R., Johnston, J. P., and Kline, S. J. "Performance and Design of Straight, Two-Dimensional Diffusers." Journal of Basic Engineering, Transaction of ASME, Series D, March 1967, pp. 141-150.

2. Boldman, D. R. and Newmann, H. E. "Experimental and Analytical Study of a Conically Diffused Flow with a Nearly Separated Boundary Layer." NASA TN D-7486, November 1973.

3. Dolan, F. X. and Runstadler, P. W., Jr. "Pressure Recovery Performance of Conical Diffusers at High Subsonic Mach Numbers." NASA CR-2299, August 1973.

4. Okwuobi, P. A. C. and Azad, R. S. "Turbulence in a Conical Diffuser with Fully Developed Flow at Entry." Journal of Fluid Mechanics, Vol. 57, Part 3, 1973, pp. 603-622.

5. Barnett, D. O. and Giel, T. V., Jr. "Application of a Two-Component Bragg-Diffracted Laser Velocimeter to Turbulence Measurements in a Subsonic Jet." AEDC-TR-76-36 (ADA025355), May 1976.

6. Eckert, E. R. G., Editor. "Minnesota Symposium on Laser Anemometry Proceedings." October 22-24, 1975, Department of Conferences, Continuing Education and Extension, University of Minnesota, January 1976.

7. Bower, W. W. "An Analytical Procedure for the Calculation of Attached and Separated Subsonic Diffuser Flows." AIAA Paper No. 74-1173, AIAA 10th Propulsion Conference, San Diego, California, 1974.

8. Means, J. L., Glance, P. G., and Klassen, H. A. "Analytical Investigation of Conical Diffusers." NASA TM X-2605, August 1972.

9. Harsha, P. T. and Glassman, H. N. "Analysis of Turbulent Unseparated Flow in Subsonic Diffusers." ASME Paper No. 76-GE-26, 1976.

10. Wolf, S. and Johnston, J. P. "Effects of Nonuniform Inlet Velocity Profiles on Flow Regimes and Performance in Two-Dimensional Diffusers." Journal of Basic Engineering, Transactions of ASME, September 1969, pp. 462-474.

11. Anderson, O. L. "Finite-Difference Solution for Turbulent Swirling Compressible Flow in Axisymmetric Ducts with Struts." NASA CR-2365, February 1974.

12. Hinze, J. O. Turbulence. McGraw-Hill Book Company, New York, 1959.

13. Launder, B. E. and Spalding, D. B. Lectures in Mathematical Models of Turbulence. Academic Press, 1972.

14. Harlow, F. H., Editor. "Turbulence Transport Modeling." AIAA Selected Reprint Series, Vol. XIV, 1973.

15. Clauser, F. "The Turbulent Boundary Layer." Advanced Applied Mechanics, Vol. 4, Academic Press, 1956, pp. 1-51.

16. Van Driest, E. R. "On Turbulent Flow near a Wall." Journal of Aeronautical Sciences, Vol. 23, 1956, p. 1007.

17. Launder, B. E. and Priddin, C. H. "A Comparison of Some Proposals for the Mixing Length near a Wall." International Journal of Heat Mass Transfer, Vol. 16, 1973, p. 700.

18. Patankar, S. V. and Spalding, D. B. Heat and Mass Transfer in Boundary Layers. Intertext Books, London, 1970.

19. Cebeci, T. "Behavior of Turbulent Flow near a Porous Wall with Pressure Gradient." AIAA Journal, Vol. 8, No. 12, December 1970, pp. 2152-2156.

20. Cebeci, T. "Calculation of Compressible Turbulent Boundary Layers with Heat and Mass Transfer." AIAA Journal, Vol. 9, No. 6, June 1971, pp. 1091-1098.

21. Adams, J. C., Jr. "Implicit Finite-Difference Analysis of Compressible Laminar, Transitional, and Turbulent Boundary Layers along the Windward Streamline of a Sharp Cone at Incidence." AEDC-TR-71-235 (AD734535), December 1971.

22. Launder, B. E. "Prediction Methods for Turbulent Flows." VKI Lecture Series 76, von Karmann Institute for Fluid Dynamics, 1975.

23. Mellor, George. "The Effects of Pressure Gradients on Turbulent Flow near a Smooth Wall." Journal of Fluid Mechanics, Vol. 24, Part 2, 1966, p. 255.

24. Szablewski, W. "New Approach to the Calculation of Incompressible Turbulent Boundary Layers." Translated from I2V.AN SSSR. Mekhanika Zhidkostic Gaza. Vol. 5, No. 2, 1970, p. 121.

25. Mellor, George L. and Herring, H. James. "Two Methods of Calculating Turbulent Boundary Layer Behavior Based on Numerical Solutions of the Equation of Motion." Proceedings Computation of Turbulent Boundary Layer-1968, AFOSR-IFP-Stanford Conference, Vol. I, Stanford University 1969, p. 331.

26. Glushko, G. S. "Turbulent Boundary Layer on a Flat Plate in an Incompressible Fluid." NASA TT F-10, 080, Translation from Izvestiya Akademii Nauk SSSR, Seriya Mekhanika, No. 4, 13.

27. Alber, Irwin E. "Similar Solutions for a Family of Separated Turbulent Boundary Layers." AIAA Paper No. 71-203, AIAA 9th Aerospace Sciences Meeting, 1971.

28. Jones, W. P. and Launder, B. E. "The Prediction of Laminarization with a Two-Equation Model of Turbulence." International Journal of Heat Mass Transfer, Vol. 15, 1972, p. 301.

29. Jones, W. P. and Launder, B. E. "The Calculation of Low-Reynolds Number Phenomena with a Two-Equation Model of Turbulent." International Journal of Heat Mass Transfer, Vol. 16, 1973, p. 1119.

30. Chien, J. C. "A General Finite-Difference Formulation with Application to Navier-Stokes Equations." Journal of Computational Physics, Vol. 20, No. 3, March 1976.

31. Hirt, C. W. "Heuristic Stability Theory for Finite-Difference Equations." Journal of Computational Physics, Vol. 2, 1968, p. 339.

32. Roache, Patrick J. "Computational Fluid Dynamics." Hermosa, 1972.

33. Smith, G. D. Numerical Solution of Partial Differential Equations. Oxford University Press, 1965, p. 147.

34. Forsythe, George E. and Wasow, Wolfgang R. Finite-Difference Methods for Partial Differential Equations. John Wiley & Sons, Inc. 1960, p. 236.

35. Schlichting, H. Boundary Layer Theory. Fourth Edition, McGraw Hill Book Co. 1960.

36. Little, B. H. and Wilbur, S. W. "Performance and Boundary-Layer Data from 12 deg and 23 deg Conical Diffusers of Area Ratio 2.0 at Mach Numbers up to Choking and Reynolds Numbers up to 7.5×10^6." NACA Report No. 1201, 1954.

37. Laufer, J. "Investigation of Turbulent Flow in a Two-Dimensional Channel." NACA Report No. 1053, 1951.

38. Clark, J. A. "A Study of Incompressible Turbulent Boundary Layers in Channel Flow." Journal of Basic Engineering, Transaction of ASME, December 1968, pp. 455-468.

39. Okwuobi, P. A. C. and Azad, R. S. "Turbulence in a Conical Diffuser with Fully Developed Flow at Entry." Journal of Fluid Mechanics, Vol. 57, Part 3, 1973, pp. 603-622.

40. Patel, V. C. and Head, M. R. "Some Observations of Skin Friction and Velocity Profiles in Fully Developed Pipe and Channel Flows." Journal of Fluid Mechanics, Vol. 38, 1969, p. 181.

41. Eckelman, H. "The Structure of the Viscous Sublayer and the Adjacent Wall Region in a Turbulent Channel Flow." <u>Journal of Fluid Mechanics</u>, Vol. 65, Part 3, 1974, pp. 439-459.

42. Dean, R. B. "Reynolds Number Dependence of Skin Friction in Two-Dimensional Rectangular Duct Flow and a Discussion of the 'Law of the Wake'." IC Aero Report 74-11, Imperial College of Science and Technology, London, England, December 1974.

$$C_\mu = \frac{A}{3(a + A/b)}$$

$$a = 1,100, \quad b = 0.27$$

$$A = \sqrt{2k}\ y/\nu \times 10^4$$
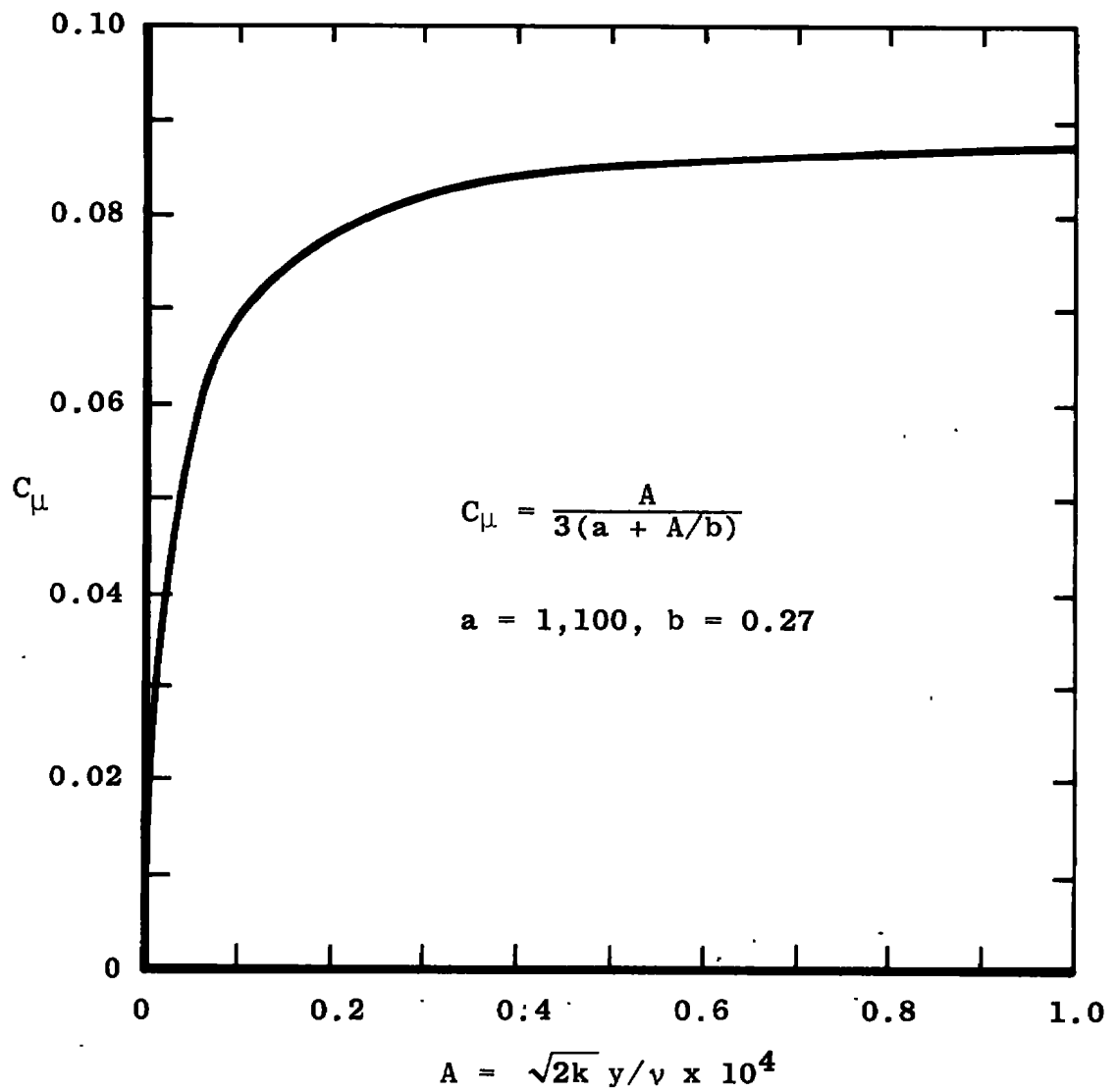
Figure 1. The coefficient (C_μ).
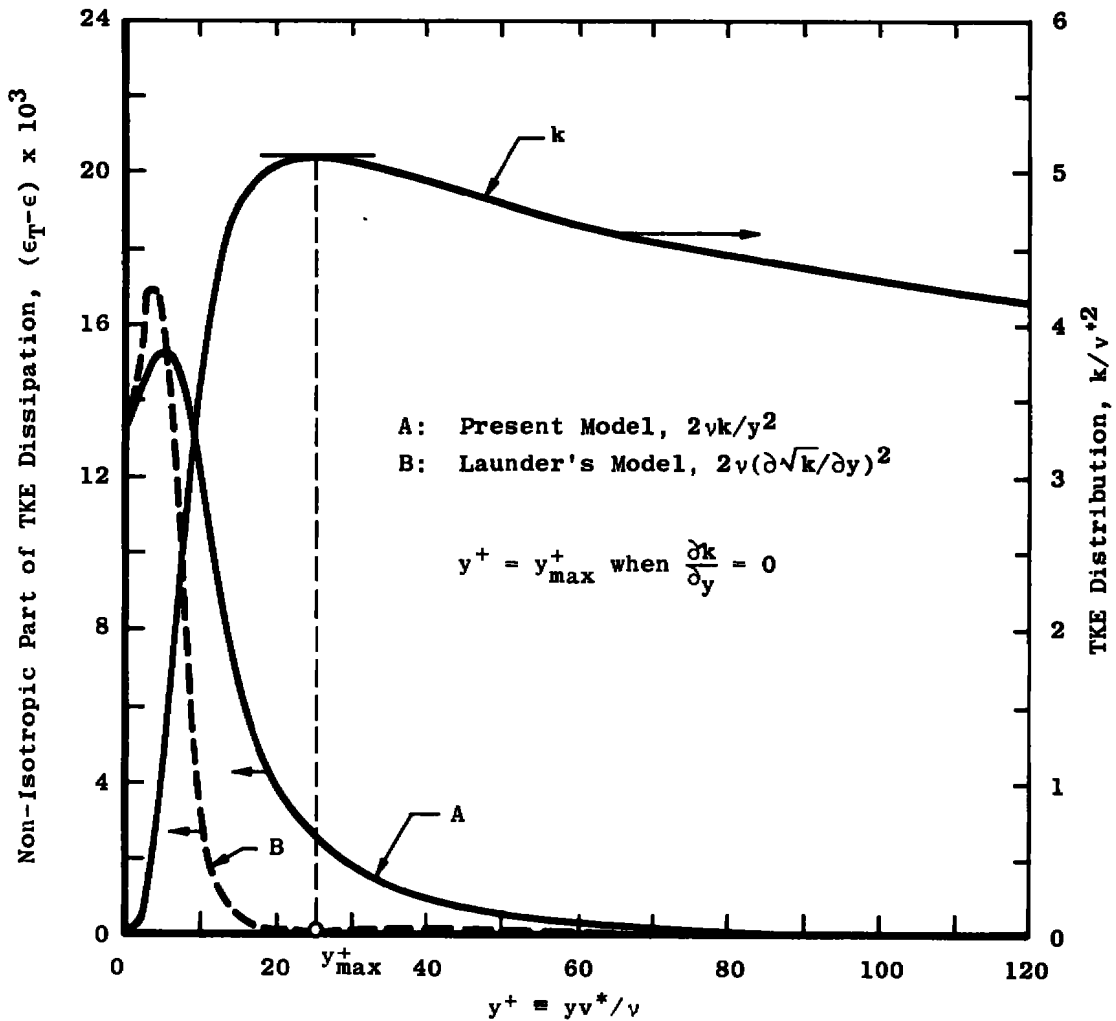
Figure 2. Turbulent kinetic energy distribution and models for the nonisotropic part of turbulent kinetic energy dissipation near a wall.
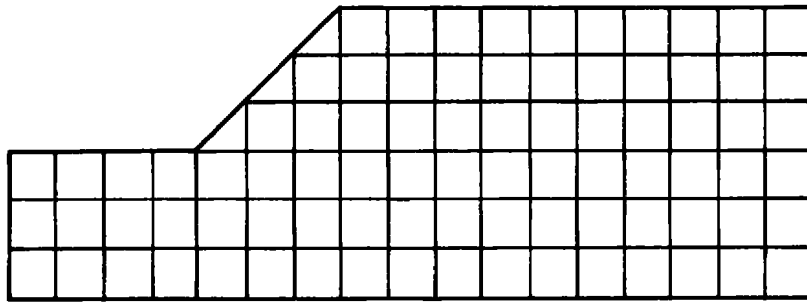
a. Uniform system, equal spacing
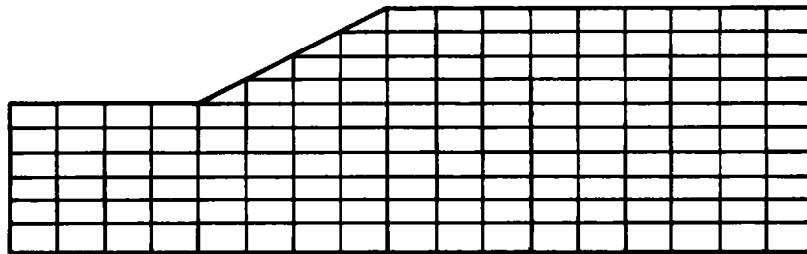
b. Uniform system, unequal spacing
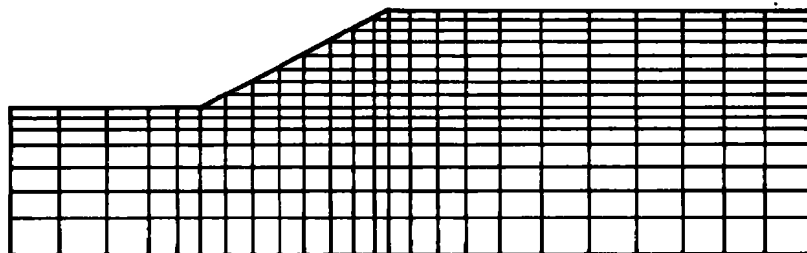
c. Nonuniform system

Figure 3. Uniform and nonuniform coordinate systems.

AEDC-TR-76-159
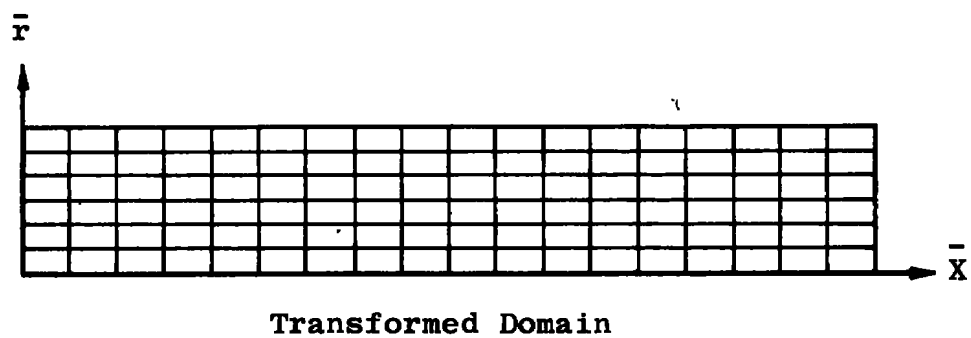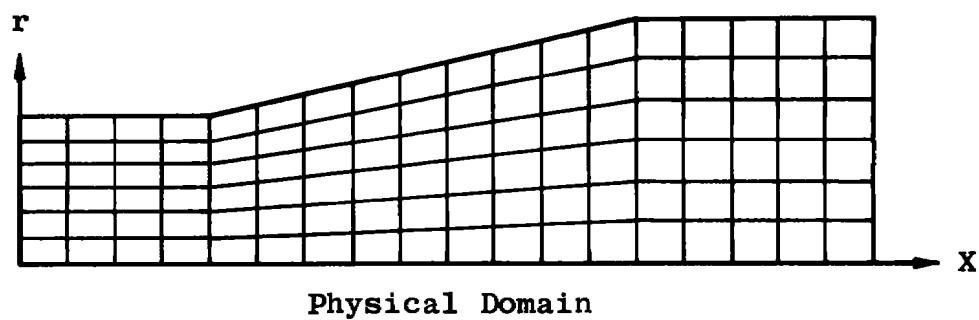
Figure 4. Body-aligned coordinate transformation.

62
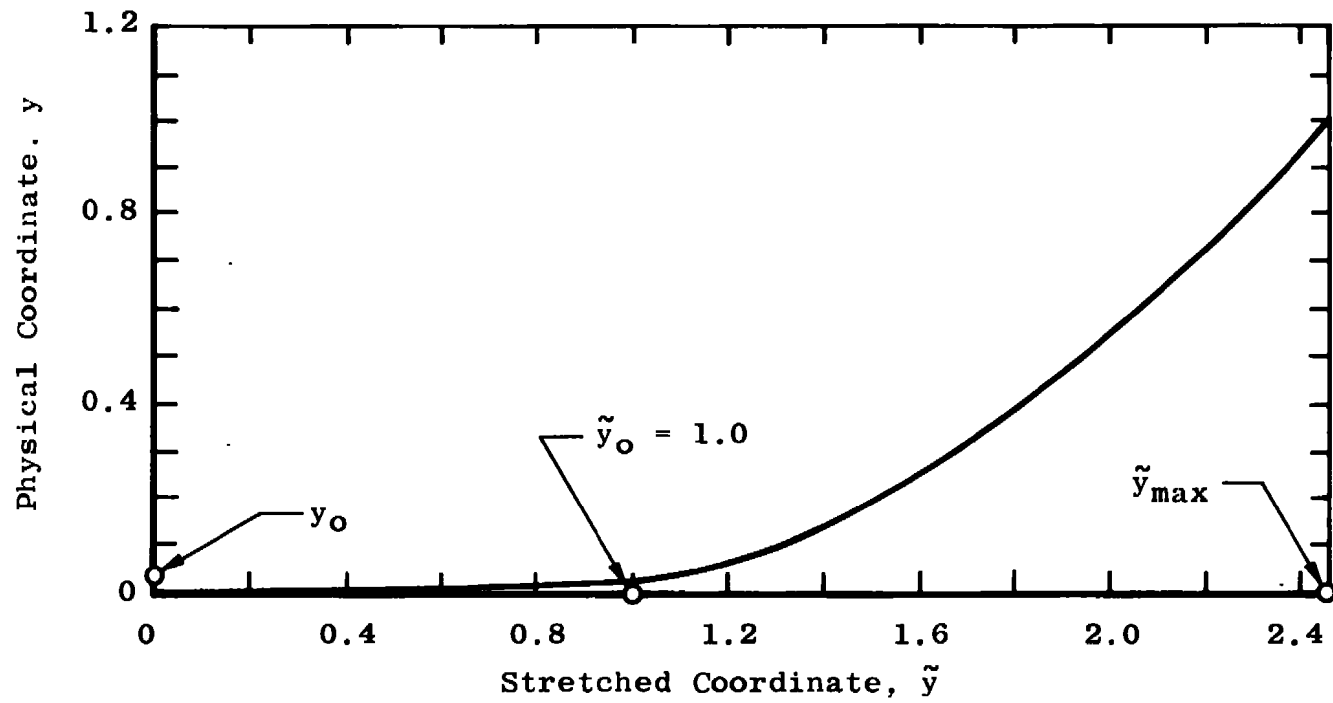
Figure 5. Coordinate transformation with a sublayer stretching.
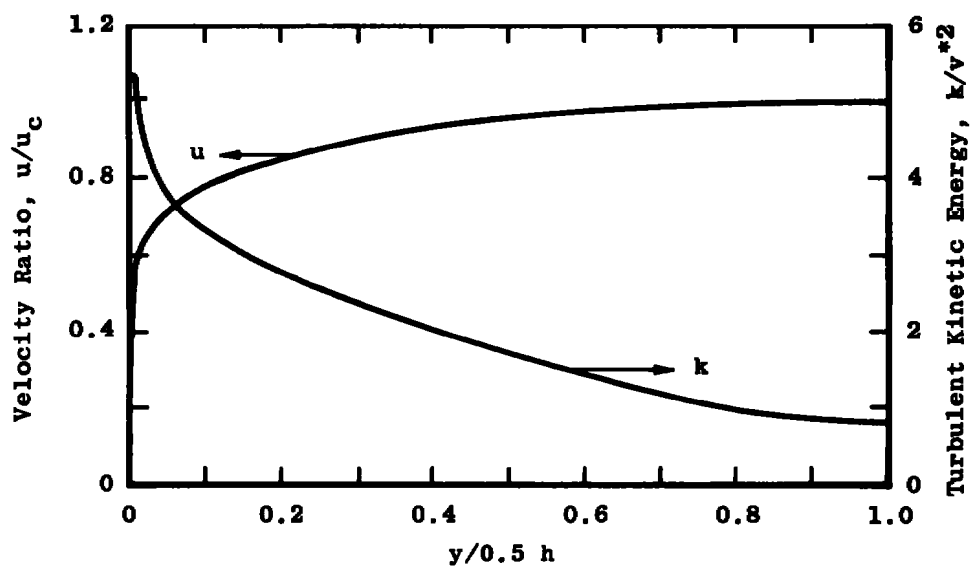
a. Physical coordinates
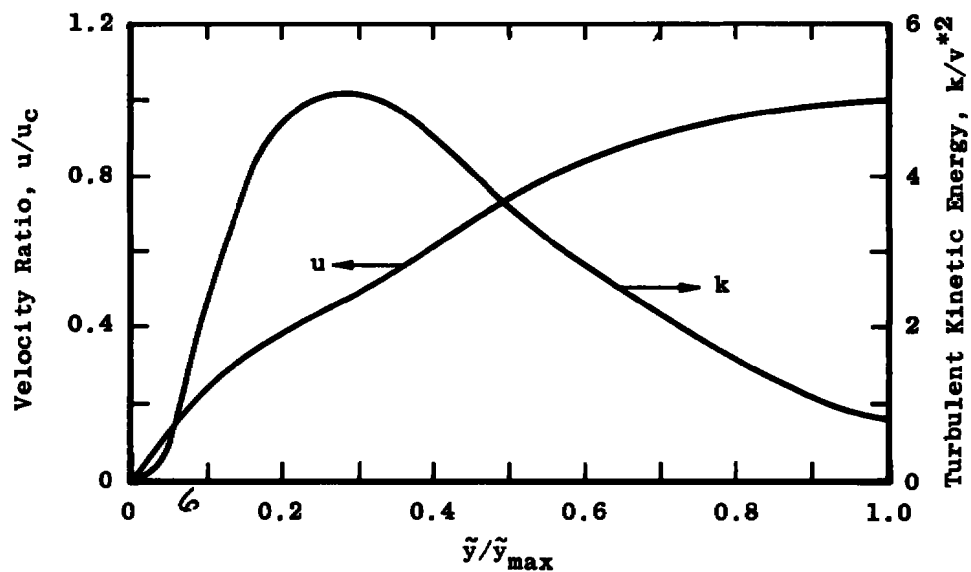
b. Transformed coordinates
with sublayer stretching

Figure 6. Velocity and turbulent kinetic energy profiles
in physical and transformed coordinates.
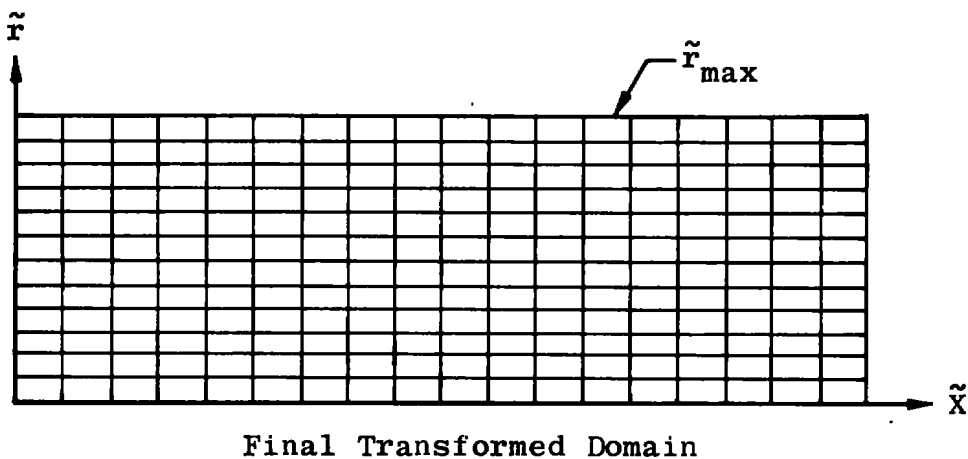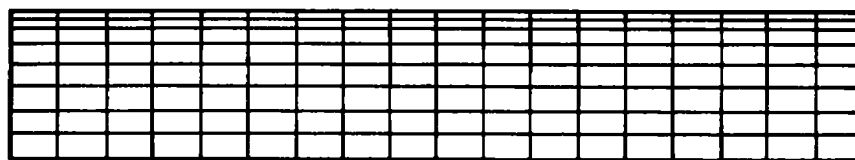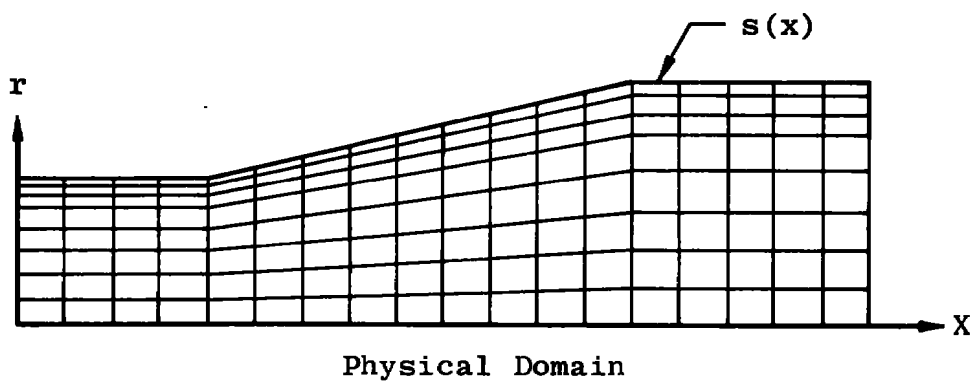
Figure 7. A complete transformation for a diffuser.
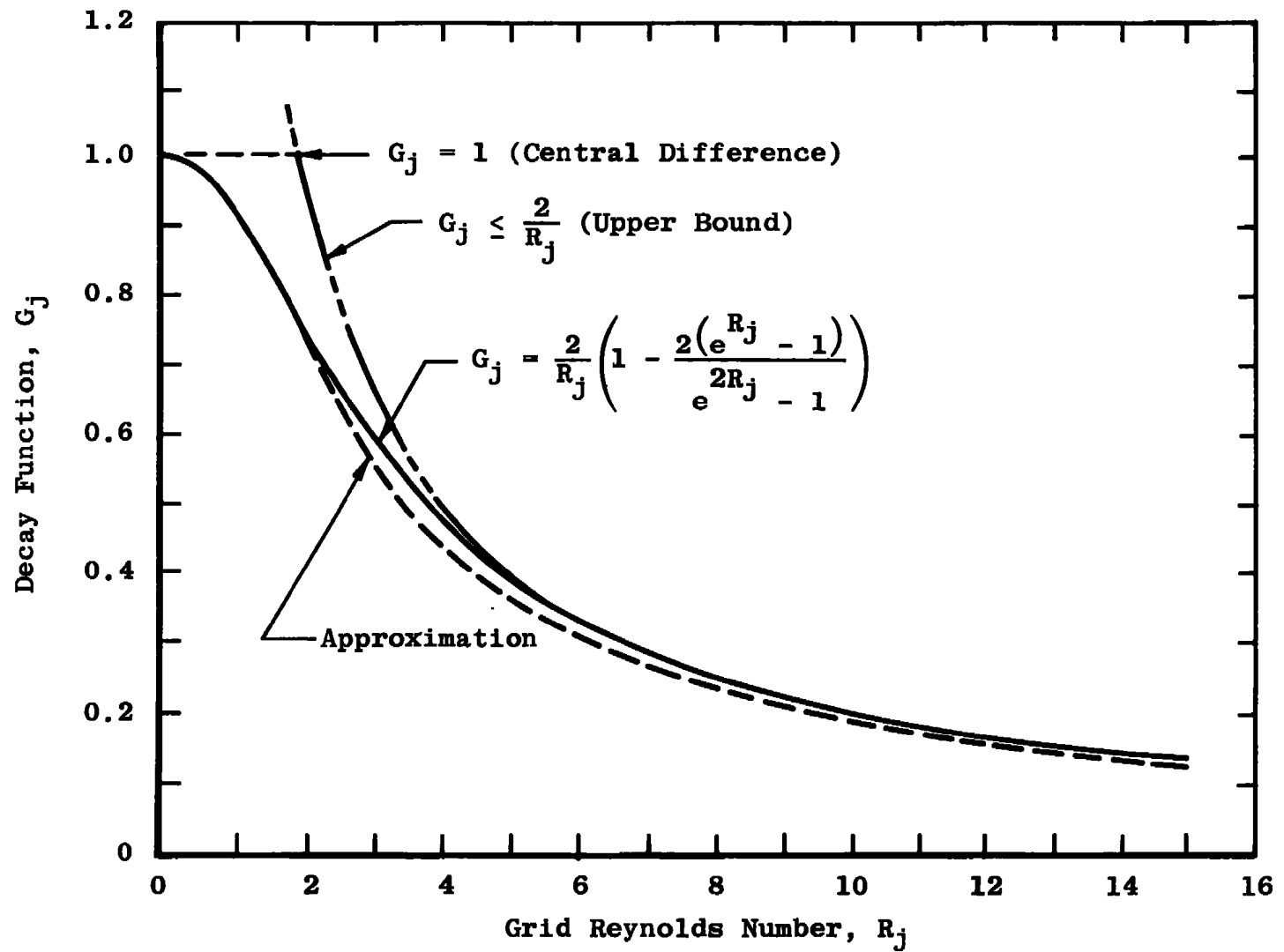
Figure 8. Decay function.
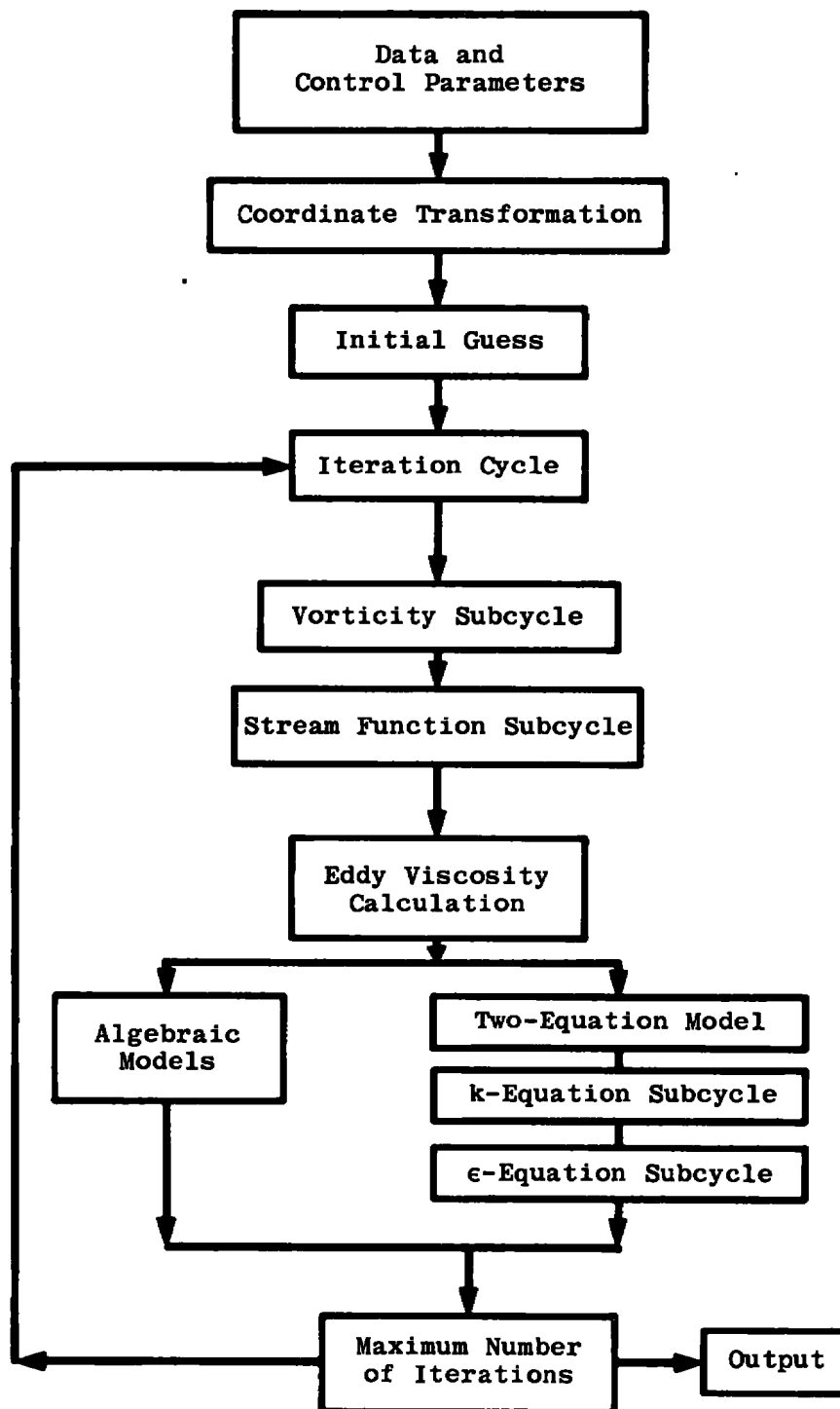
Figure 9. Flow chart of the numerical solution procedure.
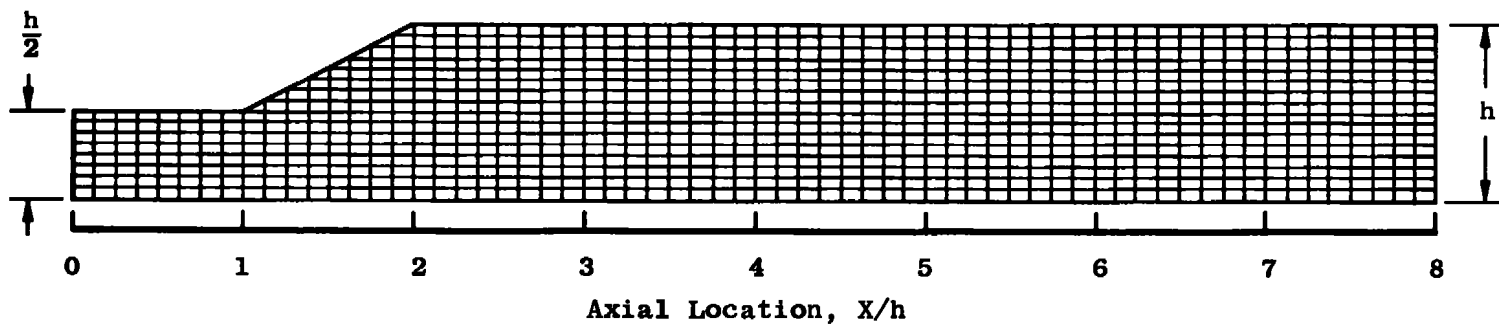
Figure 10. Two-dimensional planar diffuser and computational grid system.
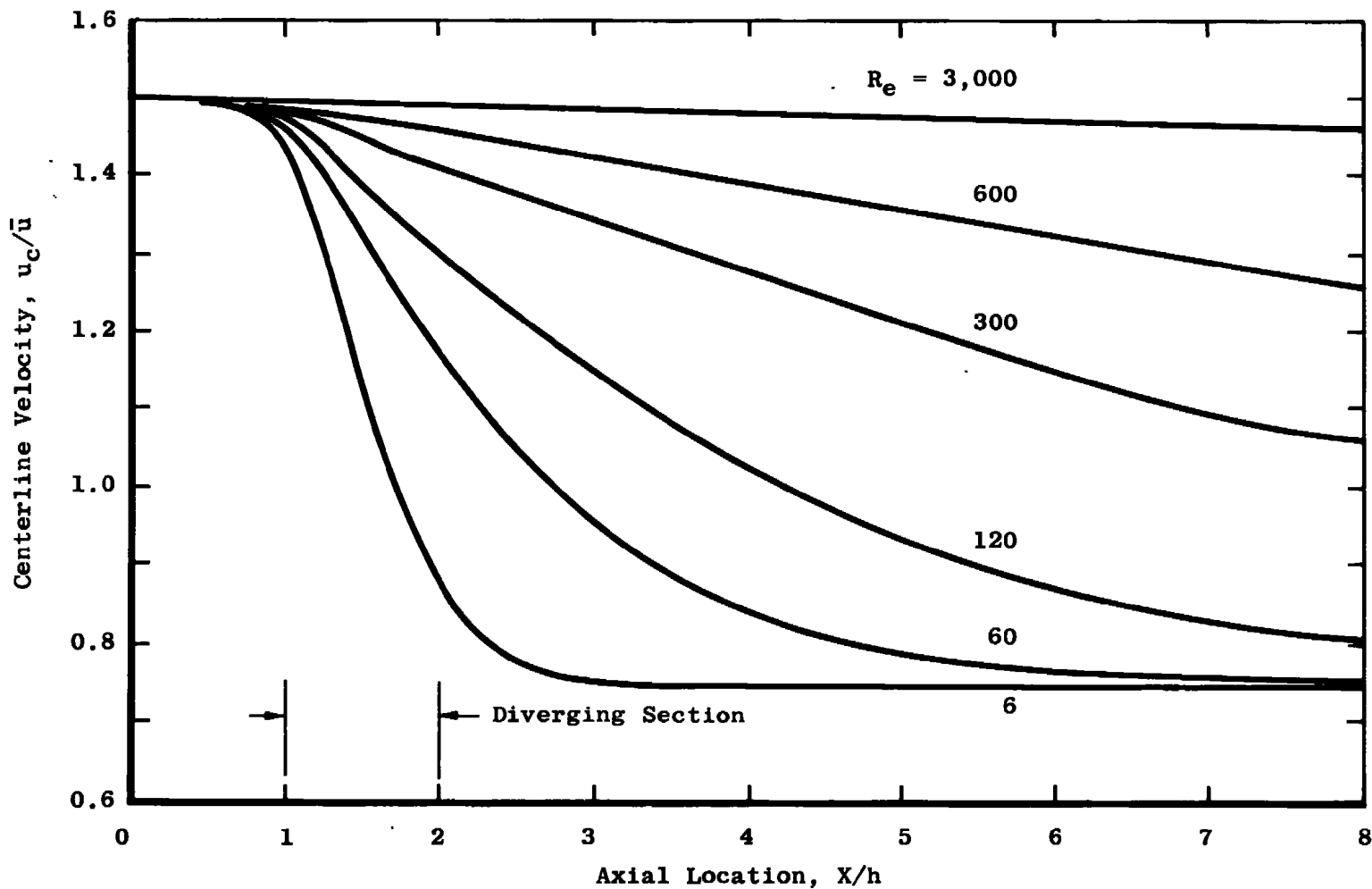
Figure 11. Centerline velocity distribution for a planar diffuser.
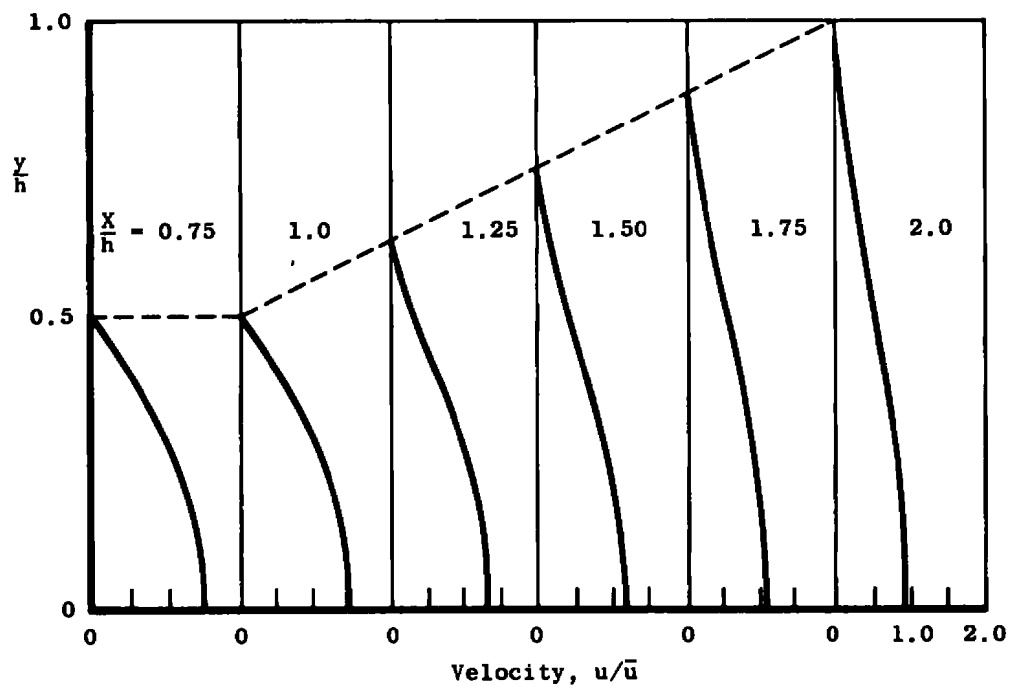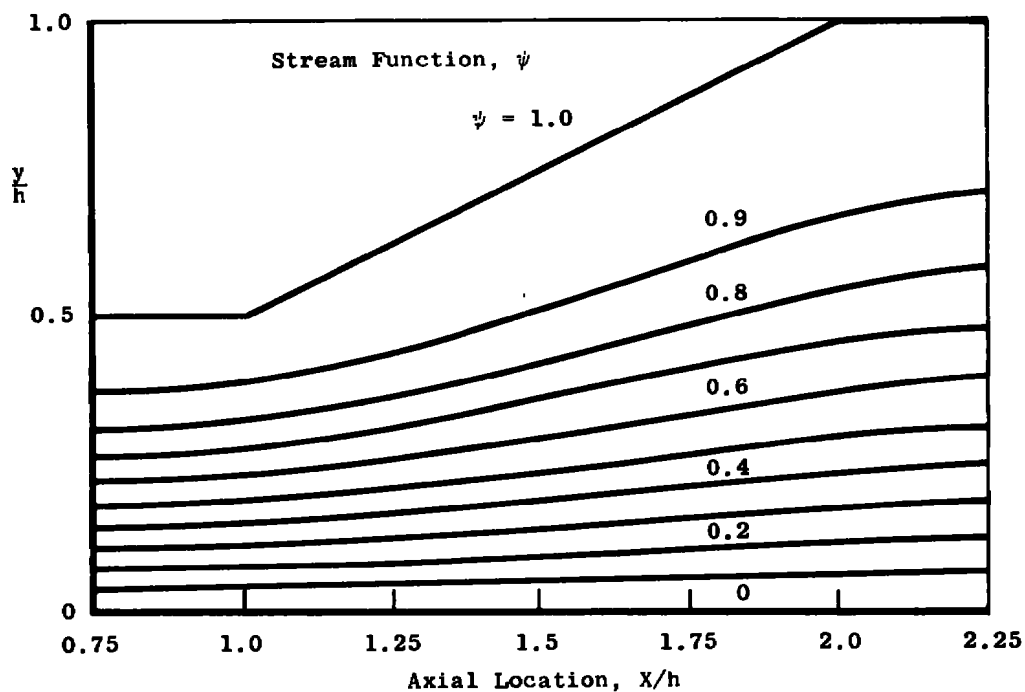
a. Re = 6

Figure 12. Velocity and stream function distribution in a planar
diffuser.

70
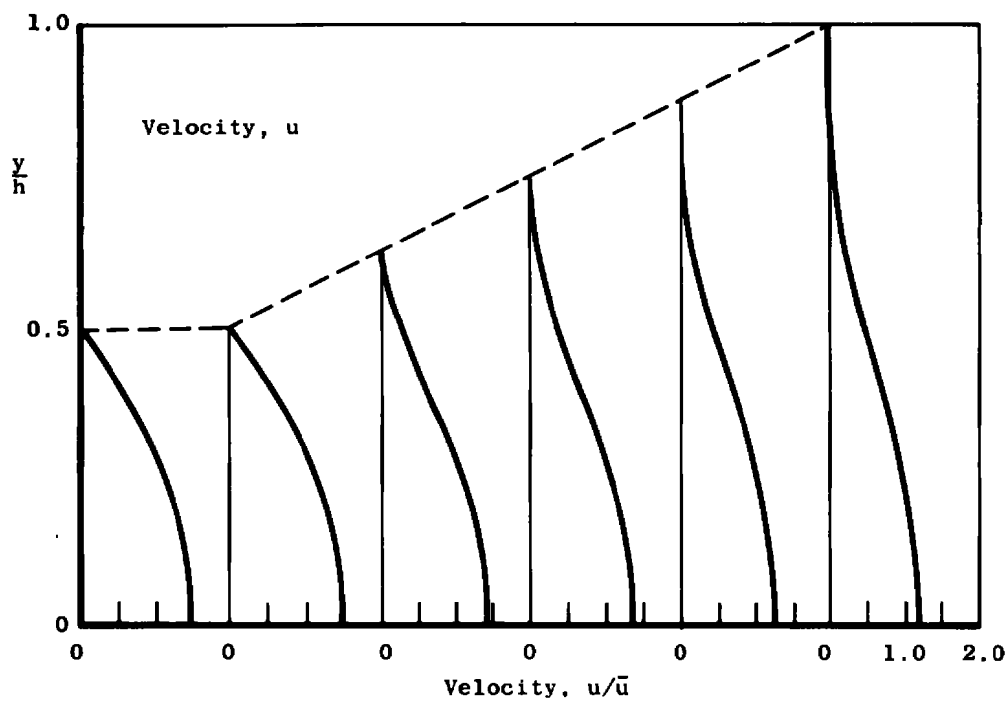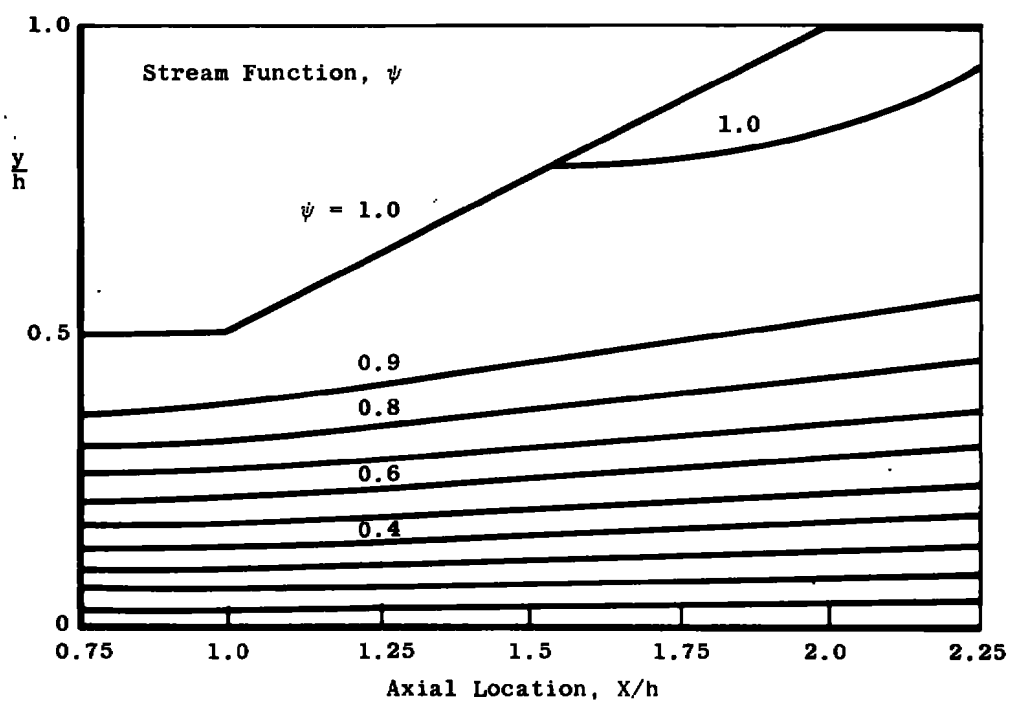
b. Re = 60
Figure 12. Continued.
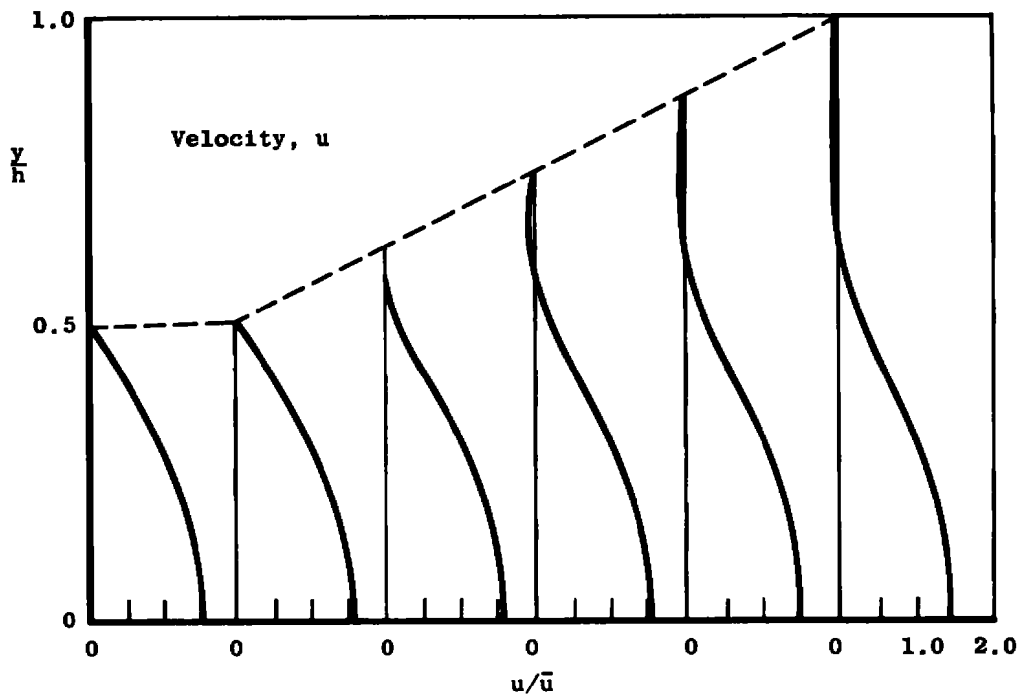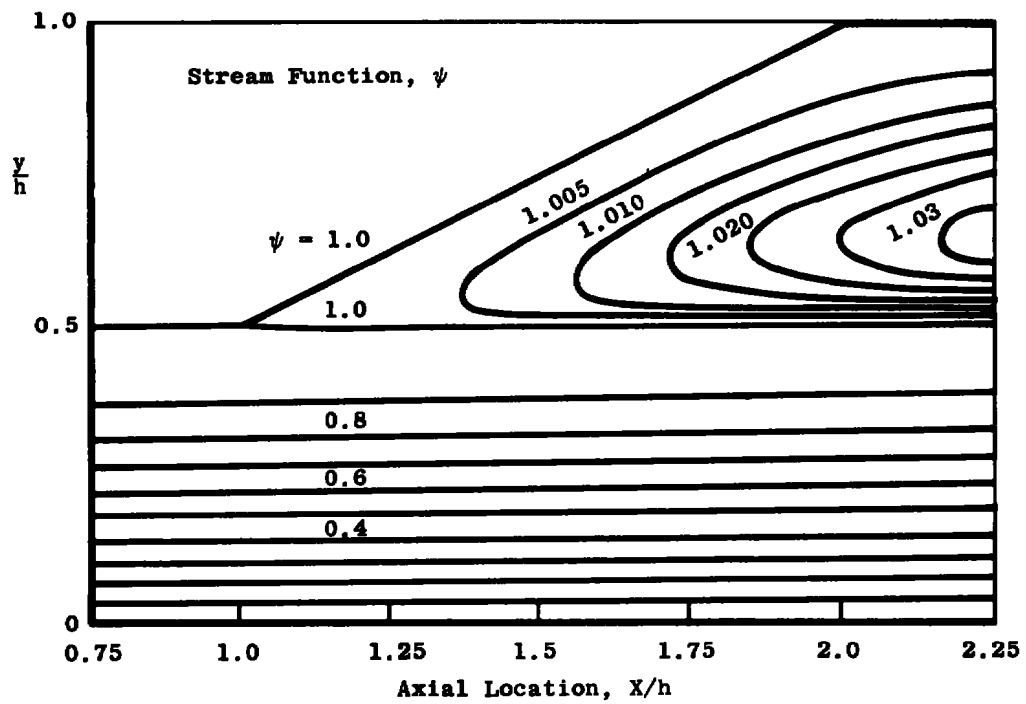
c. Re = 600
Figure 12. Concluded.
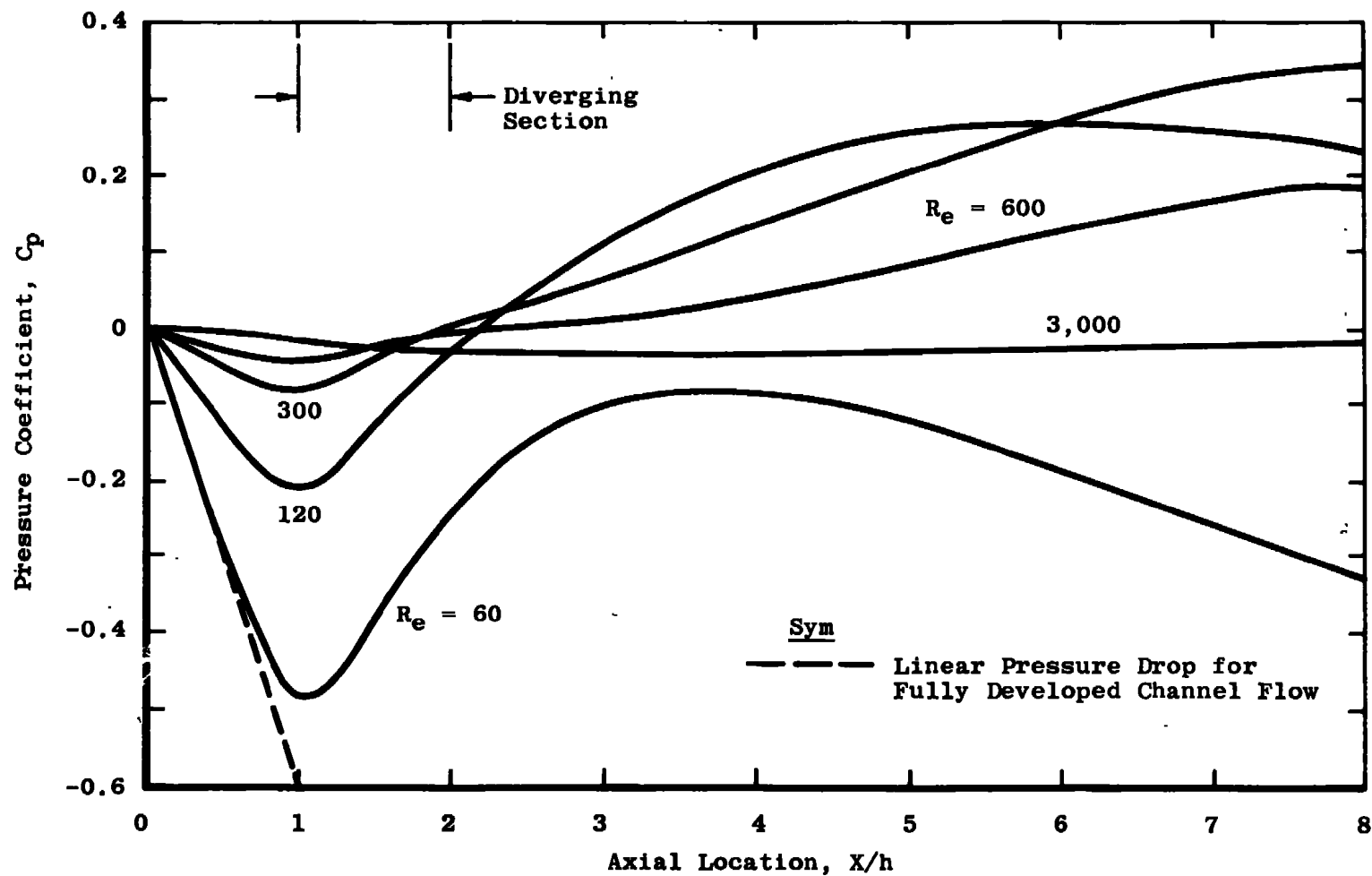
Figure 13. Centerline pressure distribution in a planar diffuser.
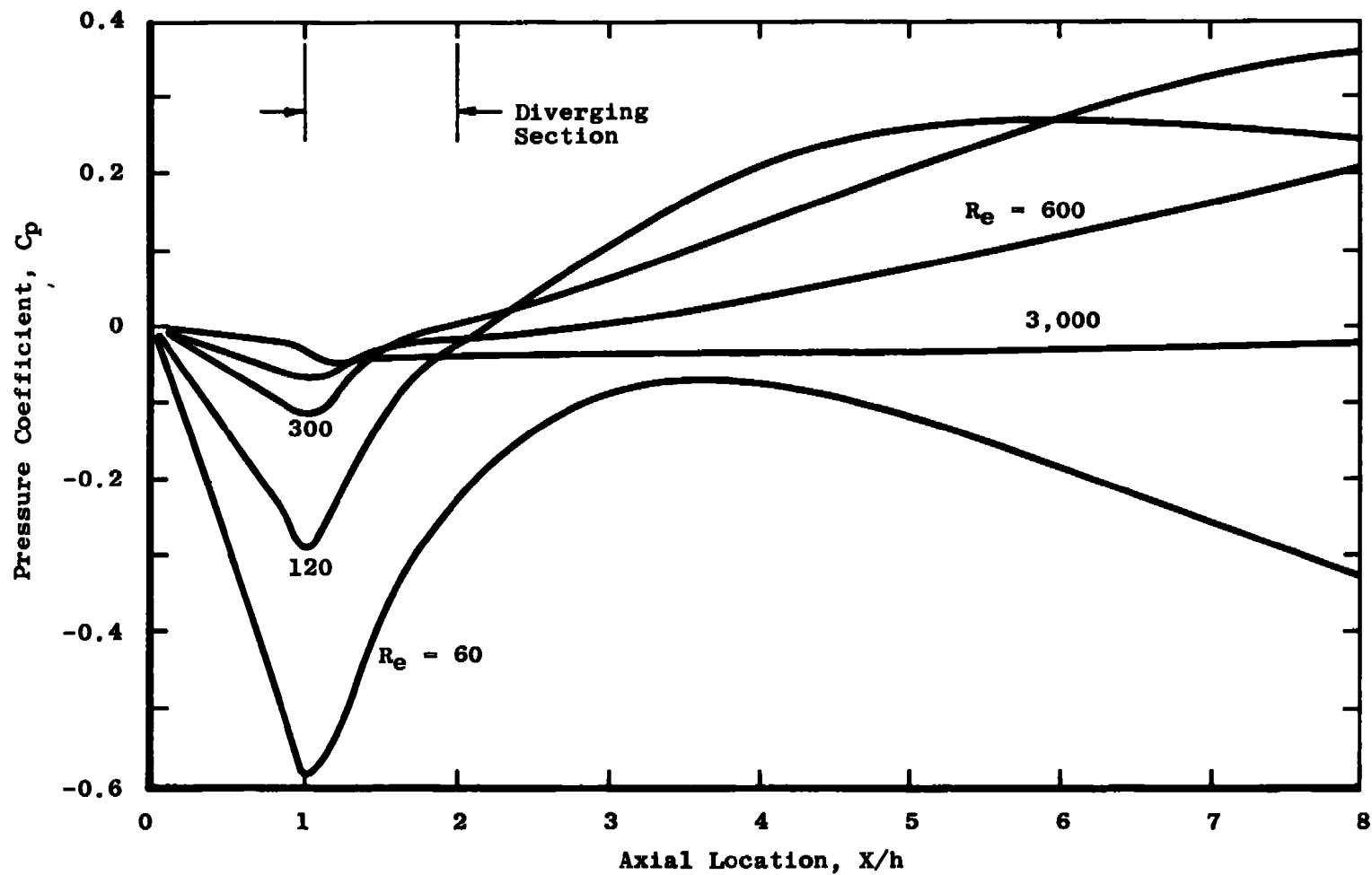
Figure 14. Wall pressure distribution in a planar diffuser.
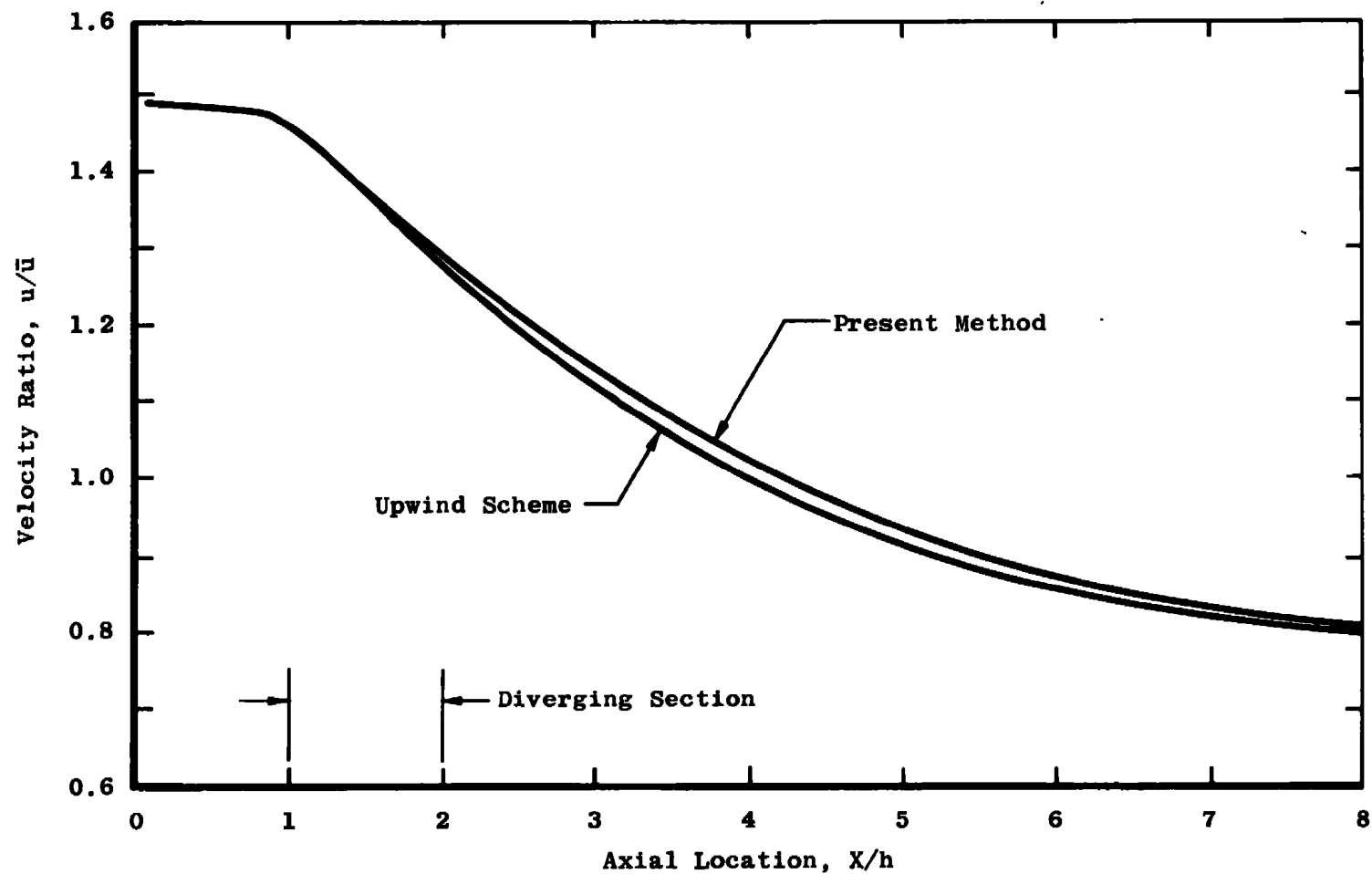
Figure 15. Centerline velocity distribution in a planar diffuser,
Re = 120.
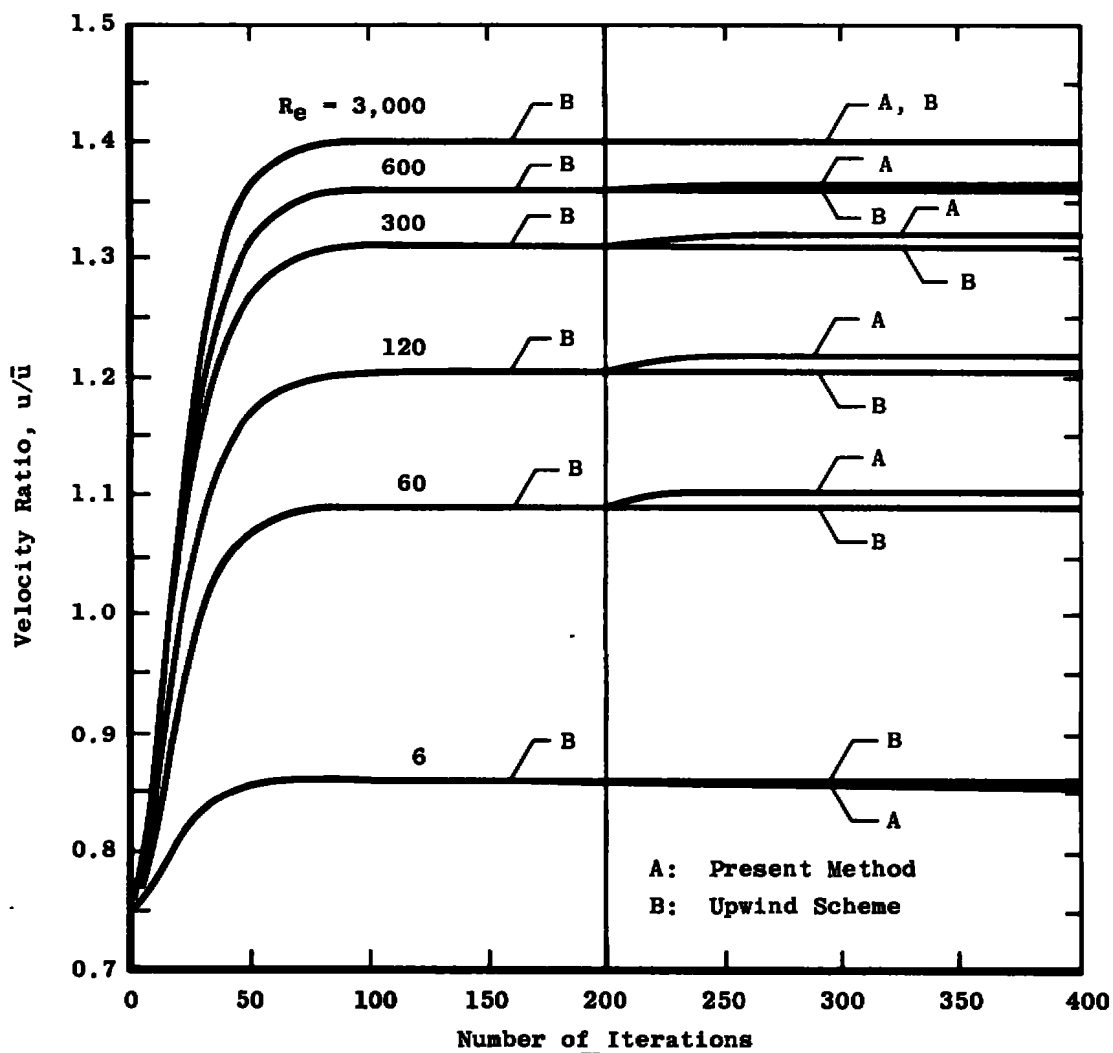
Figure 16. History of the centerline velocity convergence
at X/h = 2.0.
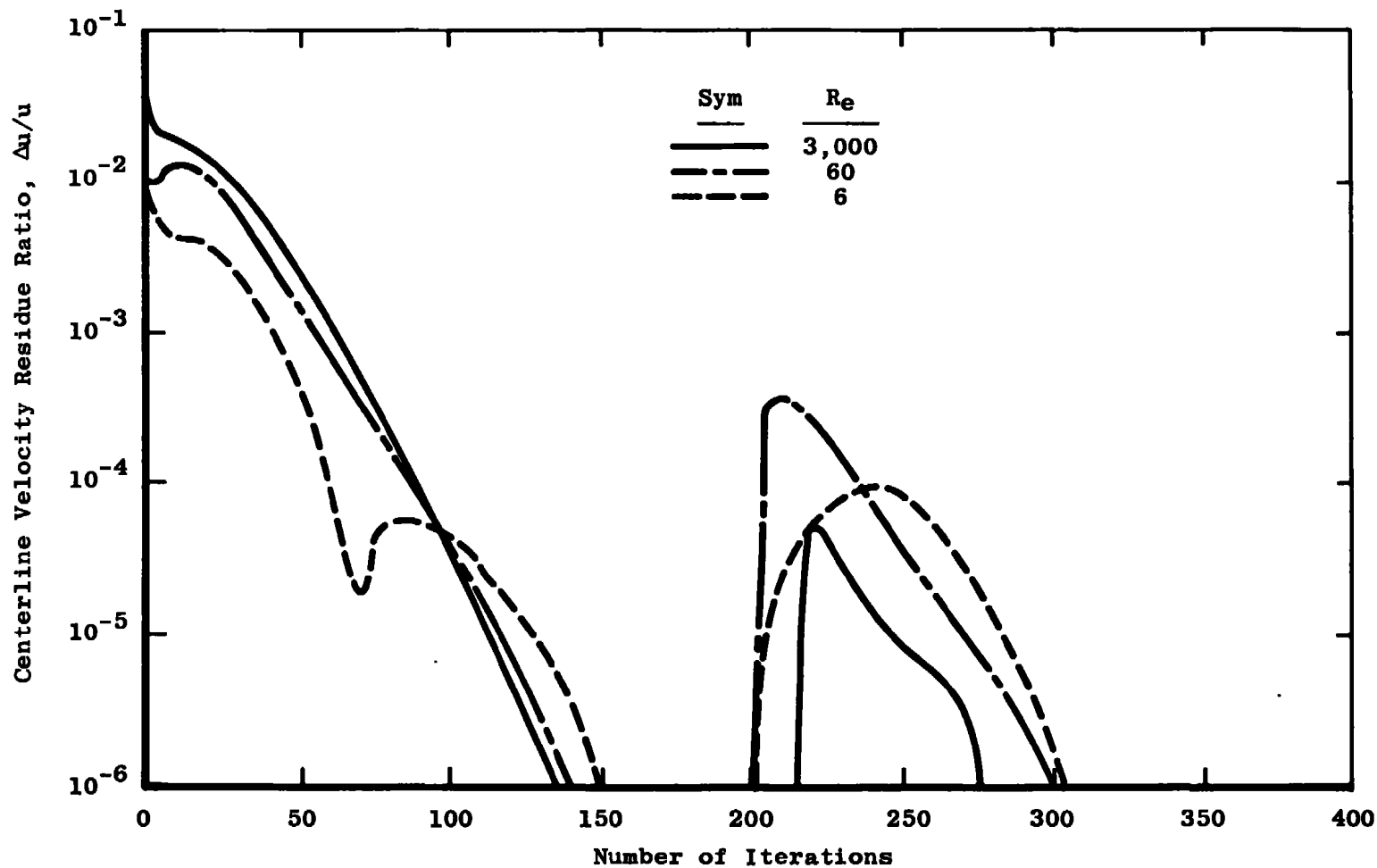
Figure 17. Variation of the centerline velocity residue ratio at
X/h = 2.0.
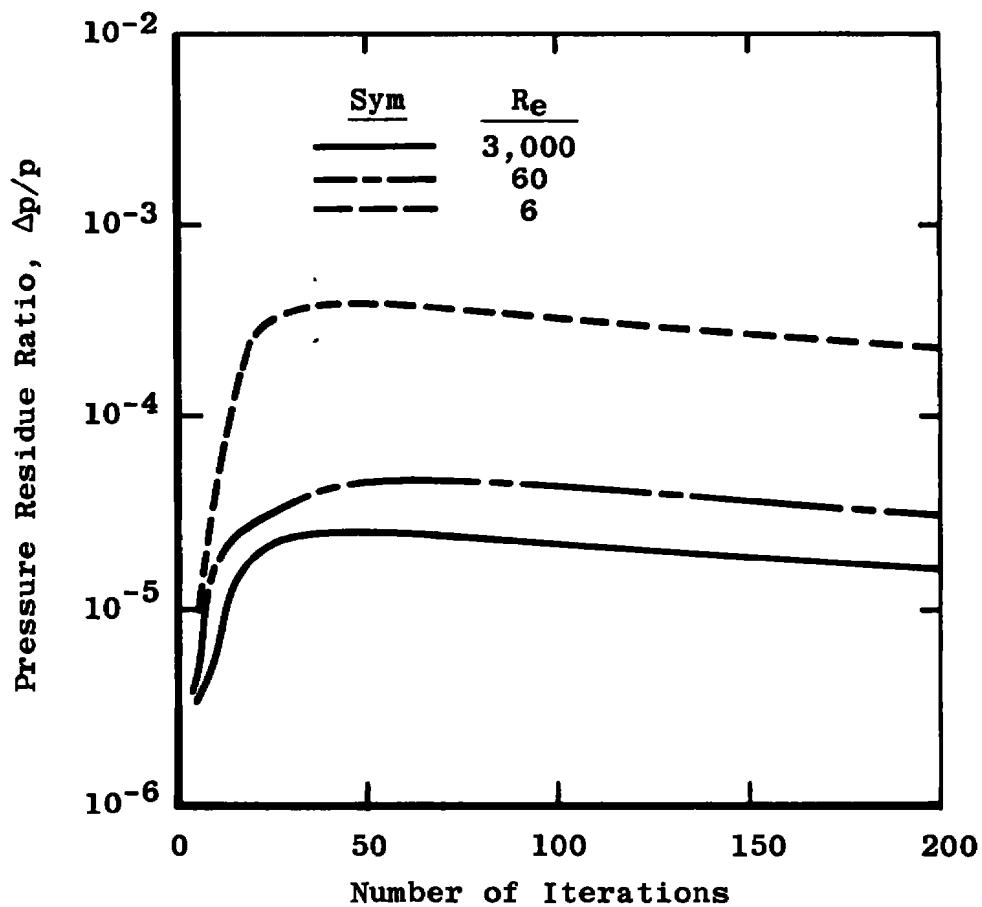
Figure 18. Variation of the pressure residue ratio at X/h = 2.0.
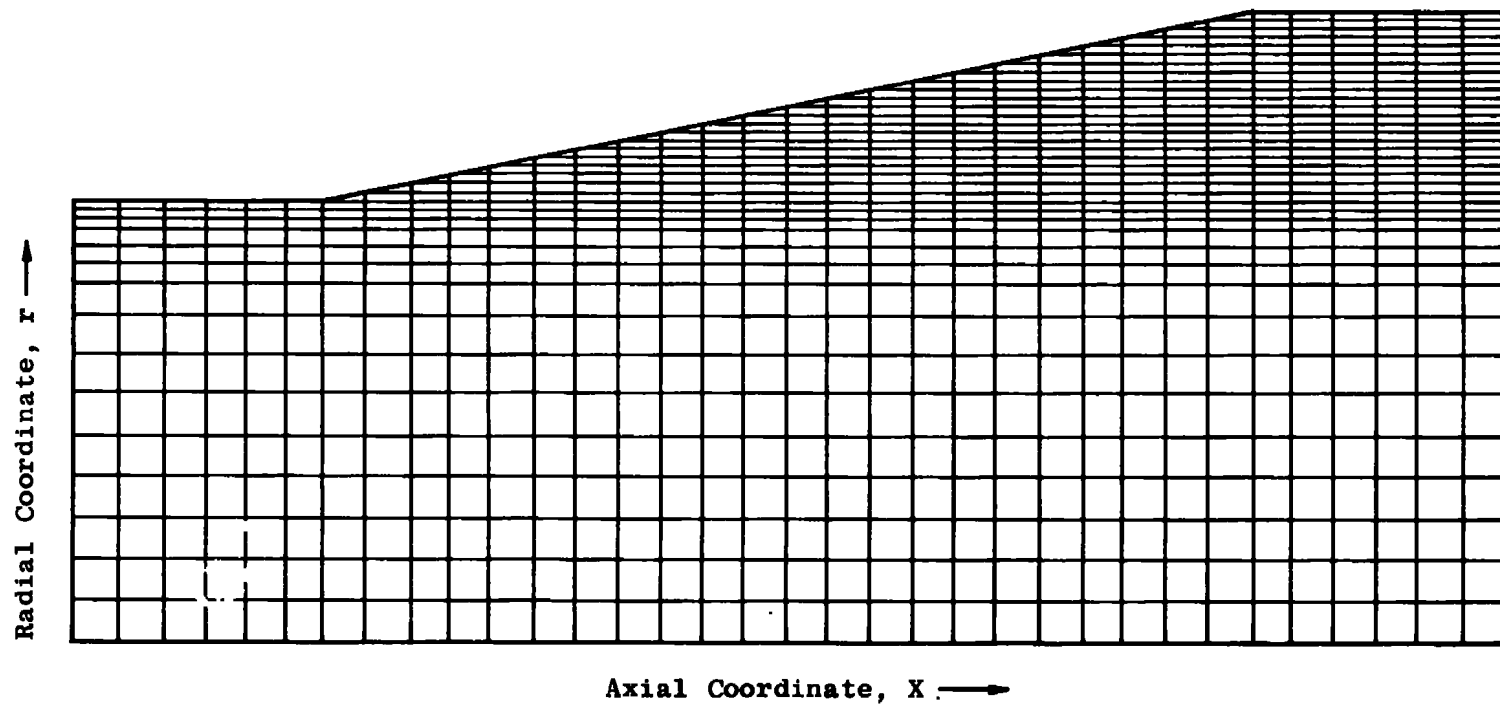
Figure 19. 23-deg conical diffuser and computational grid in radial
direction (nonuniform system).
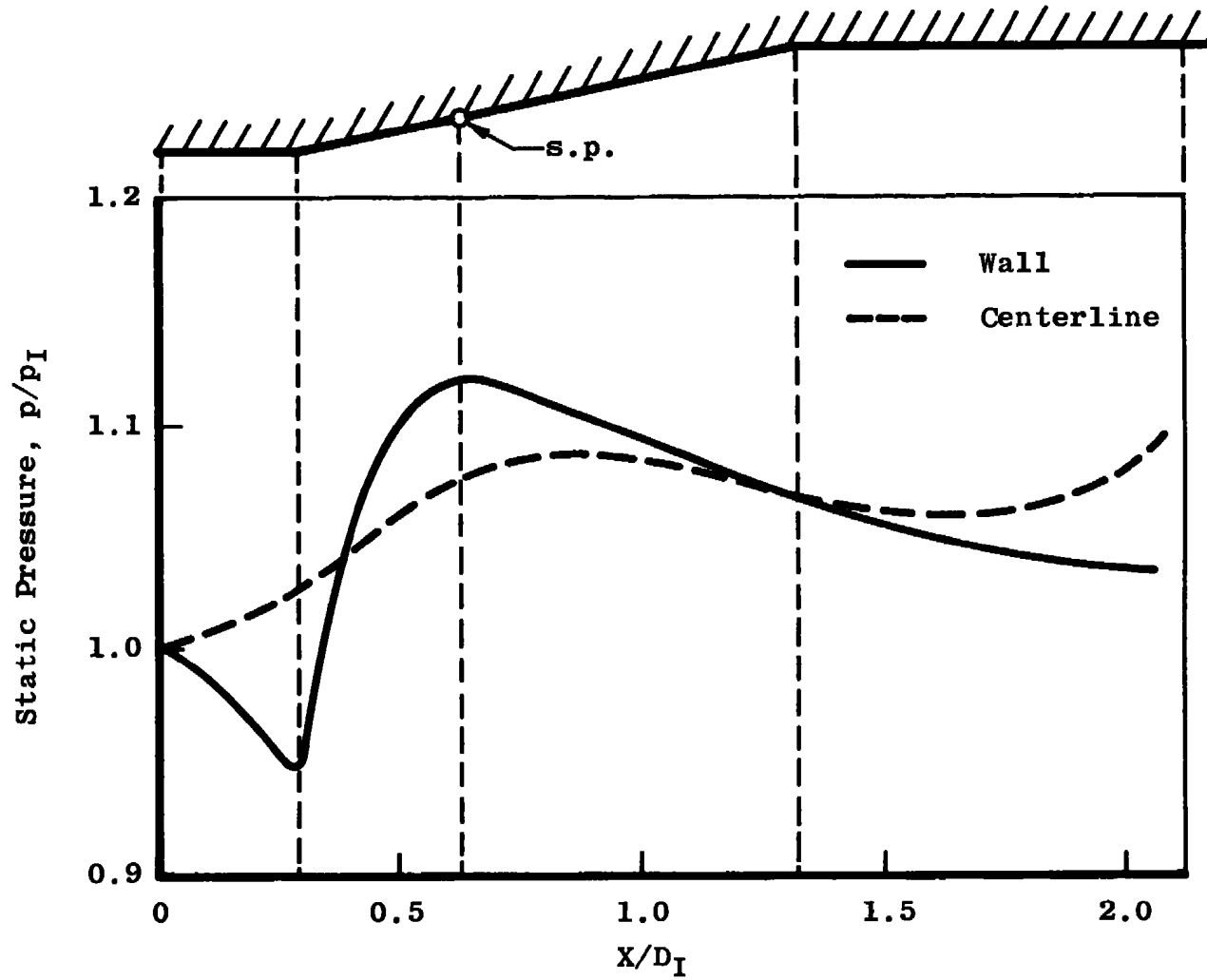
Figure 20. Wall and centerline pressure distribution with a mixing
length model.
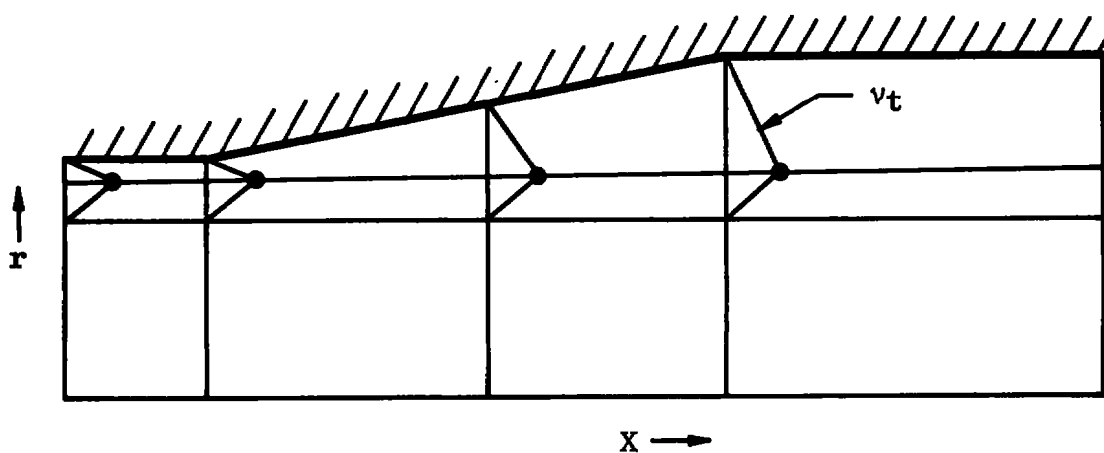
Figure 21. Schematic of a convective eddy viscosity model.
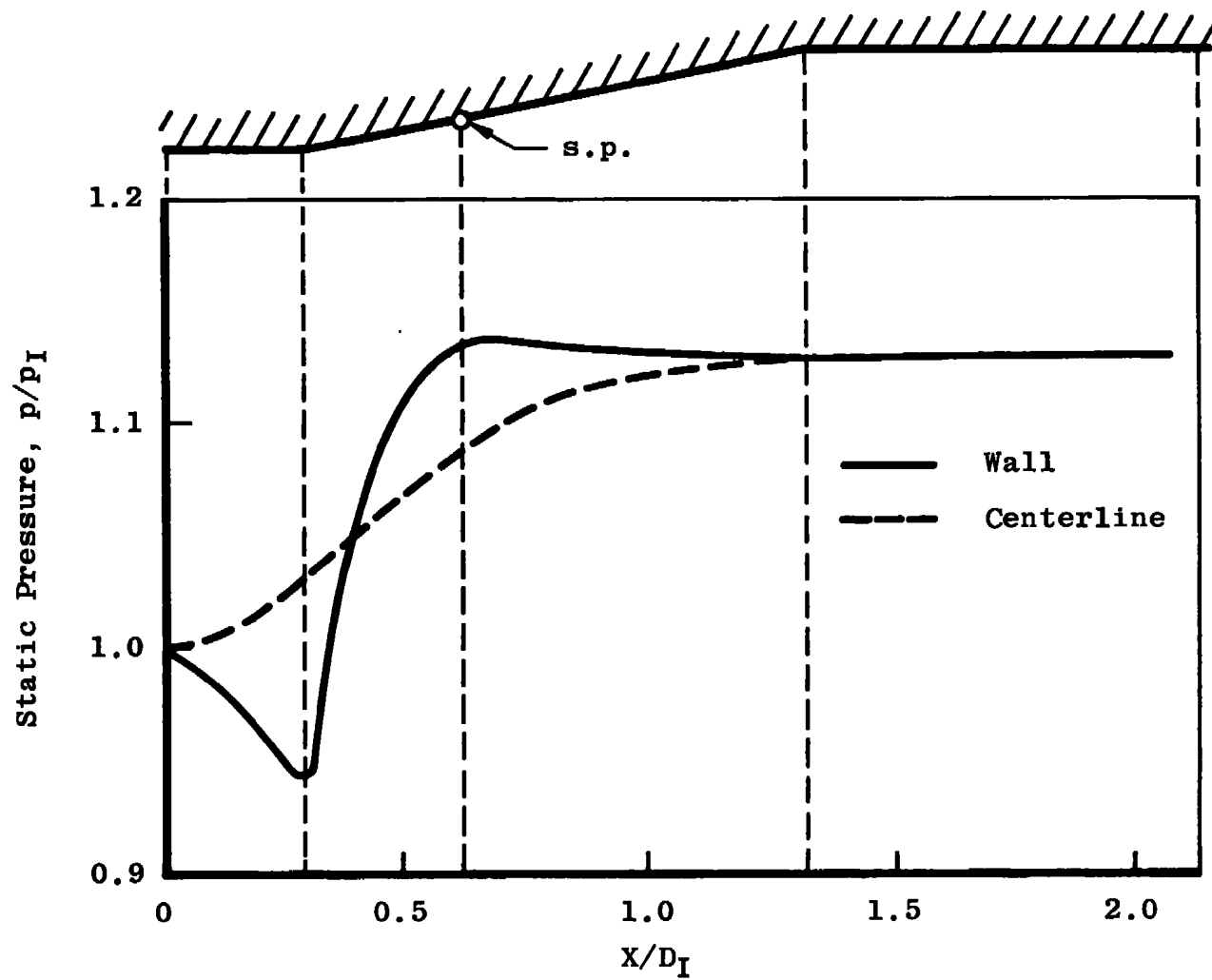
Figure 22. Wall and centerline pressure distribution with a convective model.
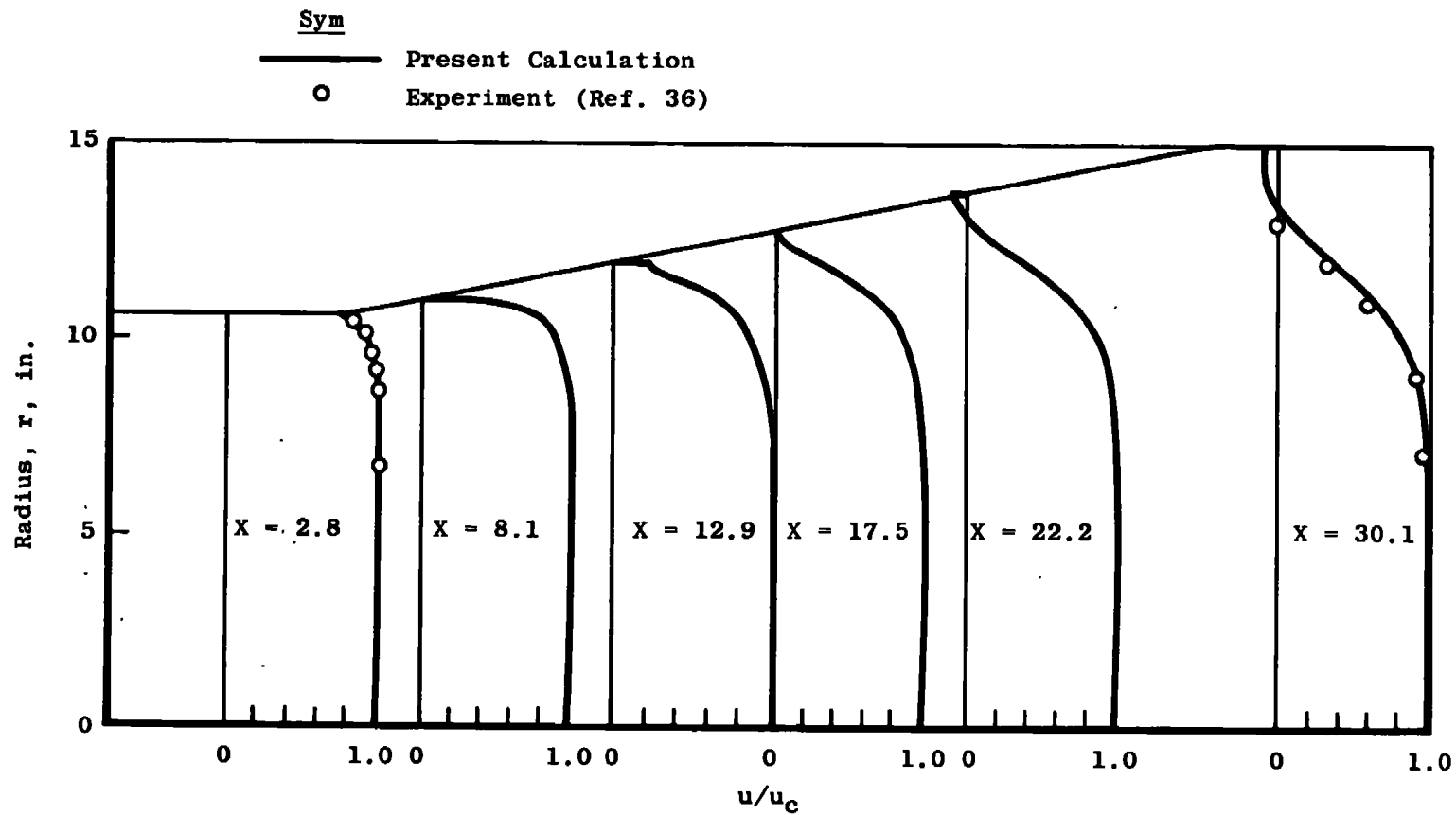
Figure 23. Velocity distribution in a 23-deg conical diffuser with
a convective eddy viscosity model.
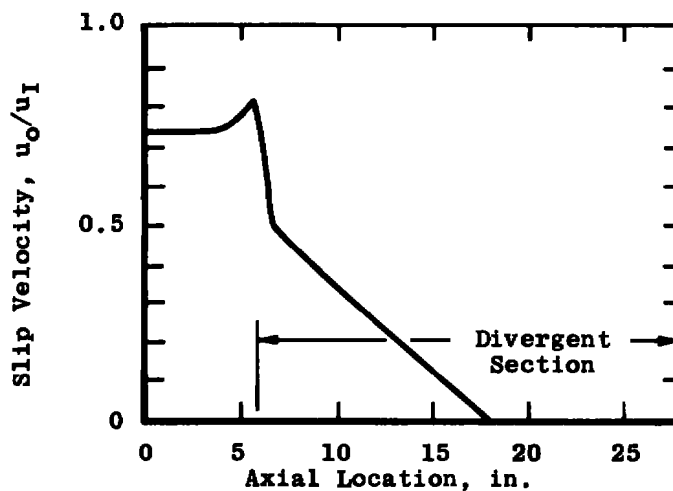
a. Assumed slip velocity, 0.1 in. from wall
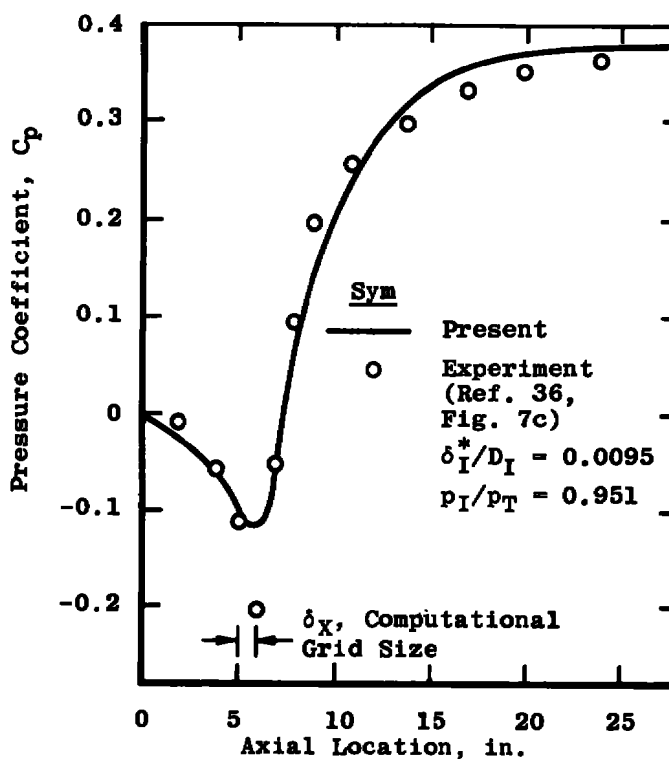
b. Wall pressure distribution

Figure 24. Wall pressure and slip velocity distributions in a separated conical diffuser.
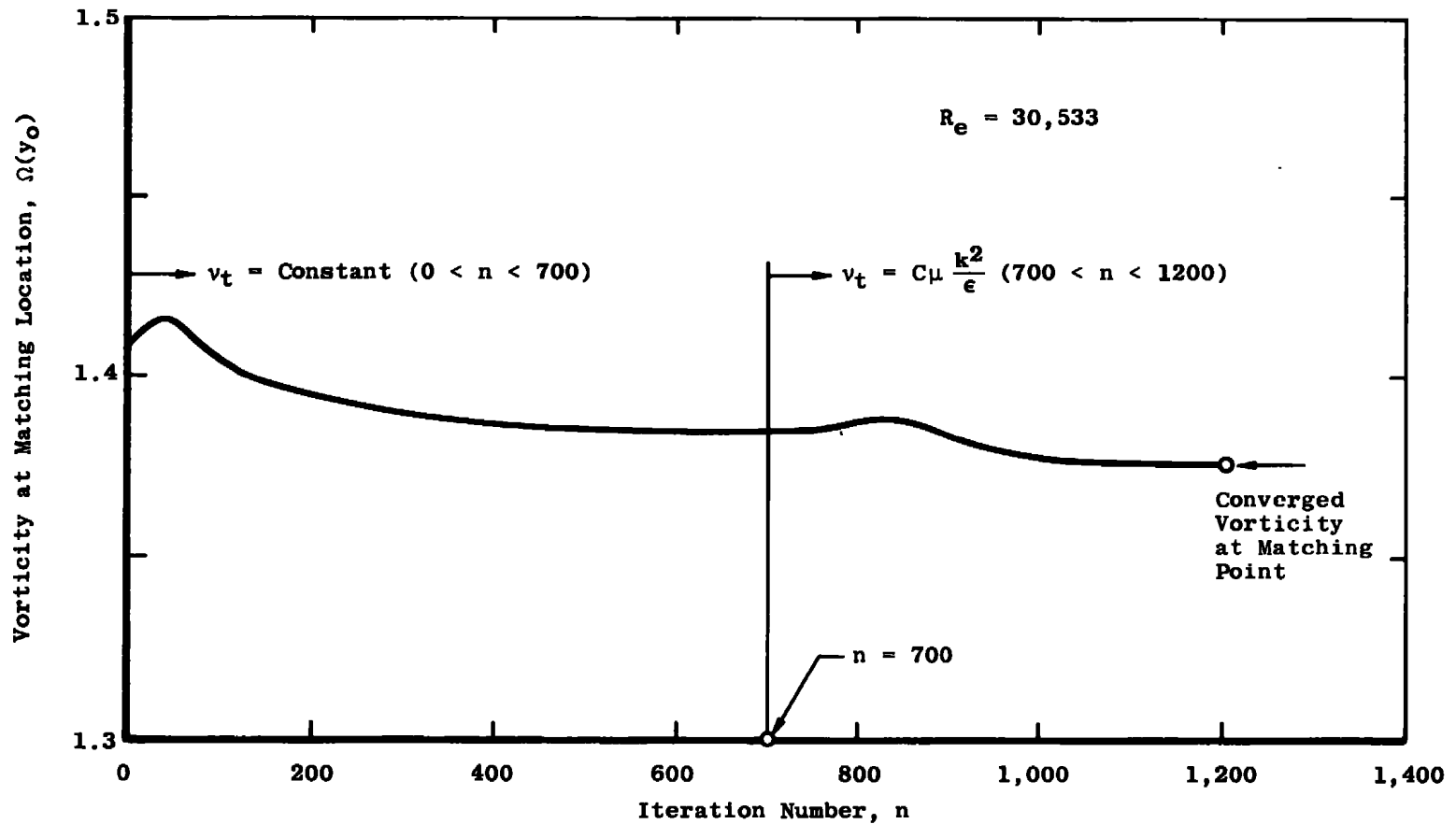
Figure 25. The convergence of the iteration process for a fully
developed channel flow calculation.
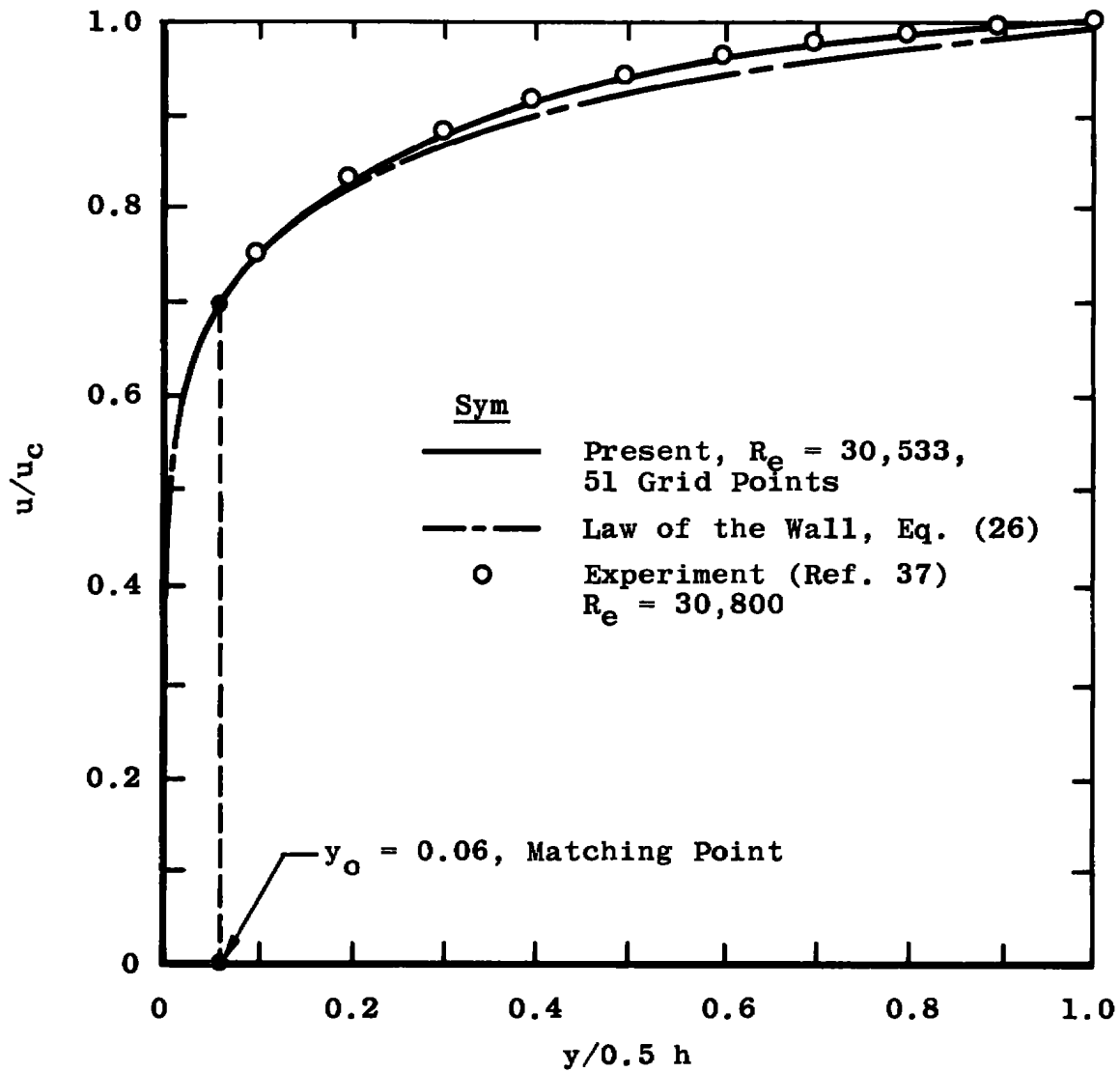
Figure 26. Velocity profile in a fully developed channel flow,
with k-ϵ model and wall matching.
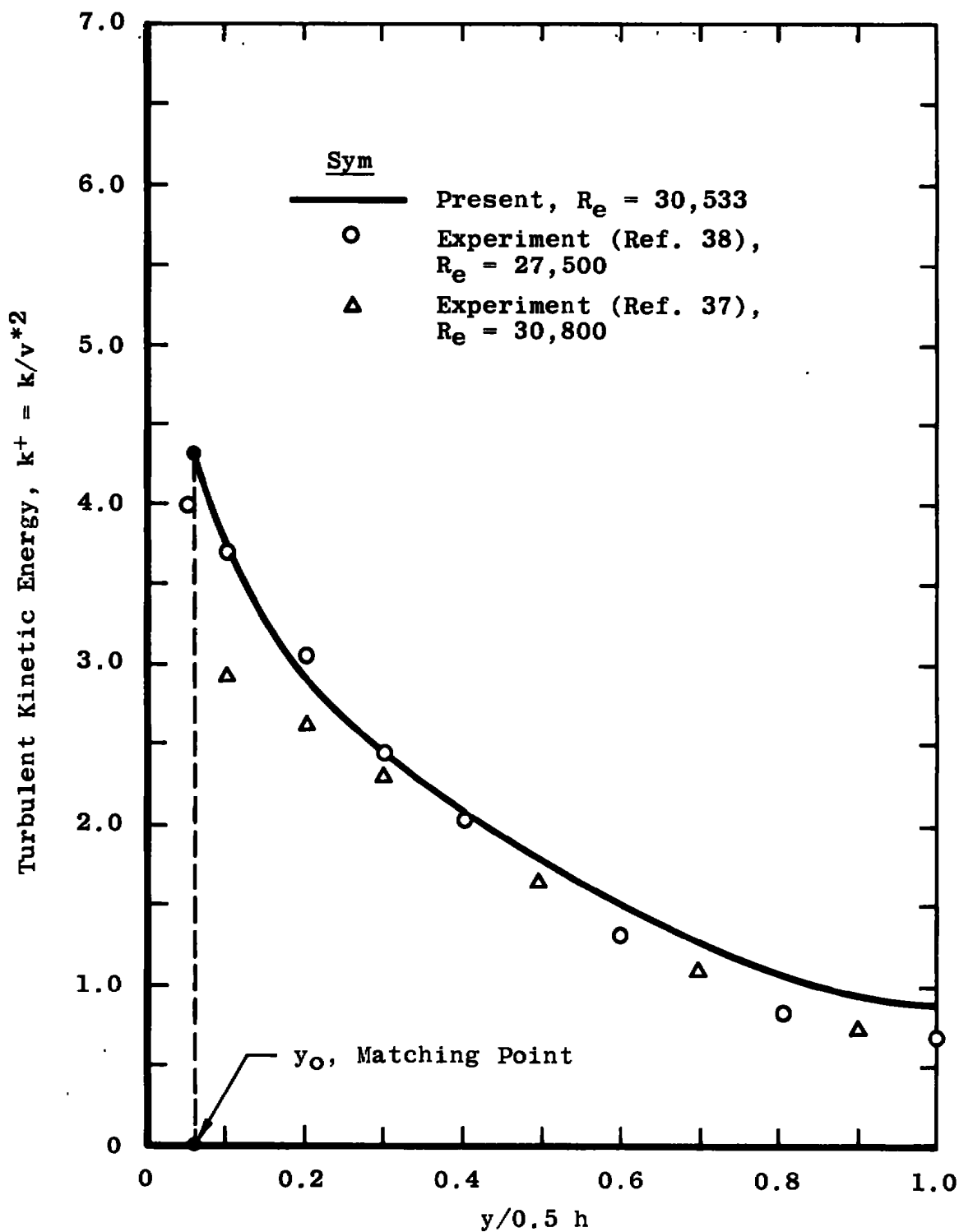
Figure 27. Turbulent kinetic energy distribution in a fully
developed channel flow.
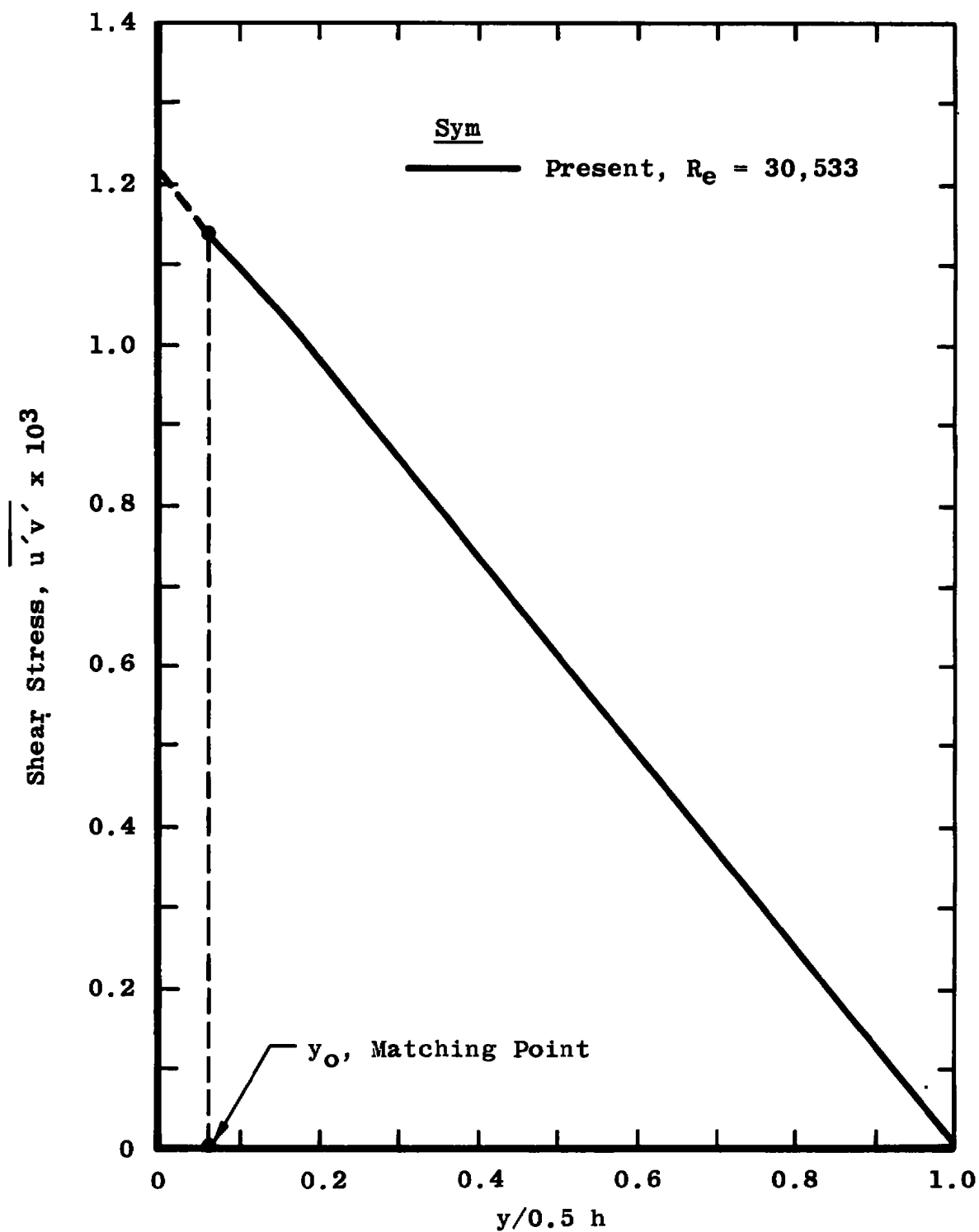
Figure 28. Shear stress distribution in a fully developed channel flow.
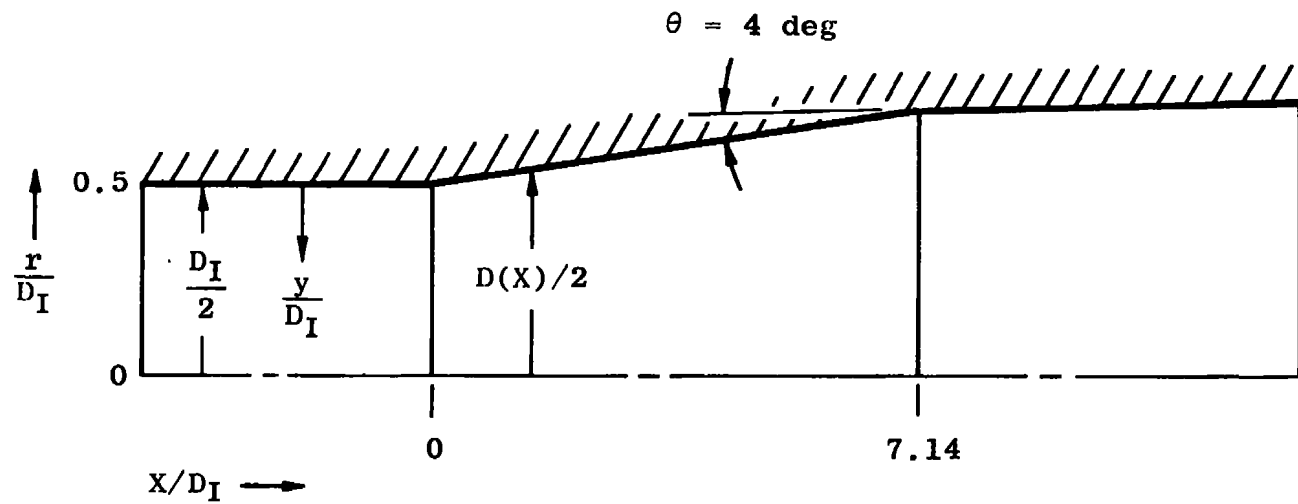
Figure 29. Conical diffuser configuration (2 θ = 8 deg).
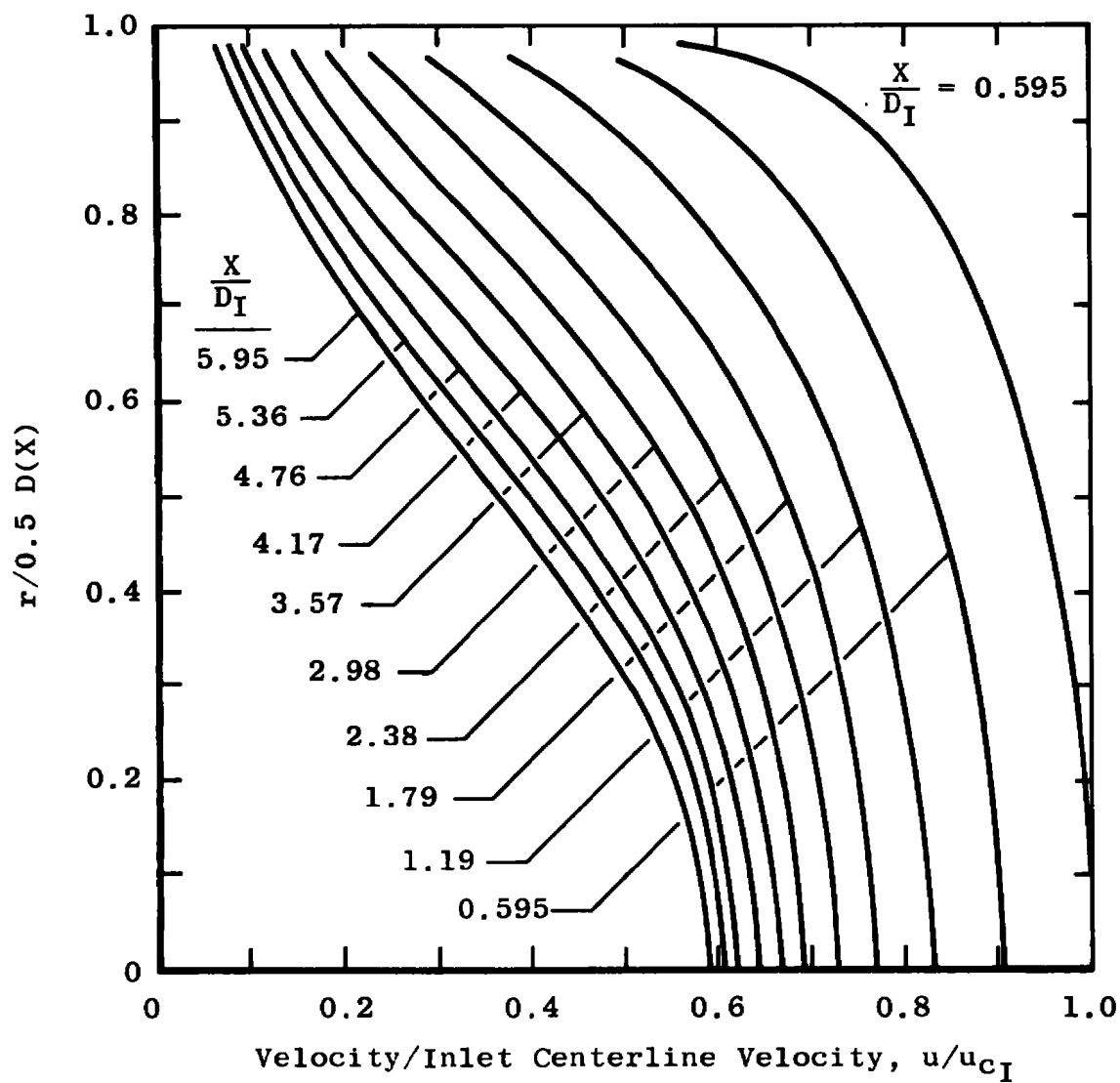
Figure 30. Velocity distribution in an 8-deg conical diffuser
at various axial stations.
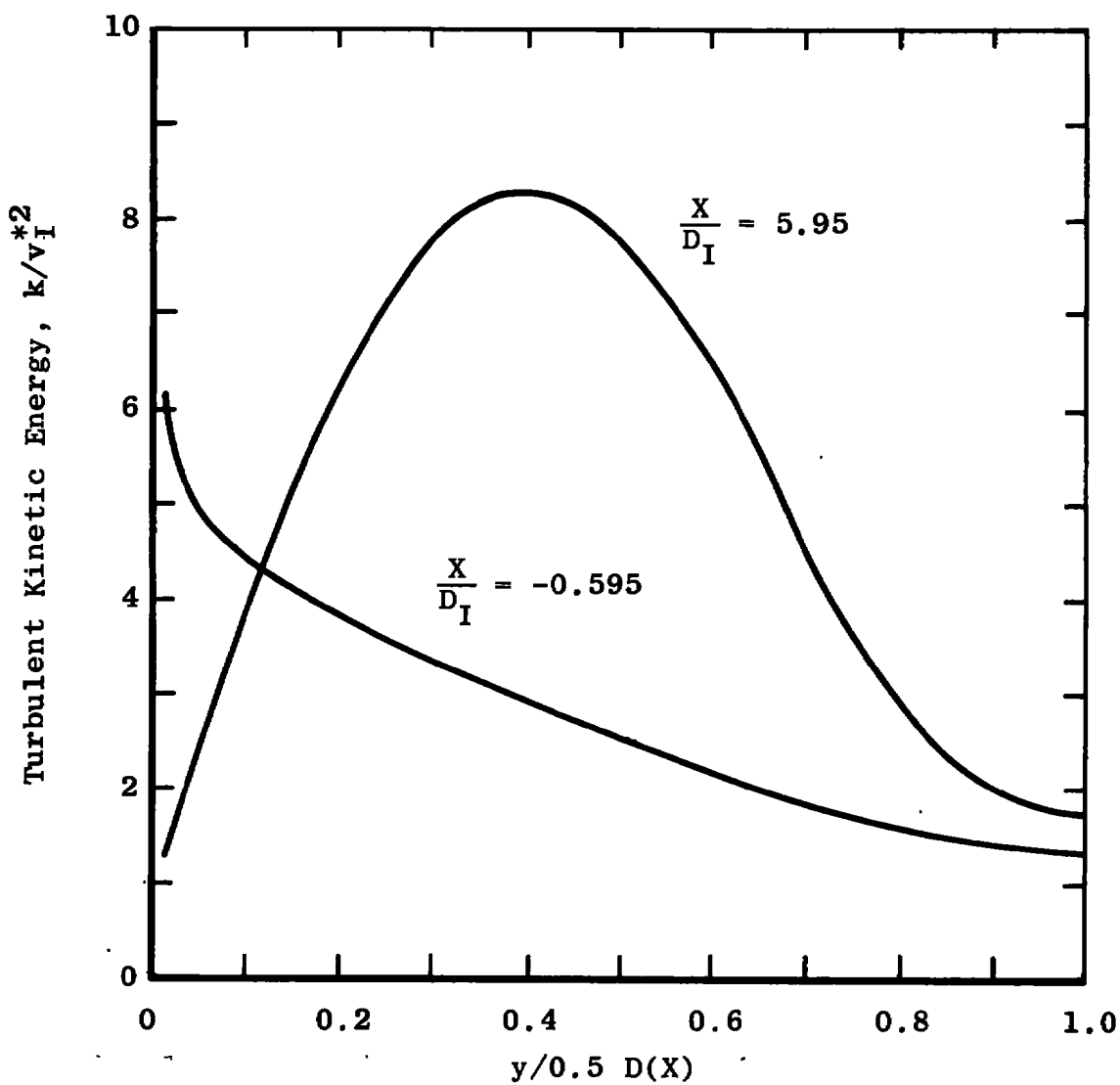
Figure 31. Turbulent kinetic energy distribution in an 8-deg
conical diffuser.
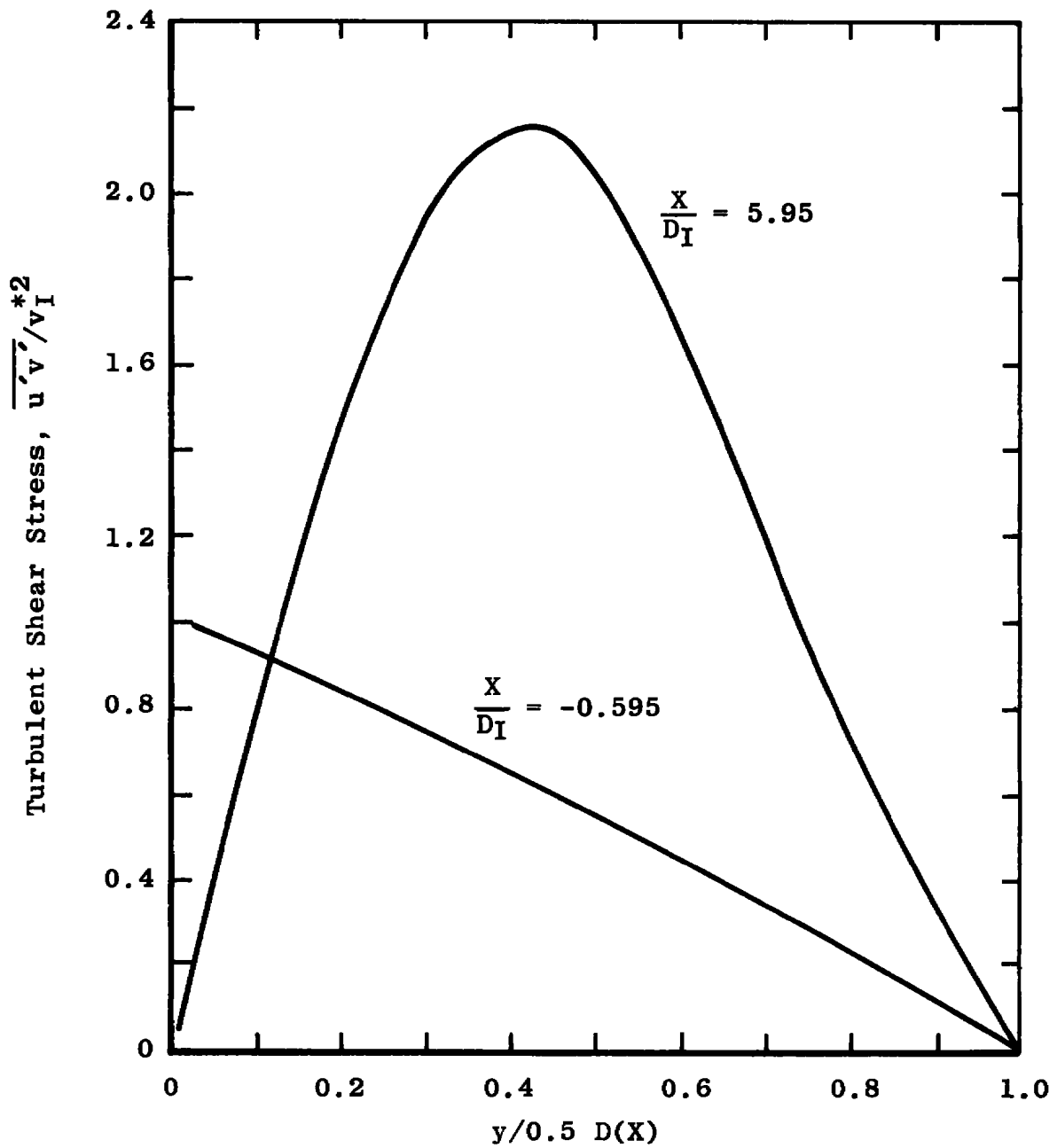
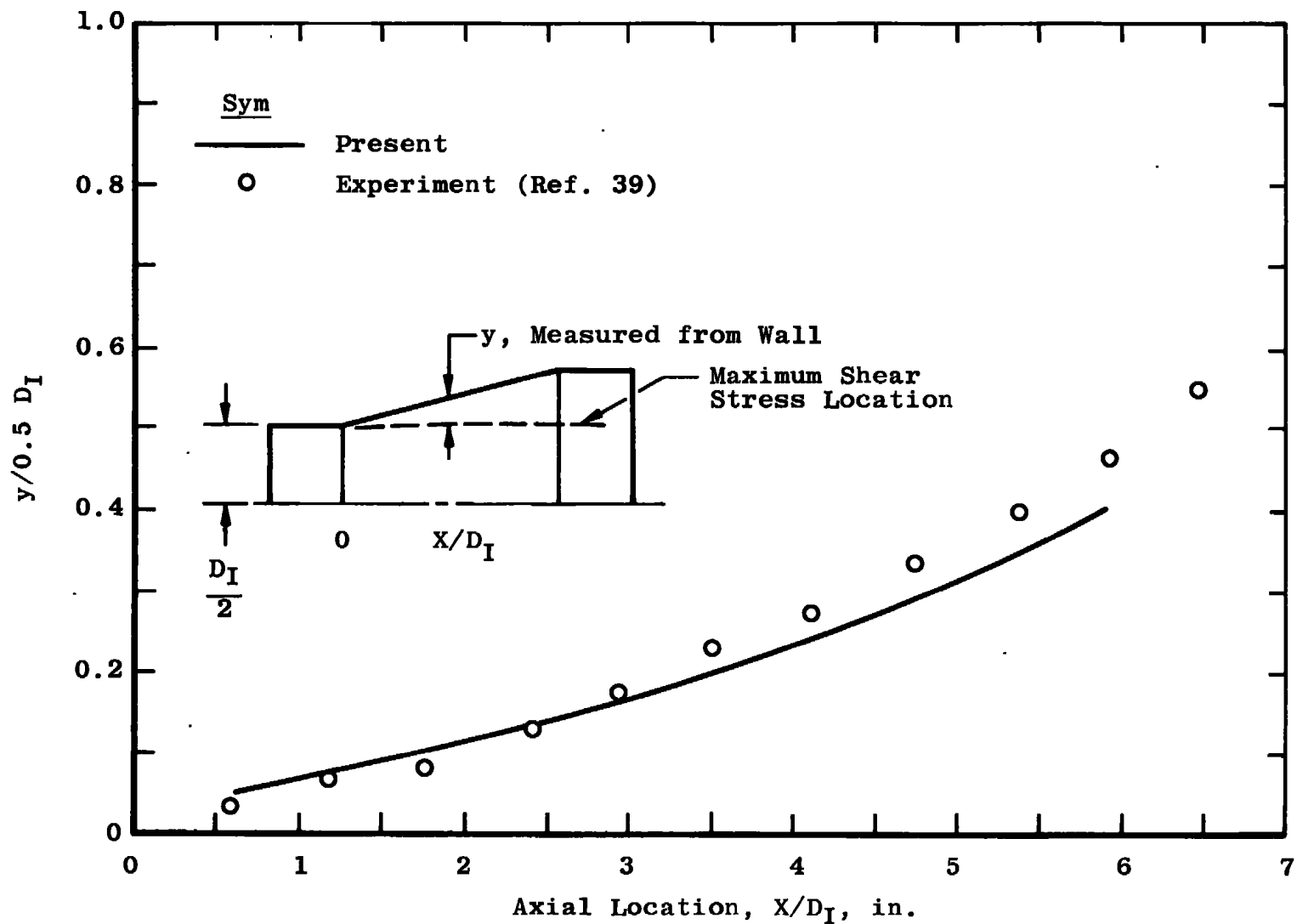Figure 32. Turbulent shear stress distribution in an 8-deg
conical diffuser.

Figure 33. Position of maximum shear stress $\overline{(u'v')}$ as a function of
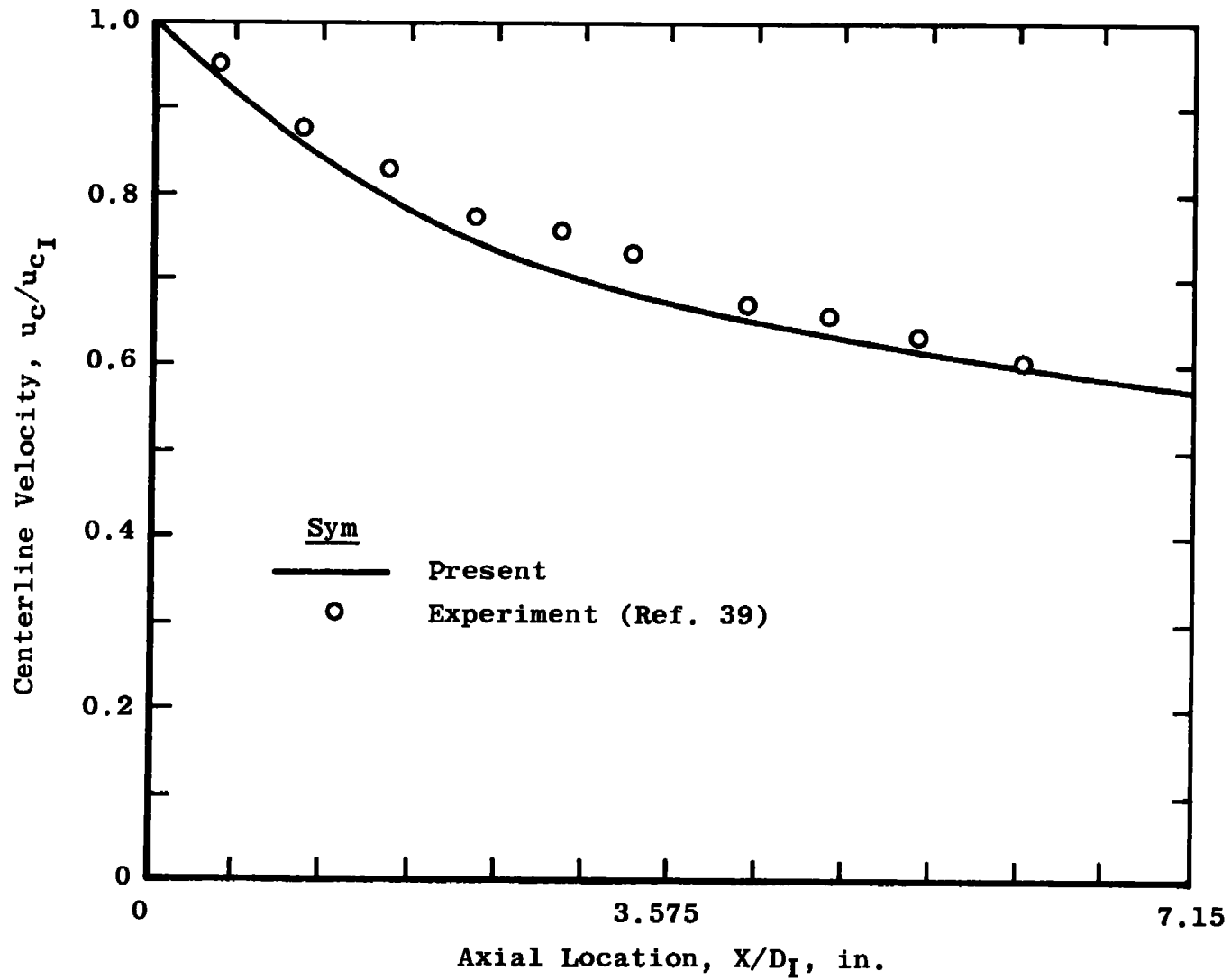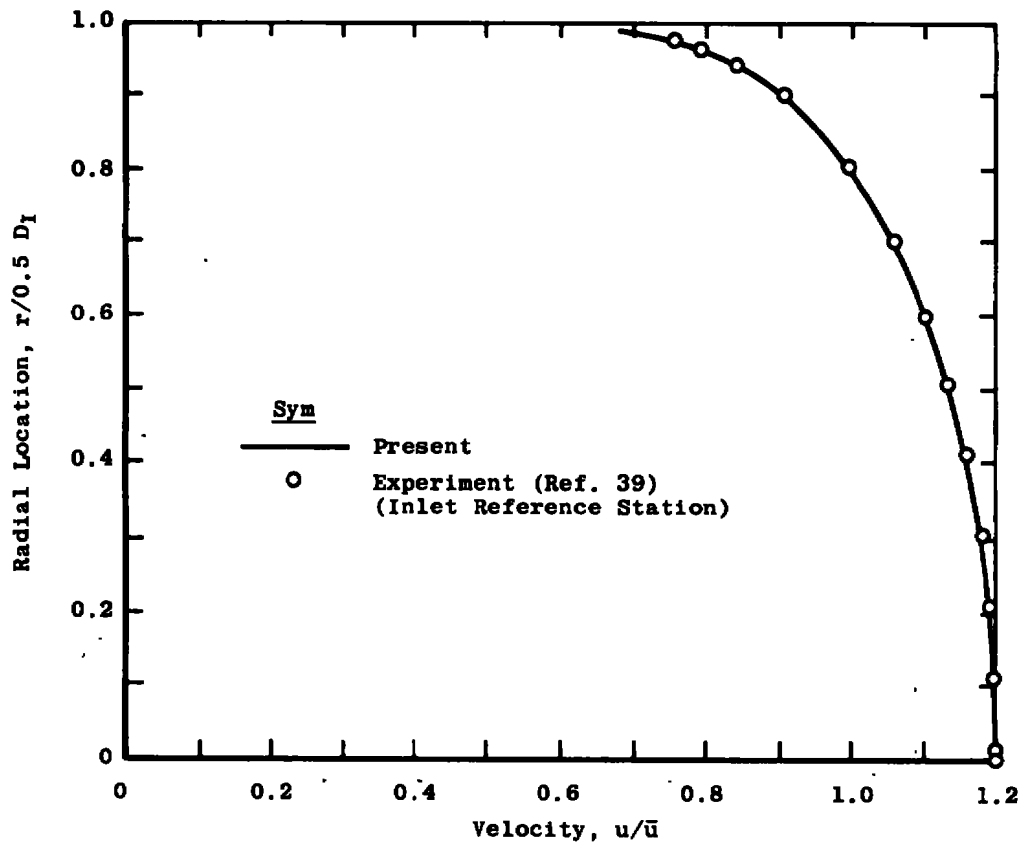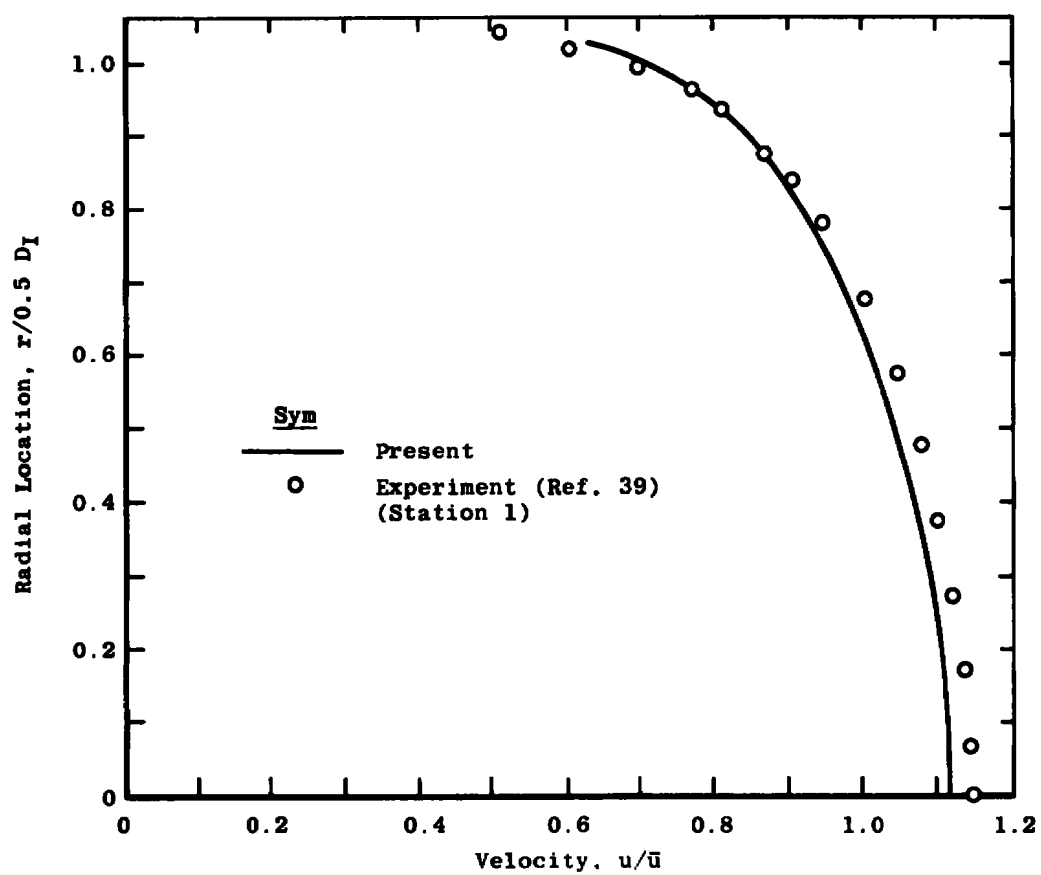axial distance.

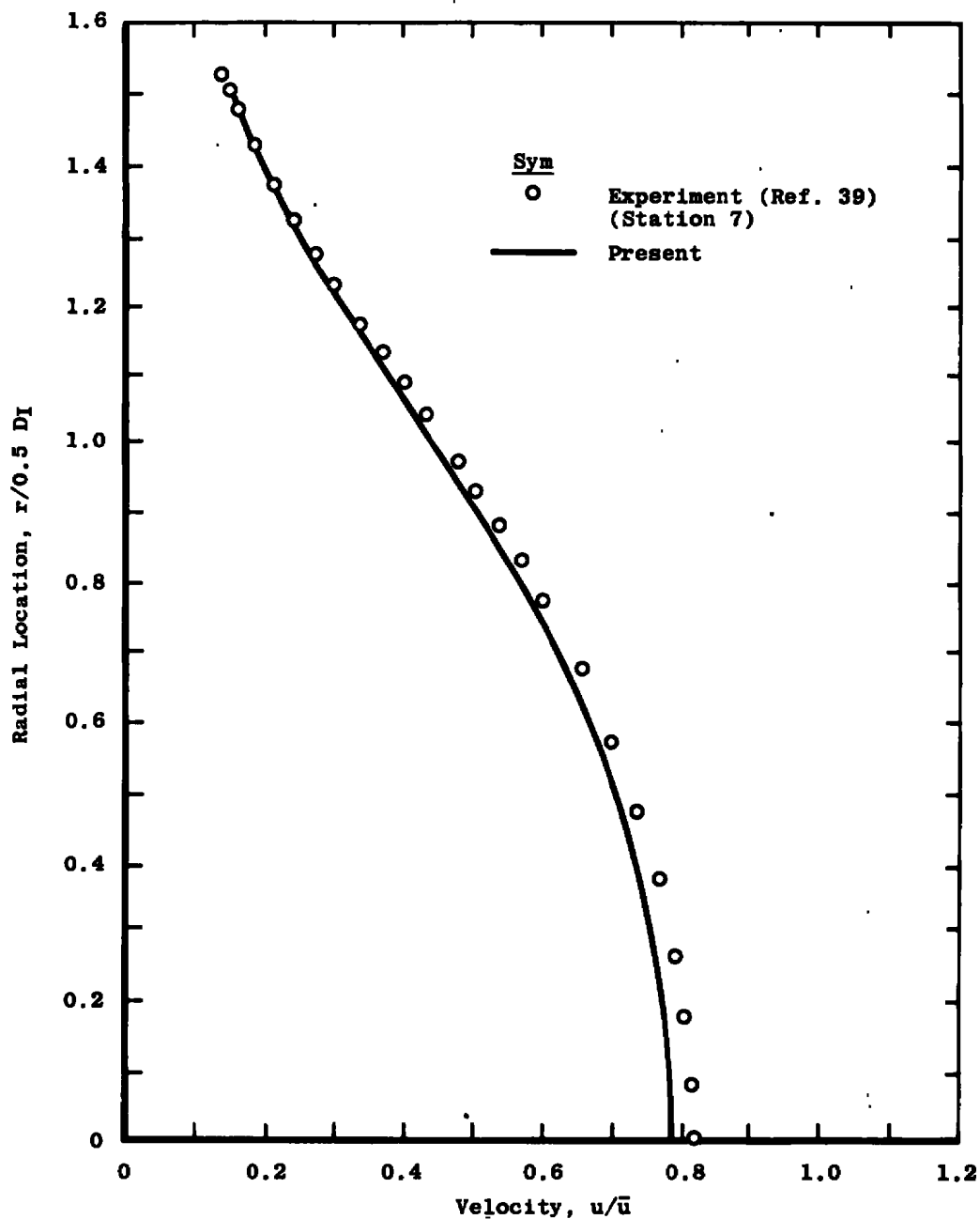Figure 34. Centerline velocity distribution in an 8-deg conical diffuser.

a. $X/D_I = -0.595$

Figure 35. Comparison between the present calculated velocity
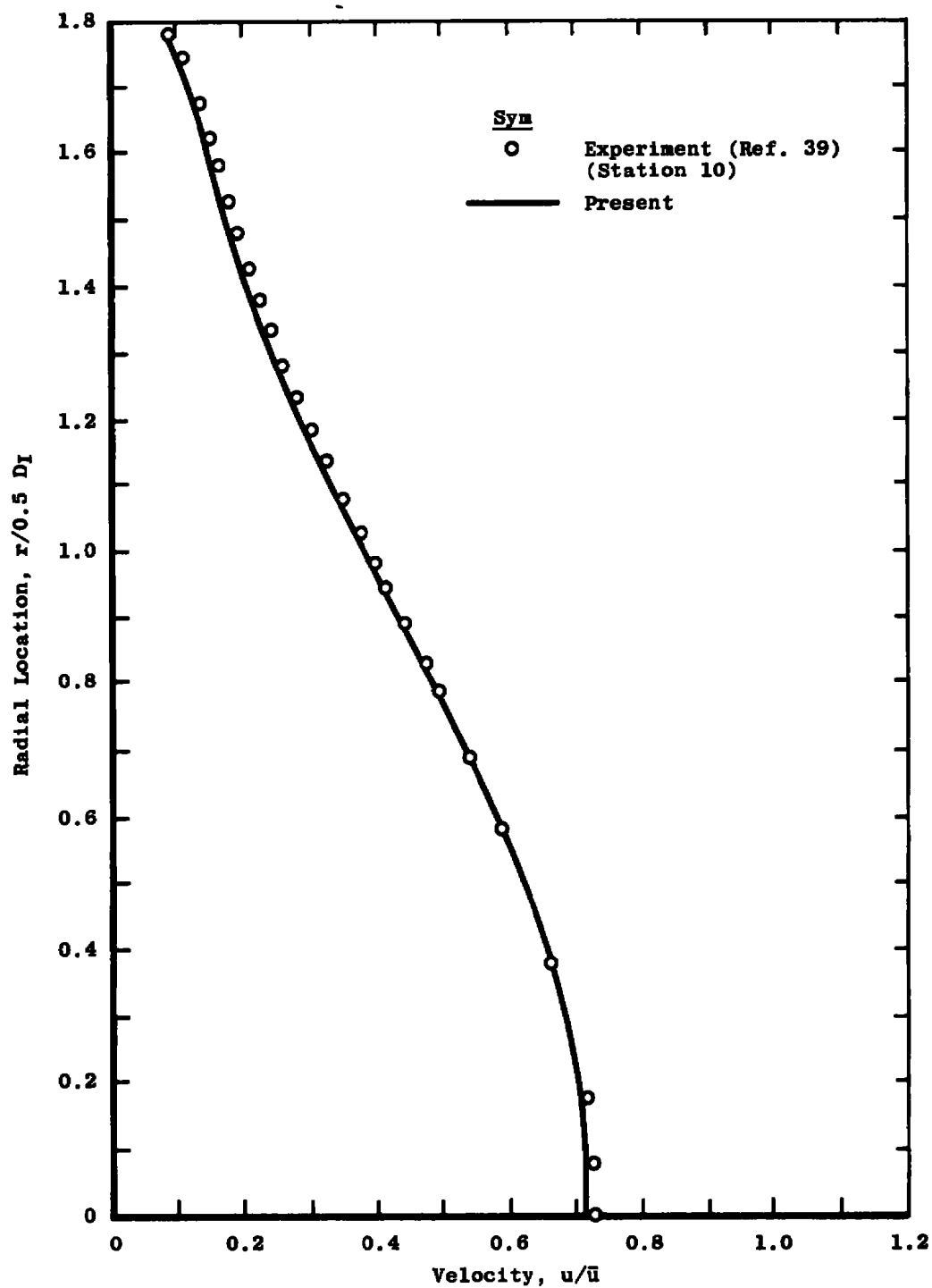distribution and experimental data.

b. $X/D_I = 0.4$
Figure 35. Continued.

c. X/D$_I$ = 4.05
Figure 35. Continued.

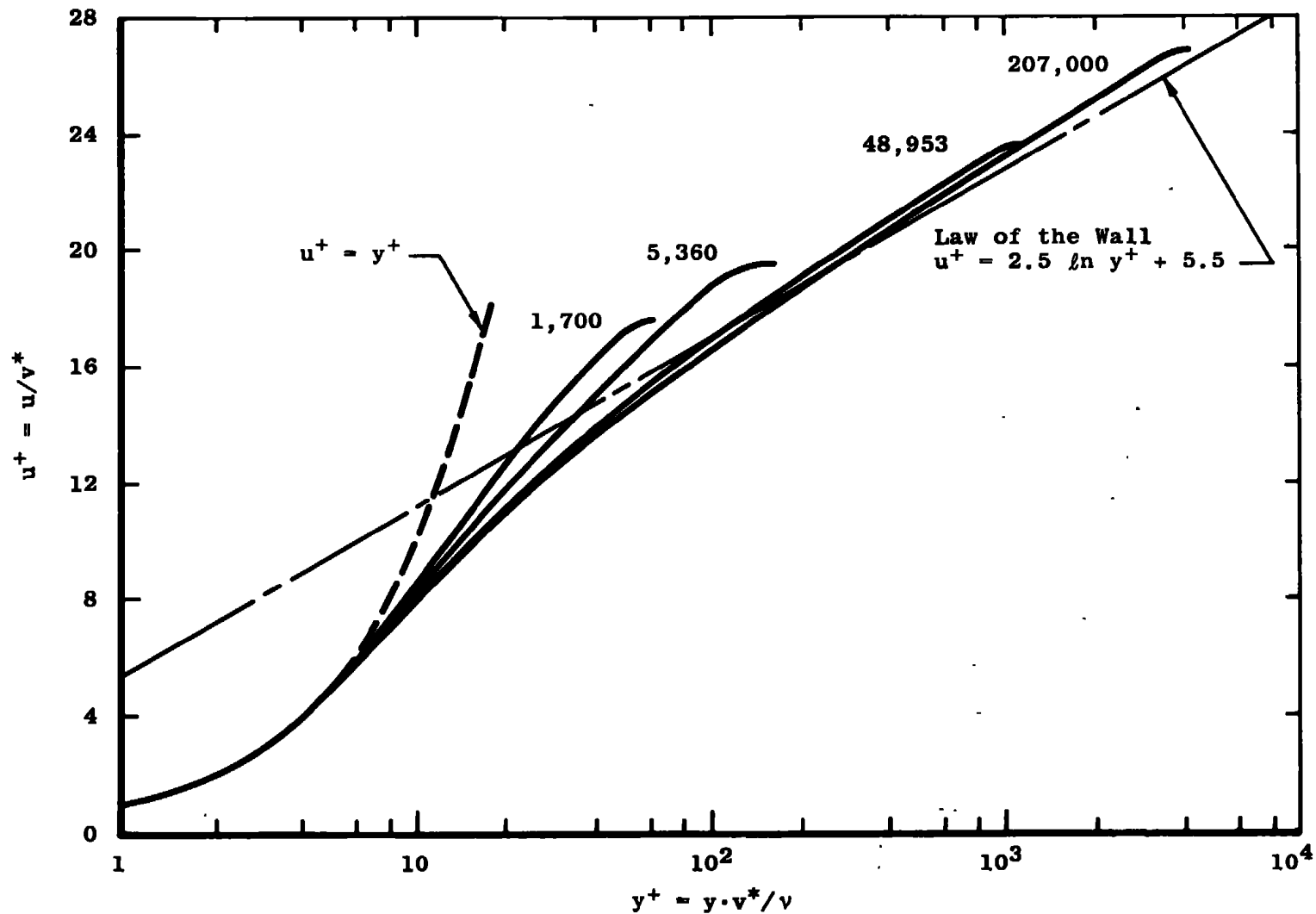d. $X/D_I = 5.95$

Figure 35. Concluded.

Figure 36. Velocity distribution in a fully developed channel flow with a low Reynolds number k-ϵ model.
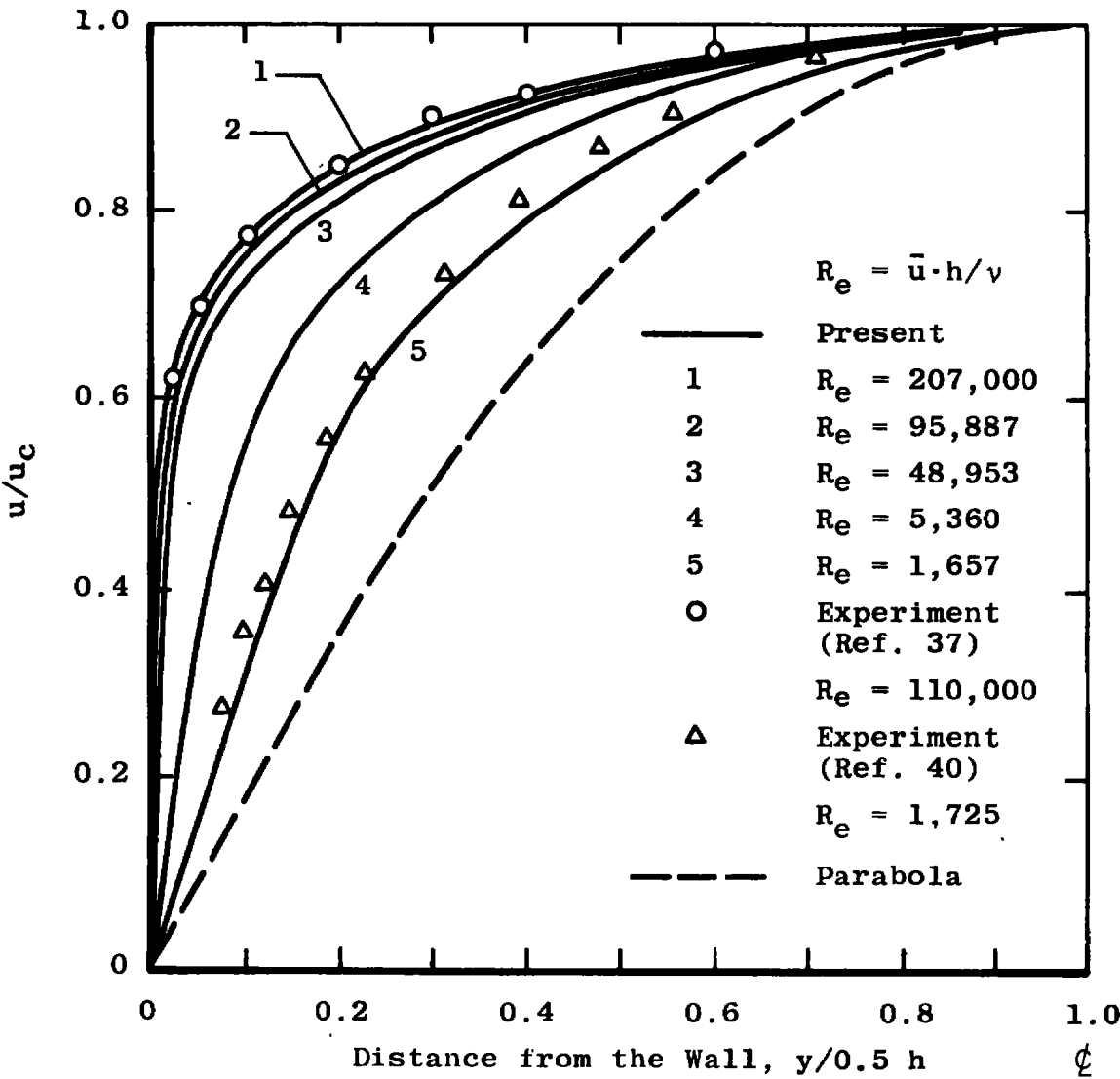
Figure 37. Velocity profiles in a fully developed channel flow.

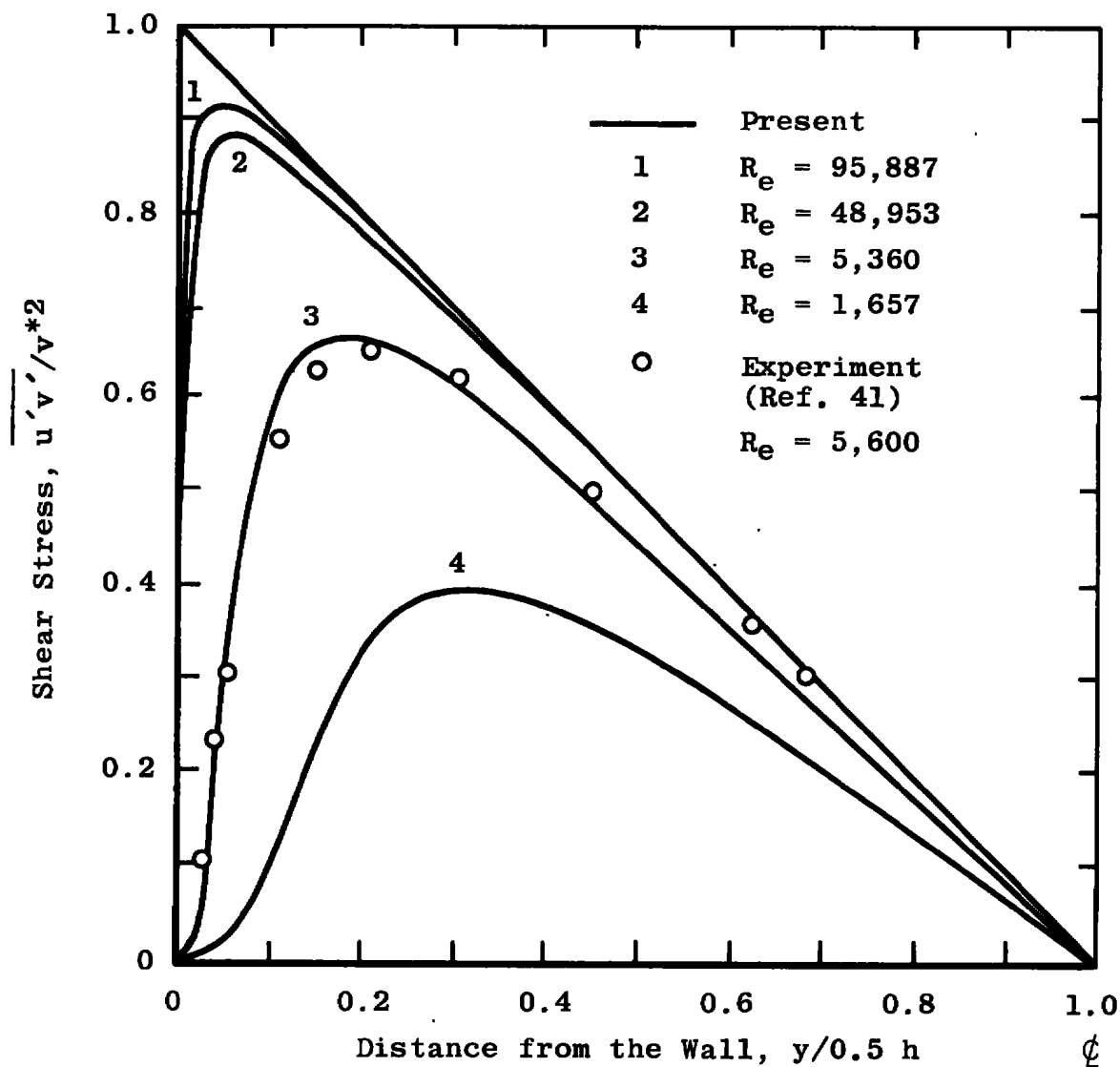Figure 38. Turbulent shear stress distributions in a fully developed channel flow.

101
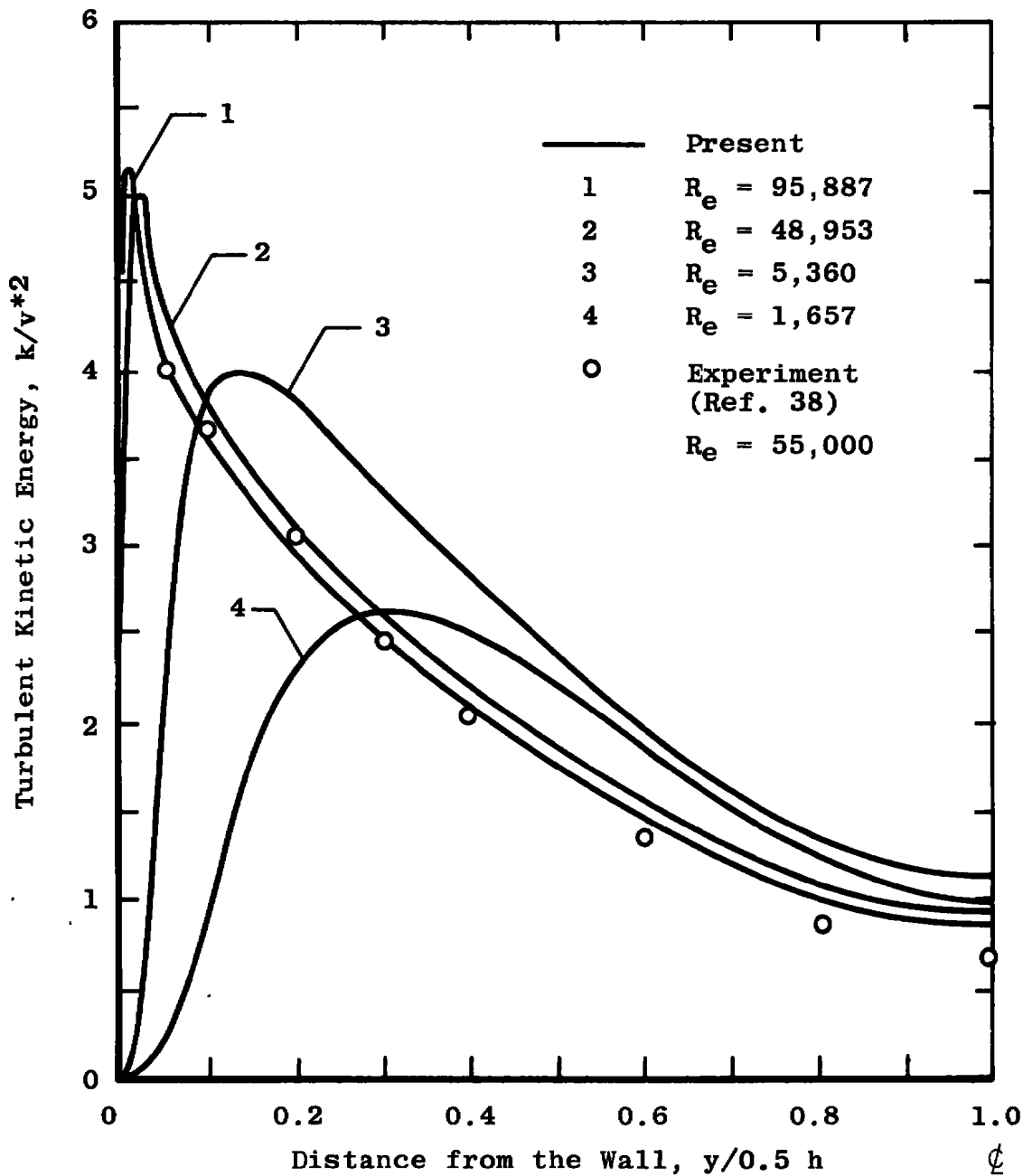
Figure 39. Turbulent kinetic energy distributions in a fully developed channel flow.
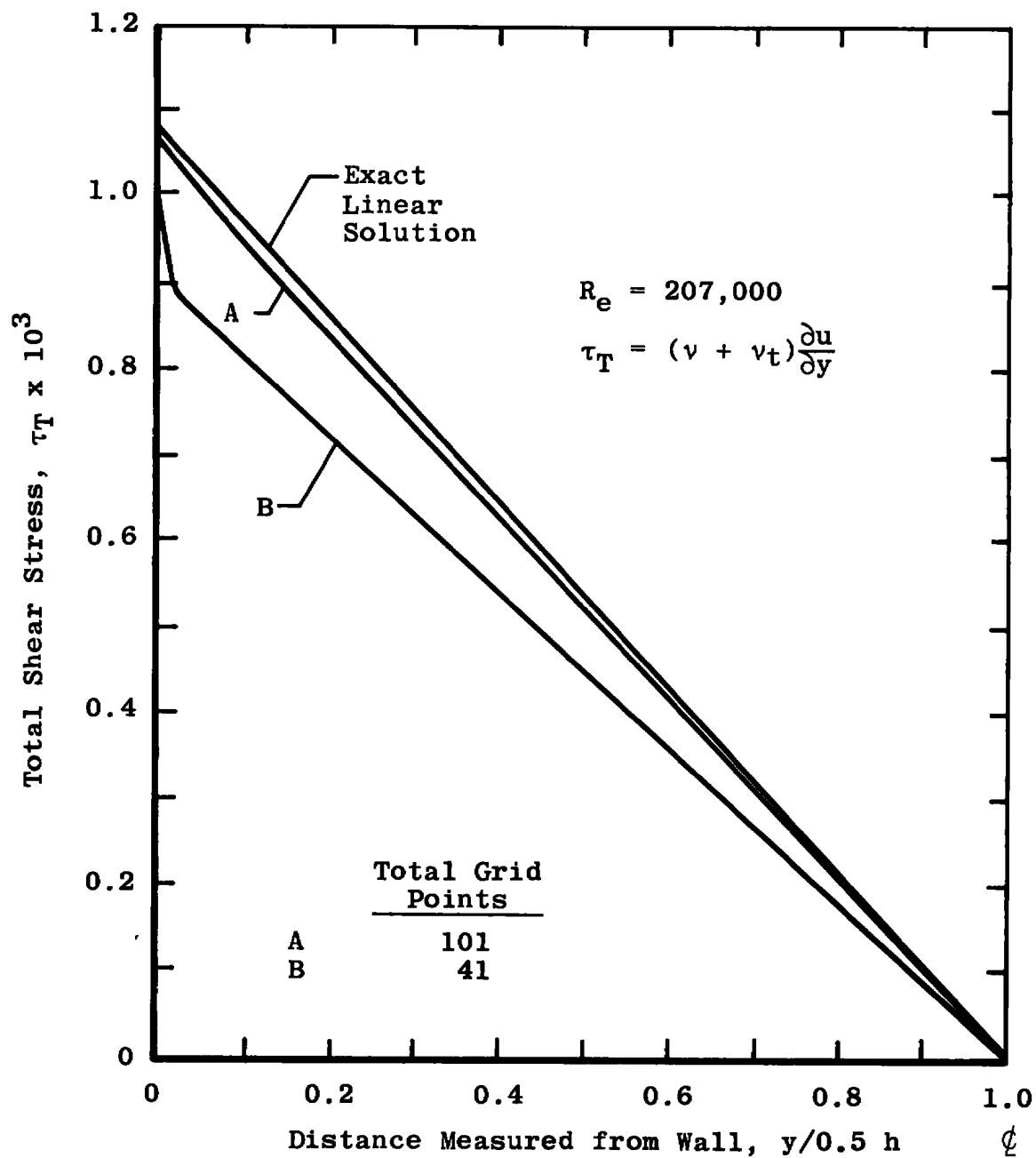
Figure 40. Effect of the total number of grid points on the total
shear stress distribution in a fully developed channel flow.
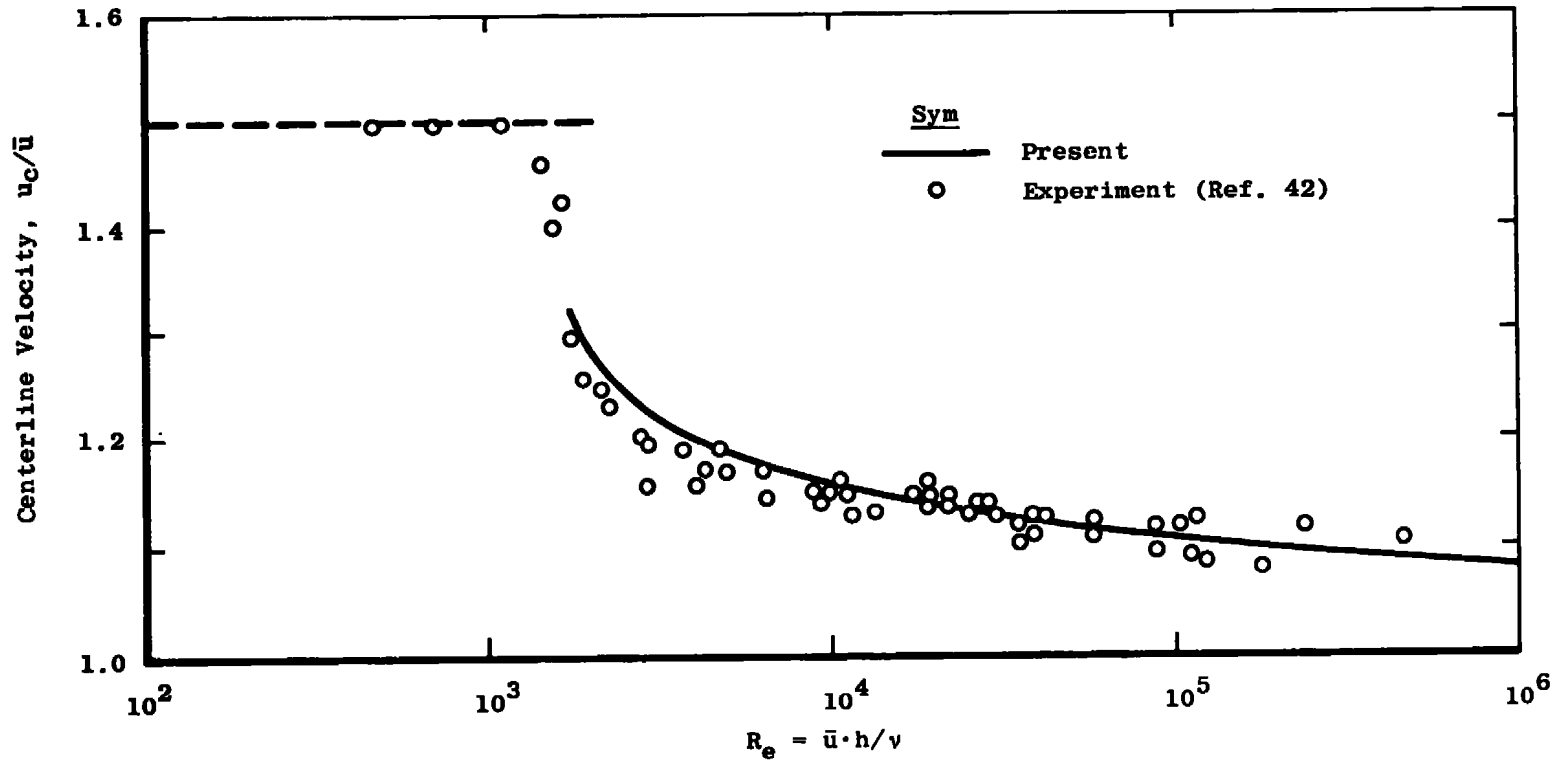
Figure 41. Comparison between the calculated and experimental centerline
velocities in a fully developed channel flow.
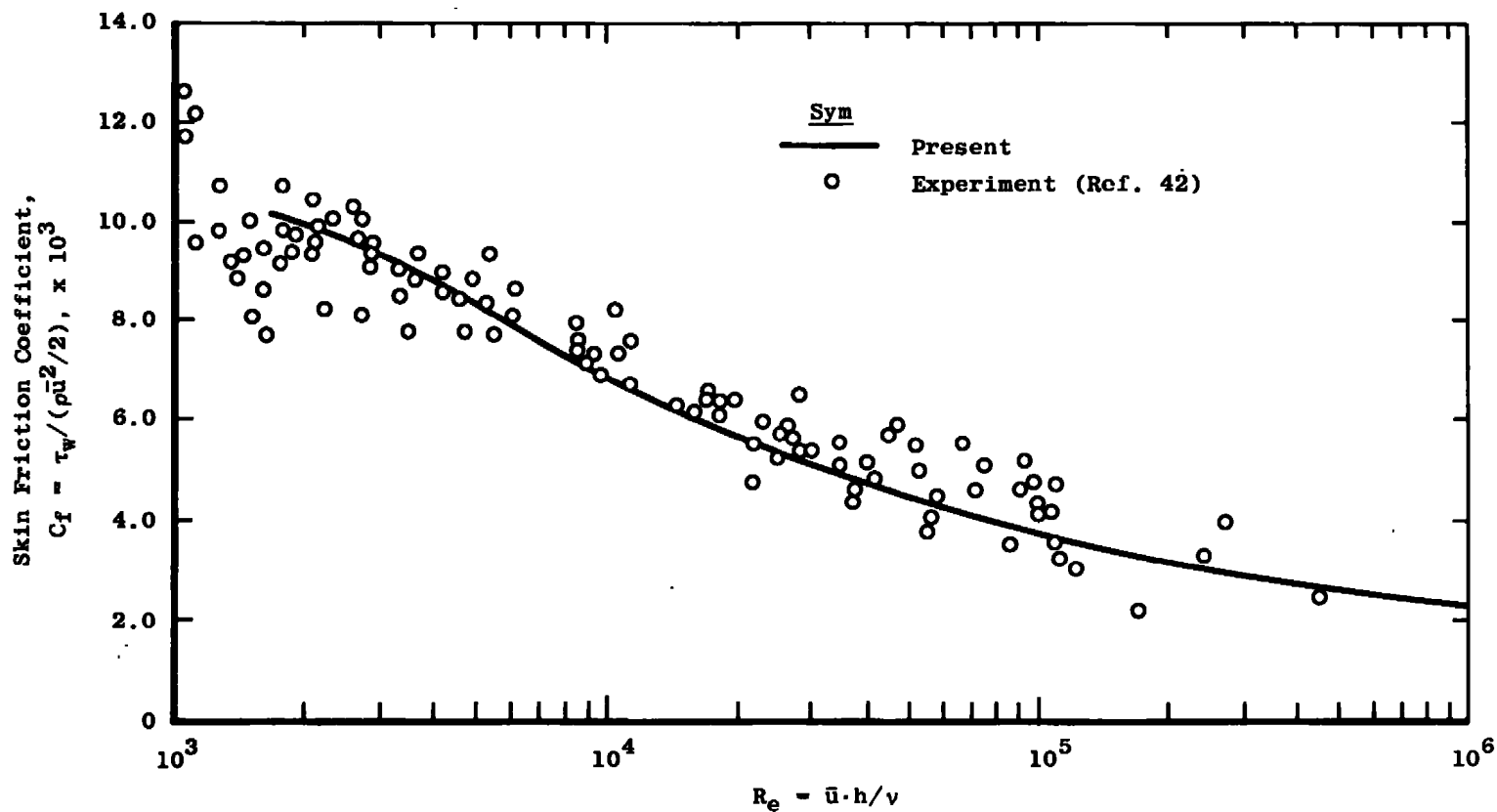
Figure 42. Comparison between the calculated and experimental skin friction coefficient in a fully developed channel flow.
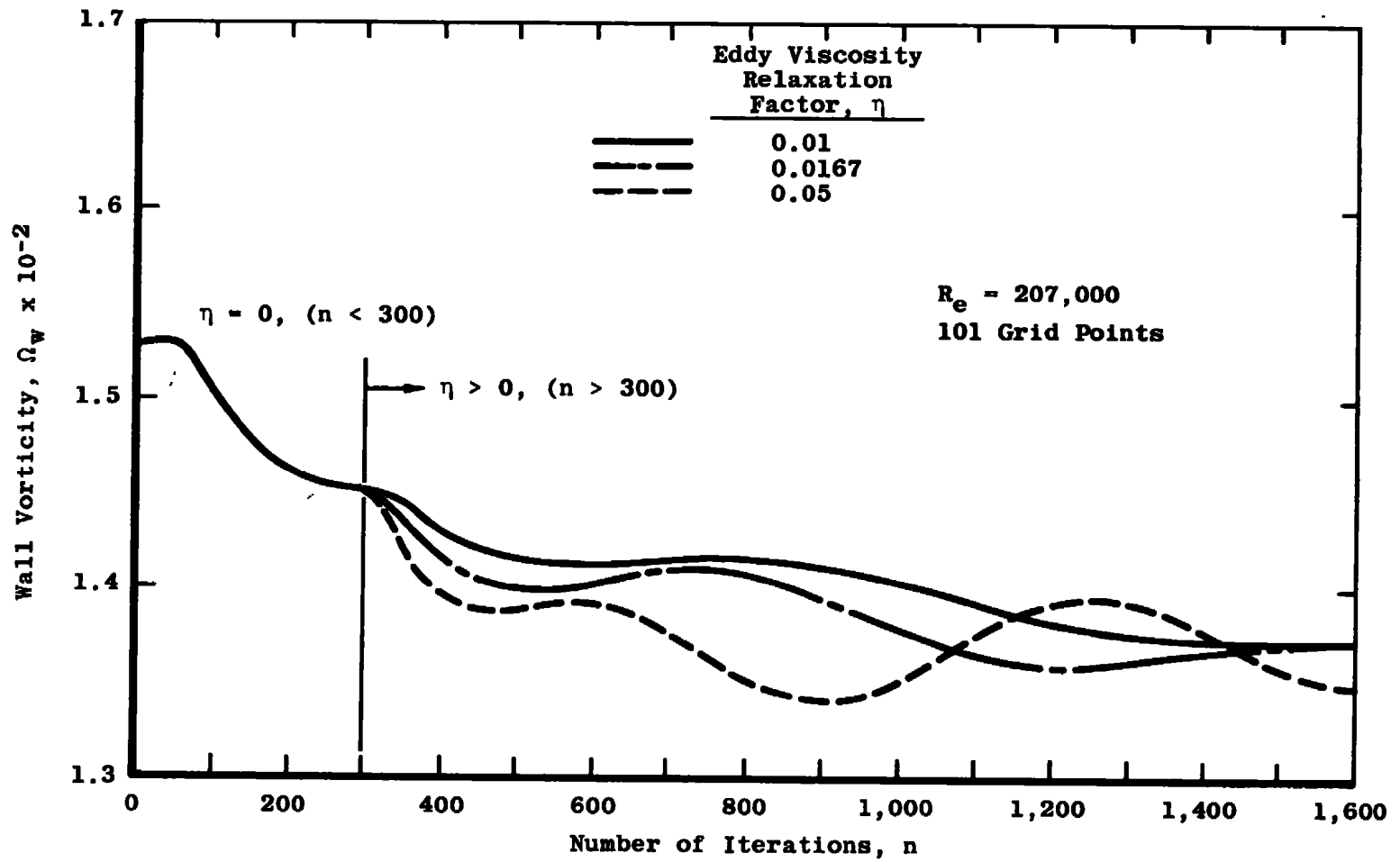
Figure 43. Effect of viscosity relaxation on the convergence of the
wall vorticity.
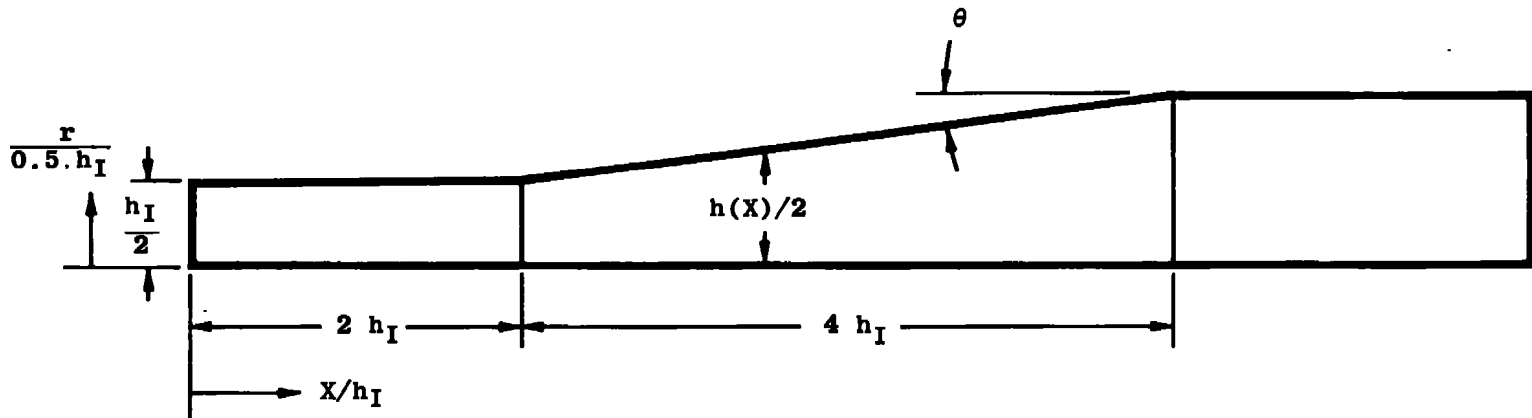
Figure 44. A 2-D planar diffuser with a 4:1 aspect ratio.
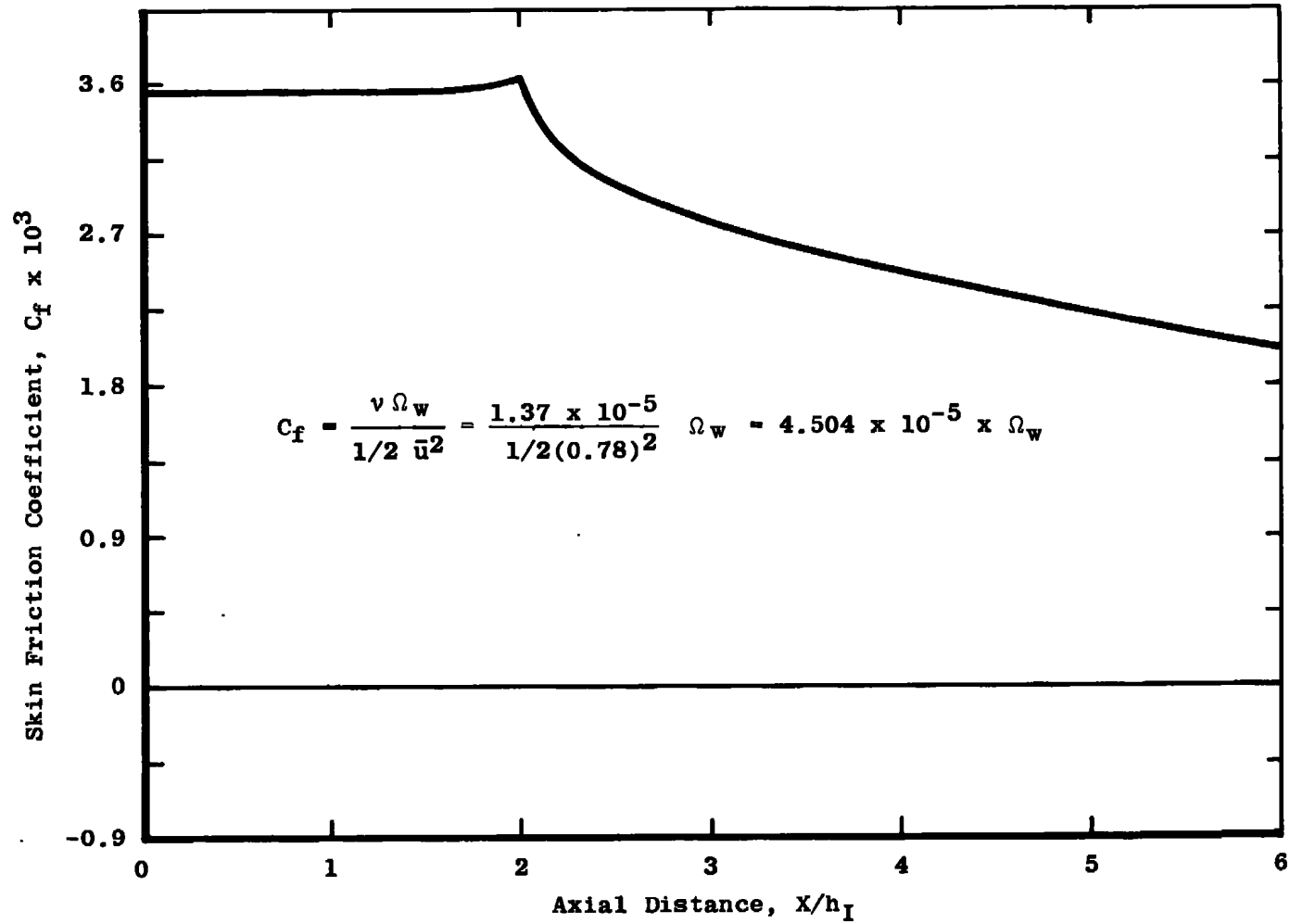
a. $2\theta = 3.58$ deg

Figure 45. Skin friction coefficient in a 2-D diffuser flow.

b. 2 θ = 7.15 deg
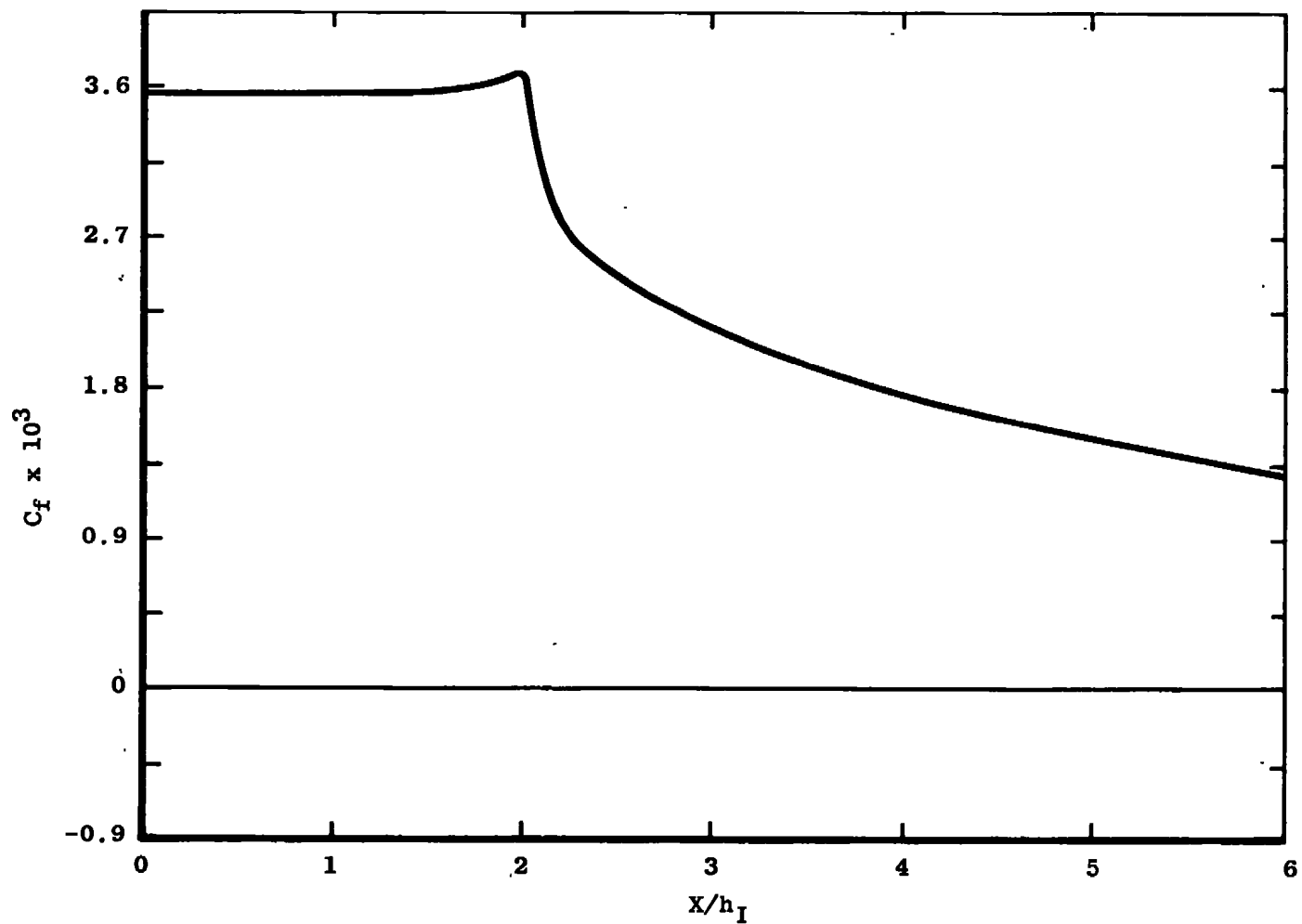
Figure 45. Continued.
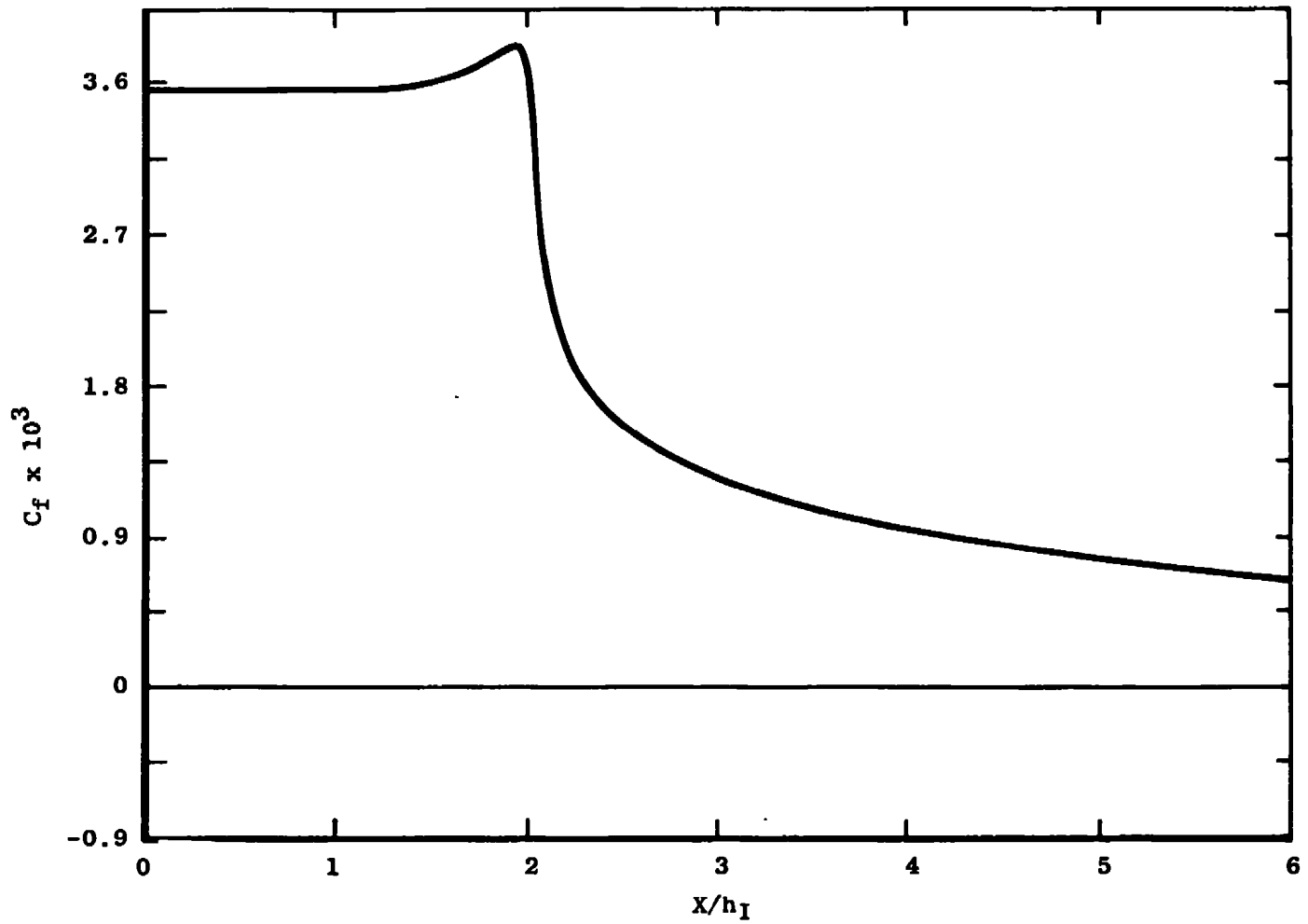
c. $2\theta = 14.25$ deg

Figure 45. Continued.

s.p.: Separation Point

s.p.
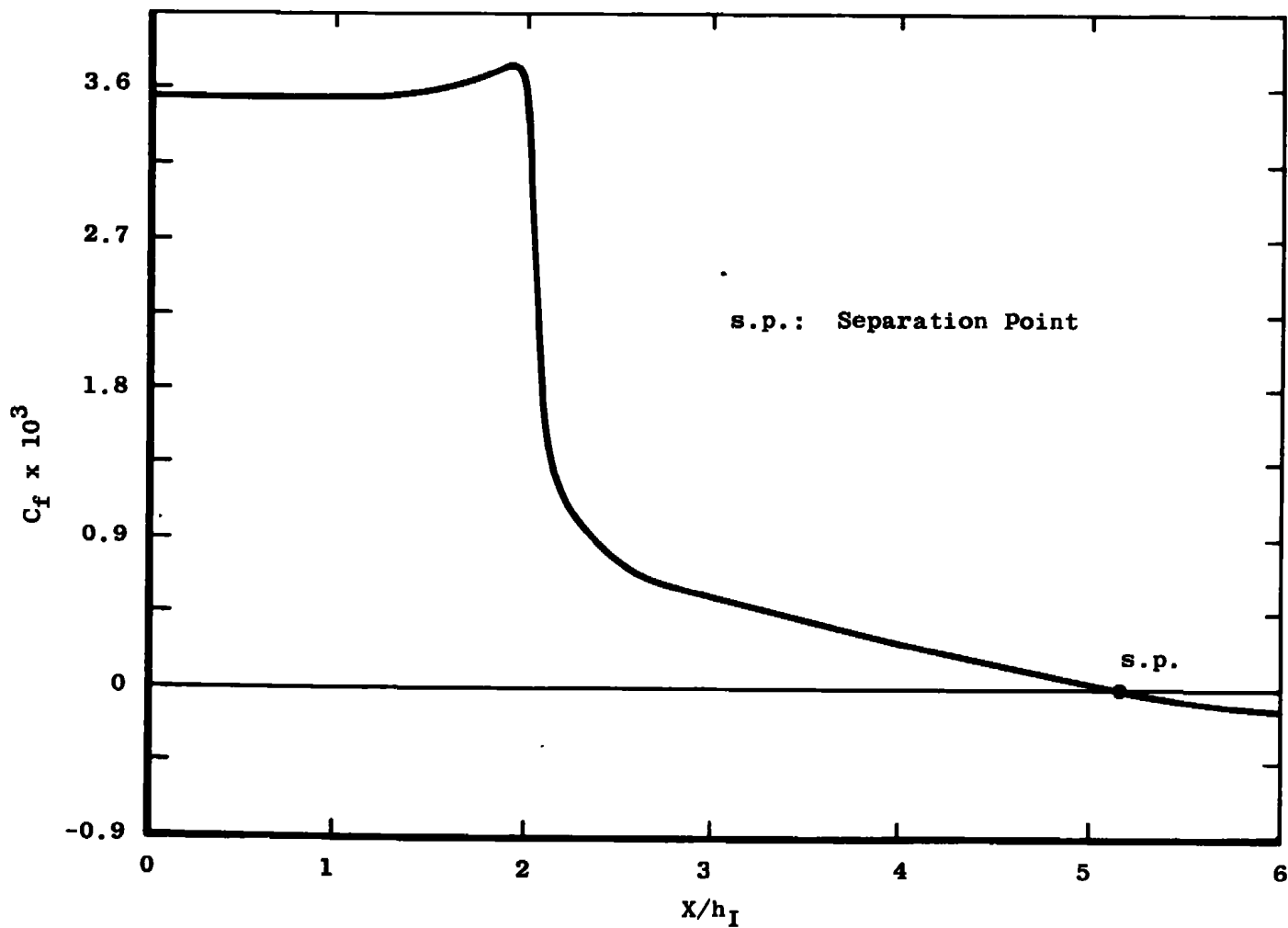
d. $2\theta = 21.2$ deg

Figure 45. Continued.
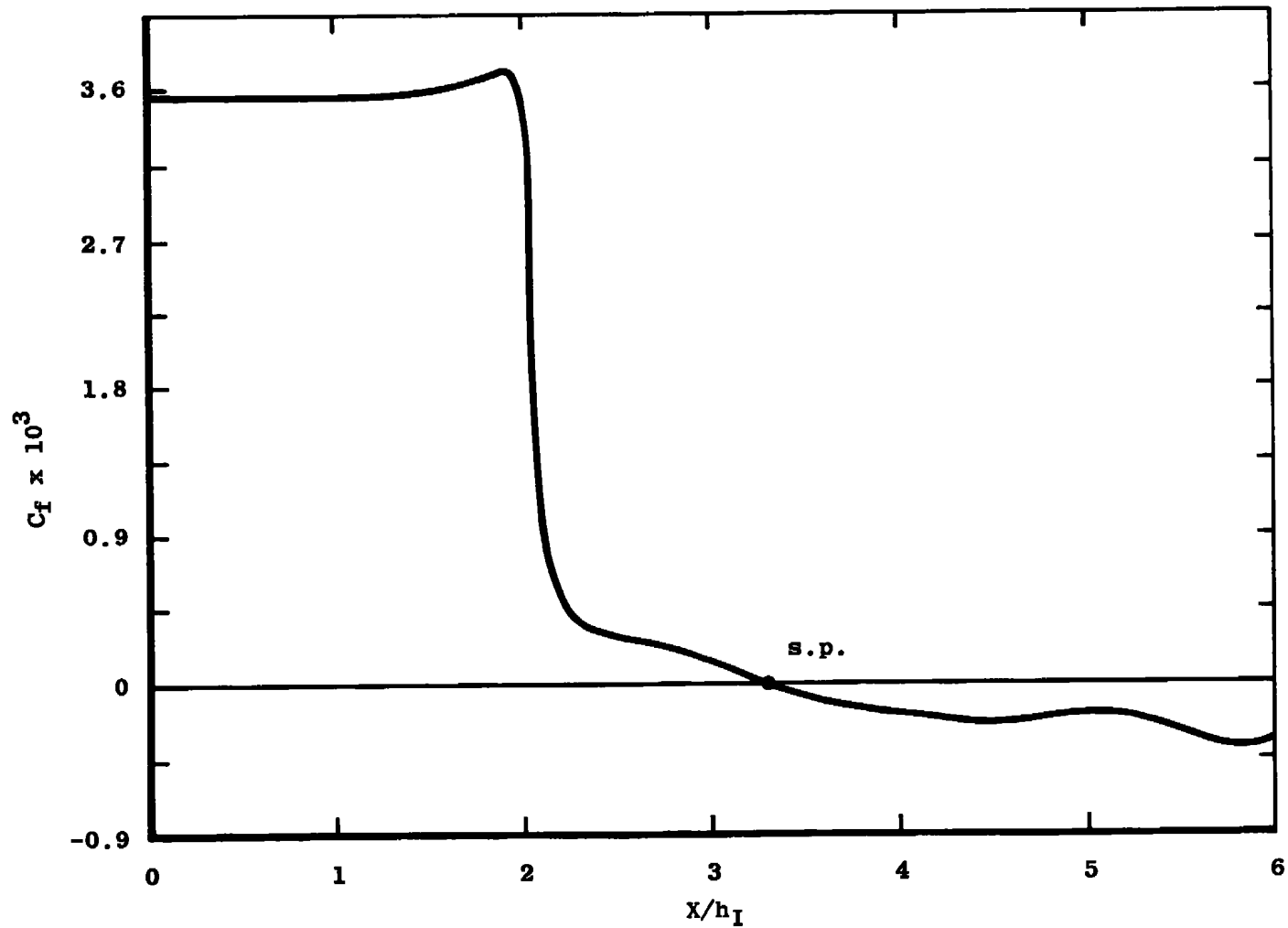
e. $2\theta = 28.1$ deg
Figure 45. Continued.
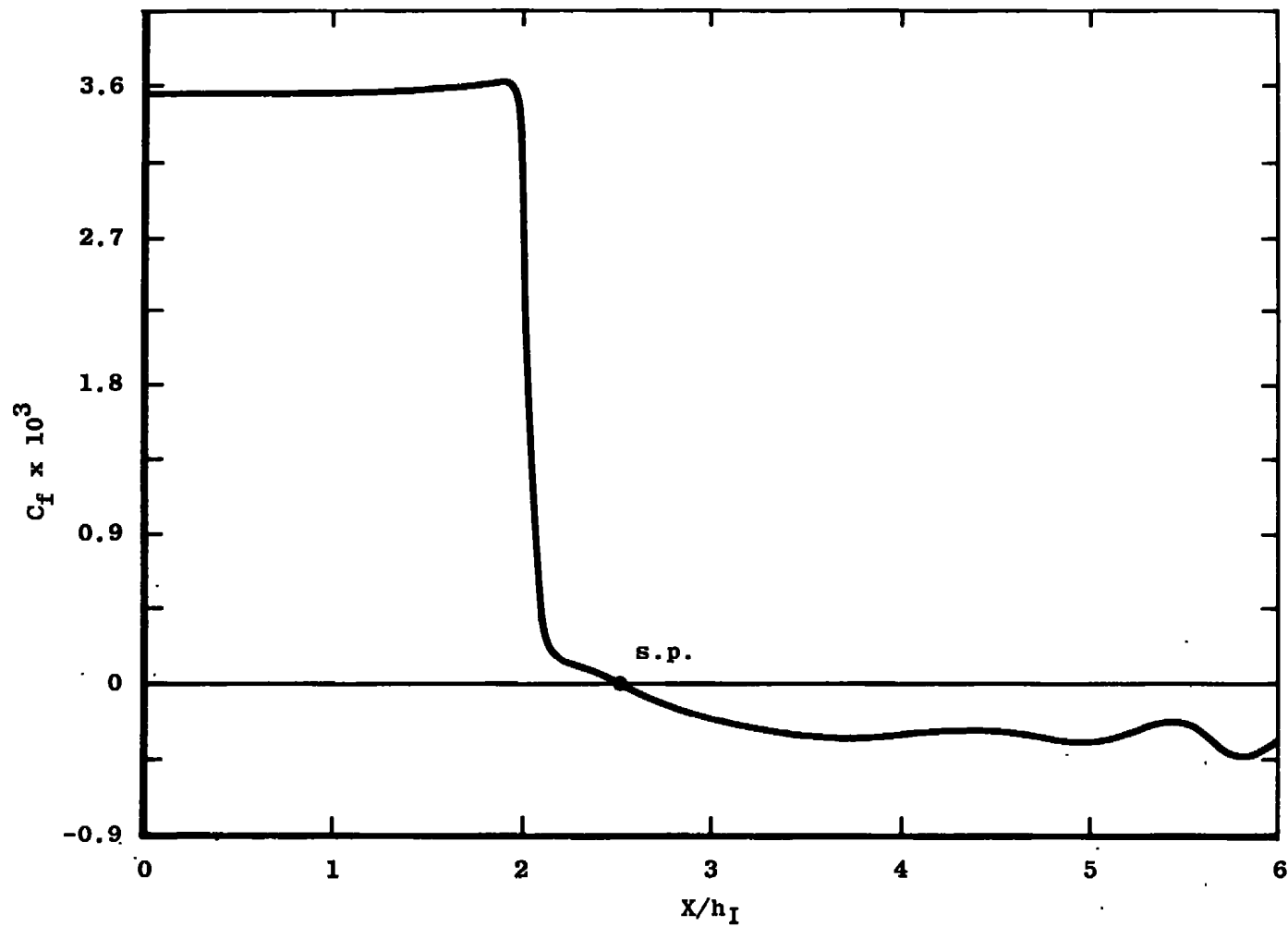
f. $2\theta = 34.7$ deg
Figure 45. Concluded.
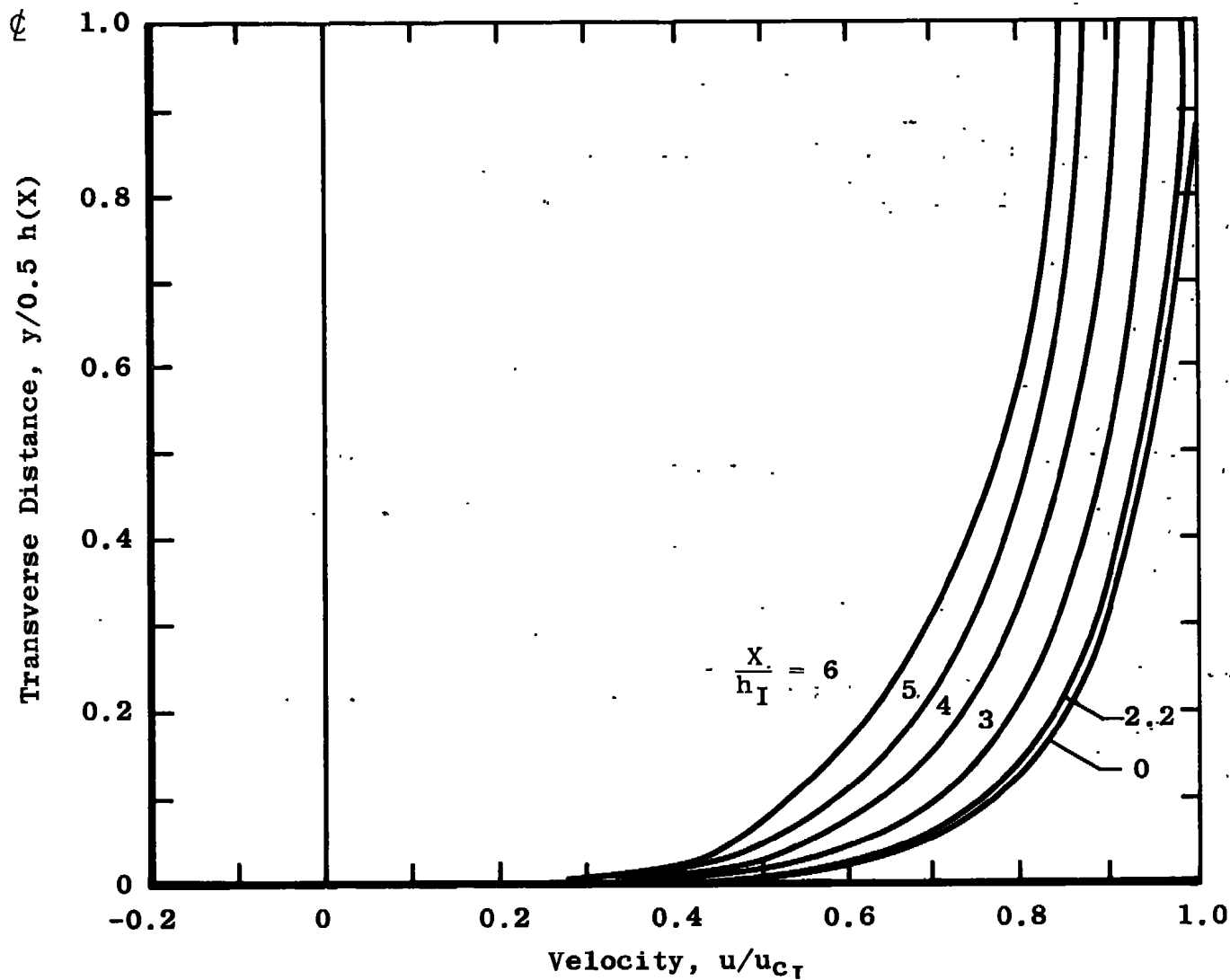
a. 2 θ = 3.58 deg

Figure 46. Velocity distribution in a 2-D diffuser.
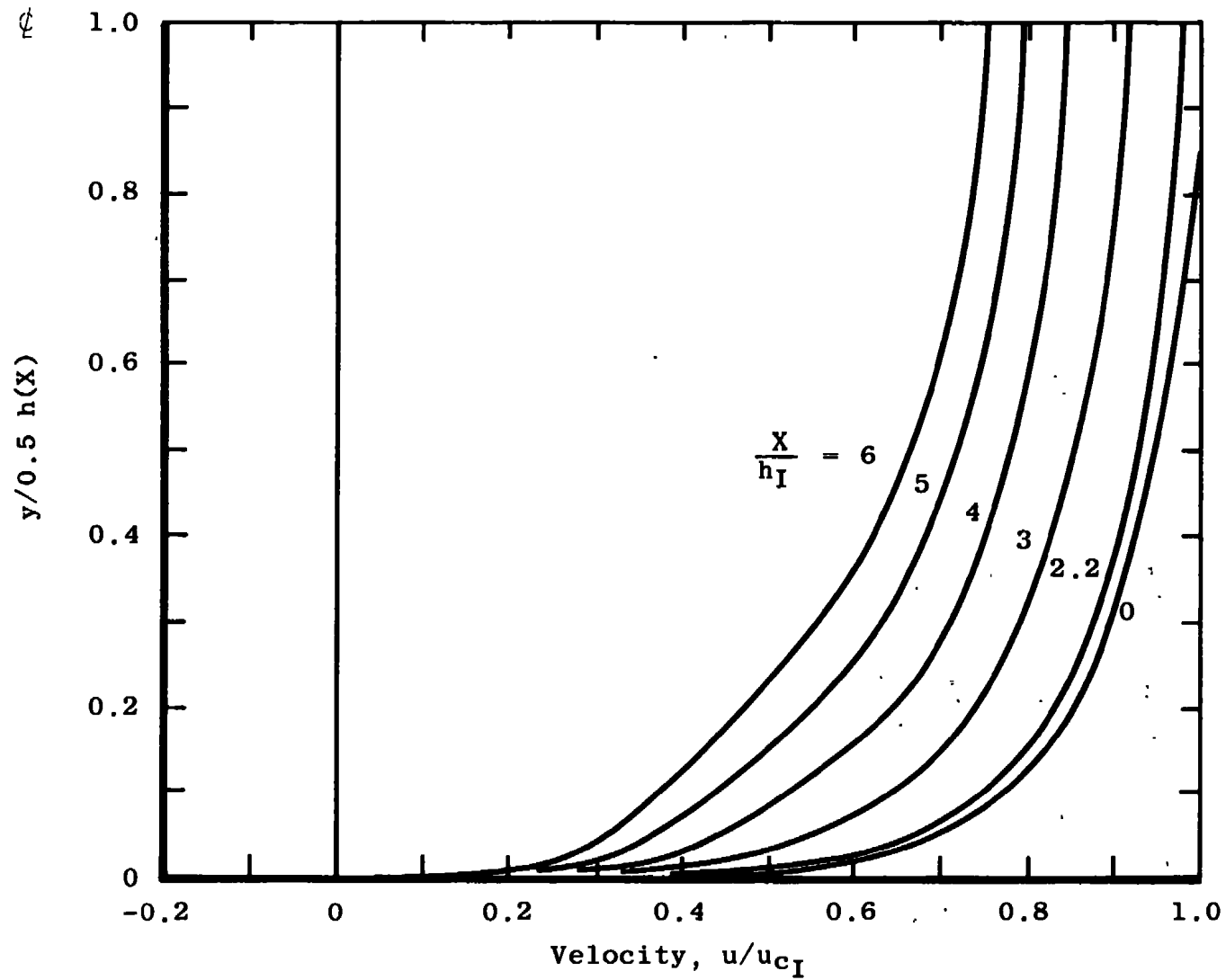
b. $2\theta = 7.15$ deg

Figure 46. Continued.
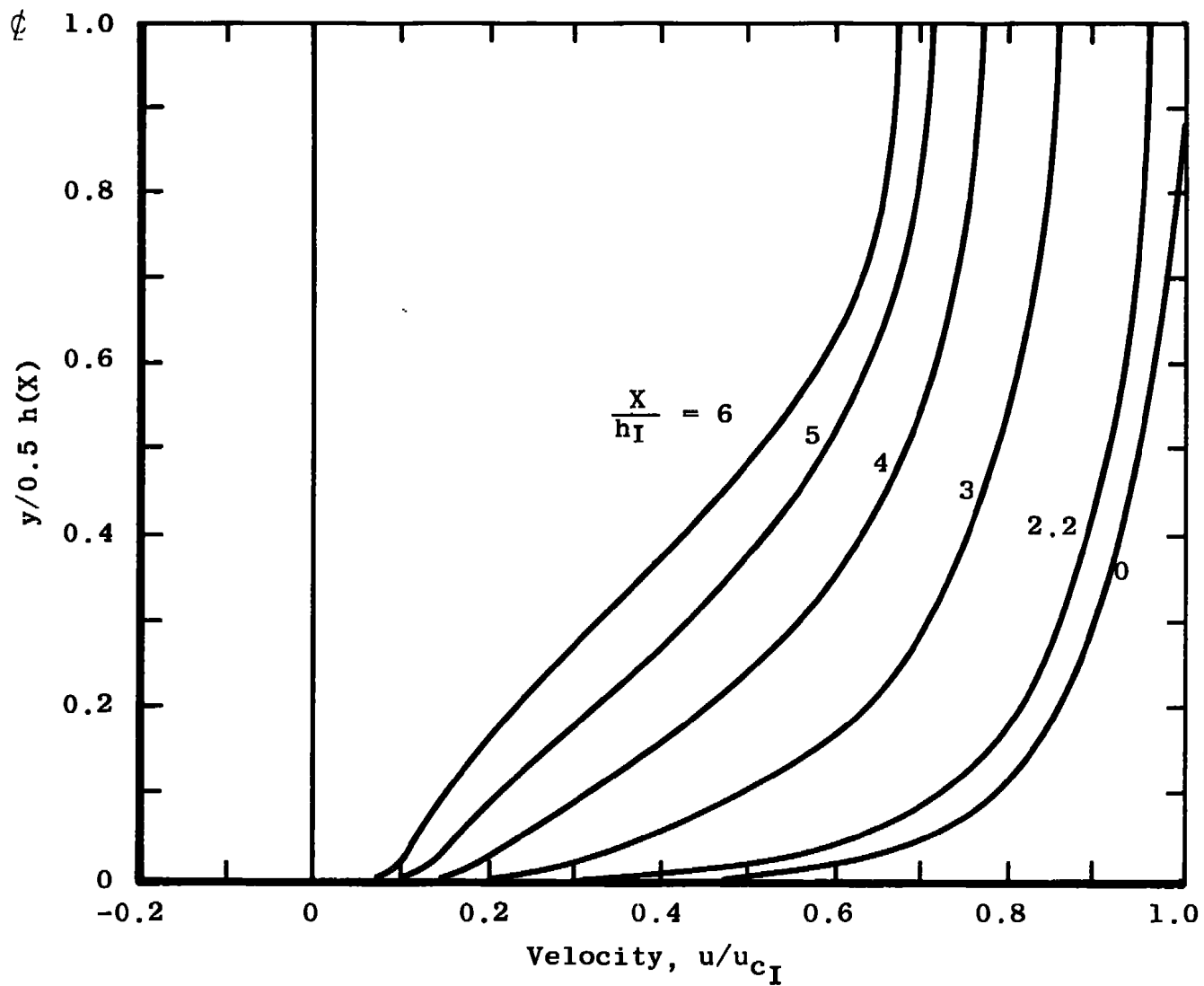
c. $2\theta = 14.25$ deg

Figure 46. Continued.
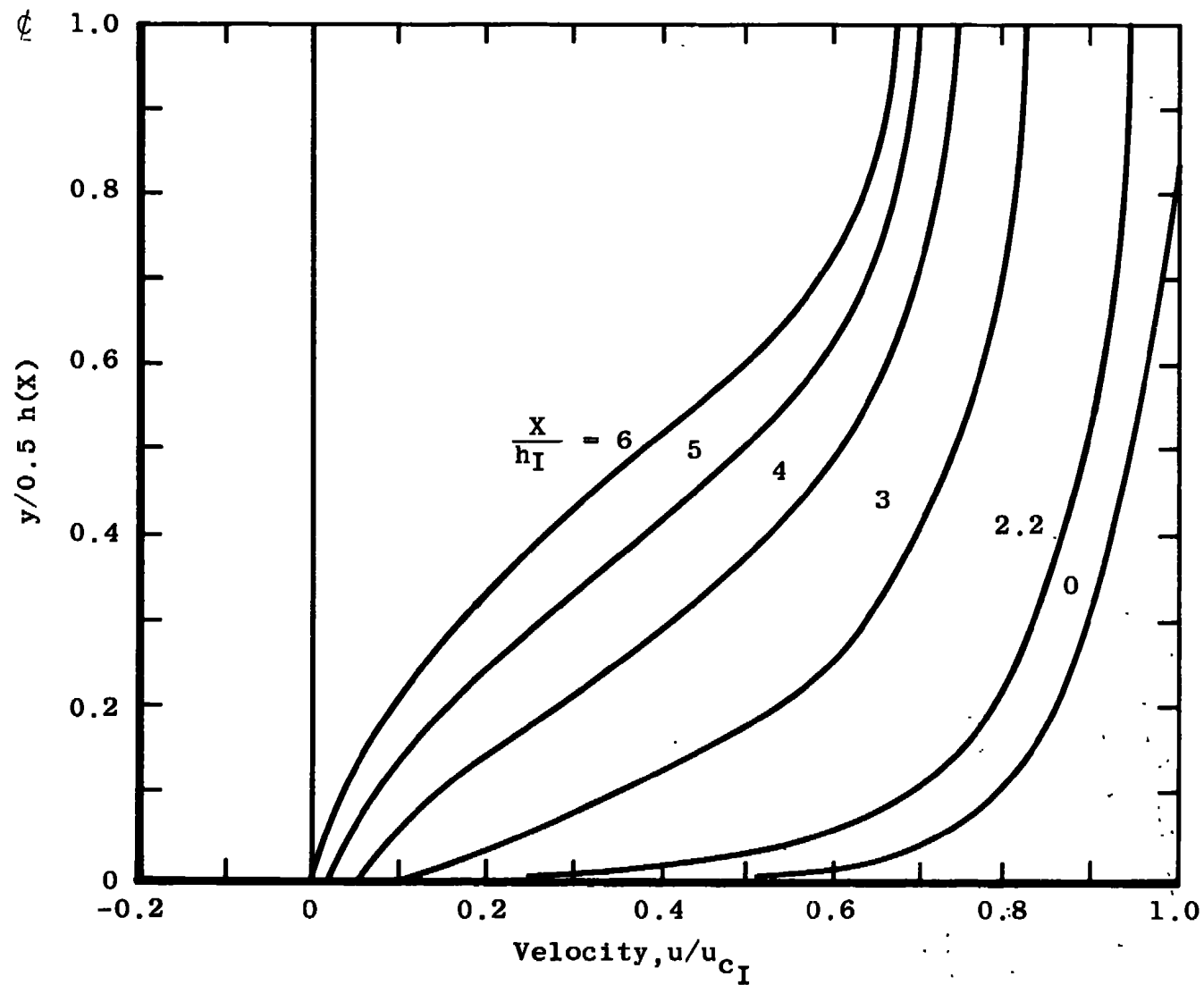
d. $2\theta = 21.2$ deg

Figure 46. Continued.
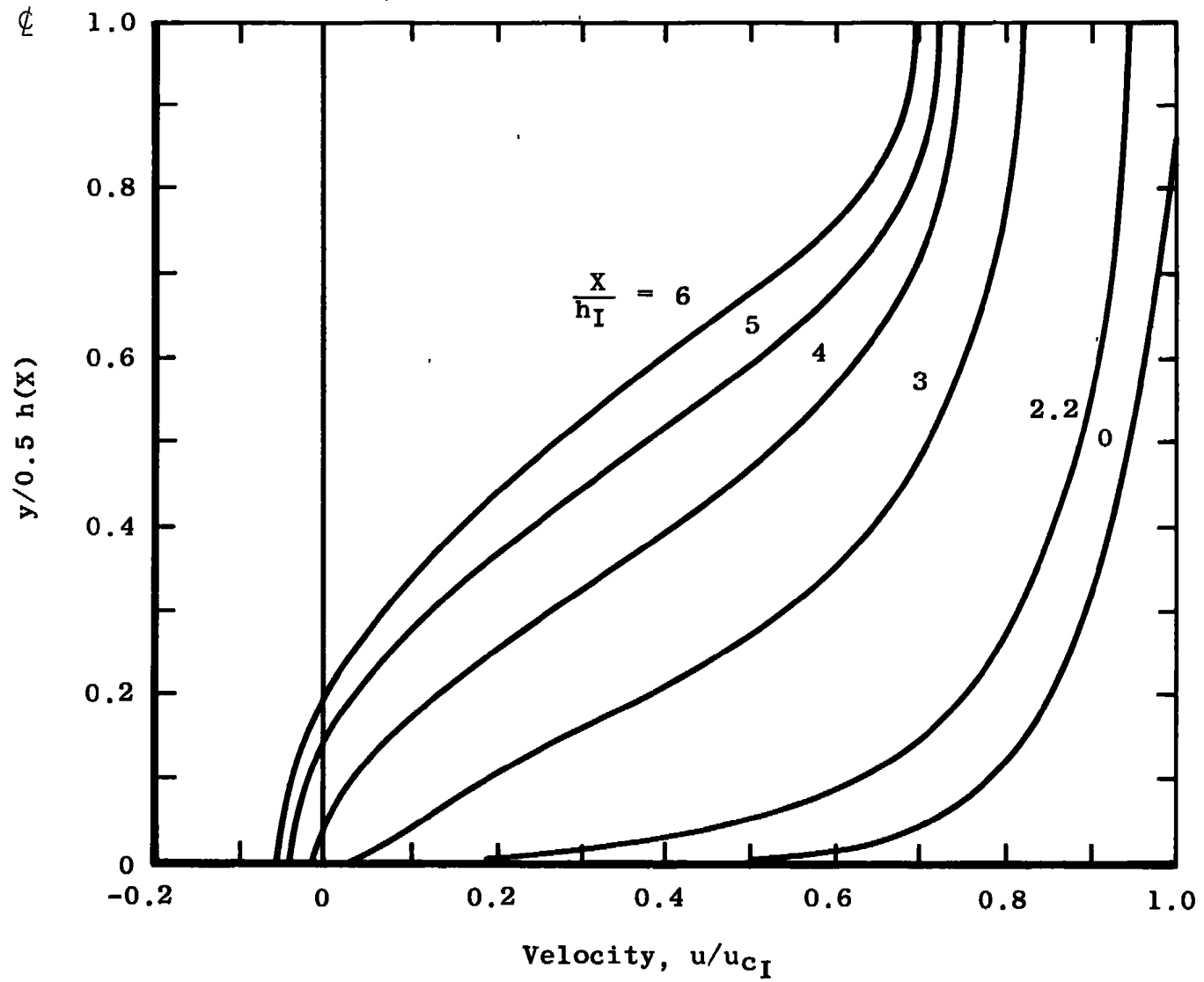
e. $2\theta = 28.1$ deg

Figure 46. Continued.
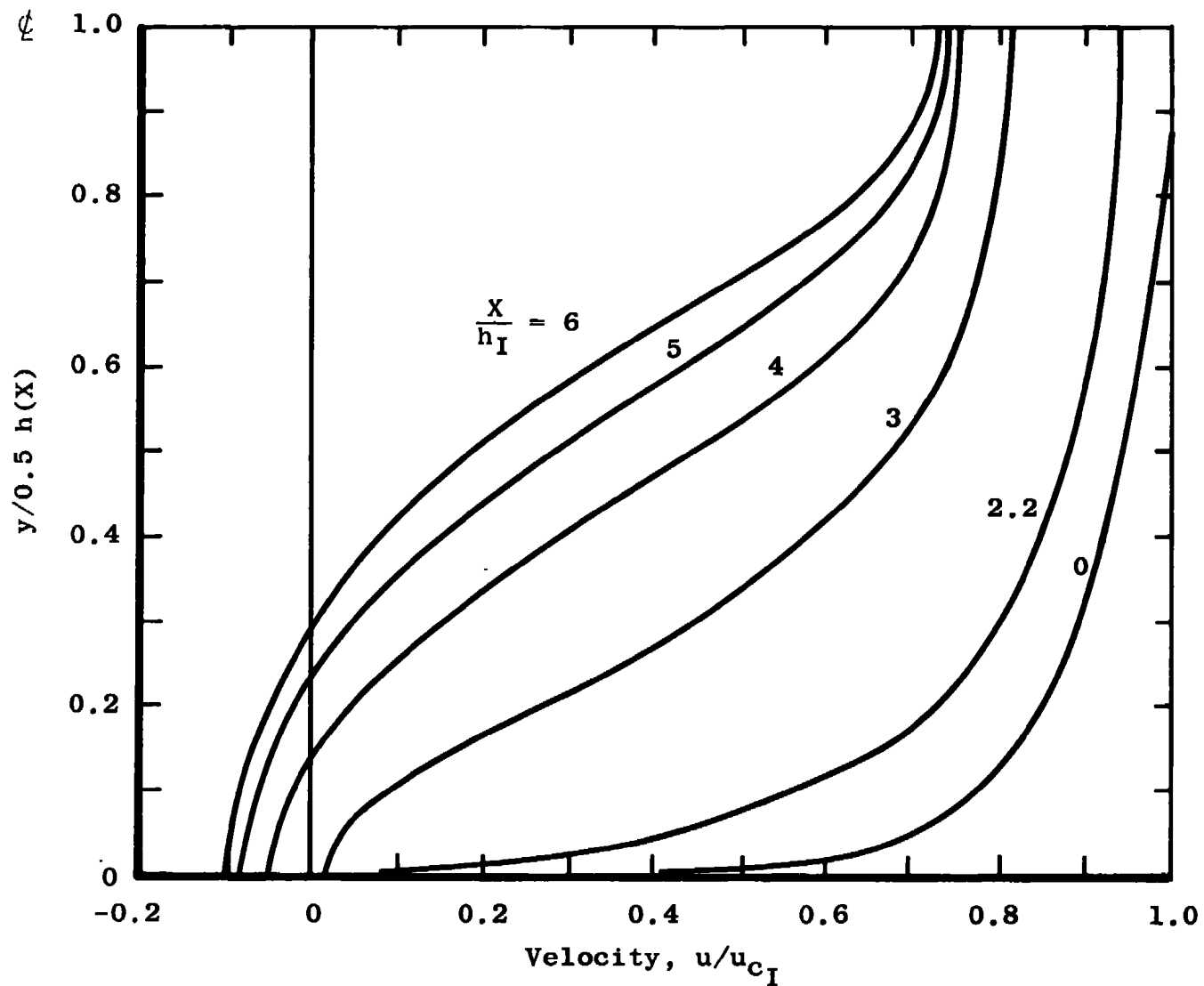
f. $2\theta = 34.7$ deg

Figure 46. Concluded.
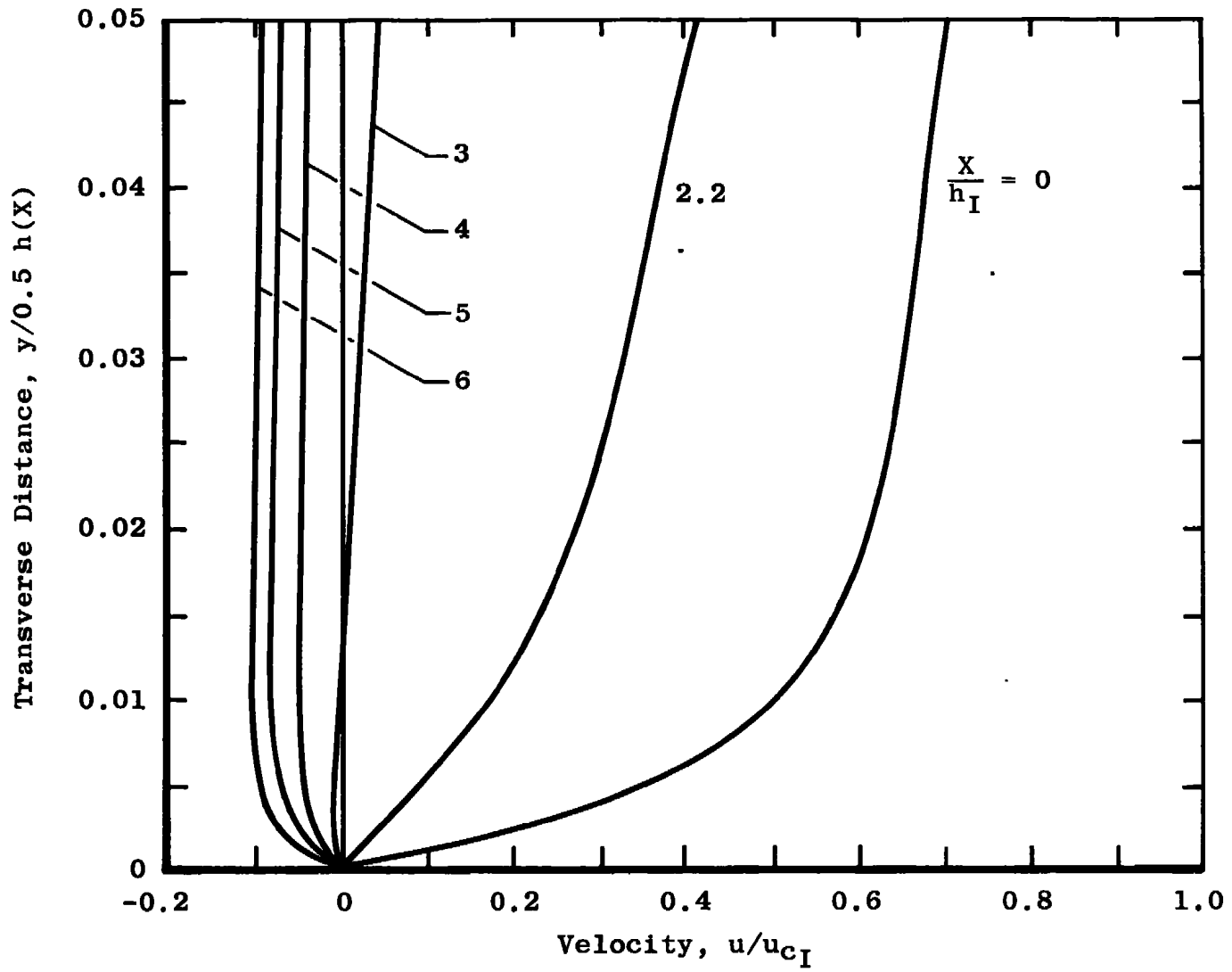
Figure 47. Sublayer velocity distribution, (2 θ = 34.7 deg).
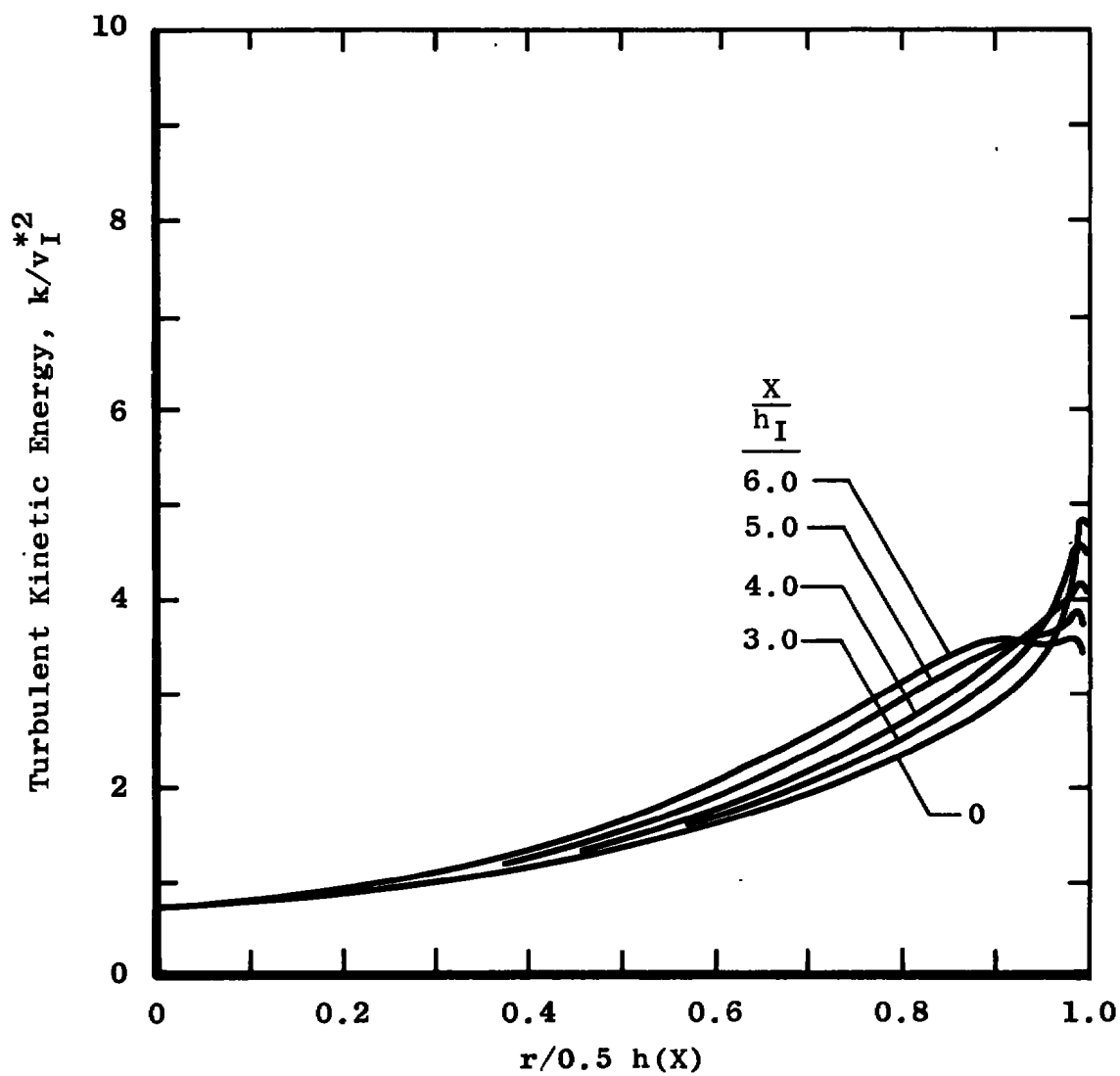
a. $2\theta = 3.58$ deg

Figure 48. Turbulent kinetic energy distribution in a 2-D diffuser.
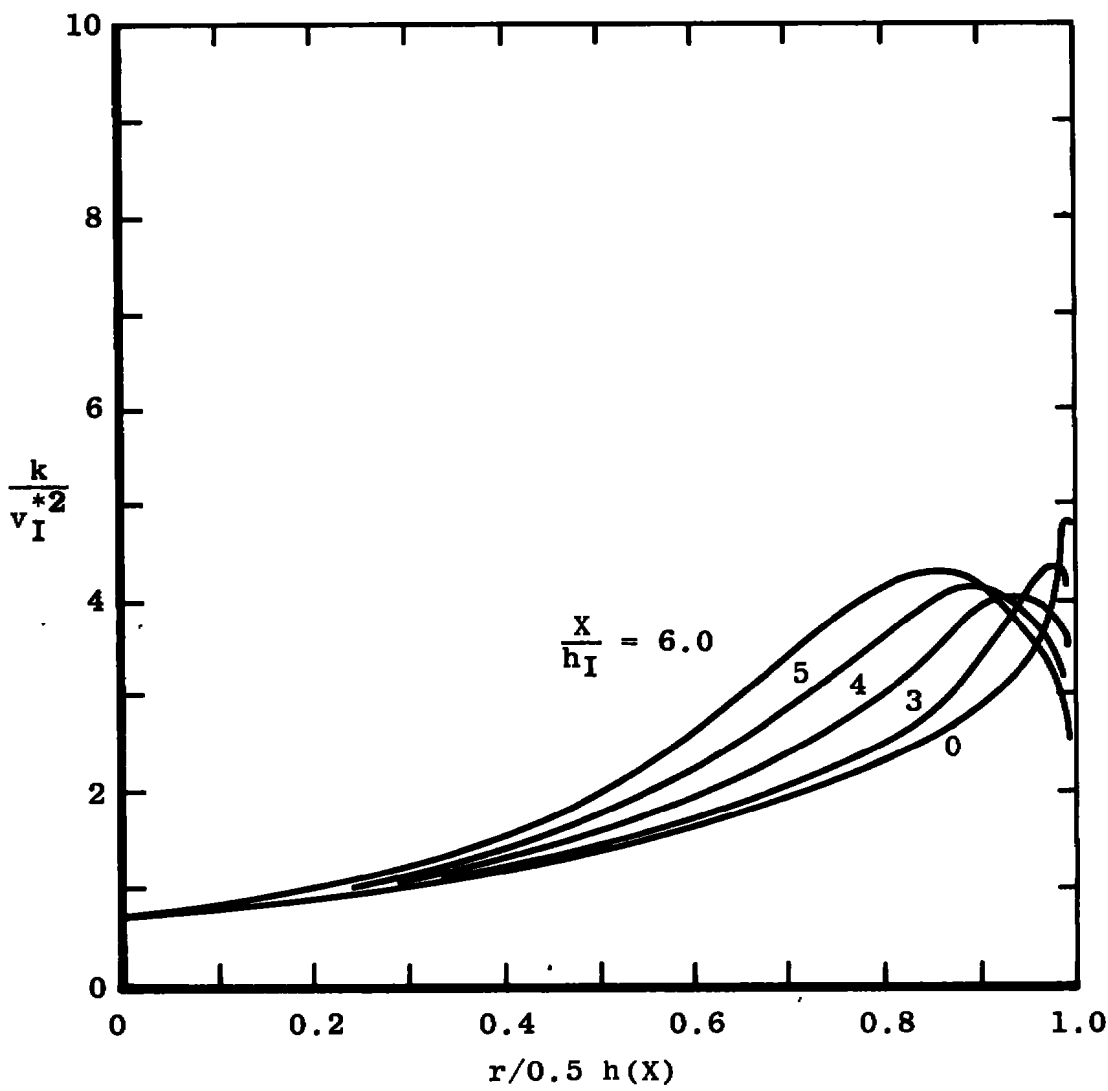
b. $2\theta = 7.15$ deg

Figure 48. Continued.
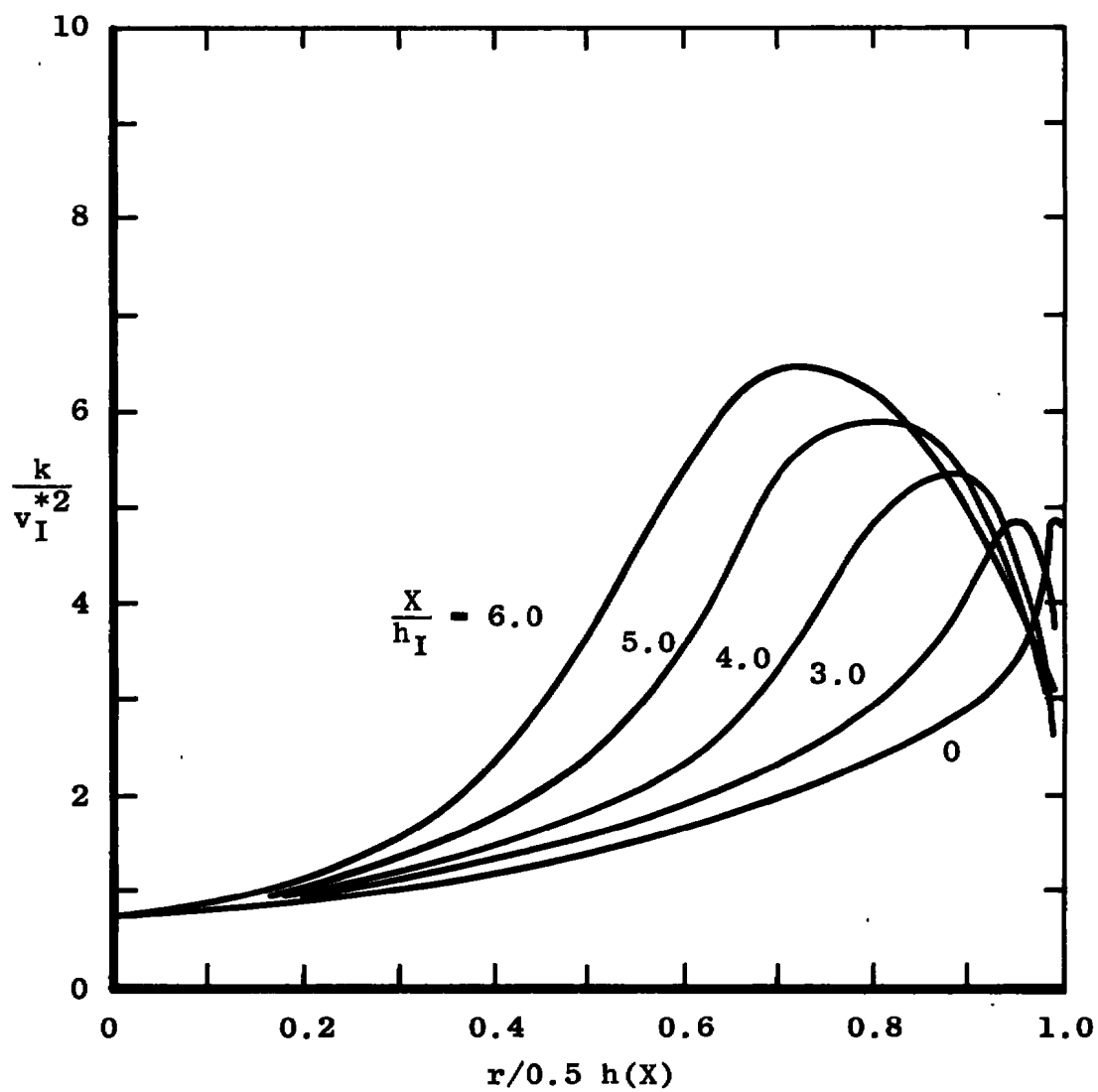
c. 2 θ = 14.25 deg
Figure 48. Continued.
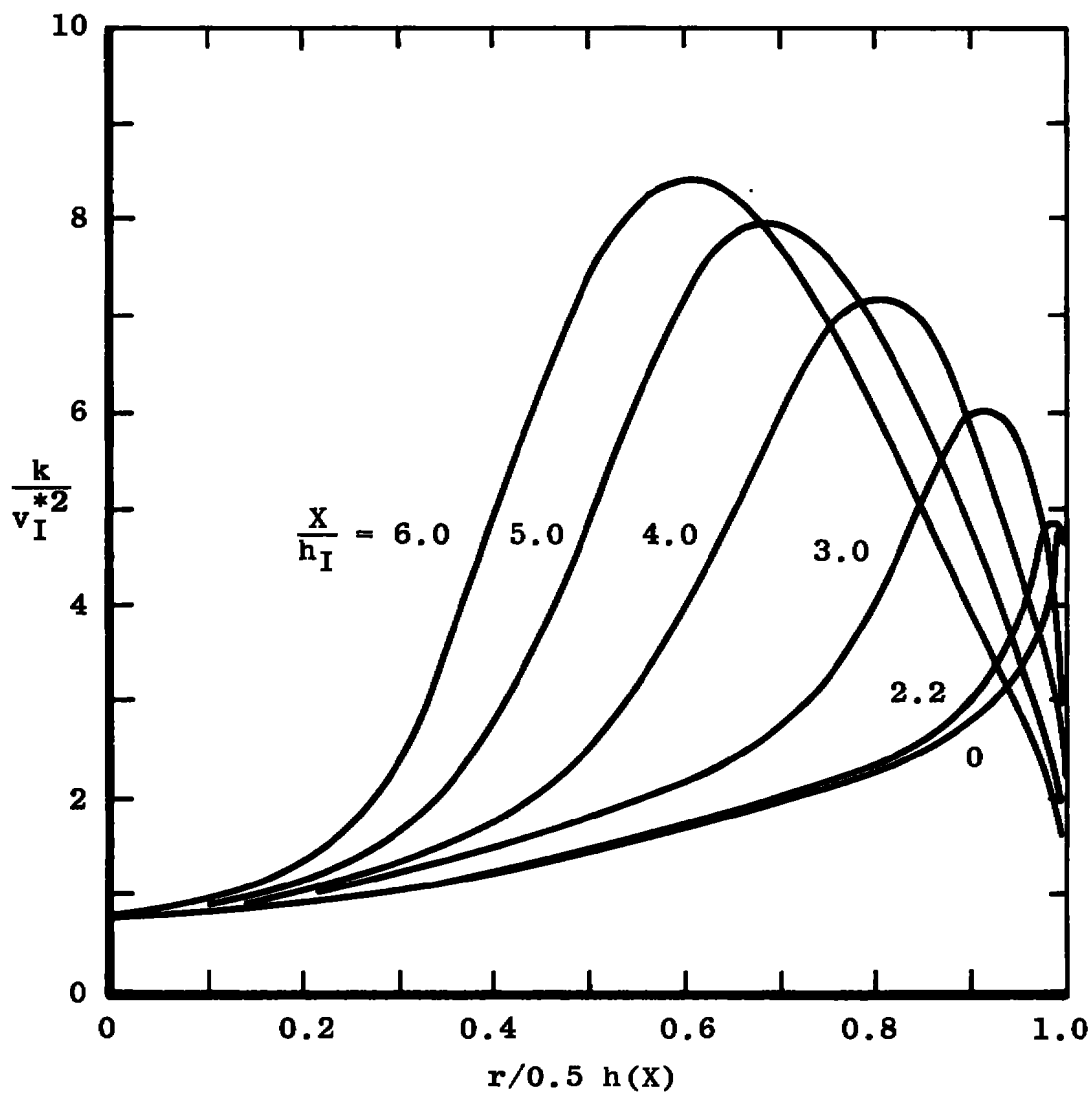
d. $2\theta = 21.2$ deg
Figure 48. Continued.
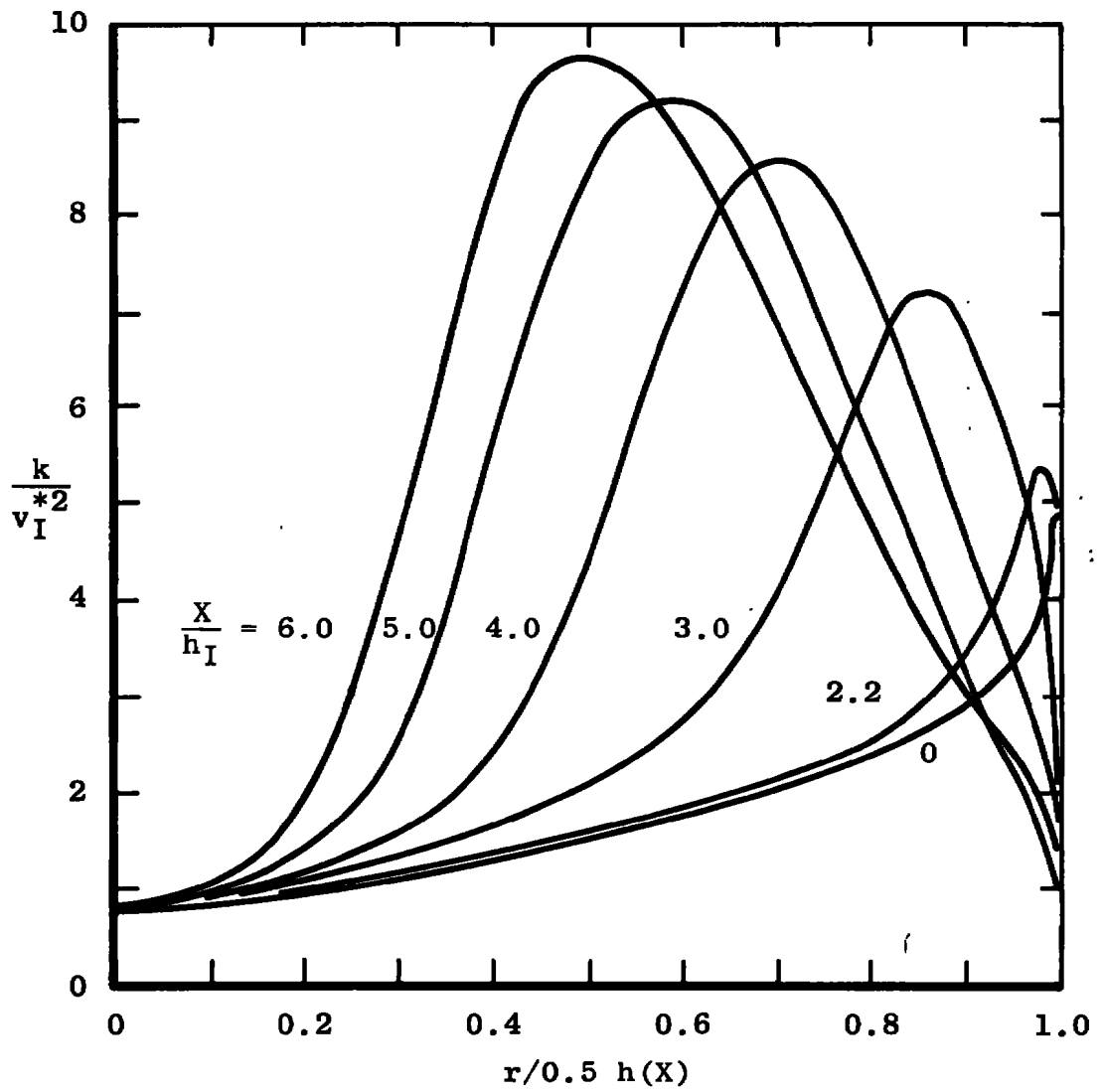
e. 2θ = 28.1 deg
Figure 48. Continued.
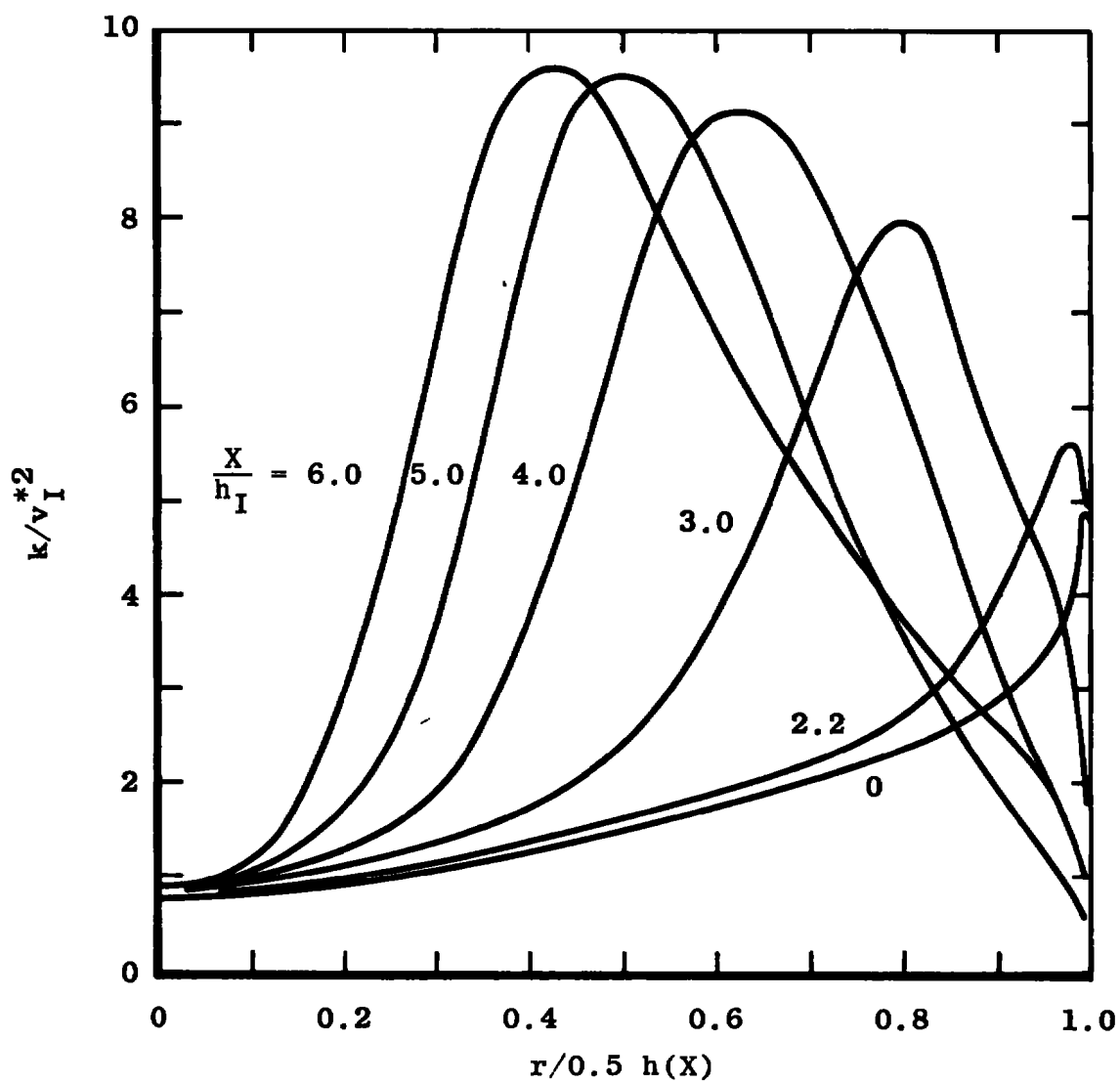
f. $2\theta = 34.7$ deg
Figure 48. Concluded.
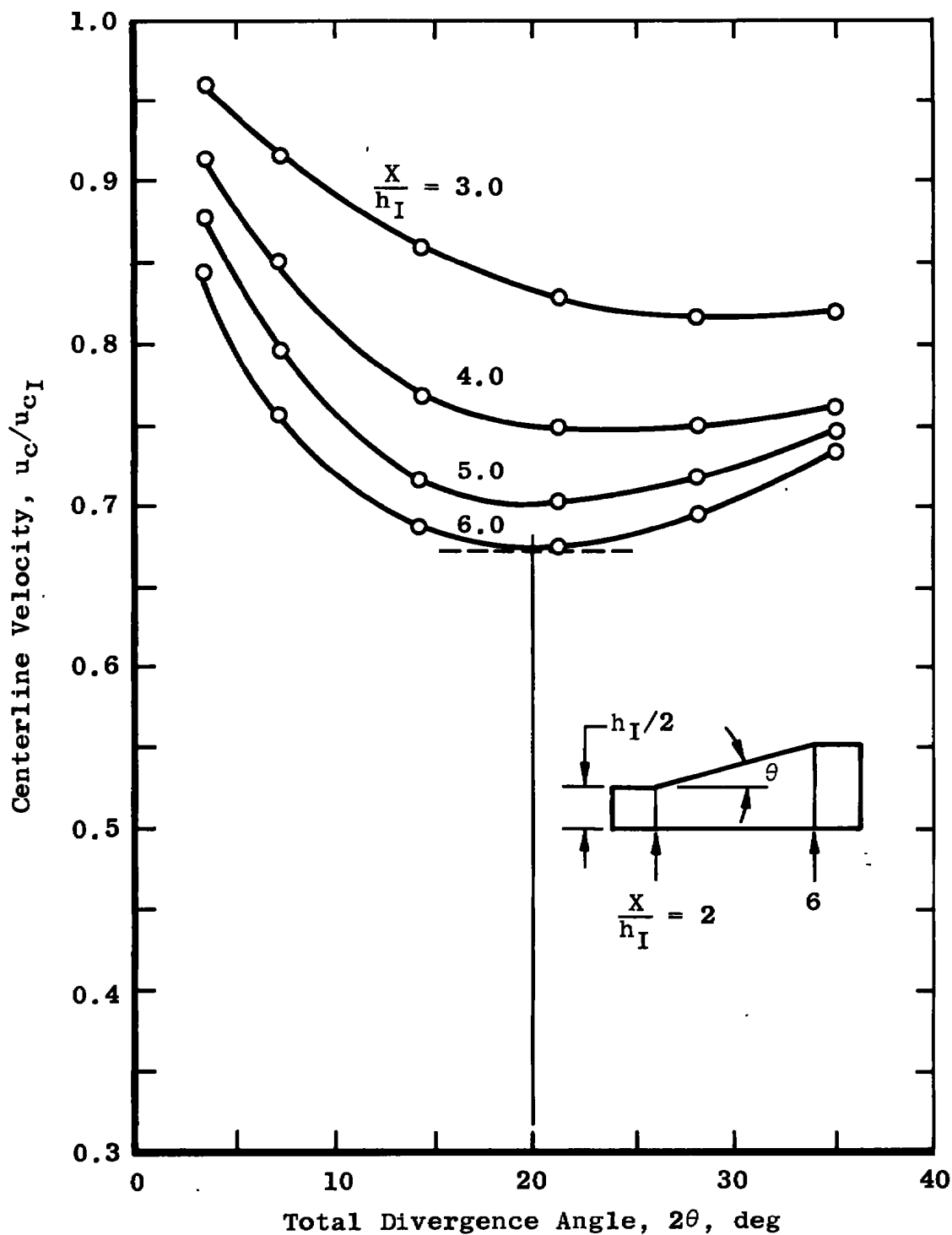
Figure 49. Centerline velocity distribution and optimum diffuser
angle.
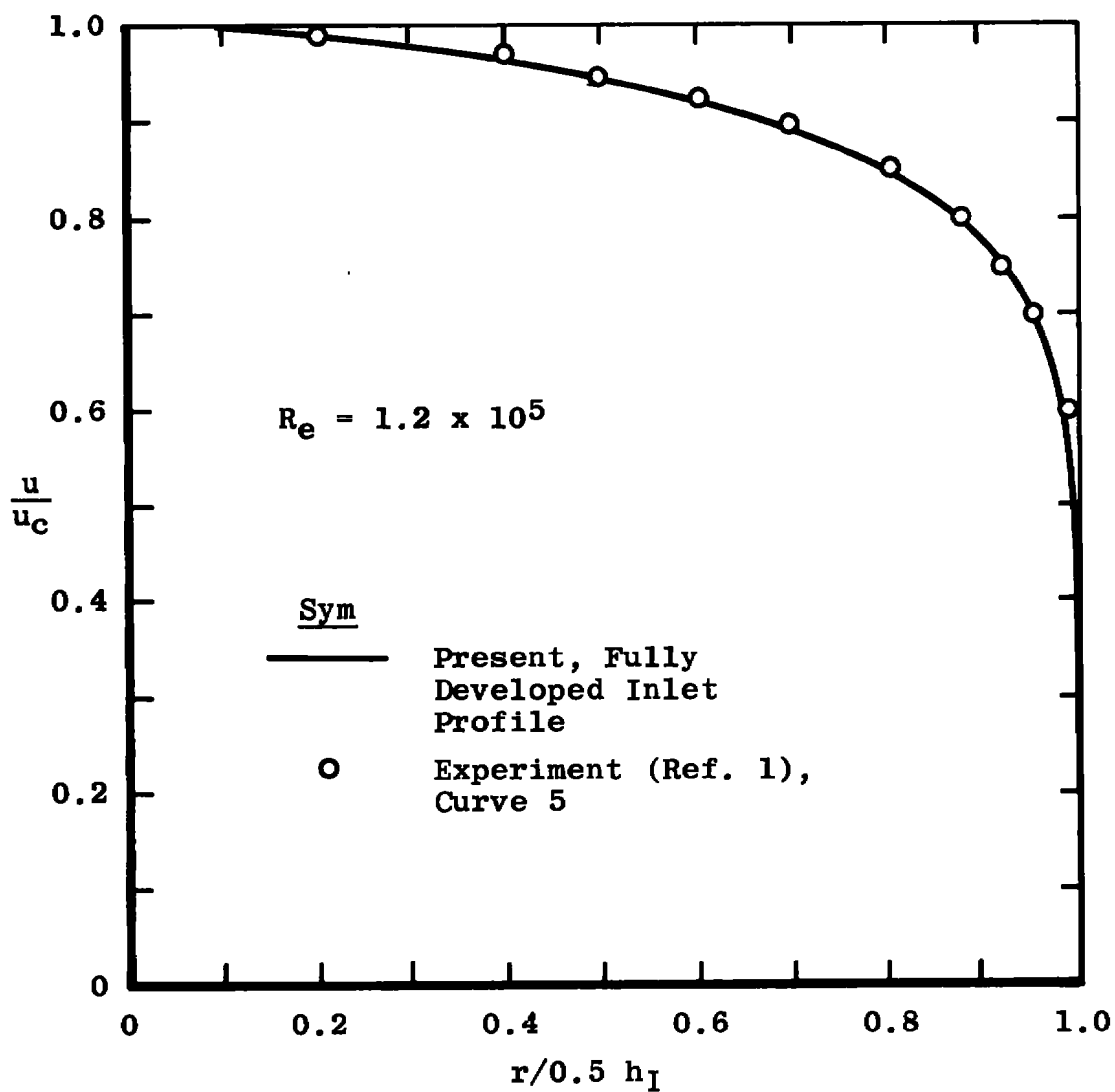
Figure 50. Inlet velocity profile, 2-D diffuser.
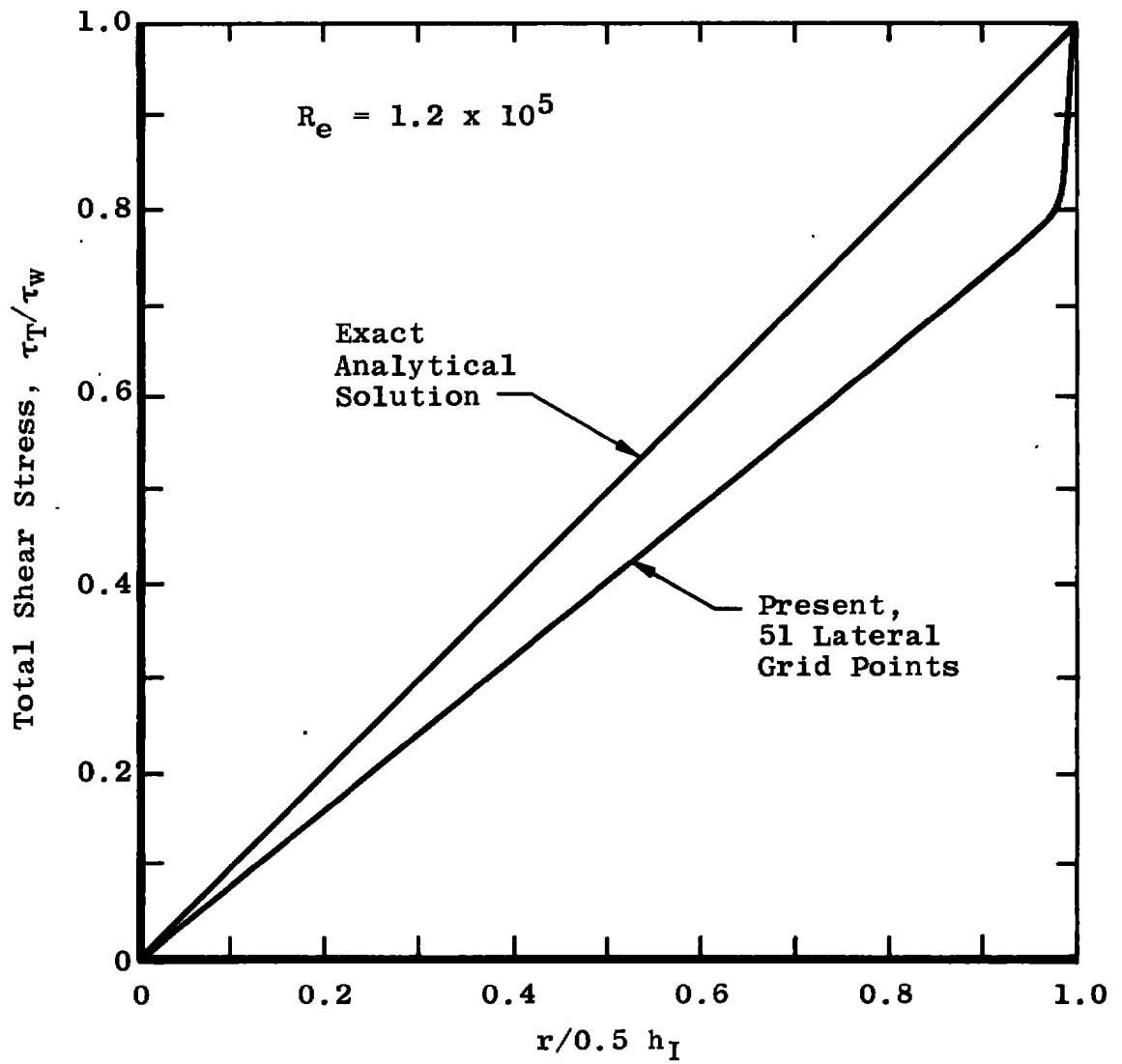
Figure 51. Accuracy of the inlet profile based on the total shear stress distribution.

Table 1. Comparison between Two Low Reynolds Number Models

	C_μ	σ_ϵ	$\mathcal{E}_T - \mathcal{E}$	Artificial Term
Present	$A/[3(a+A/b)]$	1.1	$\dfrac{2\nu k}{y^2}$	NONE
Launder's	$0.09 \exp\left(\dfrac{-3.4}{(1+R/50)^2}\right)$	1.3	$2\nu\left(\dfrac{\partial\sqrt{k}}{\partial y}\right)^2$	$2\nu\nu_t\, S\left(\dfrac{\partial^2 u}{\partial y^2}\right)$

APPENDIX A

DERIVATION OF A COORDINATE TRANSFORMATION
WITH A SUBLAYER STRETCHING

The purpose of the transformation is twofold: (1) to provide adequate resolution in the sublayer region which normally occupies only about 1 percent of the flow field, and (2) to obtain a smooth stretching of the coordinates from the sublayer to the core region. Because of the complexity of the velocity profile near the wall, separate transformation functions are derived for the sublayer and the core region. They are matched smoothly at a proper location (y_0) so that the functions are continuous up to the second derivatives.

TRANSFORMATION FUNCTION IN THE SUBLAYER

Inside the sublayer, the velocity distribution is linear. A tangent function is a suitable stretching function for the sublayer region:

$$y = \frac{\alpha}{\beta} \tan \beta \tilde{y} \tag{A-1}$$

The stretching factor $(\partial \tilde{y}/\partial y)$, which must be adjusted to provide good resolution of the sublayer velocity profile, is related to the slope of the velocity profile by

$$\left.\frac{\partial \tilde{y}}{\partial y}\right|_{y=0} = \alpha = \left.\frac{\partial u}{\partial y}\right|_{y=0} = \frac{v^{*2}}{\nu} \tag{A-2}$$

The condition determines the coefficient (α) in terms of $v*2/\nu$. The coefficient (β) will be determined through the matching procedure at y_0.

TRANSFORMATION FUNCTION IN THE CORE REGION

In the core region, there is no need to have a large coordinate stretching because the profile is rather smooth. Therefore, the stretching factor $(\partial \tilde{y}/\partial y)$ must gradually decrease to unity from the

131

sublayer to the centerline. In the present analysis, a hyperbolic function is selected for this purpose, i.e.,

$$\frac{\partial y}{\partial \tilde{y}} = c + \tanh(\tilde{y} - \tilde{y}_0) \qquad (A-3)$$

Upon integration, Eq. (A-3) becomes

$$y = c\tilde{y} + \ln(\cosh(\tilde{y} - \tilde{y}_0)) + F \qquad (A-4)$$

Equation (A-4) is the transformation function for the core region.

THE MATCHING CONDITION

The matching conditions are provided at the location (y_0) by the continuity of the function, the first and the second derivatives. With the continuity of the second derivatives at y_0, i.e.,

$$\left.\frac{\partial^2 y}{\partial \tilde{y}^2}\right|_{y_0}^{core} = \left.\frac{\partial^2 y}{\partial \tilde{y}^2}\right|_{y_0}^{sublayer} \qquad (A-5)$$

the coefficient (β) can be determined from Eqs. (A-1), (A-4), and (A-5) as

$$2\alpha\beta \sec^2\beta\tilde{y}_0 \cdot \tan\beta\tilde{y}_0 - 1 = 0 \qquad (A-6)$$

For the continuity of the first derivatives, the condition becomes

$$\left.\frac{\partial y}{\partial \tilde{y}}\right|_{y_0}^{core} = \left.\frac{\partial y}{\partial \tilde{y}}\right|_{y_0}^{sublayer} \qquad (A-7)$$

Equation (A-7) determines the coefficient (C) as

$$C = \alpha \sec^2\beta\tilde{y}_0 \qquad (A-8)$$

Finally, the continuity of the transformation functions provides the following relation for the constant (F), i.e.,

$$F = -C \, \tilde{y}_o + (\frac{\alpha}{\beta}) \tan \beta \, \tilde{y}_o \qquad \text{(A-9)}$$

By setting y = 1.0, the transformed centerline location ($\tilde{y}_{max}$) can be determined from Eq. (A-4) as

$$1 - C \, \tilde{y}_{max} - \ell_n \left(\cosh \left(\tilde{y}_{max} - \tilde{y}_o \right) \right) - F = 0 \qquad \text{(A-10)}$$

Equations (A-2), (A-6), (A-8), and (A-9) permit the transformation functions (A-1) and (A-4) to be written in terms of $v*^2/v$ and $\tilde{y}_o$, which are characteristic parameters of the sublayer.

NUMERICAL PROCEDURE

The numerical procedure used to calculate the coordinate transformation functions is outlined in Fig. A-1. First the parameter ($v*^2/v$) is determined based on some flow condition, such as the inlet condition to a diffuser. The stretched sublayer thickness is then set equal to unity so that enough resolution can be obtained. In addition, the number of grid points is specified in the transformed $\tilde{y}$ coordinate. The coefficients (α, C, and F) can be calculated directly from Eqs. (A-2), (A-8), and (A-9), respectively. On the other hand, coefficients such as β and $\tilde{y}_{max}$ must be determined iteratively by Newton's method, i.e.,

$$\beta_{n+1} = \beta_n - \frac{f(\beta_n)}{f'(\beta_n)} \qquad \text{(A-11)}$$

where β_{n+1} represents the (n+1)[th] value and β_n represents the old value.

The functions (f and f′) are obtained from Eq. (A-6) as

$$f(\beta_n) = 2 \alpha \beta_n \sec^2 \beta_n \cdot \tan \beta_n - 1 \qquad \text{(A-12)}$$

$$f'(\beta_n) = \frac{\partial f}{\partial \beta}\Big|_{\beta_n} = 2 \alpha \sec^2 \beta_n \left(\tan \beta_n + \beta_n \sec^2 \beta_n + 2 \beta_n \tan^2 \beta_n \right)$$
$$\text{(A-13)}$$

where $\tilde{y}_o$ = 1.0 has been used in the derivation. The converging solution for β is obtained by applying Eq. (A-11) successively from

an initial guess until a convergence criterion is reached. Since the Newton's method converges fairly rapidly with a good initial guess, the maximum number of iteration is often specified to terminate the calculation.

The coefficient (F) can also be determined in a similar manner, i.e.,

$$\tilde{y}_{max,n+1} = \tilde{y}_{max,n} - \frac{f(\tilde{y}_{max,n})}{f'(\tilde{y}_{max,n})} \qquad \text{(A-14)}$$

where f and f' are now derived from Eq. (A-10) as

$$f = -1 + c\,\tilde{y}_{max,n} + \ln\left(\cosh\left(\tilde{y}_{max,n} - 1\right)\right) + F \qquad \text{(A-15)}$$

$$f' = c + \tanh\left(\tilde{y}_{max,n} - 1\right) \qquad \text{(A-16)}$$

With all the coefficients determined, one can proceed to determine the uniform grid spacing ($\Delta y = (\tilde{y}_{max}/\text{JNM})$), the stretched coordinate ($\tilde{y} = (N \cdot \Delta\tilde{y})$), and the physical coordinate (y) by Eqs. (A-1) and (A-4). The coordinate transformation as a function of v^{*2}/ν is shown in Fig. A-2.

The transformation factors derived from Eqs. (A-1) and (A-4) are in the sublayer, $0 \leq \tilde{y} \leq \tilde{y}_0$:

$$\frac{\partial\tilde{y}}{\partial y} = \frac{1}{\alpha}\cos^2\beta\tilde{y}$$

$$\frac{\partial^2\tilde{y}}{\partial y^2} \Big/ \left(\frac{\partial\tilde{y}}{\partial y}\right)^2 = -2\beta\tan(\beta\tilde{y}) \qquad \text{(A-17)}$$

and in the core region, $\tilde{y}_0 \leq \tilde{y} \leq \tilde{y}_{max}$:

$$\frac{\partial\tilde{y}}{\partial y} = \frac{1}{c + \tanh(\tilde{y} - \tilde{y}_0)}$$

$$\frac{\partial^2\tilde{y}}{\partial y^2} \Big/ \left(\frac{\partial\tilde{y}}{\partial y}\right)^2 = -\left[\,\text{sech}^2(\tilde{y} - \tilde{y}_0)\right] \Big/ \left[c + \tanh(\tilde{y} - \tilde{y}_0)\right] \qquad \text{(A-18)}$$
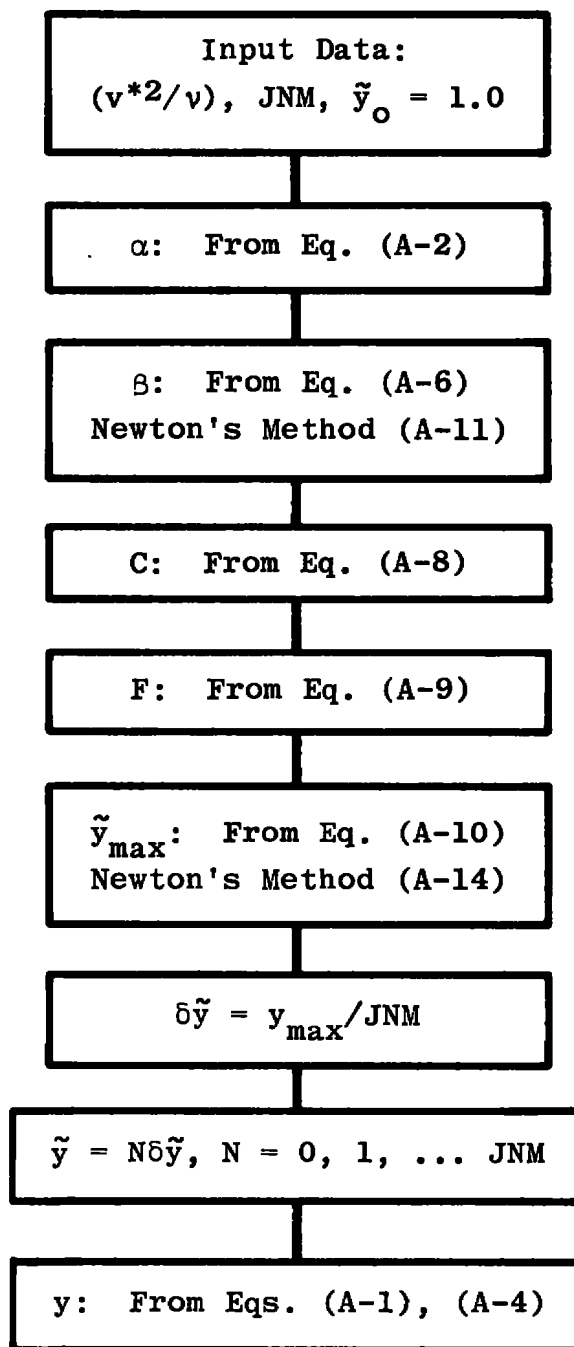
Figure A-1. Numerical procedure to determine the
coordinate transformation function.
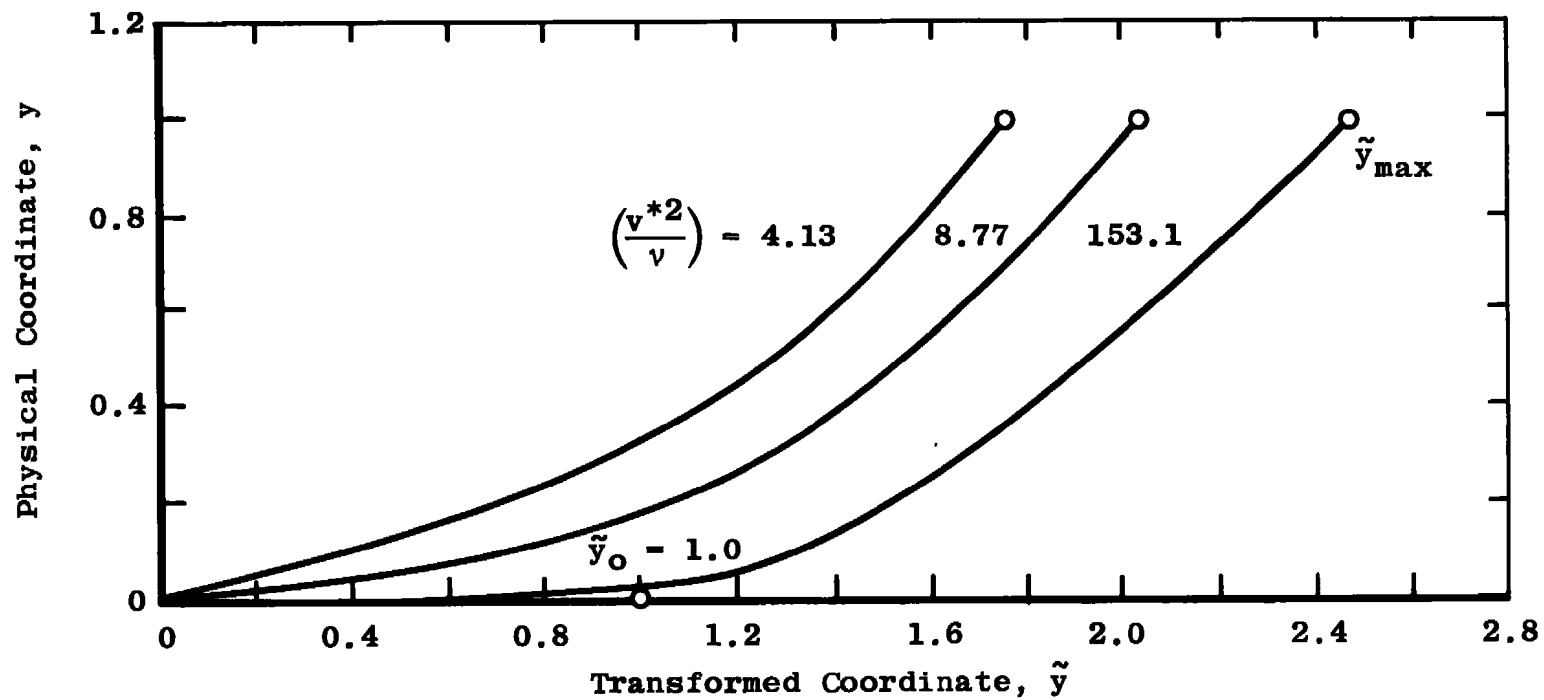
Figure A-2. Coordinate transformation as a function of the sublayer parameter (v^{*2}/ν).

APPENDIX B
DERIVATION OF DECAY FUNCTIONS

The derivation of decay functions is illustrated by using the steady-state vorticity equation. The derivation of the decay function for the time-dependent equation is given in Ref. 30. The one-dimensional vorticity equation is

$$\gamma \left(\frac{\partial^2 \Omega}{\partial y^2}\right) - v \left(\frac{\partial \Omega}{\partial y}\right) = 0 \qquad \text{(B-1)}$$

The finite difference expressions with the decay functions for a uniform grid system are

$$\frac{\partial^2 \Omega}{\partial y^2} \approx \frac{\Omega_{j+1} - 2\Omega_j + \Omega_{j-1}}{\delta y^2} \cdot \frac{1}{G_j}$$

$$\frac{\partial \Omega}{\partial y} \approx \frac{\Omega_{j+1} - \Omega_{j-1}}{2 \delta y} \cdot \frac{1}{F_j} \qquad \text{(B-2)}$$

The resulting finite difference equation is

$$\left\{ \frac{\Omega_{j+1} - 2\Omega_j + \Omega_{j-1}}{\delta y^2} \cdot \frac{1}{G_j} - \left(\frac{v}{\gamma}\right)_j \frac{\Omega_{j+1} - \Omega_{j-1}}{2 \delta y} \right\} = 0 \qquad \text{(B-3)}$$

The function (F_j) is not explicitly used in Eq. (B-3) because only one decay function is required for an equation with only two terms. For a nonuniform grid system, one obtains the finite difference equation.

$$\left\{ \frac{(\Omega_{j+1} - \Omega_j)/\delta y_1 - (\Omega_j - \Omega_{j-1})/\delta y_2}{(\delta y_1 + \delta y_2)/2} \cdot \frac{1}{G_j} - \left(\frac{v}{\gamma}\right)_j \frac{(\Omega_{j+1} - \Omega_{j-1})}{(\delta y_1 + \delta y_2)} \right\} = 0 \qquad \text{(B-4)}$$

where δy_1 and δy_2 are the grid spacing between (j+1) and (j), (j) and (j-1) grid points, respectively. After re-arrangement, Eq. (B-4) becomes

$$\Omega_j = \Omega_{j-1} + (\Omega_{j+1} - \Omega_{j-1}) \left\{ \frac{\delta y_2}{(\delta y_1 + \delta y_2)} - \left(\frac{v}{\gamma}\right)_j \frac{(\delta y_1 \cdot \delta y_2) \cdot G_j}{2(\delta y_1 + \delta y_2)} \right\} \qquad \text{(B-5)}$$

The local analytical solution of Eq. (B-1) can be obtained by assuming that v is locally constant, i.e., v_j. The analytical solution of Eq. (B-1) is

$$\Omega = C_1 + C_2 \cdot e^{\left(\frac{v}{\gamma}\right)_j \cdot y} \qquad \text{(B-6)}$$

The local boundary condition is

$$y = 0 \qquad , \quad \Omega = \Omega_{j-1}$$

$$y = \delta y_2 + \delta y_1 \quad , \quad \Omega = \Omega_{j+1} \qquad \text{(B-7)}$$

The final expression for $y = \delta y_2$ is obtained by combining Eqs. (B-6) and (B-7).

$$\Omega_j = \Omega_{j-1} + (\Omega_{j+1} - \Omega_{j-1}) \left\{ \frac{e^{\left(\frac{v}{\nu}\right)_j \delta y_2} - 1}{e^{\left(\frac{v}{\nu}\right)_j (\delta y_1 + \delta y_2)} - 1} \right\} \qquad \text{(B-8)}$$

The decay function (G_j) can be easily obtained by direct comparison of Eqs. (B-5) and (B-8). The result is

$$G_j = \frac{(\delta y_1 + \delta y_2)}{\left(\frac{v}{\nu}\right)_j \left(\frac{\delta y_1 \cdot \delta y_2}{2}\right)} \left\{ \frac{\delta y_2}{(\delta y_1 + \delta y_2)} - \frac{e^{\left(\frac{v}{\nu}\right)_j \delta y_2} - 1}{e^{\left(\frac{v}{\nu}\right)_j (\delta y_1 + \delta y_2)} - 1} \right\} \qquad \text{(B-9)}$$

for a uniform grid system, $\delta y_1 = \delta y_2 = \delta y$, and Eq. (B-9) reduces to

$$G_j = \frac{2}{\left(\frac{v}{\nu}\right)_j \delta y} \left\{ 1 - \frac{2(e^{\left(\frac{v}{\nu}\right)_j \delta y} - 1)}{(e^{2\left(\frac{v}{\nu}\right)_j \delta y} - 1)} \right\} \qquad \text{(B-10)}$$

or in terms of the grid Reynolds number $(R_j \equiv (v/\nu)_j \, \delta y)$,

$$G_j = \frac{2}{R_j} \left(1 - \frac{2(e^{R_j} - 1)}{e^{2R_j} - 1} \right) \qquad \text{(B-11)}$$

Equations (B-9) and (B-11) represent the decay functions in a non-uniform and a uniform grid system, respectively.

APPENDIX C
FINITE DIFFERENCE FORMULATION OF A 2-D FLOW
WITH A CONSTANT VISCOSITY

The governing equations for a two-dimensional planar steady-state flow of an incompressible fluid with a constant viscosity can be written as:

$$\frac{\partial u}{\partial x} + \frac{\partial v}{\partial y} = 0 \tag{C-1}$$

$$u\frac{\partial u}{\partial x} + v\frac{\partial u}{\partial y} = -\frac{1}{\rho}\frac{\partial p}{\partial x} + \nu\left(\frac{\partial^2 u}{\partial x^2} + \frac{\partial^2 u}{\partial y^2}\right) \tag{C-2}$$

$$u\frac{\partial v}{\partial x} + v\frac{\partial v}{\partial y} = -\frac{1}{\rho}\frac{\partial p}{\partial y} + \nu\left(\frac{\partial^2 v}{\partial x^2} + \frac{\partial^2 v}{\partial y^2}\right) \tag{C-3}$$

Equations (C-1) through (C-3) can be written in terms of the vorticity-stream function formulation as

$$\frac{\partial^2 \Omega}{\partial x^2} + \frac{\partial^2 \Omega}{\partial y^2} - \frac{1}{\nu}\left(u\frac{\partial \Omega}{\partial x} + v\frac{\partial \Omega}{\partial y}\right) = 0 \tag{C-4}$$

$$\Omega = \frac{\partial^2 \psi}{\partial x^2} + \frac{\partial^2 \psi}{\partial y^2} \tag{C-5}$$

A second-order pressure equation can also be derived as

$$\frac{\partial^2 p}{\partial x^2} + \frac{\partial^2 p}{\partial y^2} = -2\left\{\left(\Omega + \frac{\partial^2 \psi}{\partial y^2}\right)\left(\frac{\partial^2 \psi}{\partial y^2}\right) + \left(\frac{\partial v}{\partial y}\right)^2\right\} \tag{C-6}$$

where the source term of Eq. (C-6) has been written in terms of the derivatives in the y-direction for ease in the numerical computation. The velocity field (u, v) is obtained from the relation

$$u = \frac{\partial \psi}{\partial y} \quad , \quad v = -\frac{\partial \psi}{\partial x} \tag{C-7}$$

The corresponding finite difference equations for the general network shown in Fig. C-1 are:

Vorticity Equation (Ω)

$$\frac{(\Omega_{i+1,j}-2\Omega_{i,j}+\Omega_{i-1,j})}{\delta x^2}\cdot\frac{1}{G_i}-\left(\frac{u}{\nu}\right)_{i,j}\frac{(\Omega_{i+1,j}-\Omega_{i-1,j})}{2\delta x}$$

$$+\frac{(\Omega_{i,j+1}-2\Omega_{i,j}+\Omega_{i,j-1})}{\delta y^2}\cdot\frac{1}{G_j}-\left(\frac{v}{\nu}\right)_{i,j}\frac{(\Omega_{i,j+1}-\Omega_{i,j-1})}{2\delta y}=0 \tag{C-8}$$

where the decay functions G_i and G_j are defined as

$$G_i=(2/R_i)(1-2(e^{R_i}-1)/(e^{2R_i}-1)) \tag{C-9}$$

$$G_j=(2/R_j)(1-2(e^{R_j}-1)/(e^{2R_j}-1)) \tag{C-10}$$

$$R_i\equiv(u/\nu)_{i,j}\delta x \quad,\quad R_j\equiv(v/\nu)_{i,j}\delta y \tag{C-11}$$

Stream Function Equation (ψ)

$$(\psi_{i+1,j}-2\psi_{i,j}+\psi_{i-1,j})/\delta x^2+(\psi_{i,j+1}-2\psi_{i,j}+\psi_{i,j-1})/\delta y^2=-\Omega_{i,j} \tag{C-12}$$

Pressure Equation (p)

$$(p_{i+1,j}-2p_{i,j}+p_{i-1,j})/\delta x^2+(p_{i,j+1}-2p_{i,j}+p_{i,j-1})/\delta y^2$$

$$=-2\left\{[\Omega_{i,j}+(\psi_{i,j+1}-2\psi_{i,j}+\psi_{i,j-1})/\delta y^2][(\psi_{i,j+1}-2\psi_{i,j}+\psi_{i,j-1})/\delta y^2]\right.$$

$$\left.+[(V_{i,j+1}-V_{i,j-1})/2\delta y]^2\right\} \tag{C-13}$$

Velocity Relation (u, v)

$$u_{i,j}=(\psi_{i,j+1}-\psi_{i,j-1})/2\delta y \quad,\quad V_{i,j}=-(\psi_{i+1,j}-\psi_{i-1,j})/2\delta x \tag{C-14}$$

When Eqs. (C-8), (C-12), and (C-13) are solved iteratively by Gauss-Seidel iterative method, the corresponding successive substitution formula can be derived as

$$\phi_{i,j} = \frac{(C_1 \cdot \phi_{i+1,j} + C_2 \cdot \phi_{i-1,j} + C_3 \cdot \phi_{i,j+1} + C_4 \cdot \phi_{i,j-1} + \text{SOURCE})}{CU}$$

$$(C\text{-}15)$$

The corresponding C_1, C_2, C_3, C_4, SOURCE, and CU terms for each function are:

Ω-Equation

$$C_1 = 1/G_i - R_i/2$$

$$C_2 = 1/G_i + R_i/2$$

$$C_3 = (1/G_j - R_j/2) \cdot (\delta x/\delta y)^2$$

$$C_4 = (1/G_j + R_j/2) \cdot (\delta x/\delta y)^2 \qquad (C\text{-}16)$$

$$\text{SOURCE} = 0$$

$$CU = (2/G_i) + (2/G_j) \cdot (\delta x/\delta y)^2$$

and the decay functions are approximated as

$$G_i = 1.0 - 0.0625 \cdot (R_i)^2 \qquad , \ |R_i| < 2$$

$$= \frac{2}{|R_i|} - \frac{1}{(R_i)^2} \qquad , \ |R_i| \geq 2$$

$$\qquad (C\text{-}17)$$

$$G_j = 1.0 - 0.0625 \cdot (R_j)^2 \qquad , \ |R_j| < 2$$

$$= \frac{2}{|R_j|} - \frac{1}{(R_j)^2} \qquad , \ |R_j| \geq 2$$

ψ-Equation:

$$C_1 = 1 \qquad\qquad C_4 = (\delta x/\delta y)^2$$

$$C_2 = 1 \qquad\qquad CU = 2 + 2 \cdot (\delta x/\delta y)^2$$

$$C_3 = (\delta x/\delta y)^2 \qquad \text{SOURCE} = \Omega_{i,j} (\delta x)^2 \qquad (C\text{-}18)$$

p-Equation:

$$C_1 = 1$$

$$C_2 = 1$$

$$C_3 = (\delta x / \delta y)^2$$

$$C_4 = (\delta x / \delta y)^2 \tag{C-19}$$

$$CU = 2 + 2 \cdot (\delta x / \delta y)^2$$

$$SOURCE = 2\left\{ [\Omega_{i,j} + (\psi_{i,j+1} - 2\psi_{i,j} + \psi_{i,j-1})/\delta y^2] \cdot \right.$$
$$\left. [(\psi_{i,j+1} - 2\psi_{i,j} + \psi_{i,j-1})/\delta y^2] + [(v_{i,j+1} - v_{i,j-1})/2\delta y]^2 \right\}$$

The boundary conditions used for the planar diffuser calculation are:

UPSTREAM BOUNDARY CONDITION

A fully developed parabolic velocity profile is specified at the inlet of the diffuser in the present analysis to represent the non-uniform inlet condition. However, any other inlet profile can also be specified. The corresponding vorticity and the stream function distributions are derived from the velocity profile. The inlet static pressure profile is assumed to be uniform.

DOWNSTREAM BOUNDARY CONDITIONS

When the length of the exit section of the diffuser is long enough for a parallel flow to be established, the parallel flow condition can be expressed as

$$\frac{\partial \Omega}{\partial x} = \frac{\partial \psi}{\partial x} = 0 \tag{C-20}$$

The corresponding downstream condition for the pressure can be derived from the momentum Eq. (A-2) as

$$\frac{\partial p}{\partial x} = -\nu \frac{\partial \Omega}{\partial y} \tag{C-21}$$

SYMMETRY CONDITION

Along the line of symmetry, both the vorticity and the stream function are set equal to zero.

The pressure boundary condition along the line of symmetry can be obtained from Eq. (C-3) by integration in y direction, i.e.,

$$\int_1^2 (u\frac{\partial v}{\partial x} + v\frac{\partial v}{\partial y})\,dy = -\int_1^2 (\frac{\partial p}{\partial x})\,dy + \nu\int_1^2 (\frac{\partial \Omega}{\partial x})\,dy \qquad \text{(C-22)}$$

Subscripts 1 and 2 represent the centerline and its neighboring grid point, respectively (see Fig. C-1). By assuming that the integrands are linear function of y, one obtains

$$P_1 = \left[P + \frac{\delta y}{2}(u\frac{\partial v}{\partial x} - v\frac{\partial u}{\partial x}) - \frac{\nu \cdot \delta y}{2}(\frac{\partial \Omega}{\partial x}) \right]_2 \qquad \text{(C-23)}$$

where the continuity equation has been used for $\partial v/\partial y$. The second and the third terms inside the bracket represent the higher order term which vanishes in the limits as the ∂y goes to zero.

WALL BOUNDARY CONDITION

At the wall, the velocity components vanish and the stream function is a constant value along the solid wall, i.e.,

$$u = v = 0 \quad, \quad \psi = \psi_{wall} \qquad \text{(C-24)}$$

The vorticity at the wall can be obtained by the integration

$$\int_p^w \Omega\,dy = \int_p^w (\frac{\partial v}{\partial x} - \frac{\partial u}{\partial y})\,dy \qquad \text{(C-25)}$$

where w and p represent the wall and its neighboring points. Note that the integration can be performed in either the x- or y-direction. Assuming that the integrand in Eq. (C-25) is linear, one obtains

$$\Omega_w = +\frac{2u_p}{\delta y} + (\frac{\partial v}{\partial x})_p - \Omega_p \qquad \text{(C-26)}$$

Similarly, the wall boundary condition can be derived by integration of the momentum Eqs. (C-2) and (C-3) in either the x- or y-direction. For example, the pressure boundary condition along a

143

diverging diffuser wall is obtained by integrating Eq. (C-2) in the x-direction,

$$P_w = P_p - \frac{\nu \cdot \delta x}{2}\left[\left(\frac{\partial \Omega}{\partial y}\right)_w + \left(\frac{\partial \Omega}{\partial y}\right)_p\right] + \frac{\delta x}{2}\left[u\frac{\partial v}{\partial y} - v\frac{\partial u}{\partial y}\right]_p \quad \text{(C-27)}$$
$$+ \frac{\delta x}{2}\left[u\frac{\partial v}{\partial y} - v\frac{\partial u}{\partial y}\right]_w$$

For the horizontal inlet and exit walls, the condition (Eq. (C-27)) can be reduced to

$$P_w = P_p - \frac{\nu \cdot \delta x}{2}\left[\left(\frac{\partial \Omega}{\partial y}\right)_w + \left(\frac{\partial \Omega}{\partial y}\right)_p\right] + \frac{\delta x}{2}\left[u\frac{\partial v}{\partial y} - v\frac{\partial u}{\partial y}\right]_p \quad \text{(C-28)}$$

The formulation is fairly general in that it can be used for calculating most 2-D planar flows with proper assignment of the boundary conditions.
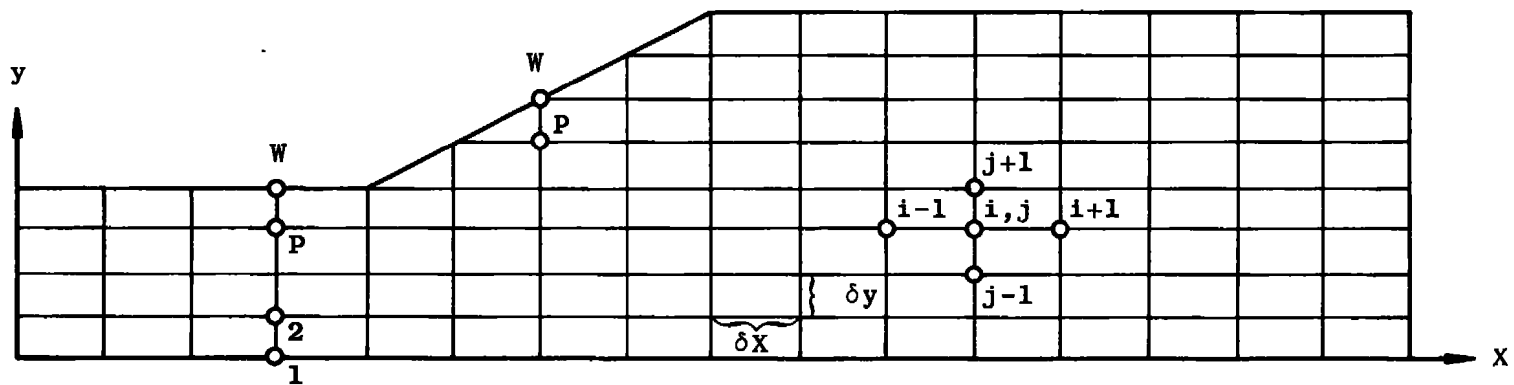
Figure C-1. 2-D diffuser and computational grid system.

APPENDIX D
FORMULATION OF A FULLY DEVELOPED CHANNEL FLOW WITH A HIGH REYNOLDS NUMBER TWO-EQUATION k-ε MODEL AND WALL MATCHING

For high Reynolds number fully developed channel flow, the governing equation is one dimensional. Since the sublayer is replaced by a law of the wall matching procedure, the effect of the molecular viscosity can be ignored. The complete set of governing equations is:

Vorticity Equation (Ω)

$$\frac{\partial^2 \Omega}{\partial r^2} - \frac{1}{\nu_t}\left\{-2\frac{\partial \nu_t}{\partial r} - \frac{\nu_t}{r}\cdot\delta\right\}\frac{\partial \Omega}{\partial r} + \delta\cdot\frac{\Omega}{\nu_t}\left\{\frac{1}{r}\frac{\partial \nu_t}{\partial r} - \frac{\nu_t}{r^2}\right\}$$
$$+ \frac{1}{\nu_t}\left\{-\frac{\partial^2 \nu_t}{\partial r^2}\cdot\frac{\partial u}{\partial r}\right\} = 0 \qquad (D-1)$$

Stream Function Equation (ψ)

$$\frac{\partial^2 \psi}{\partial r^2} - \delta\left(\frac{1}{r}\right)\frac{\partial \psi}{\partial r} + r^\delta\cdot\Omega = 0 \qquad (D-2)$$

Velocity Recovery (u)

$$u = \left(\frac{1}{r}\right)^\delta \frac{\partial \psi}{\partial r} \qquad (D-3)$$

Turbulent Kinetic Energy Equation (k)

$$\frac{\partial^2 k}{\partial r^2} - \frac{1}{\nu_t}\left\{-\frac{\partial \nu_t}{\partial r} - \frac{\nu_t}{r}\cdot\delta\right\}\frac{\partial k}{\partial r} + \left(\frac{\partial u}{\partial r}\right)^2 - \frac{\varepsilon}{\nu_t} = 0 \qquad (D-4)$$

Turbulent Kinetic Energy Dissipation Equation (ε)

$$\frac{\partial^2 \varepsilon}{\partial r^2} - \frac{\sigma_\varepsilon}{\nu_t}\left\{-\frac{\partial}{\partial r}\left(\frac{\nu_t}{\sigma_\varepsilon}\right) - \frac{\delta}{r}\left(\frac{\nu_t}{\sigma_\varepsilon}\right)\right\}\frac{\partial \varepsilon}{\partial r} + C_1 \sigma_\varepsilon \frac{\varepsilon}{k}\left(\frac{\partial u}{\partial r}\right)^2 - C_2 \frac{\varepsilon^2}{k}\left(\frac{\sigma_\varepsilon}{\nu_t}\right) = 0$$
$$(D-5)$$

Prandtl-Kolmogorov Eddy Viscosity Model

$$\nu_t = C_\mu \frac{k^2}{\varepsilon} \qquad (D-6)$$

146

The constants used are $C_\mu = 0.09$, $C_1 = 1.44$, and $C_2 = 1.92$. The boundary conditions along the centerline can be written as

$$\psi = constant \quad , \quad \Omega = \frac{\partial k}{\partial r} = \frac{\partial \varepsilon}{\partial r} = 0 \qquad (D-7)$$

The matching condition near the wall is provided by the law of the wall. The boundary condition and the related variables are

$$v^* = u_p /(2.5 \ln(v^* y_p /\nu)+5.5) \qquad k = v^{*2}/\sqrt{C_\mu}$$

$$u = v^*(2.5 \ln(v^* y_o /\nu)+5.5) \qquad \varepsilon = v^{*3}/(0.41 \, y_o)$$

$$\psi = 0 \qquad \Omega = -\frac{\partial u}{\partial r}$$
$$(D-8)$$

where y_o is the matching location measured from the wall and y_p is the distance one point next to the matching point. The governing equations written in the standard form are

$$\left\{\frac{\partial^2 \phi}{\partial r^2}\right\} - a\left\{\frac{\partial \phi}{\partial r}\right\} + d = 0 \qquad (D-9)$$

where coefficients a and d are given in the following table for a fully developed channel flow high Reynolds number model:

ϕ	a	d
Ω	$\frac{1}{\nu_t}\left\{-2\frac{\partial \nu_t}{\partial r}-\frac{\delta}{r}\nu_t\right\}$	$\delta\frac{\Omega}{\nu_t}\left\{\frac{1}{r}\frac{\partial \nu_t}{\partial r}-\frac{\nu_t}{r^2}\right\}+\frac{1}{\nu_t}\left\{-\frac{\partial^2 \nu_t}{\partial r^2}\frac{\partial u}{\partial r}\right\}$
ψ	$\left\{\frac{\delta}{r}\right\}$	$r^\delta \cdot \Omega$
k	$\frac{1}{\nu_t}\left\{-\frac{\partial \nu_t}{\partial r}-\frac{\delta}{r}\nu_t\right\}$	$(\frac{\partial u}{\partial r})^2-(\frac{C_\mu \cdot k}{\nu_t^2})\cdot k$
ε	$\frac{\sigma_\varepsilon}{\nu_t}\left\{-\frac{\partial}{\partial r}(\frac{\nu_t}{\sigma_\varepsilon})-\frac{\delta}{r}(\frac{\nu_t}{\sigma_\varepsilon})\right\}$	$C_1\sigma_\varepsilon(\frac{\partial u}{\partial r})^2\frac{C_\mu k}{\nu_t}-C_2(\frac{\varepsilon}{k}\frac{\sigma_\varepsilon}{\nu_t})\cdot\varepsilon$

147

The general finite difference formulation of Eq. (D-9) becomes

$$\left\{\frac{\phi_{j+1}-2\phi_j+\phi_{j-1}}{\delta r^2}\right\}\frac{1}{G_j} - a_j\left\{\frac{\phi_{j+1}-\phi_{j-1}}{2\delta r}\right\} + d_j = 0 \qquad (D\text{-}10)$$

where the decay function (G_j) is calculated from

$$G_j = 1.0 - 0.0625\,(R_j)^2 \qquad , \ |R_j| < 2$$

$$= \frac{2}{|R_j|} - \frac{1}{(R_j)^2} \qquad , \ |R_j| \geq 2 \qquad (D\text{-}11)$$

$$R_j \equiv a_j \cdot \delta r$$

The source terms (d_j) are calculated from the conventional central difference scheme. Note that the coefficient $(a_j$ and $R_j)$ do not necessarily represent the physical convective velocity and the Reynolds number. The coordinate system used and the variation of the eddy viscosity both contribute to the "effective" Reynolds number (R_j).

APPENDIX E

FORMULATION OF 2-D OR AXISYMMETRIC TURBULENT FLOWS WITH A TWO-EQUATION HIGH REYNOLDS NUMBER TURBULENCE MODEL

The governing equations for 2-D or axisymmetrical flows in physical coordinates are:

Vorticity Equation (Ω)

$$\left\{\frac{\partial^2\Omega}{\partial x^2}+\frac{\partial^2\Omega}{\partial r^2}\right\} - \frac{1}{\nu_t}\left\{\left[u-2\frac{\partial\nu_t}{\partial x}\right]\frac{\partial\Omega}{\partial x} + \left[v-2\frac{\partial\nu_t}{\partial r}-\frac{\nu_t}{r}\cdot\delta\right]\frac{\partial\Omega}{\partial r}\right\} + \frac{\delta}{r}\frac{\Omega}{\nu_t}\left\{v+\frac{\partial\nu_t}{\partial r}-\frac{\nu_t}{r}\right\}$$

$$+\frac{1}{\nu_t}\left\{\left(\frac{\partial^2\nu_t}{\partial x^2}-\frac{\partial^2\nu_t}{\partial r^2}\right)\left(\frac{\partial u}{\partial r}+\frac{\partial v}{\partial x}\right)+2\frac{\partial^2\nu_t}{\partial x\,\partial r}\left(\frac{\partial v}{\partial r}-\frac{\partial u}{\partial x}\right)\right\}=0 \qquad \text{(E-1)}$$

Stream Function Equation (ψ)

$$\left\{\frac{\partial^2\psi}{\partial x^2}+\frac{\partial^2\psi}{\partial r^2}\right\}-\frac{\delta}{r}\frac{\partial\psi}{\partial r}=-r^\delta\Omega \qquad \text{(E-2)}$$

Velocity Recovery (u, v)

$$u=\frac{1}{r^\delta}\frac{\partial\psi}{\partial r} \qquad , \quad v=-\frac{1}{r^\delta}\frac{\partial\psi}{\partial x} \qquad \text{(E-3)}$$

Prandtl-Kolmogorov Eddy Viscosity Model

$$\nu_t=C_\mu\frac{k^2}{\varepsilon} \qquad \text{(E-4)}$$

Turbulent Kinetic Energy Equation (k)

$$\left\{\frac{\partial^2 k}{\partial x^2}+\frac{\partial^2 k}{\partial r^2}\right\}-\frac{1}{\nu_t}\left\{\left[u-\frac{\partial\nu_t}{\partial x}\right]\frac{\partial k}{\partial x}+\left[v-\frac{\partial\nu_t}{\partial r}-\delta\frac{\nu_t}{r}\right]\frac{\partial k}{\partial r}\right\} \qquad \text{(E-5)}$$

$$+\left\{2\left[\left(\frac{\partial u}{\partial x}\right)^2+\left(\frac{\partial v}{\partial r}\right)^2+\delta\left(\frac{v}{r}\right)^2\right]+\left(\frac{\partial u}{\partial r}+\frac{\partial v}{\partial x}\right)^2\right\}-\frac{\varepsilon}{\nu_t}=0$$

Turbulent Kinetic Energy Dissipation Equation (ϵ)

$$\left\{\frac{\partial^2 \epsilon}{\partial x^2} + \frac{\partial^2 \epsilon}{\partial r^2}\right\} - \frac{\sigma_\epsilon}{\nu_t}\left\{\left[u - \frac{\partial}{\partial x}(\frac{\nu_t}{\sigma_\epsilon})\right]\frac{\partial \epsilon}{\partial x} - \left[v - \frac{\partial}{\partial r}(\frac{\nu_t}{\sigma_\epsilon}) - \frac{\epsilon}{r}(\frac{\nu_t}{\sigma_\epsilon})\right]\frac{\partial \epsilon}{\partial r}\right\}$$

$$+ C_1 \sigma_\epsilon \frac{\epsilon}{k}\left\{2\left[(\frac{\partial u}{\partial x})^2 + (\frac{\partial v}{\partial r})^2 + (\frac{v}{r})^2 \cdot \delta\right] + (\frac{\partial u}{\partial r} + \frac{\partial v}{\partial x})^2\right\} - C_2 (\frac{\epsilon^2}{k})\frac{\sigma_\epsilon}{\nu_t} = 0$$

$$\tag{E-6}$$

where

$$C_\mu = 0.09 \quad , \quad C_1 = 1.44 \quad , \quad C_2 = 1.92 \quad , \quad \sigma_\epsilon = 1.1$$

For diffuser flows, a transformation is applied to the above set of equations, i.e.,

$$\tilde{r} = \frac{r}{S(x)} \quad , \quad \tilde{x} = x \tag{E-7}$$

where (r, x) represents the physical coordinate system and $(\tilde{r}, \tilde{x})$ represents the transformed coordinate system. The chain rule and the corresponding transformation factors are

$$\frac{\partial}{\partial x} = \frac{\partial}{\partial \tilde{x}} + \frac{\partial}{\partial \tilde{x}} \cdot (\frac{\partial \tilde{r}}{\partial x})$$

$$\frac{\partial^2}{\partial x^2} = \frac{\partial}{\partial \tilde{x}^2} + (\frac{\partial \tilde{r}}{\partial x})^2 \frac{\partial^2}{\partial \tilde{r}^2} + 2(\frac{\partial \tilde{r}}{\partial x})\frac{\partial^2}{\partial \tilde{x}\partial \tilde{r}} + (\frac{\partial^2 \tilde{r}}{\partial x^2})\frac{\partial}{\partial \tilde{r}}$$

$$\frac{\partial}{\partial r} = \frac{\partial}{\partial \tilde{r}}(\frac{\partial \tilde{r}}{\partial r}) \tag{E-8}$$

$$\frac{\partial^2}{\partial r^2} = (\frac{\partial \tilde{r}}{\partial r})^2 \frac{\partial^2}{\partial \tilde{r}^2}$$

$$\frac{\partial^2}{\partial x\partial r} = (\frac{\partial \tilde{r}}{\partial r})\frac{\partial^2}{\partial \tilde{x}\partial \tilde{r}} + (\frac{\partial \tilde{r}}{\partial r})(\frac{\partial \tilde{r}}{\partial x})\frac{\partial^2}{\partial \tilde{r}^2} + \frac{\partial}{\partial \tilde{r}}(\frac{\partial^2 \tilde{r}}{\partial x\partial r})$$

where the transformation factors are

$$(\frac{\partial \tilde{r}}{\partial r}) = \frac{1}{S(x)}$$

$$(\frac{\partial \tilde{r}}{\partial x}) = -\tilde{r}(\frac{S'(x)}{S(x)})$$

$$(\frac{\partial^2 \tilde{r}}{\partial x^2}) = -(\frac{\partial \tilde{r}}{\partial x})(\frac{S'(x)}{S(x)}) - \tilde{r}\left[\frac{S''(x)}{S(x)} - (\frac{S'(x)}{S(x)})^2\right] \tag{E-9}$$

$$(\frac{\partial^2 \tilde{r}}{\partial x\partial r}) = -(\frac{S'(x)}{S(x)^2})$$

The governing equations written in the transformed coordinates in the standard form of:

$$\left\{ a_1 \frac{\partial^2 \phi}{\partial \tilde{x}^2} + a_2 \frac{\partial^2 \phi}{\partial \tilde{r}^2} \right\} - \left\{ b_1 \frac{\partial \phi}{\partial \tilde{x}} + b_2 \frac{\partial \phi}{\partial \tilde{r}} \right\} + d = 0 \tag{E-10}$$

are

Ω-Equation

$$a_1 = 1$$

$$a_2 = \left[\left(\frac{\partial \tilde{r}}{\partial x} \right)^2 + \left(\frac{\partial \tilde{r}}{\partial r} \right)^2 \right]$$

$$b_1 = \frac{1}{\gamma_t} \left\{ u - 2 \left[\frac{\partial \gamma_t}{\partial \tilde{x}} + \left(\frac{\partial \tilde{r}}{\partial x} \right) \frac{\partial \gamma_t}{\partial \tilde{r}} \right] \right\}$$

$$b_2 = \frac{1}{\gamma_t} \left\{ \left[v - 2 \left(\frac{\partial \gamma_t}{\partial \tilde{r}} \right) \left(\frac{\partial \tilde{r}}{\partial r} \right) - \frac{\delta}{r} \gamma_t \right] \left(\frac{\partial \tilde{r}}{\partial r} \right) + \left[u - 2 \left(\frac{\partial \gamma_t}{\partial \tilde{x}} + \left(\frac{\partial \tilde{r}}{\partial x} \right) \frac{\partial \gamma_t}{\partial \tilde{r}} \right) \right] \left(\frac{\partial \tilde{r}}{\partial x} \right) - \gamma_t \left(\frac{\partial^2 \tilde{r}}{\partial x^2} \right) \right\}$$

$$d = 2 \left(\frac{\partial \tilde{r}}{\partial x} \right) \frac{\partial^2 \Omega}{\partial \tilde{x} \partial \tilde{r}} + \frac{\delta}{r} \frac{\Omega}{\gamma_t} \left\{ v + \frac{\partial \gamma_t}{\partial \tilde{r}} \left(\frac{\partial \tilde{r}}{\partial r} \right) - \frac{\gamma_t}{r} \right\} + \frac{1}{\gamma_t} \left\{ \left(\frac{\partial^2 \gamma_t}{\partial \tilde{x}^2} + \left(\frac{\partial \tilde{r}}{\partial x} \right)^2 \frac{\partial^2 \gamma_t}{\partial \tilde{r}^2} \right. \right.$$

$$+ 2 \left(\frac{\partial \tilde{r}}{\partial x} \right) \frac{\partial^2 \gamma_t}{\partial \tilde{x} \partial \tilde{r}} + \left(\frac{\partial^2 \tilde{r}}{\partial x^2} \right) \left(\frac{\partial \gamma_t}{\partial \tilde{r}} \right) - \left(\frac{\partial \tilde{r}}{\partial r} \right)^2 \frac{\partial^2 \gamma_t}{\partial \tilde{r}^2} \right) \left(\left(\frac{\partial \tilde{r}}{\partial r} \right) \frac{\partial u}{\partial \tilde{r}} + \frac{\partial v}{\partial \tilde{x}} + \left(\frac{\partial \tilde{r}}{\partial x} \right) \frac{\partial v}{\partial \tilde{r}} \right)$$

$$+ 2 \left(\frac{\partial^2 \gamma_t}{\partial \tilde{x} \partial \tilde{r}} \left(\frac{\partial \tilde{r}}{\partial r} \right) + \left(\frac{\partial \tilde{r}}{\partial r} \right) \left(\frac{\partial \tilde{r}}{\partial x} \right) \frac{\partial^2 \gamma_t}{\partial \tilde{r}^2} + \frac{\partial \gamma_t}{\partial \tilde{r}} \left(\frac{\partial^2 \tilde{r}}{\partial x \partial r} \right) \right) \left(\left(\frac{\partial \tilde{r}}{\partial r} \right) \frac{\partial v}{\partial \tilde{r}} - \frac{\partial u}{\partial \tilde{x}} \right.$$

$$\left. \left. - \left(\frac{\partial \tilde{r}}{\partial x} \right) \frac{\partial u}{\partial \tilde{r}} \right) \right\} \tag{E-11}$$

ψ-Equation

$$a_1 = 1$$

$$a_2 = \left[\left(\frac{\partial \tilde{r}}{\partial x} \right)^2 + \left(\frac{\partial \tilde{r}}{\partial r} \right)^2 \right]$$

$$b_1 = 0$$

$$b_2 = - \left(\frac{\partial^2 \tilde{r}}{\partial x^2} \right)$$

$$d = - \delta \cdot u + 2 \left(\frac{\partial \tilde{r}}{\partial x} \right) \frac{\partial^2 \psi}{\partial \tilde{x} \partial \tilde{r}} + r^\delta \cdot \Omega \tag{E-12}$$

151

k-Equation

$$a_1 = 1$$

$$a_2 = \left[\left(\frac{\partial \tilde{r}}{\partial x}\right)^2 + \left(\frac{\partial \tilde{r}}{\partial r}\right)^2\right]$$

$$b_1 = \frac{1}{\nu_t}\left\{ u - \left(\frac{\partial \nu_t}{\partial \tilde{x}} + \left(\frac{\partial \tilde{r}}{\partial x}\right)\frac{\partial \nu_t}{\partial \tilde{r}}\right)\right\}$$

$$b_2 = \frac{1}{\nu_t}\left\{ \left[v - \left(\frac{\partial \tilde{r}}{\partial r}\right)\frac{\partial \nu_t}{\partial \tilde{r}} - \frac{\delta}{r}\nu_t\right]\left(\frac{\partial \tilde{r}}{\partial r}\right) + \left[u - \left(\frac{\partial \nu_t}{\partial \tilde{x}} + \left(\frac{\partial \tilde{r}}{\partial x}\right)\frac{\partial \nu_t}{\partial \tilde{r}}\right)\right]\left(\frac{\partial \tilde{r}}{\partial x}\right) \right.$$
$$\left. - \nu\left(\frac{\partial^2 \tilde{r}}{\partial x^2}\right)\right\}$$

$$d = 2\left(\frac{\partial \tilde{r}}{\partial x}\right)\frac{\partial^2 k}{\partial \tilde{x}\,\partial \tilde{r}} + 2\left\{\left[\frac{\partial u}{\partial \tilde{x}} + \frac{\partial u}{\partial \tilde{r}}\left(\frac{\partial \tilde{r}}{\partial x}\right)\right]^2 + \left[\frac{\partial v}{\partial \tilde{r}}\left(\frac{\partial \tilde{r}}{\partial r}\right)\right]^2 \right.$$
$$\left. + \left(\frac{v}{r}\right)^2 \cdot \delta\right\} + \left[\frac{\partial u}{\partial \tilde{r}}\left(\frac{\partial \tilde{r}}{\partial r}\right) + \frac{\partial v}{\partial \tilde{x}} + \left(\frac{\partial \tilde{r}}{\partial x}\right)\frac{\partial v}{\partial \tilde{r}}\right]^2 - \frac{\varepsilon}{\nu_t} \qquad \text{(E-13)}$$

ε-Equation

$$a_1 = 1$$

$$a_2 = \left[\left(\frac{\partial \tilde{r}}{\partial x}\right)^2 + \left(\frac{\partial \tilde{r}}{\partial r}\right)^2\right]$$

$$b_1 = \frac{1}{\nu_t}\left\{ \sigma_\varepsilon \cdot u - \left(\frac{\partial \nu_t}{\partial \tilde{x}} + \left(\frac{\partial \tilde{r}}{\partial x}\right)\frac{\partial \nu_t}{\partial \tilde{r}}\right)\right\}$$

$$b_2 = \frac{1}{\nu_t}\left\{ \left[\sigma_\varepsilon \cdot v - \left(\frac{\partial \tilde{r}}{\partial r}\right)\frac{\partial \nu_t}{\partial \tilde{r}} - \frac{\delta}{r}\nu_t\right]\left(\frac{\partial \tilde{r}}{\partial r}\right) \right.$$
$$\left. + \left[\sigma_\varepsilon \cdot u - \left(\frac{\partial \nu_t}{\partial \tilde{x}} + \left(\frac{\partial \tilde{r}}{\partial x}\right)\frac{\partial \nu_t}{\partial \tilde{r}}\right)\right]\left(\frac{\partial \tilde{r}}{\partial x}\right) - \nu_t\frac{\partial^2 \tilde{r}}{\partial x^2}\right\}$$

$$d = 2\left(\frac{\partial \tilde{r}}{\partial x}\right)\frac{\partial^2 k}{\partial \tilde{x}\,\partial \tilde{r}} + C_1\,\sigma_\varepsilon \frac{C_\mu k}{\nu_t}\left\{ 2\left[\frac{\partial u}{\partial \tilde{x}} + \frac{\partial u}{\partial \tilde{r}}\left(\frac{\partial \tilde{r}}{\partial x}\right)\right]^2 \right.$$
$$\left. + 2\left(\frac{v}{r}\right)^2 \cdot \delta + \left[\frac{\partial u}{\partial \tilde{r}}\left(\frac{\partial \tilde{r}}{\partial r}\right) + \frac{\partial v}{\partial \tilde{x}} + \left(\frac{\partial \tilde{r}}{\partial x}\right)\frac{\partial v}{\partial \tilde{r}}\right]^2\right\}$$
$$- C_2\,\sigma_\varepsilon \frac{C_\mu \cdot k}{\nu_t^2} \cdot \varepsilon \qquad \text{(E-14)}$$

Velocity Recovery (u, v)

$$u = \frac{1}{r^\delta}\left(\frac{\partial \tilde{r}}{\partial r}\right)\frac{\partial \psi}{\partial \tilde{r}}$$

$$v = \frac{-1}{r^\delta}\left[\frac{\partial \psi}{\partial \tilde{x}} + \frac{\partial \psi}{\partial \tilde{r}}\left(\frac{\partial \tilde{r}}{\partial x}\right)\right] \qquad \text{(E-15)}$$

APPENDIX F
FORMULATION OF A FULLY DEVELOPED CHANNEL FLOW WITH A LOW REYNOLDS NUMBER TWO-EQUATION k-ε MODEL AND SUBLAYER COORDINATE STRETCHING

The complete governing equations for a fully developed channel flow are:

Vorticity Equation (Ω)

$$\frac{\partial^2 \Omega}{\partial r^2} - \frac{1}{(\nu + \nu_t)} \left\{ -2 \frac{\partial \nu_t}{\partial r} - \frac{\delta}{r}(\nu + \nu_t) \right\} \frac{\partial \Omega}{\partial r} + \frac{1}{(\nu + \nu_t)} \frac{\partial^2 \nu_t}{\partial r^2} \cdot \Omega$$
$$+ \delta \frac{\Omega}{(\nu + \nu_t)} \left\{ \frac{1}{r} \frac{\partial \nu_t}{\partial r} - \frac{1}{r^2}(\nu + \nu_t) \right\} = 0 \qquad \text{(F-1)}$$

Stream Function Equation (ψ)

$$\frac{\partial^2 \psi}{\partial r^2} = -\Omega \, r^\delta + \frac{\delta}{r} \frac{\partial \psi}{\partial r} \qquad \text{(F-2)}$$

Velocity Recovery (u)

$$u = \frac{1}{r^\delta} \frac{\partial \psi}{\partial r} \qquad \text{(F-3)}$$

Prandtl-Kolmogorov Eddy Viscosity Model

$$\nu_t = \zeta_\mu \frac{k^2}{\varepsilon} \qquad \text{(F-4)}$$

Turbulent Kinetic Energy Equation (k)

$$\frac{\partial^2 k}{\partial r^2} - \frac{1}{(\nu + \nu_t)} \left\{ -\frac{\partial \nu_t}{\partial r} - \frac{\delta}{r}(\nu + \nu_t) \right\} \frac{\partial \Omega}{\partial r} + \frac{\nu_t}{(\nu + \nu_t)} \left(\frac{\partial u}{\partial r} \right)^2$$
$$- \frac{1}{(\nu + \nu_t)} \left\{ \varepsilon + \frac{2 \nu k}{y^2} \right\} = 0 \qquad \text{(F-5)}$$

Turbulent Kinetic Energy Dissipation Equation (ε)

$$\frac{\partial^2 \varepsilon}{\partial r^2} - \frac{1}{(\nu + \nu_t / \sigma_\varepsilon)} \left\{ -\frac{\partial}{\partial r} \left(\frac{\nu_t}{\sigma_\varepsilon} \right) - \frac{\delta}{r} \left(\nu + \frac{\nu_t}{\sigma_\varepsilon} \right) \right\} \frac{\partial \varepsilon}{\partial r}$$
$$+ C_1 \frac{\varepsilon}{k} \frac{\nu_t}{(\nu + \nu_t / \sigma_\varepsilon)} \left(\frac{\partial u}{\partial r} \right)^2 - C_2 \frac{\varepsilon^2}{k} \frac{1}{(\nu + \nu_t / \sigma_\varepsilon)} = 0 \qquad \text{(F-6)}$$

153

The coefficients (C_μ, C_1, C_2, and σ_ϵ) are

$$\varsigma_\mu = A/[3(1100 + A/0.27)]$$
$$C_1 = 1.44$$
$$C_2 = 1.92 \, [1.0 - 0.3 \exp(-R^2)]$$
$$\sigma_\epsilon = 1.1$$

(F-7)

$$A = \sqrt{2k}\, y/\nu \qquad , \qquad R \equiv k^2/(\nu \cdot \epsilon)$$

For a given coordinate transformation, such as

$$\tilde{r} = \tilde{r}(r)$$

(F-8)

the above set of equations can be written in the standard form,

$$\frac{\partial^2 \phi}{\partial \tilde{r}^2} - a \frac{\partial \phi}{\partial \tilde{r}} + d = 0$$

(F-9)

The coefficients (a and d) are listed in the following table for a fully developed channel flow low Reynolds number model:

ϕ	a	d
Ω	$\frac{1}{(\nu+\nu_t)}\left\{-2\frac{\partial \nu_t}{\partial \tilde{r}} - \frac{\delta}{r}\frac{(\nu+\nu_t)}{F_1}\right\}$ $-F_2$	$\frac{\Omega}{(\nu+\nu_t)}\left(\frac{\partial^2 \nu_t}{\partial \tilde{r}^2} + F_2 \frac{\partial \nu_t}{\partial \tilde{r}}\right)$ $+\frac{\delta \Omega}{(\nu+\nu_t)}\left\{\frac{1}{r}\frac{\partial \nu_t}{\partial \tilde{r}}\frac{1}{F_1} - \frac{1}{r^2}\frac{(\nu+\nu_t)}{(F_1)^2}\right\}$
ψ	$-F_2 + \frac{\delta}{r}\frac{1}{F_1}$	$r^\delta \frac{\Omega}{(F_1)^2}$
k	$\frac{1}{(\nu+\nu_t)}\left\{-\frac{\partial \nu_t}{\partial \tilde{r}} - \frac{\delta}{r}\frac{(\nu+\nu_t)}{F_1}\right\}$ $-F_2$	$\frac{\nu_t}{(\nu+\nu_t)}\left(\frac{\partial u}{\partial \tilde{r}}\right)^2$ $-\frac{k}{(\nu+\nu_t)}\left\{\frac{\varsigma_\mu k}{\nu_t} + \frac{2\nu}{y^2}\right\}\frac{1}{(F_1)^2}$
ϵ	$\frac{1}{(\nu+\nu_t/\sigma_\epsilon)}\left\{-\frac{\partial}{\partial \tilde{r}}\left(\frac{\nu_t}{\sigma_\epsilon}\right)\right\}$ $-\frac{\delta}{r}\frac{(\nu+\nu_t/\sigma_\epsilon)}{F_1} - F_2$	$C_1 \frac{\varsigma_\mu k}{(\nu+\nu_t/\sigma_\epsilon)}\left(\frac{\partial u}{\partial \tilde{r}}\right)^2$ $- C_2 \frac{\epsilon}{(\nu+\nu_t/\sigma_\epsilon)}\left(\frac{\varsigma_\mu k}{\nu_t}\right)\frac{1}{(F_1)^2}$
$F_1 \equiv \partial\tilde{r}/\partial r \quad , \quad F_2 \equiv (\partial^2\tilde{r}/\partial r^2)/(\partial\tilde{r}/\partial r)^2$		

NOMENCLATURE

A	Parameter
a	Coefficient
a_1, a_2	Coefficients
b	Constant
b_1, b_2	Coefficient
C_1, C_2	Coefficients
C_f	Skin friction coefficient
C_p	Pressure coefficient
C_μ	Eddy viscosity coefficient
C	Transform coefficient
D	Local diameter
d	Source term
e	Difference in finite difference equations
F	Transform parameters
G_i, G_j	Decay functions
h	Channel or 2-D diffuser height, $\tilde{y}$
JNM	Number of grid points along the $\tilde{r}$ or $\tilde{y}$ coordinate
k	Turbulent kinetic energy
L	Differential operator
ℓ	Prandtl mixing length
n	Iteration number
p	Pressure

R	Parameter, $k^2/\nu\epsilon$
Re	Reynolds number
R_i, R_j	Grid Reynolds number
r, $\widetilde{r}$	Radial coordinate in physical and transformed plane, respectively
$\widetilde{r}_{max}$	Diffuser wall coordinate in transform plane
s(x)	Diffuser wall coordinate in physical plane
u	Axial velocity
$\bar{u}$	Average axial velocity at diffuser inlet
u, v, w	Velocity components
u´, v´, w´	Trubulent velocity components
u^+	Sublayer velocity, $u/\nu *$
X	Axial coordinate
α, β	Transform parameters
γ	Trucation error
δ	Index, zero for planar configurations, 1 for axisymmetric configurations or incremental
$\delta *$	Boundary layer displacement thickness
ϵ	Isotropic part of the total turbulent energy dissipation, $k^{3/2}/\ell$
ϵ_T	Total turbulent kinetic energy dissipation
η	Relaxation factor
2θ	Total diffuser divergence angle
ν	Molecular viscosity

ν_t	Eddy viscosity
ρ	Density
σ_ϵ	Constant
τ	Shear stress
ϕ	Dependent variable
Ψ	Stream function
Ω	Vorticity

SUBSCRIPTS

c	Centerline
f	Finite difference
I	Inlet section
max	Maximum
o	Sublayer, core region solution matching location
p	Neighboring point
ref	Reference
sep	Separation
T	Total
w	Wall